Interfacial Stresses and Debonding Failures in Plated Beams

Vijayabaskar Narayanamurthy

Thesis presented for the Degree of

Doctor of Philosophy

Heriot-Watt University

February 2011

Abstract

Extensive research and recent developments in structural engineering has shown that adhesive bonding of fibre-reinforced polymer (FRP) composite, steel or any other metallic plate to the tension face of a reinforced concrete (RC), metallic or timber beam can effectively enhance its strength and other aspects of structural performance. This technique is now popularly adopted for retro-fitment and rehabilitation of existing structures. These plated beams often fail prematurely well before attaining the full flexural capacity by either plate end debonding (PED) or intermediate crack-induced interfacial debonding (ICD) failure. Concentration of higher interfacial shear and normal stresses at the plate end due to a geometric discontinuity is believed to be responsible for PED that initiates at the plate end and propagates inwards. PED includes concrete cover separation and interfacial debonding initiated at the plate end; and such failure initiated at a critical diagonal crack. ICD initiates at an intermediate major flexural or flexural-shear crack in the soffit of the original beam due to high bond stress and propagates towards one of the plate ends (type-1) or an adjacent crack (type-2).

This thesis presents a study of interfacial stresses and debonding failures in plated beams. It first presents a simple and novel theoretical solution of interfacial stresses applicable to any loading considering major deformations like axial and flexural deformations in the beam and plate within linear elastic range. This solution is then enhanced with the inclusion of the effect of adherends' shear deformation by approximating the displacement field for interfacial shear stress and using Timoshenko's beam theory for interfacial normal stress, achieving a better understanding of the effect of shear deformation which is ill-understood. This resulted in a first ever solution to include the effect of adherends' shear deformation under both interfacial shear and normal stresses. This solution is further advanced by developing a rigorous and a versatile closed-form solution fully based on Timoshenko's beam theory that offered a significant insight.

Interfacial stresses at the plate end cannot be measured directly using available measurement techniques, and may only be interpreted indirectly from measured plate strains. The conventional interpretation is based on the assumption that the plate is under pure tension. A significant drawback of this is that the interfacial normal stresses

cannot be deduced. A new technique is developed to deduce both interfacial shear and normal stresses from strain measurements.

The thesis presents three PED strength models for the special case of an RC beam with the plate terminated in the constant moment region: a theoretical model based on interfacial fracture mechanics with a reasonable accuracy; a semi-empirical model with greater accuracy; and an empirical model that is slightly less accurate but simpler to apply than the semi-empirical model. This is followed by the development of a shear debonding model to predict the debonding failure in an RC beam with the plate terminated in high shear and a very low or zero moment region. The two models for PED failure in pure bending and pure shear zones are then combined to result in an accurate shear-bending interaction debonding model. An assessment of these models against a carefully constructed large test database shows that they are more accurate than existing models and suitable for implementation in design codes or guidelines.

Finally, a structural mechanics formulation for an FRP-to-concrete bonded joint between two adjacent cracks is developed. It considers axial forces, transverse shear forces and bending moments in the adherends and uses a linearly softening bond-slip model. A section analysis with partial interaction and a rotational spring method are used to relate the applied loading to the interfacial deformation. A closed-form solution is obtained that may form the basis of a rational ICD design method.

To my maternal grand parents

Acknowledgements

My foremost and heartfelt thanks go to my two supervisors Dr. Jian-Fei Chen from The University of Edinburgh (UoE) and Dr. John Cairns from Heriot-Watt University (HWU) for their excellent motivation, enlightening guidance and continued encouragement. I am thankful to them as well as to the two Universities for offering me the Edinburgh Research Partnership in Engineering and Mathematics-Joint Research Institute (ERP-JRI) Doctoral Fellowship that in turn benefited me with the best resources in both Universities.

I am grateful to Dr. JF Chen for his admirable practice of conducting weekly review of the research besides his all time approachability in spite of being fully engaged that has really accelerated the pace and depth of research. He initiated numerous excellent ideas for me to follow throughout my candidature. His deep insights in structural mechanics and behaviour and adherence to rigorous research methodology ensured the quality of the research presented in this thesis. He also initiated the weekly review presentations that immensely helped me to get valuable feed backs from Prof. Michael Rotter, Prof. Jin Ooi, Prof. Yong Lu and all my friends in structures and granular mechanics group at UoE for which I am obliged. I appreciate Dr. John for his keen interest and valuable time in reviewing the manuscripts even while he was busy on a sabbatical. I am thankful to his numerous prolific comments.

I am also grateful to Prof. Ananth Ramaswamy (Indian Institute of Science) and Prof. Deric Oehlers (University of Adelaide) for their valuable review and fruitful comments about the research in Chapters 3 and 6 respectively. I sincerely thank my beloved previous adviser Prof. C. Lakshmana Rao (Indian Institute of Technology Madras) and mathematics teacher Prof. R. Sekar (Pondicherry Engineering College) for their passionate encouragement.

This studentship provided me an opportunity to benefit from the excellent lectures on theory and design of structures; plastic analysis; mechanics of repairing and strengthening; non-linear mechanics and FEM provided by Dr. JF Chen; Dr. Pankaj; Dr. Vengadesan Venugopal; Dr. Tim Stratford; Dr. Luke Bisby; Prof. Rotter; and Prof. Asif Usmani at UoE and Dr. David Haldane at HWU. I am thankful to all these wonderful faculties. I should really thank Dr. Chen and Dr. John again here for their

encouragement to attend such lectures and many other researcher development programmes held at both Universities and various conferences in and out of UK from day one.

I am thankful to Gillian Rae (HWU) and Margaret Taylor (UoE) for their administrative services and helps.

I was fortunate to have a nice team of good friends Tao Yi; Xiaoqin Li; Dr. Jun Ai; Ying Liu; Shiqing Li; Dr. Chong Zhou; Yin Wang; Dr. Adam Sadowski; Finn Ewan Donaldson; Noel Conlisk; Lei Chen; Nick Brown; John Morrisey; Dr. Kiran Tota Maharaj; Dr. Mical Johnston; Dr. Jin Sun; Subash Thakur; and Prashant Gupta from UoE where I spent the majority of my time and Abdul Sangi; Nicoloas; Sudip Pal; Aysha Akter; Soni; and Srinivas from HWU for making my University life more enjoyable with many fruitful discussions. I am also thankful to many life long friends and seniors in India and elsewhere for their perpetual friendship and moral support.

I thank Dr. Chen and his family for their kind efforts and fervour in organising periodical social get-togethers for all the researchers and their family from structures and granular mechanics group at UoE that were fondly memorable.

I have been gifted to have great teachers through out my life who offered selfless services with their excellent teachings and induced inherent interest in academics. I am indebted to all my teachers who stayed as role models in Government Primary School, Jawahar Navodaya Vidyalaya, Motilal Nehru Government Polytechnic, Pondicherry Engineering College and Indian Institute of Technology Madras.

Finally, my special thanks go to my maternal grandparents, mother, brother, maternal relatives and teachers who made my school and higher educations possible in an extremely difficult period; to my wife Sathya for her adorable character, care and confidence; and to my daughter Charuroopa for providing me a wonderful and more enjoyable life and for her kindness in permitting me to continue my works in week ends after our regular and memorable library, park and shopping trips.

ACADEMIC REGISTRY
Research Thesis Submission

Name*:*	VIJAYABASKAR NARAYANAMURTHY		
School/PGI:	School of the Built Environment		
Version: *(i.e. First, Resubmission, Final)*	Final	Degree Sought (Award **and** Subject area)	Doctor of Philosophy (Structural Engineering)

Declaration

In accordance with the appropriate regulations I hereby submit my thesis and I declare that:

1) the thesis embodies the results of my own work and has been composed by myself
2) where appropriate, I have made acknowledgement of the work of others and have made reference to work carried out in collaboration with other persons
3) the thesis is the correct version of the thesis for submission and is the same version as any electronic versions submitted*.
4) my thesis for the award referred to, deposited in the Heriot-Watt University Library, should be made available for loan or photocopying and be available via the Institutional Repository, subject to such conditions as the Librarian may require
5) I understand that as a student of the University I am required to abide by the Regulations of the University and to conform to its discipline.

* *Please note that it is the responsibility of the candidate to ensure that the correct version of the thesis is submitted.*

Signature of Candidate*:*		Date:	28.02.2011

Submission

Submitted By *(name in capitals):*	VIJAYABASKAR NARAYANAMURTHY
Signature of Individual Submitting:	
Date Submitted:	28.02.2011

For Completion in Academic Registry

Received in the Academic Registry by *(name in capitals):*			
Method of Submission *(Handed in to Academic Registry; posted through internal/external mail):*	*Handed in to Academic Registry*		
E-thesis Submitted (mandatory for final theses from January 2009)			
Signature:		Date:	28.02.2011

Contents

Publications and Awards

This research was conducted under the direct supervision of Dr. Jian-Fei Chen at the School of Engineering at the University of Edinburgh and guided by Dr. John Cairns at Heriot-Watt University. This research has resulted in the following publications and awards.

Journal Publications

1. Narayanamurthy, V., Chen, J. F. and Cairns, J. (2010). "A general analytical method for the analysis of interfacial stresses in plated beams under arbitrary loading". *Advances in Structural Engineering*, 13 (5), 975-988.

2. Narayanamurthy, V., Chen, J. F., Cairns, J. and Ananth, R. (2011). "Effect of shear deformation on interfacial stresses of plated beams subjected to arbitrary loading". *International Journal of Adhesion and Adhesives, (under review).*

3. Narayanamurthy, V., Chen, J. F., Cairns, J., Oehlers, D.J. (2011). "Plate end flexural debonding model for plated beams". *ASCE Journal of Composites for Construction, (under review).*

Conference Presentations and Publications

4. Narayanamurthy, V., Chen, J. F. and Cairns, J. (2009). "A new Approach for interfacial stress analysis of beams with a bonded soffit plate. *In: Seracino, R. and Oehlers, D.J. (eds.), Proceedings of Ninth International Symposium on Fiber Reinforced Polymer Reinforcement for Reinforced Concrete Structures (FRPRCS-9)*, July 13-15, Sydney, Australia.

5. Narayanamurthy, V., Chen, J. F. and Cairns, J. (2009). "A solution for plated beam including shear deformation effect". *In: Halliwell, S. (ed.), Proceedings of Advanced Composites in Construction (ACIC-09)*, September 1-3, Edinburgh, UK.

6. Narayanamurthy, V., Chen, J. F. and Cairns, J. (2010). "A new technique for deducing interfacial stresses from experiments in a plated beam". *In: Ford, M.C, (ed.), Proceedings of Thirteenth International Conference on Structural Faults and Repair (SFR-2010)*, June 15-17, Edinburgh, UK.

7. Narayanamurthy, V., Chen, J. F. and Cairns, J. (2010). "A rigorous solution for interfacial stresses in plated beams". *In: Feng, P. et al. (eds.), Proceedings of Fifth International Conference on FRP Composites in Civil Engineering (CICE 2010)*, September 27-29, Beijing, China.

8. Chen, J. F., Narayanamurthy, V. and Cairns, J. (2010). "A technique for deducing interfacial stresses from plate strain measurements in FRP or steel plated beams". *In: Ghugal, Y. M. and Londhe, R. S. (eds.), Proceedings of the International Conference on Innovative World of Structural Engineering (ICIWSE-2010)*, September 17-19, Aurangabad, India.

9. Narayanamurthy, V., Chen, J. F. and Cairns, J. (2011). "A solution for intermediate crack-induced debonding in plated beams". *Accepted for presentation and publication at the Tenth International Symposium on Fiber Reinforced Polymer Reinforcement for Reinforced Concrete Structures (FRPRCS-10)*, April 2-4, 2010, Tampa, Florida, USA.

10. Narayanamurthy, V., Chen, J. F. and Cairns, J. (2011). "Effect of flexural deformation on IC debonding behaviour of plated beams". *Abstract submitted for Advanced Composites in Construction (ACIC-2011)*, June 1-3, Warwick, UK.

Poster Presentations

11. Narayanamurthy, V., Chen, J. F. and Cairns, J. (2008). "A novel method for the analysis of interfacial stresses in plated beams". *Poster presented at the International Conference on Granular Materials and Structures-From Scientific Principles to Engineering Applications*, Royal Society of Edinburgh, June 30-July 2, Edinburgh, UK.

12. Narayanamurthy, V., Chen, J. F. and Cairns, J. (2010). "An analytical method for interpretation of interfacial stresses from experiments in a plated beam". *Poster presented at the Edinburgh Research Partnership in Engineering Mathematics (ERPem) Industry Evening Seminar*, January 21, The University of Edinburgh, UK.

13. Narayanamurthy, V., Chen, J. F. and Cairns, J. (2010). "Modelling of interfacial stresses and debonding failures in plated beams". *Poster presented at the Young Researchers Conference (YRC-2010)*, Institution of Structural Engineers (IStrcutE), March 10, London, UK.

14. Narayanamurthy, V., Chen, J. F. and Cairns, J. (2010). "Solution for intermediate crack induced debonding in plated beams". *Poster presented at the Fifth Heriot-Watt Post-Graduate Research Conference*, June 3, Heriot-Watt University, Edinburgh, UK.

Awards

The following prizes/awards were received during the PhD candidature:

1. Best Research Award: 13th International Conference on Structural Faults and Repair (SFR-2010), U.K., July 2010.
2. First Prize in Poster Presentation: Young Researchers Conference, YRC-2010, IStructE, U.K., March 2010.
3. Best Poster Award in Structures: Edinburgh Research Partnership in Engineering Mathematics (ERPem) Industry Evening Seminar, UoE, U.K, January 2009.
4. First Prize in Edinburgh Area Branch Graduates & Students Papers Competition-ICE, U.K., February 2009.
5. First Prize in East of Scotland Graduates & Students Papers Competition, ICE, U.K., and one among the five finalists in U.K., March 2009.
6. Best Poster Award: International Conference on Granular Materials and Structures-From Scientific Principle to Engineering Applications, Royal Society of Edinburgh, U.K., July 2008.

Chapter 1

Introduction

1.1 Background

Recent trends and extensive research to date in structural engineering have demonstrated that external adhesive bonding a plate (sheet) to the tension face of a beam (Figure 1.1) or slab, around a column or along the walls can effectively enhance its strength and structural performance without affecting the surrounding environment (Teng et al., 2002a; Hollaway and Teng, 2008). The original structural member (beam, slab, column or wall) could be made of reinforced concrete (RC), masonry, metal or timber and the plate is generally made of fibre reinforced polymer (FRP) composite, steel, aluminium or another metal. Such a member is called a plated structural member or hybrid structural member. This technique is commonly used for the retro-fitment and rehabilitation of existing structures and is potentially of use in many other engineering applications. The external plate augments flexural strength if plated on the tension face and shear strength if wrapped around or plated on the side faces in RC beams; flexural strength of RC slabs; confinement and axial capacity in columns; and blast resistance of walls and can even act as an effective seismic retro-fit of a structural member.

This thesis is concerned with plating of beams and slabs to improve their flexural strength. The scope is restricted to unprestressed and unanchored soffit plates. This bonded plate enhances the flexural strength of an original beam through the additional tensile capacity of the plate that supplements conventional embedded reinforcement, if any. For simplicity, all discussions in this thesis are presented with explicit reference to a simply supported beam (Figure 1.1), but the information is also commonly applicable

to indeterminate beams by treating each segment between two points of inflection as a simply-supported beam.

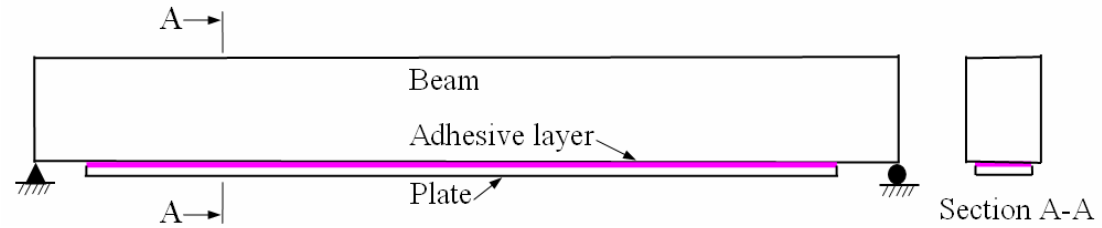

Figure 1.1. A plated beam

1.1.1 Flexural strengthening with FRP composites

The use of FRP composites for strengthening RC structures was first investigated as an alternative to steel plate bonding for beam strengthening at the Swiss Federal Laboratory for Materials Testing and Research (EMPA) where tests on RC beams strengthened with CFRP plates started in 1984, but most of the research on FRP plating has been carried out in the last 15 years. The main advantages of FRP composites are their high strength-to weight ratio, high corrosion resistance, light weight and ease of application. FRP bonding/wrapping has been found to be the most cost-effective solution in many strengthening projects (Hollaway and Teng, 2008). The most widely used FRP composites are glass-fibre-reinforced polymer (GFRP) composites, carbon-fibre-reinforced polymer (CFRP) composites, aramid-fibre-reinforced polymer (AFRP) composites and basalt- fibre-reinforced polymer (BFRP) composites. Two common methods of constructing FRPs in strengthening RC structures are wet lay-up method and factory prefabrication (pultruded plates). CFRP composites have superior properties to GFRP, AFRP and BFRP composites, but the latter are significantly cheaper. The stress–strain behaviour of all FRP is linearly elastic until rupture.

1.1.2 Failure modes

In addition to the flexural failure modes pertinent to a classical RC beam, plated RC beams in particular are vulnerable to various premature debonding failure modes prior to attaining their full flexural capacity. This premature debonding failure prevents the full intended utilization of the bonded plate that needs to be prevented to ensure widespread practical application of this technique. A schematic representation of these

failure modes are shown in Figures 1.2 and 1.3. The flexural failure of an FRP plated RC section can be due to the tensile rupture of the FRP plate or crushing of concrete that occurs when the ultimate flexural capacity of the beam is reached (Figure 1.2) at a critical section only if the plates are properly anchored. Composite action between bonded plate and beam continues until this form of flexural failure. The steel reinforcement will usually yield prior to these flexural failures unless it is located far from the tension face. In general, however, debonding of the plate from the original beam is the controlling failure mode in plated beams. Debonding failures observed in experiments can be broadly classified under two major failure types: (1) plate end debonding (PED) associated with high interfacial stresses near the ends of the bonded plate; and (2) intermediate crack induced interfacial debonding (ICD) induced by a flexural or flexural-shear crack (intermediate crack) away from the plate ends. This debonding can propagate toward either of the two plate ends.

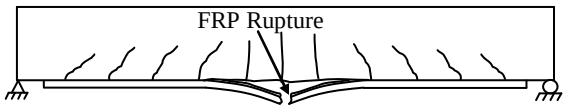

a) FRP rupture

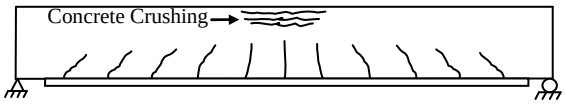

b) Crushing of compressive concrete

Figure 1.2. Conventional flexural failure modes of an FRP-plated RC beam (Teng and Chen, 2009)

PED can occur in five different modes: (a) critical diagonal crack (CDC) induced interfacial debonding (Figure 1.3a); (b) CDC with concrete cover separation (Figure 1.3b); (c) concrete cover separation (Figure 1.3c); (d) plate end interfacial debonding (Figure 1.3d); (e) mixed mode debonding with concrete cover separation followed by interfacial debonding (Figures 1.3c,d). The actual photographs with more details of two flexural failures and the first four PED failures can be found in Teng and Chen (2009) and Hollaway and Teng (2008) respectively and the last PED failure in Smith and Teng (2002a, b). CDC induced interfacial debonding occurs when the plate is terminated in a region of high shear force but low moment (closer to point of contraflexure or support) and the amount of steel shear reinforcement is limited. In this case, a major diagonal

shear crack (or CDC) forms and intersects the plate inducing high interfacial stresses, eventually leading to the interfacial debonding of the plate towards the plate end. If the same plated beam has more shear reinforcement, multiple shear cracks dominate the behaviour and leads to local detachment of the plate end which in turn moves the plate end to a new location with a larger moment from where CDC with cover separation begins.

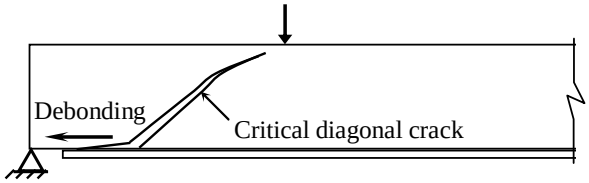

a) CDC induced interfacial debonding

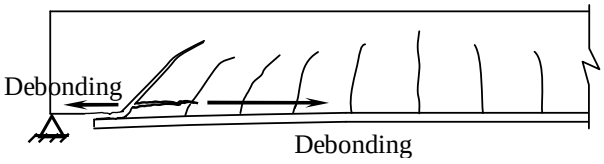

b) CDC debonding with concrete cover separation

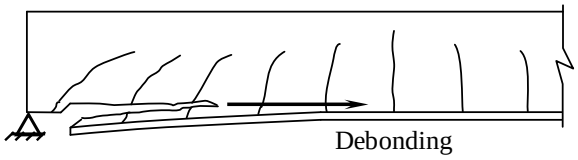

c) Concrete cover separation

d) Plate end interfacial debonding

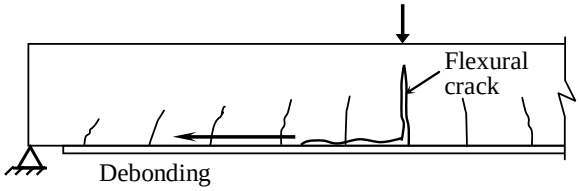

e) Intermediate crack induced interfacial debonding

Figure 1.3. Debonding failure modes of RC beams bonded with a soffit FRP plate (Teng and Chen, 2009)

Concrete cover separation involves crack propagation along the level of the steel tension reinforcement. Failure of the concrete cover is initiated by the formation of a crack near the plate end that propagates to and then along the level of the steel tension reinforcement, resulting in the separation of the concrete cover. Plate end interfacial debonding is initiated by high interfacial shear and normal stresses near the end of the plate that exceed the strength of the weakest element, generally the concrete, where it initiates at the adhesive-concrete interface and propagates towards the mid-span of the beam. This failure generally occurs when the plate is narrower than the beam section. Mixed mode debonding with cover separation followed by plate end interfacial debonding occurs in few cases of plated beams lying in between the two former cases.

ICD is initiated when a major flexural or flexural-shear crack formed in the concrete induces a large local strain concentration and leads to a much localized debonding of the plate from the concrete. The tensile stresses released by the cracked concrete are transferred to the plate and steel rebars, inducing high local interfacial stresses between the adhesive-to-concrete interface near the crack. The increase in applied loading further increases the tensile stresses in the plate and hence these interfacial stresses near the crack. When these stresses reach critical values, debonding starts to propagate towards one of the nearer plate ends (type-1) or adjacent crack (type-2) due to the stress gradient in the plate. ICD (Figure 1.3e) failures are more likely to occur in shallow beams that are more prone to flexural cracking.

1.1.3 Interfacial stresses and debonding models

High interfacial shear and normal stresses are generated between the plate and beam near the plate ends (Narayanamurthy et al., 2010) that may play an important role in some of the PED failure modes including concrete cover separation and plate end interfacial debonding although it is not simple to relate directly the magnitude of interfacial stresses based on an elastic analysis to debonding failures which is inherently nonlinear. Many analytical solutions, all based on linear elastic analysis have been developed for interfacial stresses but simple approximate closed-form solutions that sufficiently illustrate the stress concentration phenomenon in the vicinity of the plate end are shown to be suitable for exploitation in design (Teng et al., 2002a). They led to the development of interfacial stress based debonding models. Concurrently, many other PED models have been presented based on shear capacity of concrete and

concrete tooth formed by the cracks (Smith and Teng, 2002a, b), although their accuracy and approach still require a sound assessment.

Solutions have been presented for interfacial stress concentrations near the intermediate flexural or flexural shear cracks based on simple pull-off tests, simplifying assumptions and bond-slip behaviour for the plate-to-concrete interface (Yuan et al., 2004; Teng et al., 2006; Chen et al., 2007). They have been extremely useful for understanding the mechanics of ICD failures and laid the path for the development of ICD models. But the bond models need to be developed with minimal approximations to widen the scope of existing knowledge and for better prediction of these premature failures.

Available interfacial stress based solutions are applicable for one or two simple loading arrangements. There is no generic and simple solution with good accuracy. The effect of shear deformation on interfacial stresses remains poorly understood and only two approximate solutions exist which provide only a limited insight. Existing techniques used for interpreting the interfacial stresses in experiments are approximate and cannot quantify the effect of peeling between the plate and beam. Interfacial fracture mechanics based PED models are at their preliminary stages and are very few (De Lorenzis et al., 2008), and while robust models may be in development elsewhere none are as yet in the literature. The two existing complete models (Oehlers, 1992; Teng and Yao, 2007) are phenomenological (empirical), rather complex for use in design, and their accuracies need to be assessed against test data. A sound understanding on type-1 knowledge is really inadequate to explain the type-2 behaviour of ICD due to the differences in the failure mechanics. Very few studies existing on type-2 ICD need to be advanced for future exploitation in design against ICD. This thesis results from an endeavour to find the solutions to the above problems and contribute to the little advancement in the theory of plated beams.

1.2 Objectives and Methodologies

This research has the overall aim of improving the current understanding of interfacial stresses and modelling of debonding failures in plated beams from a structural mechanics perspective. The specific objectives and methodologies are as follows:

1. To develop a generic, simple and accurate theoretical solution for the analysis of interfacial stresses in plated beams subjected to arbitrary loading considering axial and flexural deformations;

2. To study the effect of shear deformation in adherends on interfacial stresses by developing an enhanced solution that includes the shear deformation effect on interfacial shear stress by an approximation of displacement field in adherends and on interfacial normal stress by Timoshenko's beam theory;

3. To derive a rigorous closed-form solution based on linear-elastic analysis considering all deformations simultaneously for any plated beam under any loading fully based on Timoshenko's beam theory;

4. To develop a new technique to interpret the interfacial shear stress and additionally quantify the interfacial normal stress from experimental plate strain measurements;

5. To develop a PED model based on interfacial fracture mechanics for a plated RC beam with plates terminated in a pure bending region;

6. To develop a phenomenological and simple PED model for a plated RC beam with plates terminated in high shear-low(zero) moment region (nearer to points of contraflexure);

7. To treat the above two models as two extreme boundary conditions to the general case of a plate terminated in any shear-bending interaction region; and develop an accurate and a general PED model suitable for direct implementation in any design codes or guidelines;

8. To develop a structural mechanics model to characterise the type-2 ICD behaviour using a local softening interface deformation model; relate the applied loading with plate deformation using rotational springs that simulate the crack flexibility at ends or a sectional analysis with partial interaction method; and provide solutions to all states of interfaces in different possible failure processes; and

9. To understand the effect of flexural deformation on type-2 ICD behaviour.

1.3 Structure of the Thesis

This thesis is constituted by nine chapters including this introductory chapter and seven core chapters followed by a summarising chapter. A brief introduction to each chapter is provided in this section.

Chapter 2 provides a simple, accurate and a general theoretical solution for analysing the interfacial stresses in plated beams. This solution considers a linear material behaviour for the plate and beam similar to all existing solutions, adopts a superposition technique and compatibility of longitudinal and vertical deformations at the adhesive and adherend's interfaces. This is applicable to all loadings, any cross-section of beam and any thickness of bonded plate.

Chapter 3 introduces the effect of shear deformation of beam and plate on both interfacial stresses. This accounts the effect of shear deformation on interfacial shear stress by a reasonable approximation of displacement field and on interfacial normal stress by Timoshenko's beam theory. This is the first solution to provide a right assessment of shear deformation effect.

Chapter 4 provides a rigorous closed-form theoretical solution for interfacial stresses by treating the plated beam as bi-Timoshenko beams. This solution explains the real effect of shear deformation on interfacial shear and normal stresses and provides a better understanding.

Chapter 5 highlights the development of a new technique to interpret the interfacial stresses from experimentally measured plate strains. This technique is advantageous compared to the traditional deduction method. It provides the peeling stresses additionally and the deduced interfacial shear stress accounts the effect of flexural deformation in beam and plate. This is applicable for all loading arrangements.

Chapter 6 reports the development of a first interfacial fracture mechanics based flexural PED model for the plates terminated in pure bending region. This is assessed with a constructed large flexural debonding test database and shown to be reasonably accurate. Calibration of this theoretical model with test database resulted in another semi-empirical model with highest accuracy. A phenomenological model is also

provided that is slightly less accurate but simpler than the semi-empirical model. The latter two models are shown to be the accurate of all existing and proposed models.

Chapter 7 gives a review of flexural, shear and shear-bending interaction models respectively for a plate terminated in pure bending, high shear-low (or zero) moment and shear-bending interaction regions. Then it provides a simple and an explicit shear debonding strength model followed by a shear-bending interaction model. Comparisons using a large test database with 226 test results and the predictions demonstrate the simplicity and the accuracy of the proposed models that can easily be incorporated in any design codes and guidelines.

Chapter 8 is related to the development of a structural mechanics model to characterise the type-2 ICD behaviour using a local softening interface deformation model. The applied loading is related to the plate deformation using rotational springs that simulate the crack flexibility at crack locations as well as using a sectional analysis with partial interaction method. Provide solutions to all states of interfaces in different possible failure processes. Effect of flexural deformation on type-2 ICD behaviour is demonstrated with parametric studies.

Chapter 9 summarises all the findings and contributions of this thesis. Future research essential to strengthen the concepts, simplify the solutions and improve the methodologies and accuracies are identified and recommendations are provided.

This thesis is organised in an incremental fashion that involves a diverse background literature and research methodologies. So, the literature review is divided and integrated into each core chapter for a better understanding and completeness of each chapter instead of providing a separate individual chapter on literature review. Moreover, the core chapters of this thesis are self contained as each will form the basis of a manuscript for submission to scientific journals. As a result, there is some repetition of fundamental concepts in the introduction of each core chapter and some differences in the writing style. Furthermore, notations were chosen to be simple and clear for each core chapter rather than for the thesis as a whole; consequently, the notations may not be identical from one chapter to another although effort has been made to retain identical notations where ever possible.

Chapter 2

A Simple General Method for Interfacial Stresses

Abstract

Recent developments in structural engineering have demonstrated effective enhancement in strength and performance of reinforced concrete (RC) and metallic beams bonded with a fibre reinforced polymer (FRP) composite or steel plate on their tension face. This technique is now popularly adopted for the retrofitting and strengthening of existing structures. Under applied loading after strengthening, interfacial shear and normal stresses are developed between the adherends in such plated beams due to the transfer of stresses between the bonded plate and the original beam. The combination of these stresses may be responsible for premature plate end debonding failure of the plate from the original beam in a brittle manner. Consequently, many analytical solutions have been developed to quantify these interfacial stresses. However, almost all of these solutions are applicable only to thin plates bonded to the beam and are specific to pre-defined simple loading arrangements, so each solution is commonly only applicable to a specific loading.

This chapter presents a new analytical solution for the interfacial stresses in a simply supported beam bonded with a thin or thick plate to the tension face. The solution is generic and applicable to beams and plates made of any structural materials within the linear elastic range, in common with almost all previous studies. The novelty of this work lies in the application of the superposition principle so that the simple solution is applicable to any arbitrary loading arrangement. Numerical comparison of the new solution with one of the existing solutions and finite element predictions for three loading cases illustrate the accuracy and applicability of the new analytical solution.

2.1 Introduction

Extensive research has shown that bonding a fibre-reinforced polymer (FRP) composite or metallic plate to the tension face of a reinforced concrete (RC) or metallic beam is effective in enhancing its strength (Teng et al., 2002a). Such strengthened beams (Figure 2.1) are called plated beams for brevity in this chapter. This method is popularly adopted for retrofitting existing structures. When the plated beam is loaded, longitudinal normal (i.e., axial) stresses are generated in the bonded plate. During the transfer of the stresses between the bonded plate and the original beam, interfacial shear and normal stresses are developed between the adherends (i.e. the original beam and the external plate) in the plated beam. These interfacial shear and normal stresses usually have their maximum values near the plate ends. The combined effect of these stresses may lead to the premature plate end debonding failure of the plate from the original beam in a brittle manner. Consequently, the interfacial stresses between the plate and the original beam have attracted a great interest in the last few decades and many analytical solutions have been developed to quantify them. A significant limitation of the majority of these solutions is that they are load specific, i.e. the form of the solution is different for each different loading scheme. Furthermore, most are only applicable to beams strengthened with thin plates.

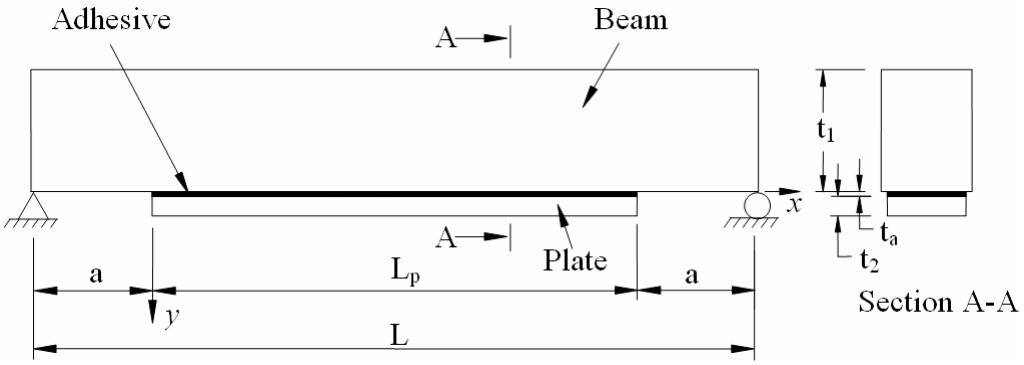

Figure 2.1. A plated beam

All the analytical solutions available to date are applicable only to linear elastic materials. Most also adopt an important assumption of constant interfacial stresses through the thickness of the adhesive layer. This assumption helps in deriving relatively simple closed form solutions.

Two different approaches have been used in developing the existing solutions, namely the deformation compatibility approach and the staged analysis approach. Smith and Teng (2001), Vilnay (1988), Liu and Zhu (1994), Taljsten (1997) and Malek et al. (1998) and almost all solutions developed after 2001 (e.g. Stratford and Cadei, 2006; Yang and Wu, 2007; Xu and Wu, 2009; Yang et al., 2009) considered the deformation compatibility between the beam and the bonded plate while Roberts (1989) and Roberts and Haji-Kazemi (1989) used a staged analysis approach to derive the interfacial stresses. A review by Smith and Teng (2001) suggests that the deformation compatibility approach which enforce the interaction of the beam and the plate during deformation is more advantageous compared to the staged analysis approach which allows deformation of the adherends without interaction.

Under loading a plated beam experiences bending, axial and shear deformations of both adherends. Solutions differ in the extent to which they account for axial, bending and shear deformations in either the beam, in the bonded plate or in both. All existing solutions take account of the bending deformation in the beam and axial deformation in the bonded plate in determining the interfacial shear stress. The effects of axial deformation in the beam and the bending deformation in the plate are considered in the solutions of Roberts (1989), Roberts and Haji-Kazemi (1989), Malek et al. (1998) and Smith and Teng (2001) and ignored in other solutions such as Vilnay (1998) and Liu and Zhu (1994) in deriving the interfacial shear stress. Taljsten (1997) included axial deformation of the beam and ignored the bending deformation of the plate in finding the interfacial shear stress. In obtaining the interfacial normal stress, the effect of bending deformation in the beam is accounted in a few solutions such as Smith and Teng (2001), Liu and Zhu (1994), Taljsten (1997) and Malek et al. (1998) and ignored in other solutions such as Vilnay (1998), Roberts (1989) and Roberts and Haji-Kazemi (1989). Many of the existing solutions were specifically developed for RC beams bonded with a thin plate in which case the bending stiffness of the plate may be neglected in deriving both the interfacial shear and normal stresses. Solutions ignoring the bending deformation in the beam in determining the interfacial normal stress are found (Smith and Teng, 2001) to be unsuitable for plated beams when the flexural rigidity of the beam and the bonded plate are more comparable.

Smith and Teng (2001) considered the shear deformation of the adherends within the governing differential equations but neglected it when deriving the general solutions.

This is recently solved by Yang and Wu (2007) based on a superposition technique as a sum of Smith and Teng's (2001) solution and an additional part which considers the shear deformation effect and represented by a series solution. Liu and Zhu (1994) considered the effect of shear deformation of the beam within the general solution of interfacial shear stress but neglected it in the governing equation of interfacial normal stress. This solution is found to be incomplete in the sense that the constants of integration in the general solution of interfacial shear stress are not evaluated although the boundary conditions are specified. Abdelouahed (2006) included the effect of adherend shear deformations by assuming a linear shear stress variation through the thickness of the adherends in Smith & Teng's (2001) solution. However, the shear deformation is considered only in predicting the interfacial shear stress. The effect of the shear deformations of the adherends is neglected in all other solutions including the present one as it is believed to be insignificant for practical beams.

Many of these solutions were specifically developed for plated beams under a specific kind of loading. Smith and Teng (2001) provided specific interfacial stress expressions applicable for three load cases: an arbitrarily positioned point load, two symmetrically positioned point loads and a UDL. The solution of Malek et al. (1998) is general in loading to an extent provided the external moment is expressed in terms of a quadratic equation with the plate length as the variable. The solution of Vilnay (1988) is applicable only to a single point load at the mid span, Taljsten's (1997) is for an arbitrarily positioned single point load and Roberts and Haji-Kazemi's (1989) solution is limited to a UDL. Roberts' (1989) solution is general in terms of loading but it is based on staged analysis approach intended for thin plated RC beams and is rather complex. Yang et al. (2009) presented a higher order solution for arbitrary symmetrical loading. Stratford and Cadei (2006) developed a classical solution for interfacial shear and normal stresses in a plated beam with varying cross sections based on finite difference method and Xu and Wu (2009) provided a similar solution based on the finite element method but only for the interfacial shear stress.

All simple closed-form solutions do not satisfy the free stress condition that the shear stress at the ends of the adhesive layer and of the plate is equal to zero. Higher order analyses (e.g. Rabinovich and Frostig, 2000; Shen et al., 2001; and Yang et al., 2002, 2004, 2009) are required to satisfy this condition. However, such solutions are very complex. The limitation of the simple closed-form solutions is found to have a very

small effect in a small zone near the end of the plate (Roberts, 1989). This chapter proposes a simple analysis giving a closed-form solution.

This chapter presents a new analytical solution generic in nature for determining the interfacial stresses in simply supported beams bonded with a thin or a thick plate and subjected to any kind of external loading. The solution is based on linear elastic material behaviour which is common to all the existing solutions and is derived considering deformation compatibility between the adherends. The novelty in this solution lies in the application of the superposition principle so that the simple solution is applicable to any arbitrary loading arrangement. Numerical comparison of the new solution is given for three important load cases: a UDL, an arbitrarily positioned point load and a complex loading arrangement. The first two load cases are compared with the solutions of Smith and Teng (2001) and finite element (FE) results. The third load case is compared with FE results only as no analytical solution is available for such a complex loading case.

2.2 Assumptions

The following assumptions are employed in deriving the new solution in this chapter:

a) the beam, adhesive and plate are linear elastic;
b) plane stress conditions are assumed;
c) the shear and normal stresses across the thickness of the adhesive layer are assumed to be constant although the shear stress variation is partially captured within the capability of the composite beam theory;
d) the curvatures of the beam and the plate are assumed to be the same only in determining the interfacial shear stress (this assumption is not used in determining the interfacial normal stress); and
e) compatibility of deformation is considered between the beam and the adhesive and between the plate and the adhesive.

The first four assumptions other than the shear stress variation across the adhesive thickness are common to all the existing solutions while the fifth is common to almost all solutions published after 1990.

2.3 Methodology

Consider a simply supported beam either symmetrically or asymmetrically strengthened with a soffit plate as shown in Figure 2.1. The beam may or may not have an initial loading, but only additional loading applied after plating is considered in the following analysis. This additional loading after plating can be arbitrary (Case-1 in Figure 2.2) which is decomposed into Case-2 and Case-3. Case-2 includes all the external loading plus an axial force and a bending moment at each end of the plate. The magnitude of these axial forces and moments are determined from the deformation of the un-plated beam so that both ends of the plate deform compatibly with the un-plated beam under the external loading and the case can be analysed using the classical composite beam theory. Case-3 is the plated beam under the same but opposite plate end loading as in Case-2. The combined solutions from Cases 2 and 3 give the solution for the original problem in Case-1.

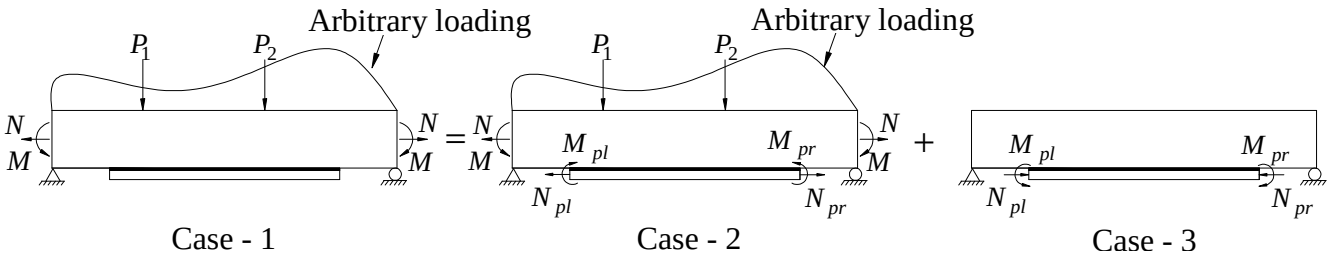

Figure 2.2. Principle of super position in the interfacial stress analysis of plated beam

Let the axial stiffness ratio R_a and bending stiffness ratio R_b of the plate to the beam, and the ratio between the axial stiffness of the plate and the bending stiffness of the beam R_{ab} be

$$R_a = \frac{E_2 A_2}{E_1 A_1};\ R_b = \frac{E_2 I_2}{E_1 I_1};\ R_{ab} = \frac{E_2 A_2}{E_1 I_1} \tag{2.1}$$

The axial force N and bending moment M at the plate ends for the composite beam in Case-2 (Figure 2.2) are given as:

$$N_{pl} = M(0)(y_1 + t_a + y_2)R_{ab} + NR_a \tag{2.2}$$

$$N_{pr} = M(L_p)(y_1 + t_a + y_2)R_{ab} + NR_a \tag{2.3}$$

$$M_{pl} = M(0)R_b \tag{2.4}$$

$$M_{pr} = M(L_p)R_b \tag{2.5}$$

where y_1 and y_2 are the distances from the bottom of adherend-1 (the original beam) and the top of adherend-2 (the plate) to their respective centroids (as shown in Figure 2.4); subscripts *pl* and *pr* refer respectively to the left and right plate ends; subscripts 1, 2 and *a* respectively refer to adherend-1, adherend-2 and adhesive; *M(0)* and $M(L_p)$ denote the bending moment at $x=0$ and $x=L_p$ respectively on the beam under the original loading; and *E, A, I, b* and *t* refer to the elastic modulus, cross sectional area, second moment of area about the centroid of the concerned adherend (i.e. beam or plate), breadth and thickness (or depth) respectively.

2.4 Solution for the Composite Beam (Case-2)

The interfacial stress in Case-2 can be obtained using the classical composite beam theory. The equivalent second moment of area of the composite beam section is given by

$$I_e = I_{1c} + I_{ac} + I_{2c} \tag{2.6}$$

where I_{1c}, I_{ac} and I_{2c} are the equivalent second moment of area of the original beam, adhesive and plate sections respectively about the centroid of the composite beam section. They can be explicitly written as

$$I_{1c} = I_1 + A_1\left[y_c - (t_1 - y_1)\right]^2 \tag{2.7}$$

$$I_{ac} = \left[\frac{b_a t_a{}^3}{12} + b_a t_a (t_1 + 0.5t_a - y_c)^2\right] R_{ma} \tag{2.8}$$

$$I_{2c} = \left[\frac{b_2 t_2{}^3}{12} + b_2 t_2 (t_1 + t_a + y_2 - y_c)^2\right] R_{m2} \tag{2.9}$$

in which y_c is the distance of the centroid of the composite beam section from the top surface

$$y_c = \frac{A_1(t_1 - y_1) + R_{ma} b_a t_a (t_1 + 0.5t_a) + R_{m2} b_2 t_2 (t_1 + t_a + y_2)}{A_1 + R_{ma} b_a t_a + R_{m2} b_2 t_2} \tag{2.10}$$

where the modular ratios R_{ma} and R_{m2} are given as

$$R_{ma} = \frac{E_a}{E_1};\ R_{m2} = \frac{E_2}{E_1} \tag{2.11}$$

Considering a point in the adhesive layer with *y* distance from bottom of the beam to adhesive interface (so *y* ranges from 0 to t_a within the adhesive), the first moment of

area of the equivalent plate and adhesive section below the considered position about the centroid of the composite beam section is given by

$$Q_e(y) = R_{m2} b_2 t_2 [t_1 + t_a + y_2 - y_c] + R_{ma} b_2 (t_a - y)[t_1 + 0.5(t_a + y) - y_c] \quad (2.12)$$

The shear stress at the considered position within the adhesive layer is thus

$$\tau(x, y) = m_c(y) V_{Tc}(x) \quad (2.13)$$

where $V_{Tc}(x)$ is the total shear force on the composite beam section at a distance of x from the plate end due to all the loading in Case-2 (including the contribution from plate end loadings) and

$$m_c(y) = \frac{Q_e(y)}{I_e b_2} \quad (2.14)$$

The interfacial normal stress from this theory is zero, $\sigma(x) \approx 0$.

2.5 Governing Differential Equations and General Solutions for Case-3

The governing differential equations and general solutions for the interfacial shear and normal stresses between the adherends of the plated beam shown in Case-3 (Figure 2.2) are derived in this section.

2.5.1 Interfacial shear stress

The moment in the beam and that in the plate can be related assuming equal curvatures in both of them. This gives

$$R_b M_1(x) = M_2(x) \quad (2.15)$$

Longitudinal equilibrium of a differential segment of the plated beam as shown in Figure 2.3 gives

$$-\frac{dN_1(x)}{dx} = b_2 \tau(x) = \frac{dN_2(x)}{dx} \quad (2.16)$$

$$N_{pl} - N_{pr} - N_1(x) = b_2 \int_0^x \tau(x) dx = N_2(x) + N_{pl} \quad (2.17)$$

where $\tau(x)$ is the interfacial shear stress between the adherends. Eq. 2.17 is obtained from axial equilibrium of the left part of the structure shown in Figure 2.4.

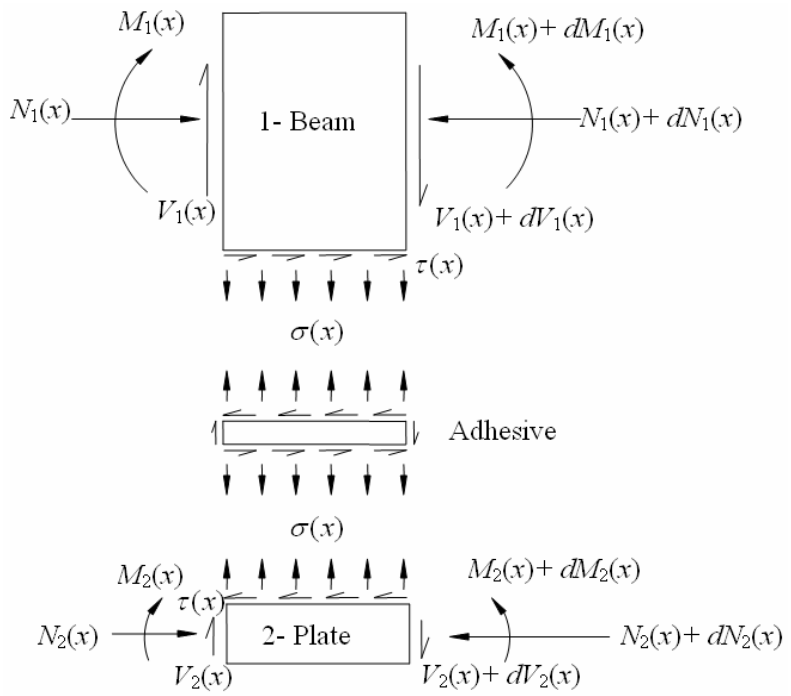

Figure 2.3. Differential segment of a plated beam

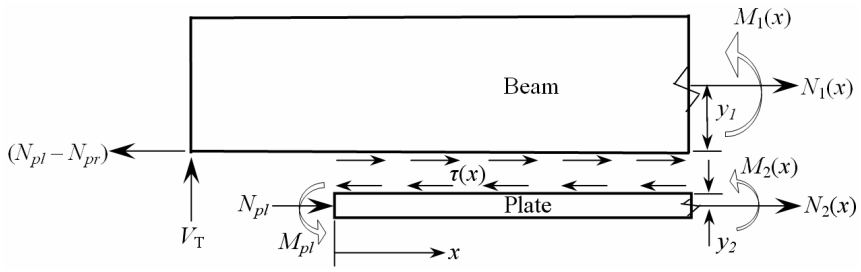

Figure 2.4. Free body diagram of the left segment of the plated beam

Assuming that the beam is on a pinned support at the left and roller support on the right as shown in Figure 2.2, the total shear force at any section of the plated beam $V_T(x)$ can be expressed in terms of the plate end loadings as

$$V_T(x) = \frac{1}{L}\left[M_{pl} - M_{pr} + (N_{pl} - N_{pr})(t_a + y_2)\right] = V_T \tag{2.18}$$

The total applied moment at any section of the plated beam $M_T(x)$ can be related to the moment and axial force on each of the adherend as

$$M_T(x) = M_1(x) + M_2(x) + N_2(x)[t_1 + t_a + y_2 - y_c] - N_1(x)[y_c - (t_1 - y_1)] \tag{2.19}$$

From Eqs 2.15 and 2.19 the bending moment in each adherend can be found as

$$M_i(x) = \left(\frac{E_i I_i}{E_1 I_1 + E_2 I_2} \right) \left(M_T(x) - N_2(x)[t_1 + t_a + y_2 - y_c] + N_1(x)[y_c - (t_1 - y_1)] \right) \qquad (2.20)$$

where subscript i = 1, 2 refer respectively to adherend-1 and adherend-2.

Substituting Eq. 2.16 into the first derivative of Eq. 2.20 gives the following relationship between the bending moments in each adherend with the total shear force:

$$\frac{dM_i(x)}{dx} = \left(\frac{E_i I_i}{E_1 I_1 + E_2 I_2} \right) \left(V_T(x) - b_2 [y_1 + t_a + y_2] \tau(x) \right); \qquad i = 1, 2 \qquad (2.21)$$

The longitudinal strain at the bottom of adherend-1 $\varepsilon_1(x)$ and at the top of adherend-2 $\varepsilon_2(x)$ are

$$\varepsilon_i(x) = \frac{du_i(x)}{dx} = (-1)^{i+1} \frac{y_i}{E_i I_i} M_i(x) + \frac{1}{E_i A_i} N_i(x); \qquad i = 1, 2 \qquad (2.22)$$

Based on the theory of elasticity, the shear stress in the adhesive layer can be found from

$$\tau(x) = G_a \left(\frac{du(x,y)}{dy} + \frac{dv(x,y)}{dx} \right) \qquad (2.23)$$

where G_a is the shear modulus of adhesive and $u(x,y)$ and $v(x,y)$ are the horizontal and vertical displacement in the adhesive layer.

The first derivative of Eq. 2.23 with respect to x is

$$\frac{d\tau(x)}{dx} = G_a \left(\frac{d^2 u(x,y)}{dxdy} + \frac{d^2 v(x,y)}{dx^2} \right) \qquad (2.24)$$

The moment-curvature relation for a differential segment of the plated beam gives

$$\frac{d^2 v(x,y)}{dx^2} = -\frac{1}{E_1 I_e} M_T(x) \qquad (2.25)$$

Assuming that the shear stress is uniform through the thickness of the adhesive layer in Case-3, $u(x,y)$ varies linearly across t_a, so

$$\frac{du(x,y)}{dy} = \frac{1}{t_a} [u_2(x) - u_1(x)] \qquad (2.26)$$

The first derivative of the above equation with respect to x is given by

$$\frac{d^2 u(x,y)}{dxdy} = \frac{1}{t_a} \left(\frac{du_2(x)}{dx} - \frac{du_1(x)}{dx} \right) \qquad (2.27)$$

Substituting Eqs 2.25 and 2.27 into Eq. 2.24 gives

$$\frac{d\tau(x)}{dx} = \frac{G_a}{t_a}\left(\frac{du_2(x)}{dx} - \frac{du_1(x)}{dx}\right) - \frac{G_a}{E_1 I_e} M_T(x) \tag{2.28}$$

The third term on the right side in Eq. 2.28 is not considered in previous solutions to avoid complexity in the solution. This term is usually very small. Very small differences are found in the results between the new solution and Smith & Teng (2001) due to the inclusion of the above term.

Substituting Eqs 2.19 and 2.22 into Eq. 2.28 yields

$$\frac{d\tau(x)}{dx} = \frac{G_a}{E_1}\left[-r_1 M_1(x) - r_2 M_2(x) - r_3 N_1(x) + r_4 N_2(x)\right] \tag{2.29}$$

where

$$r_1 = \left[\frac{y_1}{t_a I_1} + \frac{1}{I_e}\right] \tag{2.29a}$$

$$r_2 = \left[\frac{y_2}{t_a R_{m2} I_2} + \frac{1}{I_e}\right] \tag{2.29b}$$

$$r_3 = \left[\frac{1}{t_a A_1} - \frac{(y_c - t_1 + y_1)}{I_e}\right] \tag{2.29c}$$

$$r_4 = \left[\frac{1}{t_a R_{m2} A_2} - \frac{(t_1 + t_a + y_2 - y_c)}{I_e}\right] \tag{2.29d}$$

Differentiating Eq. 2.29 once with respect *x* and substituting Eqs 2.16 and 2.21 into the resulting expression results in the following governing differential equation for the interfacial shear stress:

$$\frac{d^2\tau(x)}{dx^2} - \lambda^2 \tau(x) + m_1 \lambda^2 V_T(x) = 0 \tag{2.30}$$

where

$$\lambda^2 = \frac{G_a b_2}{t_a}\left[\frac{(y_1 + y_2)(y_1 + t_a + y_2)}{(E_1 I_1 + E_2 I_2)} + \frac{1}{E_1 A_1} + \frac{1}{E_2 A_2}\right] \tag{2.30a}$$

$$m_1 = \frac{G_a}{\lambda^2}\left[\frac{y_1 + y_2}{t_a (E_1 I_1 + E_2 I_2)} + \frac{1}{E_1 I_e}\right] \tag{2.30b}$$

Note that the expression for m_1 has the additional second term compared with Smith and Teng (2001). The general solution of the second order non-homogeneous differential equation (Eq. 2.30) is:

$$\tau(x) = B_1 \cosh(\lambda x) + B_2 \sinh(\lambda x) + m_1 V_T \tag{2.31}$$

where B_1 and B_2 are constants of integration to be determined from appropriate boundary conditions.

The boundary conditions available in Case-3 are:

$$M_1(x)\big|_{x=0} = \frac{a}{L}\left[M_{pl} - M_{pr} + (N_{pl} - N_{pr})\left(\frac{L}{a} y_1 + y_2 + t_a\right)\right] = M_1(0) \tag{2.32a}$$

$$M_2(x)\big|_{x=0} = -M_{pl} \tag{2.32b}$$

$$N_1(x)\big|_{x=0} = N_{pl} - N_{pr} \tag{2.32c}$$

$$N_2(x)\big|_{x=0} = -N_{pl} \tag{2.32d}$$

$$M_1(x)\big|_{x=L_p} = -\frac{a}{L}\left(M_{pl} - M_{pr} + (N_{pl} - N_{pr})(y_2 + t_a)\right) = M_1(L_p) \tag{2.32e}$$

$$M_2(x)\big|_{x=L_p} = -M_{pr} \tag{2.32f}$$

$$N_1(x)\big|_{x=L_p} = 0 \tag{2.32g}$$

$$N_2(x)\big|_{x=L_p} = -N_{pr} \tag{2.32h}$$

$$V_2(x)\big|_{x=0} = 0 \text{ ; hence, } V_1(x)\big|_{x=0} = V_T - b_2 t_a \tau(x)\big|_{x=0} \tag{2.32i}$$

Applying Eqs 2.32a-d to Eq. 2.29 gives

$$\left.\frac{d\tau(x)}{dx}\right|_{x=0} = \frac{G_a}{E_1}\left(-r_1 M_1(0) + r_2 M_{pl} - (r_3 + r_4) N_{pl} + r_3 N_{pr}\right) \tag{2.33}$$

The first derivative of Eq. 2.31 with respect to x at x=0 is

$$\left.\frac{d\tau(x)}{dx}\right|_{x=0} = B_2 \lambda \tag{2.34}$$

From Eqs 2.33 and 2.34,

$$B_2 = \frac{G_a}{E_1 \lambda}\left(-r_1 M_1(0) + r_2 M_{pl} - (r_3 + r_4) N_{pl} + r_3 N_{pr}\right) \tag{2.35}$$

Applying Eqs 2.32e-h to Eq. 2.29 gives

$$\left.\frac{d\tau(x)}{dx}\right|_{x=L_p} = \frac{G_a}{E_1}\left(-r_1 M_1(L_p) + r_2 M_{pr} - r_4 N_{pr}\right) \tag{2.36}$$

The first derivative of Eq. 2.31 with respect to x at $x=L_p$ is

$$\left.\frac{d\tau(x)}{dx}\right|_{x=L_p} = \lambda[B_1 \sinh(\lambda L_p) + B_2 \cosh(\lambda L_p)] \tag{2.37}$$

From Eqs 2.36 and 2.37,

$$B_1 = -\frac{B_2}{\tanh(\lambda L_p)} + \frac{G_a}{E_1 \lambda \sinh(\lambda L_p)}\left(-r_1 M_1(L_p) + r_2 M_{pr} - r_4 N_{pr}\right) \tag{2.38}$$

It is found that λL_p is generally greater than 10 for practical cases. Hence, $\tanh(\lambda L_p) \approx 1$ and $[1/\sinh(\lambda L_p)] \approx 0$. So the second term in Eq. 2.38 is negligible and it reduces to

$$B_1 = -B_2 \tag{2.39}$$

2.5.2 Interfacial normal stress

The interfacial normal stress exists between the adherends due to their differential vertical displacement when the beam is loaded. If the vertical displacements of the adherends 1 and 2 are respectively $v_1(x)$ and $v_2(x)$, the interfacial normal stress, $\sigma(x)$ can be found from

$$\sigma(x) = \frac{E_a}{t_a}[v_2(x) - v_1(x)] \tag{2.40}$$

The moment-curvature relation, moment and vertical equilibrium consideration of the differential segment of adherends 1 and 2 (Figure 2.3) give

$$\frac{d^2 v_i(x)}{dx^2} = -\frac{1}{E_i I_i} M_i(x); \qquad i = 1, 2 \tag{2.41}$$

$$\frac{dM_i(x)}{dx} = V_i(x) - b_2 y_i \tau(x); \qquad i = 1, 2 \tag{2.42}$$

$$\frac{dV_i(x)}{dx} = (-1)^i b_2 \sigma(x); \qquad i = 1, 2 \tag{2.43}$$

Differentiating Eq. 2.41 once and substituting Eq. 2.42 into the resulting equation gives

$$\frac{d^3 v_i(x)}{dx^3} = -\frac{1}{E_i I_i}[V_i(x) - b_2 y_i \tau(x)]; \quad i = 1, 2 \tag{2.44}$$

Differentiating Eq. 2.44 once and substituting Eq. 2.43 into the resulting equation gives

$$\frac{d^4 v_i(x)}{dx^4} = (-1)^{i+1} \frac{b_2}{E_i I_i} \sigma(x) + \frac{b_2 y_i}{E_i I_i} \frac{d\tau(x)}{dx}; \quad i = 1, 2 \tag{2.45}$$

Differentiating Eq. 2.40 four times with respect to *x* and substituting Eq. 2.45 into the resulting equation yields the following governing differential equation for the interfacial normal stress:

$$\frac{d^4\sigma(x)}{dx^4} + (4\beta^4)\sigma(x) + (4\beta^4)n_1\frac{d\tau(x)}{dx} = 0 \tag{2.46}$$

where

$$\beta = \left[\frac{E_a b_2}{4t_a}\left(\frac{1}{E_1 I_1} + \frac{1}{E_2 I_2}\right)\right]^{\left(\frac{1}{4}\right)} \tag{2.46a}$$

$$n_1 = \left(\frac{y_1 E_2 I_2 - y_2 E_1 I_1}{E_1 I_1 + E_2 I_2}\right) \tag{2.46b}$$

The general solution to the fourth order non-homogeneous differential equation (Eq. 2.46) is:

$$\sigma(x) = e^{-\beta x}\left[C_1\cos(\beta x) + C_2\sin(\beta x)\right] + e^{\beta x}\left[C_3\cos(\beta x) + C_4\sin(\beta x)\right] - n_1\frac{d\tau(x)}{dx} \tag{2.47}$$

where C_1 to C_4 are constants of integration.

As $\sigma(x) \to 0$ for large values of *x*, $C_3 = C_4 = 0$. Hence, Eq. 2.47 reduces to

$$\sigma(x) = e^{-\beta x}\left[C_1\cos(\beta x) + C_2\sin(\beta x)\right] - n_1\frac{d\tau(x)}{dx} \tag{2.48}$$

Using Eqs 2.31 and 2.39, Eq. 2.48 can also be written as

$$\sigma(x) = e^{-\beta x}\left[C_1\cos(\beta x) + C_2\sin(\beta x)\right] - B_1 n_1\lambda\left[\sinh(\lambda x) - \cosh(\lambda x)\right] \tag{2.49}$$

The constants C_1 and C_2 can be determined from appropriate boundary conditions listed in Eq. 2.32. Differentiating Eq. 2.40 twice with respect to *x*, substituting Eq. 2.41 into the resulting expression and then applying the boundary conditions of Eqs 2.32a and 2.32e gives

$$\left.\frac{d^2\sigma(x)}{dx^2}\right|_{x=0} = \frac{E_a}{t_a E_2 I_2}\left[R_b M_1(0) + M_{pl}\right] \tag{2.50}$$

Differentiating Eq. 2.49 twice with respect to *x* and substituting *x*=0 into the resulting equation gives

$$\left.\frac{d^2\sigma(x)}{dx^2}\right|_{x=0} = B_1 n_1 \lambda^3 - 2\beta^2 C_2 \tag{2.51}$$

From Eqs 2.50 and 2.51,

$$C_2 = \frac{B_1 n_1 \lambda^3}{2\beta^2} - \frac{E_a}{2\beta^2 t_a E_2 I_2}\left[R_b M_1(0) + M_{pl}\right] \tag{2.52}$$

Differentiating Eq. 2.40 thrice with respect to *x*, substituting Eq. 2.44 into the resulting expression and then applying the boundary condition of Eq. 2.32i gives

$$\left.\frac{d^3\sigma(x)}{dx^3}\right|_{x=0} = \frac{E_a}{t_a E_1 I_1} V_T - n_2 \tau(0) \tag{2.53}$$

where

$$n_2 = \frac{E_a b_2}{t_a}\left(\frac{y_1 + t_a}{E_1 I_1} - \frac{y_2}{E_2 I_2}\right) \tag{2.53a}$$

Differentiating Eq. 2.49 three times with respect to *x* and setting *x*=0 gives

$$\left.\frac{d^3\sigma(x)}{dx^3}\right|_{x=0} = 2\beta^3\left[C_1 + C_2\right] - B_1 n_1 \lambda^4 \tag{2.54}$$

C_1 is obtained from Eqs 2.52 – 2.54 as

$$C_1 = \frac{E_a}{2\beta^3 t_a E_2 I_2}\left[R_b\left(V_T + \beta M_1(0)\right) + \beta M_{pl}\right] - \frac{n_2}{2\beta^3}\tau(0) + \frac{B_1 n_1 \lambda^3}{2\beta^3}(\lambda - \beta) \tag{2.55}$$

2.6 Solution for General Loading (Case-1)

The solutions from Case-2 and 3 are combined to give the solution for the original problem in Case-1. The interfacial shear stress is given by

$$\tau(x, y) = m_c(y) V_{Tc}(x) + B_1\left[\cosh(\lambda x) - \sinh(\lambda x)\right] + m_1 V_T \tag{2.56}$$

where $m_c(y), B_1, \lambda, m_1$ and V_T are respectively given by Eqs 2.14, 2.39, 2.30a-b and 2.18.

The interfacial normal stress is given by Eq. 2.49 where β, n_1, C_1 and C_2 are respectively given by Eqs 2.46a-b, 2.55 and 2.52. It may be noted that $M_1(0) = M_1(L_p) = V_T = 0$ when the external loading is symmetrical on the plated beam which yields simple expressions for interfacial shear stress and constants of integration.

2.7 Validation of New Analytical Solution

The general analytical solution derived above is validated in this section by considering three example plated beams under different loadings (Figure 2.5). Plated beam-1 is an RC beam of rectangular cross section bonded with a thin glass-fibre-reinforced polymer (GFRP) plate at the soffit and subjected to an uniformly distributed load, plated beam-2 is a rectangular hollow section aluminium beam bonded with a thin carbon-fibre-reinforced polymer (CFRP) soffit plate and subjected to a single point load near the left support and plated beam-3 is a I-section steel beam bonded at the soffit with a thick CFRP plate and subjected to a complex loading arrangement. The geometric and material properties of these example beams are provided in Table 2.1 and Figure 2.5.

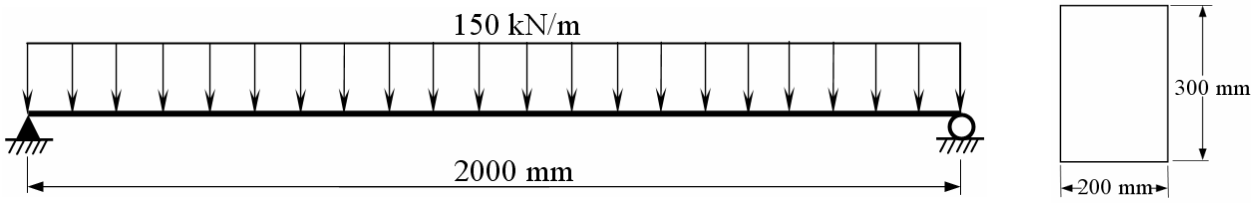

(a) GFRP plated rectangular RC beam under UDL

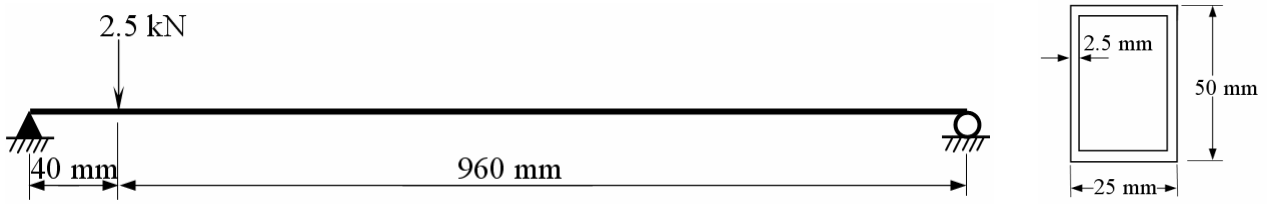

(b) CFRP plated rectangular hollow section aluminium beam under single offset point load

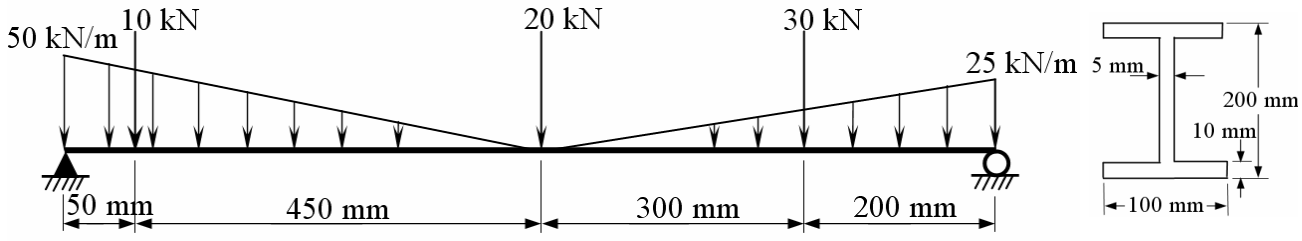

(c) CFRP plated I-section steel beam under complex loading

Figure 2.5. Example plated beams

Table 2.1: Geometric and material properties of example plated beams

Example plated beam	Component	Width (mm)	Depth (mm)	Length (mm)	Elastic Modulus (GPa)	Poisson's ratio
1	RC beam	$b_1 = 200$	$t_1 = 300$	$L_1 = 2000$	$E_1 = 30$	$\upsilon_1 = 0.17$
	Adhesive layer	$b_a = 200$	$t_a = 2.0$	$L_a = 1600$	$E_a = 2$	$\upsilon_a = 0.35$
	GFRP plate	$b_2 = 200$	$t_2 = 5.0$	$L_2 = 1600$	$E_2 = 50$	$\upsilon_2 = 0.30$
2	AL beam	$b_1 = 25$	$t_1 = 50$	$L_1 = 1000$	$E_1 = 65.3$	$\upsilon_1 = 0.28$
	Adhesive layer	$b_a = 25$	$t_a = 1.0$	$L_a = 860$	$E_a = 2$	$\upsilon_a = 0.35$
	CFRP plate	$b_2 = 25$	$t_2 = 2.0$	$L_2 = 860$	$E_2 = 100$	$\upsilon_2 = 0.35$
3	Steel beam	$b_1 = 100$	$t_1 = 200$	$L_1 = 1000$	$E_1 = 200$	$\upsilon_1 = 0.30$
	Adhesive layer	$b_a = 100$	$t_a = 2.0$	$L_a = 850$	$E_a = 2$	$\upsilon_a = 0.35$
	CFRP plate	$b_2 = 100$	$t_2 = 20.0$	$L_2 = 850$	$E_2 = 100$	$\upsilon_2 = 0.35$

The interfacial shear and normal stresses are determined for all the example plated beams. The results of the new solution for the first two plated beams are compared with the analytical solution of Smith and Teng (2001) as well as with finite element (FE) predictions (Figures 2.6 and 2.7) while the third one is compared with FE predictions only (Figure 2.8) as no other analytical solution is available for this complex loading arrangement. Numerical analysis of these example beams show that the interfacial stresses near the plate end is dominated by the effect due to the termination of the plate (i.e. the solution from Case 3). Away from the plate end, these stresses are dominated by the simple composite beam action (i.e. the solution from Case 2), while the solution from Case 3 contributes little.

All the FE analyses presented here were conducted using ANSYS 10.0 (2005). The plated beam was modelled as a plane stress problem. Four node quadrilateral plane stress elements were used in modelling the beam, plate and adhesive layer. The FE results shown in this paper were obtained for a fine mesh with an element size of 0.1mm at the plate and the adhesive near the plate end, the same as the finest mesh adopted in Teng et al. (2002b). The mesh was graded in the horizontal direction starting with an aspect ratio of 1 for the elements at the plate end to obtain reasonably accurate stresses. It should be noted that stress singularities exist at the two bi-material interfaces, i.e. at the beam-adhesive interface (BA interface) and the plate and the adhesive interface (PA interface) at the plate ends (Hein and Erdogan, 1971; Teng et al., 2002b; Chen et al., 2001). The magnitude of the stresses near the stress singularities will always increase as the element size is reduced. Therefore, a fully converged solution can never be obtained in a finite element analysis. However, the stress singularity effects are only confined to

within a couple of millimetres near the plate end for the adopted mesh (Teng et al., 2002b; Chen et al., 2001).

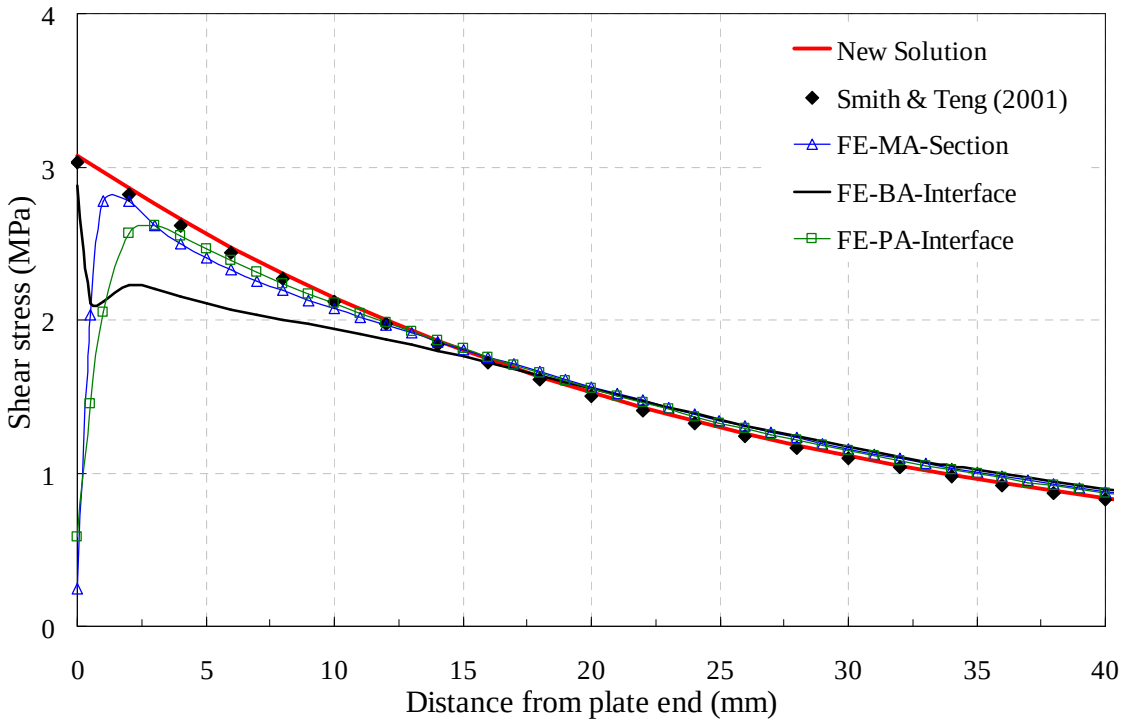

(a) Interfacial shear stress

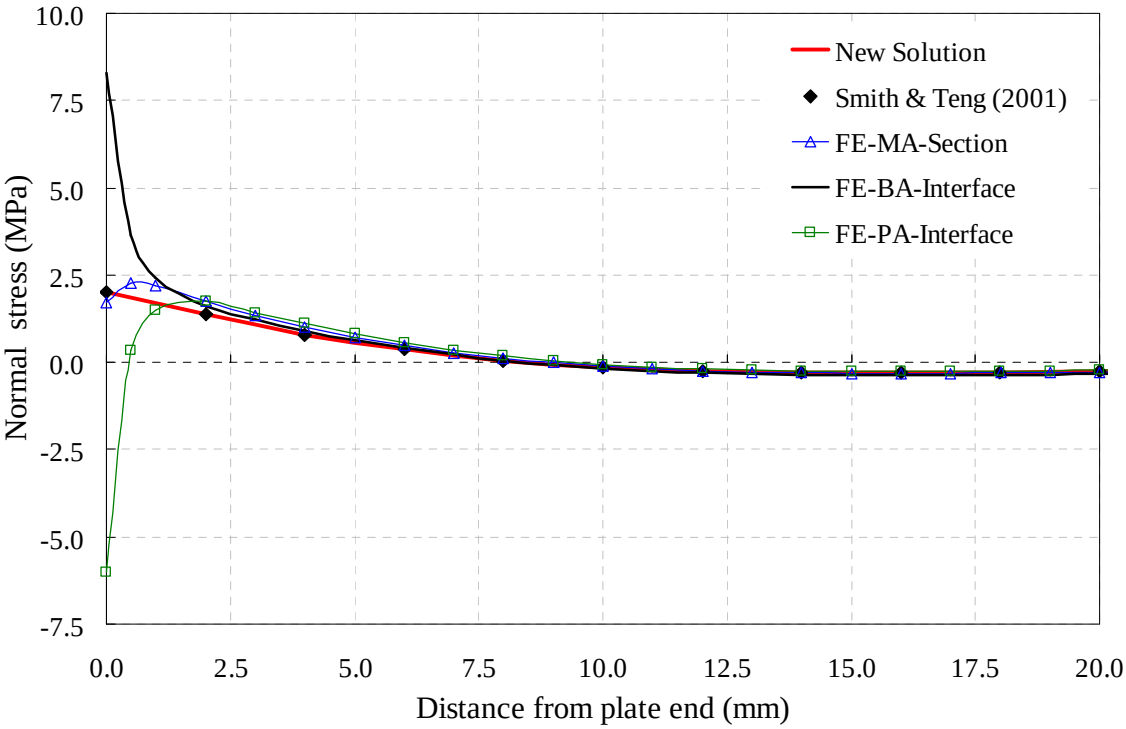

(b) Interfacial normal stress

Figure 2.6. Comparison between analytical and FE predictions of interfacial stresses in a GFRP plated RC beam (solid rectangular section) subjected to an UDL

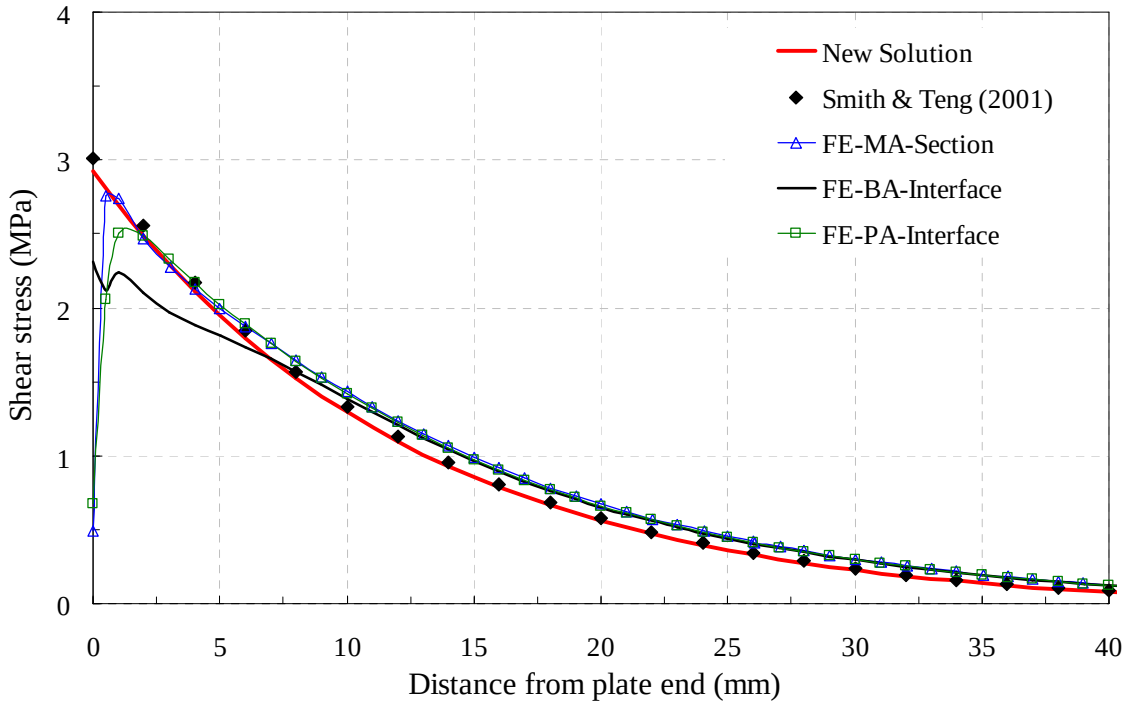

(a) Interfacial shear stress

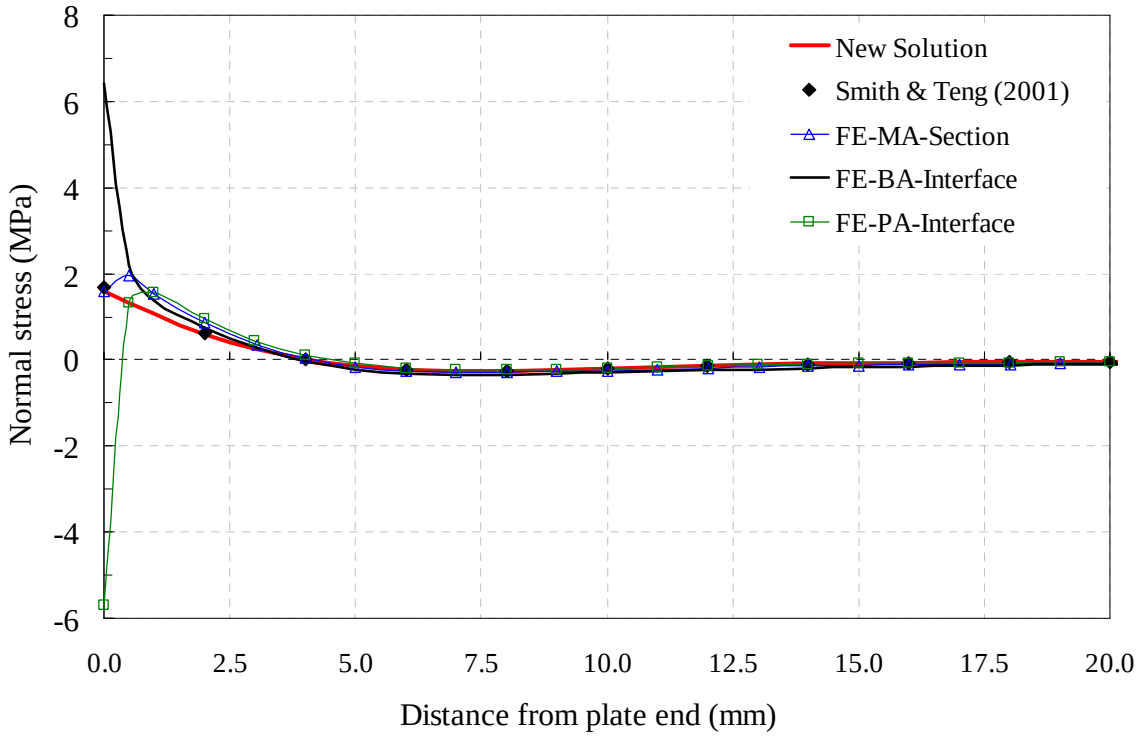

(b) Interfacial normal stress

Figure 2.7. Comparison between analytical and FE predictions for interfacial stresses in a CFRP plated rectangular hollow section aluminium beam subjected to a single point offset load

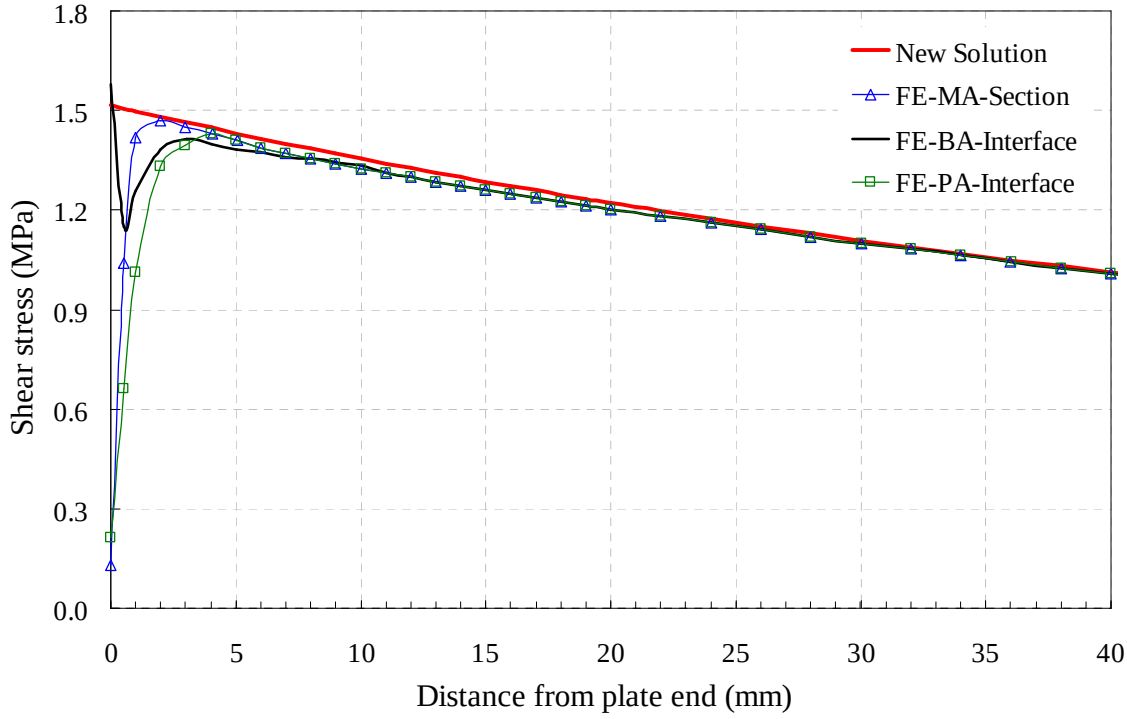

(a) Interfacial shear stress

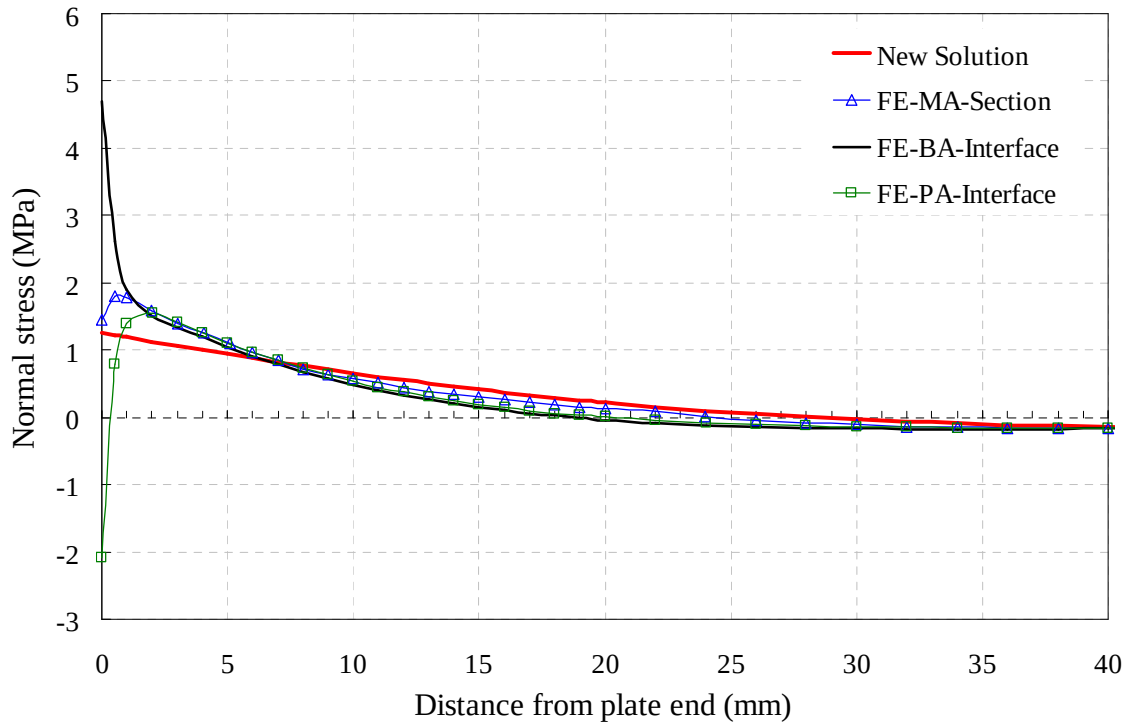

(b) Interfacial normal stress

Figure 2.8. Comparison between new analytical solution and FE predictions for interfacial stresses in a CFRP plated I-section steel beam subjected to complex loading

Table 2.2: Maximum interfacial shear and normal stresses at the plate end, MPa

Example plated beam	New solution		Smith & Teng (2001)		Finite element results					
					BA Interface		MA Section		PA Interface	
	$\tau(x)$	$\sigma(x)$	$\tau(x)$	$\sigma(x)$	$\tau(x)$	$\sigma(x)$	$\tau(x)$	$\sigma(x)$	$\tau(x)$	$\sigma(x)$
1	3.075	2.025	3.028	2.018	2.881	8.286	0.246	1.722	0.582	- 6.027
2	2.923	1.648	3.007	1.675	2.313	6.422	0.488	1.578	0.678	- 5.683
3	1.515	1.256	-	-	1.578	4.694	0.129	1.459	0.211	- 2.091

The interfacial stresses near the plate end predicted by Smith and Teng's (2001) solution, the present solution and the finite element method are shown in Figures 2.6-2.8 for the three example plated beams. It may be noted that uniform shear and normal stress distribution is assumed in Smith & Teng's (2001) and other simple solutions. This assumption is largely retained in the present solution: the variation of the shear stress across the thickness of the adhesive layer is partially considered based on the composite beam theory but the variation arisen from this consideration is found to be negligible near the plate end for the three example beams (less than 0.5%). Therefore, only the prediction at the beam-adhesive interface (BA interface) is shown in Figures 2.6-2.8 for the present solution. Because the beam was modelled as a plane stress problem in the FE analysis, the stress variation across the adhesive thickness was properly modelled. To show such variation, the FE results are plotted in Figures 2.6-2.8 at three horizontal sections in the adhesive layer, namely, BA interface, PA interface and the mid thickness of the adhesive (MA section). The predicted maximum interfacial shear and normal stresses at the plate end are listed in Table 2.2.

Figures 2.6 and 2.7 show that the predictions from the new solution are in very close agreement with those from Smith and Teng's (2001) solution for the example plated concrete beam and the example plated aluminium beam, validating the present solution. Figures 2.6-2.8 show that the present solution match closely with the FE predictions at the MA section except within about 2 mm from the plate end for all the three example beams.

The FE predictions show that the interfacial normal and shear stresses along the BA interface and the interfacial normal stress along the PA interface are very high at the plate end resulting from stress singularity as discussed above. The normal stress at the plate end is tensile at the BA interface but compressive at the PA interface, showing a very complex local stress state there. The effect of the singularity is also more

pronounced on the stresses at the BA interface than the PA interface. Except at the BA interface, the shear stress along the vertical edge of the plate end approaches zero as the mesh is refined, satisfying the free stress condition there.

It should be noted that an exact match between the results of the simple analytical solutions (both the present solution and Smith and Teng's, 2001 solution) and the FE predictions presented in this paper is not expected because different assumptions are made in these two types of analyses. In the analytical solutions, both the beam and the plate are treated as beams while the adhesive layer is effectively treated as equivalent springs due to the assumption of constant stress across its thickness. In contrast, the FE analysis presented treats the whole plated beam as a plane stress problem which accurately reflects the actual stress state. The comparison between the FE predictions and those of the analytical solution is thus more about the accuracy of, rather than validating, the present solution. If validation is the purpose of the analysis, both the original beam and the plate should be modelled using beam elements while the adhesive layer should be modelled using spring elements which are consistent with the assumptions in the analytical solution. A comprehensive investigation of the different modelling approaches for the plated beam can be found in Zhang and Teng (2010b).

2.8 Conclusions

Improvement in strength and performance is observed on metallic and RC beams when bonded with a thin plate on their tension face. Interfacial shear and normal stresses are generated between the beam and the plate in such plated beams during service which may influence the plate end debonding failures. A simple closed-form analytical solution based on the principle of superposition has been developed in this chapter to quantify these interfacial stresses. Compared with existing analytical solutions which are mostly applicable only to rectangular beams under specific loadings, the key advantage of the new general solution is that it is applicable for any prismatic beam sections under any type of transverse loading, moments and axial forces.

The new solution is demonstrated to be in close agreement with the well-known Smith and Teng (2001) solution for an example GFRP plated concrete beam under a uniformly distributed load and a CFRP plated rectangular hollow section aluminium beam under

an offset point load. Comparisons between the predictions of the new solution and the more accurate plane stress finite element predictions have also been conducted for three plated beams including a CFRP plated I-section steel beam under a complex loading arrangement. The predictions of the new solution are found to be in good agreement with the finite element predictions at the mid-adhesive section for any loading arrangements.

2.9 Notation

The following symbols are used in this chapter:

A = cross sectional area of the adhesive or adherends;

b = width of the adhesive or adherends;

E = modulus of elasticity of the adhesive or adherends;

G = shear modulus of the adhesive;

I = second moment of area of the adhesive or adherends about their centroidal axis;

I_{1c}, I_{ac}, I_{2c} = second moment of area of beam, adhesive and plate section about the centroidal axis of the composite beam section respectively;

I_e = second moment of area of the equivalent composite beam section about its centroidal axis;

L = length of the adhesive or adherends;

L_p = length of the plate;

M = bending moment in the adherends;

$M(0), M(L_p)$ = bending moment in plated beam at x=0 and x=L_p under original loading ignoring the effects of plate end loading (Case-2);

$M_1(0), M_1(L_p)$ = bending moment in beam at x=0 and x=L_p in Case-3 loading;

$M_T(x)$ = total applied bending moment at any section of the plated beam;

N = axial force in the adherends;

$N(x)$ = resultant axial force resisted by any section of the adherends;

$Q_e(x,y)$ = first moment of area of equivalent adhesive or plate section about the centroidal axis of the composite beam section;

$m_c(y)$, r_1- r_4, m_1, λ, β, n_1 = parameter defined respectively in Eq. 14, 29a-d, 30a-b and 46a-b;

t = thickness/depth of the adhesive or adherends;

u = longitudinal displacement of the adherends;

v = vertical displacement of the adherends;

$V(x)$ = shear force at any section of adherends;

$V_{Tc}(x)$ = total applied shear force at any section of the composite beam in Case-2;

V_T = total shear force at any section of the plated beam in Case-3 loading;

y_c = vertical distance from top of the beam to the centroid of the composite beam section;

y_1, y_2 = vertical distance from bottom of the beam and top of the plate to their respective centroids respectively;

$_{pl,\, pr}$ = subscripts referring respectively to the left and right end of the plate;

$_{1,\, a,\, 2}$ = subscripts referring respectively to the beam, adhesive and plate;

$\sigma(x)$ = interfacial normal stress at any section of the plated beam;

$\tau(x)$ = interfacial shear stress at any section of the plated beam;

γ_{xy} = engineering shear strain at the adhesive layer; and

$\varepsilon_1(x), \varepsilon_2(x)$ = longitudinal strain at bottom layer of beam and at top layer of plate respectively.

Chapter 3

Effect of Shear Deformation on Interfacial Stresses

Abstract

Bonding a fibre reinforced polymer (FRP) composite or metallic plate to the soffit of a reinforced concrete (RC), timber or metallic beam can significantly increase its strength and other aspects of structural performance. These hybrid beams are often found to fail due to premature debonding of the plate from the original beam in a brittle manner. This has led to the development of many analytical solutions over the last two decades to quantify the interfacial shear and normal stresses between the adherends. The adherends are subjected to axial, bending and shear deformations. However, most analytical solutions have neglected the influence of shear deformation of the adherends. For the few solutions which consider this effect in an approximate manner, their applicability is limited to one or two specific load cases. This chapter presents a general analytical solution for the interfacial stresses in plated beams under an arbitrary loading with the shear deformation of the adherends duly considered. The shear stress distribution is assumed to be parabolic through the depth of the adherends in predicting the interfacial shear stress and Timoshenko's beam theory is adopted in predicting interfacial normal stress to account for the shear deformation. The solution is applicable to a beam of arbitrary prismatic cross-section bonded symmetrically or asymmetrically with a thin or thick plate, both having linear elastic material properties. The effect of shear deformation is illustrated through an example beam. The influence of material and geometric parameters of the adherends and adhesive on the interfacial stress concentrations at the plate end is discussed.

3.1 Introduction

Bonding a fibre reinforced polymer (FRP) composite, steel or any other metallic plate to the tension face of a reinforced concrete (RC), timber or metallic beam using an adhesive (Figure 3.1) has found wide applications in structural engineering for retrofitting and rehabilitation of existing structures. The external plate enhances the strength and structural performance of the original beam without disturbing the surrounding environment. Under external loading, tensile force is generated within the bonded plate which is in turn transferred to the original beam through the adhesive layer. This process generates interfacial shear and normal stresses in the adhesive layer. The concentration of interfacial stresses is highest at the plate ends due to the geometric discontinuity at this location. The combination of high interfacial shear and normal stresses at the plate end commonly leads to a debonding failure of the plate from the original beam in a brittle manner well before the full flexural strength of the plated beam is attained.

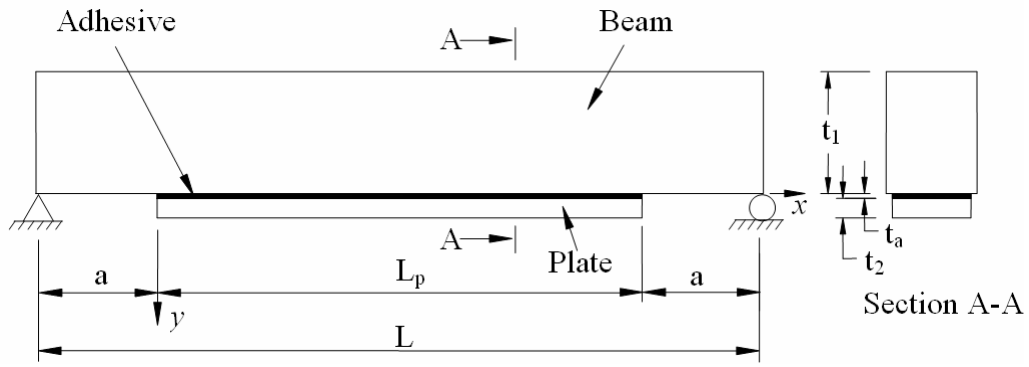

Figure 3.1. Plated beam

Many theoretical solutions (Vilnay, 1988; Roberts, 1989; Roberts and Haji-Kazemi, 1989; Liu and Zhu, 1994; Taljsten, 1997; Malek et al., 1998; Rabinovich and Frostig, 2000; Smith and Teng, 2001; Shen et al., 2001; Deng et al., 2004; Yang et al., 2004, 2009; De Lorenzis et al., 2006; Stratford and Cadei, 2006; Abdelouahed, 2006, 2009; Yang and Wu, 2007; Narayanamurthy et al., 2010; and Zhang and Teng, 2010a) have been developed over the last two decades to quantify the interfacial stresses near the ends of the plate. With the exception of the higher order solutions (Rabinovich and Frostig, 2000; Shen et al., 2001; and Yang et al., 2004, 2009) all classical solutions consider constant interfacial stresses across the thickness of the adhesive layer and

hence violate the free surface condition at the ends of the adhesive layer. Due to its simplicity and accuracy, the solution developed by Smith and Teng (2001) is popular among all the above solutions but is applicable only for uniformly distributed loads (UDL) and single point loads. The solutions of Narayanamurthy et al. (2010) and Zhang and Teng (2010a) retain the advantages of Smith and Teng's solution but are applicable to any loading arrangements, while the latter is applicable even to curved plated beams.

The adherends in a plated beam are usually subjected to axial, bending and shear deformations under external loading. However, most theoretical solutions neglect the effect of shear deformation of the adherends. Liu and Zhu (1994) considered this effect of shear deformation of the beam only in the general solution of interfacial shear stress and provided an incomplete solution without providing the expressions for the constants of integration. Smith and Teng (2001) considered the shear deformation of the adherends within the governing differential equations but neglected it when deriving the general solutions to simplify the solution from the complexities in arriving at the general solutions from the two strongly coupled governing equations. This is recently solved by Yang and Wu (2007) based on a superposition technique as a sum of Smith and Teng's (2001) solution and an additional part which considers the shear deformation effect and represented by a series solution which is complex. Tsai et al. (1998) considered the effect of shear deformation in adhesively bonded double lap joints by assuming a linear shear stress variation through the thickness of the adherends. Abdelouahed (2006) applied Tsai et al.'s (1998) assumption in Smith & Teng's (2001) solution for plated beams. A slightly different function from that used in (2006) in approximating the longitudinal displacement of the adherends was used in Abdelouahed et al. (2009) but its improvement is unclear. It appears that a mistake was made in both Abdelouahed (2006) and Abdelouahed et al. (2009) when comparing the predictions with test results reported in Jones et al. (1988).

From the above review, only three solutions (Abdelouahed, 2006; Yang and Wu, 2007; Abdelouahed et al., 2009) incorporated the effect of shear deformation approximately in the solution of interfacial shear stress in plated beams. No solutions have considered this effect on the interfacial normal stress. It may also be noted that the solutions in Abdelouahed (2006) and Abdelouahed et al. (2009) are only applicable to UDL and two single point loads while that in Yang and Wu (2007) is only applicable to UDL. From these studies, the effect of shear deformation has been found to be considerable for

plates made of FRP composites due to their low shear modulus (Tsai et al., 1998). This effect is also dependent on factors such as the elastic modulus of the adhesive, thickness of the adhesive layer and the plate (Yang and Wu, 2007).

This chapter presents a new solution which includes the effect of the shear deformation of adherends on both interfacial normal and shear stresses. This new solution is based on the principle of superposition and compatibility of longitudinal and transverse deformations between the beam-adhesive and adhesive-plate interfaces for a plane stress condition. The shear and normal stresses through the thickness of the adhesive layer are assumed to be constant although the shear stress variation is captured within the capability of the composite beam theory. In determining the interfacial shear stress, the curvatures of the beam and the plate are assumed to be the same. This solution considers axial, bending and shear deformation in both the original beam and the bonded plate. The effect of the shear deformation of the adherends on the interfacial shear stress is considered by assuming a parabolic variation of shear stress through the depths of the original beam and of the plate. In deriving the solution for interfacial normal stress, the shear deformation in adherends is accounted for in closed form using the Timoshenko's beam theory. Further, the present solution is very general in nature because it is applicable to any beam composed of linear elastic adherends, having arbitrary cross sections, with either a thick or thin plate bonded symmetrically or asymmetrically over the span of the beam, and subject to a general loading arrangement. A comparison of the present solution with other theoretical solutions is given at the end through an illustrative example to highlight the effect of shear deformation in adherends. The influence of material and geometric parameters of the adherends and adhesive on the present solution is also provided through a parametric study that offers other insights.

3.2 Methodology

Consider a simply supported beam symmetrically or asymmetrically strengthened with a soffit plate as shown in Figure 3.1. The plated beam under an arbitrary loading as shown in Case-1 (Figure 3.2) is decomposed into Case-2 and Case-3. Case-2 considers an axial force, shear force and a bending moment at each end of the plate in addition to the external loading. The magnitude of these axial forces, shear forces and moments are

determined from the deformation of the un-plated beam so that both ends of the plate deform compatibly with the un-plated beam under the external loading and the case can be analysed using the classical composite beam theory. Case-3 is the beam having a plate experiencing the same axial forces, shear forces and bending moments at the ends of the plate but in the opposite directions as in Case-2. The combined solution from Cases 2 and 3 gives the solution for the original problem in Case-1.

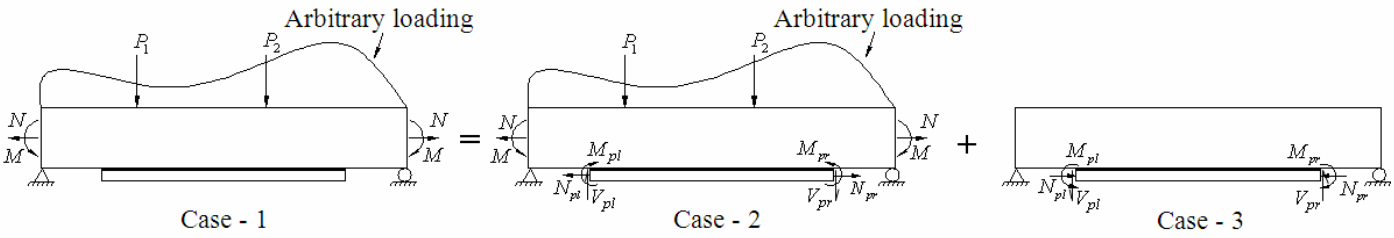

Solution for Case-1 = Solution from (Case- 2 + Case- 3)

Figure 3.2. Principle of superposition in the interfacial stress analysis of plated beam

Let the axial stiffness ratio of the plate to the beam R_a (dimensionless), bending stiffness ratio of the plate to the beam R_b (dimensionless) and the ratio between the axial stiffness of the plate and the bending stiffness of the beam R_{ab} [having dimensions of (1/Length)^2] be given by

$$R_a = \frac{E_2 A_2}{E_1 A_1}; \qquad R_b = \frac{E_2 I_2}{E_1 I_1}; \qquad R_{ab} = \frac{E_2 A_2}{E_1 I_1} \tag{3.1}$$

Let y_1 and y_2 be the distances from the bottom of the adherend-1 (the original beam) and the top of the adherend-2 (the plate) to their respective centroids and y_c be the distance of the centroid of the composite beam section from the top surface. The axial force N, shear force V and bending moment M at the plate ends for the composite beam in Case-2 (Figure 3.2) are thus given as:

$$N_{pl} = M(0)(y_1 + t_a + y_2)R_{ab} + NR_a \tag{3.2}$$

$$N_{pr} = M(L_p)(y_1 + t_a + y_2)R_{ab} + NR_a \tag{3.3}$$

$$V_{pl} = \frac{E_2 b_2 t_2^2 [2t_2 + 3(t_1 + t_a - y_c)]}{6E_1 I_e} V(0) \tag{3.4}$$

$$V_{pr} = \frac{E_2 b_2 t_2^2 [2t_2 + 3(t_1 + t_a - y_c)]}{6E_1 I_e} V(L_p) \tag{3.5}$$

$$M_{pl} = M(0)R_b \tag{3.6}$$

$$M_{pr} = M(L_p)R_b \tag{3.7}$$

where subscripts *pl* and *pr* refer respectively to the left and right plate ends; subscripts 1, 2 and *a* respectively refer to adherends 1 and 2 and the adhesive; $M(0)$, $M(L_p)$, $V(0)$ and $V(L_p)$ denote the bending moments and shear forces at $x=0$ and $x=L_p$ respectively on the beam under the original loading ignoring the plate end loads; and E, A, I, I_e, b and t refer to the elastic modulus, cross sectional area, second moment of area about the centroid of the concerned component (i.e. beam or plate), equivalent second moment of area of the composite beam section, breadth and thickness respectively.

3.3 Solution for the Composite Beam (Case-2)

As noted earlier the interfacial stress in Case-2 can be obtained using the classical composite beam theory. The equivalent second moment of area of the composite beam section is given by

$$I_e = I_{1c} + I_{ac} + I_{2c} \tag{3.8}$$

where I_{1c}, I_{ac} and I_{2c} are the equivalent second moment of area of the original beam, adhesive and plate sections respectively about the centroid of the composite beam section. They can be written as

$$I_{1c} = I_1 + A_1[y_c - (t_1 - y_1)]^2 \tag{3.9}$$

$$I_{ac} = \left[\frac{b_a t_a^{\,3}}{12} + b_a t_a (t_1 + 0.5t_a - y_c)^2\right] R_{ma} \tag{3.10}$$

$$I_{2c} = \left[\frac{b_2 t_2^{\,3}}{12} + b_2 t_2 (t_1 + t_a + y_2 - y_c)^2\right] R_{m2} \tag{3.11}$$

where y_c and the modular ratios R_{ma} and R_{m2} are given by

$$y_c = \frac{A_1(t_1 - y_1) + R_{ma} b_a t_a (t_1 + 0.5t_a) + R_{m2} b_2 t_2 (t_1 + t_a + y_2)}{A_1 + R_{ma} b_a t_a + R_{m2} b_2 t_2} \tag{3.12}$$

$$R_{ma} = \frac{E_a}{E_1}; \qquad R_{m2} = \frac{E_2}{E_1} \tag{3.13}$$

Considering a point in the adhesive layer at distance y from the beam to adhesive interface (so y ranges from 0 to t_a within the adhesive), the first moment of area of the equivalent plate and adhesive section below the considered position about the centroid of the composite beam section is given by

$$Q_e(y) = R_{m2} b_2 t_2 \left[t_1 + t_a + y_2 - y_c\right] + R_{ma} b_2 (t_a - y)\left[t_1 + 0.5(t_a + y) - y_c\right] \tag{3.14}$$

The shear stress at the considered position within the adhesive layer is thus

$$\tau(x, y) = m_c(y) V_{Tc}(x) \tag{3.15}$$

where $V_{Tc}(x)$ is the total shear force on the composite beam section at a distance of x from the left plate end due to all the loading in Case-2 (including the contribution from plate end loadings) and

$$m_c(y) = \frac{Q_e(y)}{I_e b_2} \tag{3.16}$$

The interfacial normal stress from this theory is zero, i.e. $\sigma(x) \approx 0$.

3.4 Governing Differential Equations and General Solutions for Case-3

The governing differential equations and general solutions for the interfacial shear and normal stresses between the adherends for Case-3 (Figure 3.2) are derived in this section.

3.4.1 Interfacial shear stress

The moment in the beam and the plate can be related assuming that they experience equal curvatures under the given load. This is given by

$$R_b M_1(x) = M_2(x) \tag{3.17}$$

Longitudinal equilibrium of a differential segment of the plated beam as shown in Figure 3.3 gives

$$-\frac{dN_1(x)}{dx} = b_2 \tau(x) = \frac{dN_2(x)}{dx} \tag{3.18}$$

where $\tau(x)$ is the interfacial shear stress between the adherends.

The total shear force $V_T(x)$ and total applied moment $M_T(x)$ at any section of the plated beam as obtained from plate end loadings are:

$$V_T(x) = \frac{1}{L}\left[M_{pl} - M_{pr} - (V_{pl} + V_{pr})a + (N_{pl} - N_{pr})(t_a + y_2)\right] = V_T \tag{3.19}$$

$$M_T(x) = V_{pl} a + V_T(a + x) - M_{pl} - N_{pl}(t_a + y_2) - N_{pr}(t_1 - y_c); \qquad 0 \le x \le L_p \tag{3.20}$$

where a is the distance from the support to the plate end.

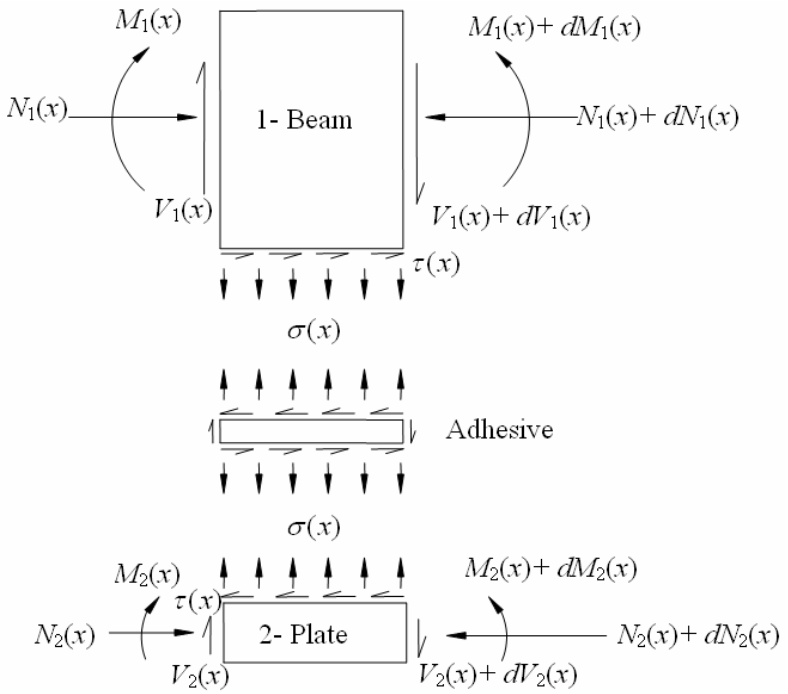

Figure 3. 3. Differential segment of a plated beam

From Eqs 3.17 and 3.20 the bending moment in each adherend can be found as

$$M_i(x)=\left(\frac{E_iI_i}{E_1I_1+E_2I_2}\right)\left[M_T(x)-N_2(x)[t_1+t_a+y_2-y_c]+N_1(x)[y_c-(t_1-y_1)]\right];\ i=1,\ 2 \tag{3.21}$$

Taking the first derivative of Eq. 3.21 with respect to *x* gives the following relationship between the bending moments in each adherend and the total shear force:

$$\frac{dM_i(x)}{dx}=\left(\frac{E_iI_i}{E_1I_1+E_2I_2}\right)\left[V_T(x)-b_2(y_1+t_a+y_2)\tau(x)\right];\qquad i=1,\ 2 \tag{3.22}$$

The moment equilibrium in adherends relates the shear force and bending moment in each adherends as

$$V_i(x)=\frac{dM_i(x)}{dx}+b_2y_i\tau(x);\quad i=1,\ 2 \tag{3.23}$$

The longitudinal strain at the bottom of adherend-1 $\varepsilon_1(x)$ and at the top of adherend-2 $\varepsilon_2(x)$ are

$$\varepsilon_i(x)=\frac{du_i(x)}{dx}=\varepsilon_{ib}(x)+\varepsilon_{im}(x);\qquad i=1,\ 2 \tag{3.24}$$

where $\varepsilon_{ib}(x)$ and $\varepsilon_{im}(x)$ are the strains induced by the bending moments and axial (membrane) forces respectively. If the displacements corresponding to the above strains are respectively given as $u_{ib}(x)$ and $u_{im}(x)$, these strains can be expressed as

$$\varepsilon_{ib}(x) = \frac{du_{ib}(x)}{dx} = (-1)^{i+1}\frac{y_i}{E_i I_i} M_i(x); \qquad i = 1, 2 \tag{3.25}$$

$$\varepsilon_{im}(x) = \frac{du_{im}(x)}{dx}; \qquad i = 1, 2 \tag{3.26}$$

Shear deformations of the adherends are incorporated in this analysis in determining $\varepsilon_{im}(x)$. The present analysis considers the actual parabolic variation of shear stress (strain) through the adherend thickness. In order to achieve the above distribution, a cubic variation in respect of y is considered for the longitudinal displacements $u_{im}(x,y)$:

$$u_{1m}(x, y_o) = a_1(x)y_o^3 + a_2(x)y_o^2 + a_3(x)y_o + a_4(x) \tag{3.27}$$

$$u_{2m}(x, y_p) = a_5(x)y_p^3 + a_6(x)y_p^2 + a_7(x)y_p + a_8(x) \tag{3.28}$$

where (x, y_o) and (x, y_p) are the local co-ordinate system with their origin at the top surface of adherend-1(original beam) and adherend-2 (plate) respectively.

The variation of the transverse displacement in the longitudinal direction is negligible, i.e. $\partial v_{im}/\partial x = 0$, so the shear strains in the adherends are given by

$$\gamma_1(x, y_o) = \frac{\partial u_{1m}}{\partial y} = 3a_1(x)y_o^2 + 2a_2(x)y_o + a_3(x) \tag{3.29}$$

$$\gamma_2(x, y_p) = \frac{\partial u_{2m}}{\partial y} = 3a_5(x)y_p^2 + 2a_6(x)y_p + a_7(x) \tag{3.30}$$

The shear stresses in the two adherends are

$$\tau_i(x, y) = G_i\gamma_i(x, y) \qquad ; \qquad i = 1,\ y = y_0 \text{ or } i = 2,\ y = y_p \tag{3.31}$$

where G_i is the transverse shear modulus of the adherends

The shear stress in the adherends must satisfy the following conditions:

$$\tau_1(x,0) = 0 \qquad ; \qquad \tau_2(x,t_2) = 0 \tag{3.32a}$$

$$\tau_1(x, y_b) = \tau_{1n}(x) \qquad ; \qquad \tau_2(x, y_2) = \tau_{2n}(x) \tag{3.32b}$$

$$\tau_1(x,t_1) = \tau(x) \qquad ; \qquad \tau_2(x,0) = \tau(x) \tag{3.32c}$$

where y_b is the distance of the centroid of the beam from its top surface, $\tau_{in}(x)$ with i=1, 2 represents the shear stress in adherends at the neutral axis (NA). $\tau_{in}(x)$ is determined based on equilibrium by considering interfacial shear stress and beam theory as

$$\tau_{in}(x) = \frac{V_i(x)}{I_i b_{in}} \int y dA_i = \frac{V_i(x)}{I_i b_{in}} Q_i(y) \qquad ;\ i = 1,\ y = y_0 \text{ or } i = 2,\ y = y_p \tag{3.33}$$

In the above equation, b_{1n} is the width of beam at NA, $b_{2n} = b_2$ and $Q_i(y)$ is the first moment of area of the section of adherend below or above the NA about the NA of the cross section. Eq. 3.32a is based on zero shear stress on the free surface at the top of adherend-1 and bottom of adherend-2. Eq. 3.32b is an approximation based on the beam theory. Eq. 3.32c results from the continuity of displacements at the interfaces between adhesive and adherends and the assumption of constant shear stress $\tau(x)$ through the thickness of the adhesive.

Application of Eqs 3.32a-c into Eq. 3.31 gives

$$\gamma_1(x, y_o) = \frac{1}{G_1 y_b t_1 (y_b - t_1)} \left\{ [t_1 \tau_{1n}(x) - y_b \tau(x)] y_o^2 - [t_1^2 \tau_{1n}(x) - y_b^2 \tau(x)] y_o \right\} \tag{3.34}$$

$$\gamma_2(x, y_p) = \frac{1}{G_2 t_2^2} \left\{ [2\tau(x) - 4\tau_{2n}(x)] y_p^2 - t_2 [3\tau(x) - 4\tau_{2n}(x)] y_p + t_2^2 \tau(x) \right\} \tag{3.35}$$

The longitudinal displacement u_{im} for the adherends are given by

$$u_{im}(x, y) = u_{im}(x,0) + \int_0^y \gamma_i(x, y) dy \qquad ;\ i = 1,\ y = y_0 \text{ or } i = 2,\ y = y_p \tag{3.36}$$

Substituting Eqs 3.34-3.35 into Eq. 3.36 gives

$$u_{1m}(x, y_o) = u_{1m}(x,0) + \frac{1}{6 G_1 y_b t_1 (y_b - t_1)} \left(2[t_1 \tau_{1n}(x) - y_b \tau(x)] y_o^3 - 3[t_1^2 \tau_{1n}(x) - y_b^2 \tau(x)] y_o^2 \right) \tag{3.37}$$

$$u_{2m}(x, y_p) = u_{2m}(x,0) + \frac{1}{6 G_2 t_2^2} \left(2[2\tau(x) - 4\tau_{2n}(x)] y_p^3 - 3t_2 [3\tau(x) - 4\tau_{2n}(x)] y_p^2 + 6 t_2^2 \tau(x) y_p \right) \tag{3.38}$$

The displacements are continuous at the interfaces between the adhesive and adherends. Hence, $u_{1m}(x,t_1) = u_{1m}$ and $u_{2m}(x,0) = u_{2m}$.

Substituting $y_0 = t_1$ into Eq. 3.37 and rearranging yields

$$u_{1m}(x,0) = u_{1m} - \frac{2[t_1 \tau_{1n}(x) - y_b \tau(x)] t_1^3 - 3[t_1^2 \tau_{1n}(x) - y_b^2 \tau(x)] t_1^2}{6 G_1 y_b t_1 (y_b - t_1)} \tag{3.39}$$

Substituting Eq. 3.39 into Eq. 3.37 gives

$$u_{1m}(x,y_o)=u_{1m}+\frac{2[t_1\tau_{1n}(x)-y_b\tau(x)](y_o^3-t_1^3)-3[t_1^2\tau_{1n}(x)-y_b^2\tau(x)](y_o^2-t_1^2)}{6G_1y_bt_1(y_b-t_1)} \tag{3.40}$$

The longitudinal resultant forces $N_i(x)$ in the adherends are given by

$$N_i=b_i\int_0^y\sigma_i(x,y)dy \qquad ; \qquad i=1,\ y=y_0 \text{ or } i=2,\ y=y_p \tag{3.41}$$

where $\sigma_i(x,y)$ is the longitudinal normal stress in the adherends. Expressing these stresses into functions of displacements at the interface between the adhesive and adherends results

$$\begin{aligned}N_1&=E_1b_1\int_0^{t_1}\frac{du_{1m}(x,y_o)}{dx}dy_o\\&=E_1A_1\left[\frac{du_{1m}}{dx}-\frac{t_1}{12G_1(y_b-t_1)}\left((4y_b-3t_1)\frac{d\tau(x)}{dx}-\frac{t_1^2}{y_b}\frac{d\tau_{1n}(x)}{dx}\right)\right]\end{aligned} \tag{3.42}$$

$$N_2=E_2b_2\int_0^{t_2}\frac{du_{2m}(x,y_p)}{dx}dy_p=E_2A_2\left[\frac{du_{2m}}{dx}+\frac{t_2}{6G_2}\left(\frac{d\tau(x)}{dx}+2\frac{d\tau_{2n}(x)}{dx}\right)\right] \tag{3.43}$$

From Eqs 3.42 and 3.43,

$$\varepsilon_{1m}=\frac{du_{1m}}{dx}=\frac{N_1(x)}{E_1A_1}+\frac{t_1}{12G_1(y_b-t_1)}\left((4y_b-3t_1)\frac{d\tau(x)}{dx}-(\frac{t_1^2}{y_b})\frac{d\tau_{1n}(x)}{dx}\right) \tag{3.44}$$

$$\varepsilon_{2m}=\frac{du_{2m}}{dx}=\frac{N_2(x)}{E_2A_2}-\frac{t_2}{6G_2}\left(\frac{d\tau(x)}{dx}+2\frac{d\tau_{2n}(x)}{dx}\right) \tag{3.45}$$

Substituting the first derivative with respect to x of Eq. 3.33 into Eqs 3.44-3.45 and using the resulting equations together with Eq. 3.25 into Eq. 3.24 yields

$$\frac{du_1(x)}{dx}=\frac{M_1(x)y_1}{E_1I_1}+\frac{N_1(x)}{E_1A_1}+\left(\frac{t_1(4y_b-3t_1)}{12G_1(y_b-t_1)}\right)\frac{d\tau(x)}{dx}-\left(\frac{t_1^3Q_1(y_o)}{12G_1y_b(y_b-t_1)I_1b_{1n}}\right)\frac{dV_1(x)}{dx} \tag{3.46}$$

$$\frac{du_2(x)}{dx}=-\frac{M_2(x)y_2}{E_2I_2}+\frac{N_2(x)}{E_2A_2}-\frac{t_2}{6G_2}\frac{d\tau(x)}{dx}-\frac{t_2Q_2(y_p)}{3G_2I_2b_2}\frac{dV_2(x)}{dx} \tag{3.47}$$

Based on the theory of elasticity, the shear stress in the adhesive layer can be found from

$$\tau(x)=G_a\left(\frac{du(x,y)}{dy}+\frac{dv(x,y)}{dx}\right) \tag{3.48}$$

where G_a is the shear modulus of adhesive and $u(x,y)$ and $v(x,y)$ are the horizontal and vertical displacement in the adhesive layer.

The first derivative of Eq. 3.48 with respect to *x* is

$$\frac{d\tau(x)}{dx} = G_a\left(\frac{d^2u(x,y)}{dxdy} + \frac{d^2v(x,y)}{dx^2}\right) \tag{3.49}$$

The moment-curvature relation for a differential segment of the plated beam is

$$\frac{d^2v(x,y)}{dx^2} = -\frac{1}{E_1 I_e} M_T(x) \tag{3.50}$$

Because the shear stress is assumed to be uniform through the thickness of the adhesive layer, $u(x,y)$ varies linearly across t_a so

$$\frac{du(x,y)}{dy} = \frac{1}{t_a}[u_2(x) - u_1(x)] \tag{3.51}$$

The first derivative of the above equation with respect to *x* is

$$\frac{d^2u(x,y)}{dxdy} = \frac{1}{t_a}\left(\frac{du_2(x)}{dx} - \frac{du_1(x)}{dx}\right) \tag{3.52}$$

Substituting Eqs 3.50 and 3.52 into Eq. 3.49 gives

$$\frac{d\tau(x)}{dx} = \frac{G_a}{t_a}\left(\frac{du_2(x)}{dx} - \frac{du_1(x)}{dx}\right) - \frac{G_a}{E_1 I_e} M_T(x) \tag{3.53}$$

Substituting Eqs 3.21, 3.46 and 3.47 into Eq. 3.53 yields

$$\frac{d\tau(x)}{dx} = \frac{G_a}{E_1}\left(-r_1 M_1(x) - r_2 M_2(x) - r_3 N_1(x) + r_4 N_2(x) - r_5 \frac{d\tau(x)}{dx} + r_6 \frac{dV_1(x)}{dx} - r_7 \frac{dV_2(x)}{dx}\right) \tag{3.54a}$$

where

$$r_1 = \frac{y_1}{t_a I_1} + \frac{1}{I_e}; \qquad r_2 = \frac{y_2}{t_a R_{m2} I_2} + \frac{1}{I_e}; \qquad r_3 = \frac{1}{t_a A_1} - \frac{(y_c - t_1 + y_1)}{I_e} \tag{3.54b}$$

$$r_4 = \frac{1}{t_a R_{m2} A_2} - \frac{(t_1 + t_a + y_2 - y_c)}{I_e}; \qquad r_5 = \frac{E_1}{6t_a}\left[\frac{t_1(4y_b - 3t_1)}{2G_1(y_b - t_1)} + \frac{t_2}{G_2}\right] \tag{3.54c}$$

$$r_6 = \frac{E_1 t_1^3 Q_1(y_o)}{12 t_a G_1 y_b (y_b - t_1) I_1 b_{1n}}; \qquad r_7 = \frac{E_1 t_2 Q_2(y_p)}{3 t_a G_2 I_2 b_2} \tag{3.54d}$$

Differentiating Eq. 3.54a once with respect to *x* and substituting Eqs 3.18, 3.22 and 3.23 into the resulting expression results in the following governing differential equation for the interfacial shear stress:

$$\frac{d^2\tau(x)}{dx^2} - (\lambda_n^{\,2})\tau(x) + (m_1\lambda_n^{\,2})V_T(x) = 0 \tag{3.55a}$$

where

$$\lambda_n^{\,2} = \alpha^2 \lambda^2 \tag{3.55b}$$

$$\alpha^2 = \left[1 + \frac{G_a}{3t_a}\left(\frac{t_1}{G_1} r_8 + \frac{t_2}{G_2} r_9\right)\right]^{-1} \tag{3.55c}$$

$$r_8 = \frac{1}{4(y_b - t_1)}\left[4y_b - 3t_1 - \frac{t_1^2 b_2 Q_1(y_o)}{y_b I_1 b_{1n}}\left(y_1 - \frac{E_1 I_1 (y_1 + y_2 + t_a)}{E_1 I_1 + E_2 I_2}\right)\right] \tag{3.55d}$$

$$r_9 = \frac{1}{2} + \left[\frac{y_2}{I_2} - \frac{E_2 (y_1 + y_2 + t_a)}{E_1 I_1 + E_2 I_2}\right] Q_2(y_p) \tag{3.55e}$$

$$\lambda^2 = \frac{G_a b_2}{t_a}\left[\frac{(y_1 + y_2)(y_1 + t_a + y_2)}{(E_1 I_1 + E_2 I_2)} + \frac{1}{E_1 A_1} + \frac{1}{E_2 A_2}\right] \tag{3.55f}$$

$$m_1 = \frac{G_a}{\lambda^2}\left[\frac{y_1 + y_2}{t_a (E_1 I_1 + E_2 I_2)} + \frac{1}{E_1 I_e}\right] \tag{3.55g}$$

The parameter λ_n accounts for the effects of flexural, axial and shear deformation in which α caters for the shear deformation and λ for the flexural and axial deformation. Parameters r_8 and r_9 are responsible for effecting parabolic variation of shear stress in adherends. Taking r_8 and r_9 values to unity leads to a linear shear stress distribution in adherends as approximated in Tsai et al. (1998) and Abdelouahed (2006), and taking their values to zero leads to (α = 1) the interfacial shear stress solution in Narayanamurthy et al. (2010). The accuracy in capturing the effect of shear deformation in the adherends lies with the accuracy in the prediction of α.

The general solution of the second order non-homogeneous differential equation (Eq. 3.55a) is:

$$\tau(x) = B_1 \cosh(\lambda_n x) + B_2 \sinh(\lambda_n x) + m_1 V_T \tag{3.56}$$

where B_1 and B_2 are the constants of integration to be determined from appropriate boundary conditions.

3.4.2 Interfacial normal stress

The interfacial normal stress exists between the adherends due to the differential vertical displacement between them when the beam is loaded. If the vertical displacements of the adherends 1 and 2 are respectively denoted by $v_1(x)$ and $v_2(x)$, the interfacial normal

stress, $\sigma(x)$ can be found from the following equation assuming a constant normal stress through the thickness of the adhesive:

$$\sigma(x) = \frac{E_a}{t_a}[v_2(x) - v_1(x)] \tag{3.57}$$

The moment-curvature relation, moment and vertical equilibrium of the differential segment of the adherends 1 and 2 (Figure 3.3) gives the following relationships

$$\frac{d^2 v_i(x)}{dx^2} = -\frac{1}{E_i I_i} M_i(x) + (-1)^i \frac{b_2}{G_i A_i \kappa_i} \sigma(x); \qquad i = 1, 2 \tag{3.58}$$

where κ_i is the Timoshenko's shear coefficient which is the ratio between the effective area resisting shear deformation and the actual cross sectional area of the adherend (e.g. κ=5/6 for rectangle and κ=5/12 for hollow thin walled square section).

The moment equilibrium is as given in Eq. 3.23.

$$\frac{dV_i(x)}{dx} = (-1)^i b_2 \sigma(x); \qquad i = 1, 2 \tag{3.59}$$

Differentiating Eq. 3.58 once with respect to x and substituting Eq. 3.23 into the resulting equation gives

$$\frac{d^3 v_i(x)}{dx^3} = -\frac{1}{E_i I_i}\left(V_i(x) - b_2 y_i \tau(x)\right) + (-1)^i \frac{b_2}{G_i A_i \kappa_i} \frac{d\sigma(x)}{dx}; \qquad i = 1, 2 \tag{3.60}$$

Differentiating Eq. 3.60 once with respect to x and substituting Eq. 3.59 into the resulting equation gives

$$\frac{d^4 v_i(x)}{dx^4} = (-1)^{i+1} \frac{b_2}{E_i I_i} \sigma(x) + (-1)^i \frac{b_2}{G_i A_i \kappa_i} \frac{d^2\sigma(x)}{dx^2} + \frac{b_2 y_i}{E_i I_i} \frac{d\tau(x)}{dx}; \qquad i = 1, 2 \tag{3.61}$$

Differentiating Eq. 3.57 four times with respect to x and substituting Eq. 3.61 into the resulting equation yields the following governing differential equation for the interfacial normal stress

$$\frac{d^4\sigma(x)}{dx^4} - \beta_1 \frac{d^2\sigma(x)}{dx^2} + \beta_2 \sigma(x) + n_2 \frac{d\tau(x)}{dx} = 0 \tag{3.62a}$$

where

$$\beta_1 = \frac{E_a b_2}{t_a}\left(\frac{1}{G_1 A_1 \kappa_1} + \frac{1}{G_2 A_2 \kappa_2}\right) \tag{3.62b}$$

$$\beta_2 = \frac{E_a b_2}{t_a}\left(\frac{1}{E_1 I_1} + \frac{1}{E_2 I_2}\right) \tag{3.62c}$$

$$n_2 = \frac{E_a b_2}{t_a}\left(\frac{y_1}{E_1 I_1} - \frac{y_2}{E_2 I_2}\right) \tag{3.62d}$$

In Eq. 3.62a, β_1 arose from Timoshenko's beam theory and reflects the effect of shear deformation. If β_1= 0 it reduces to the governing equation for interfacial normal stress without considering shear deformation as in Narayanamurthy et al. (2010).

The governing equation for the interfacial normal stress given in Eq. 3.62a is a fourth order non-homogeneous ordinary differential equation. Its general solution can have the following three forms depending on the value of parameter δ which is influenced by material and geometric properties of the adherends and adhesive.

$$\delta = 4\beta_2 - \beta_1^2 \tag{3.63}$$

$$\sigma(x) = e^{-\eta_1 x}\left[C_1\cos(\eta_2 x) + C_2\sin(\eta_2 x)\right] + e^{\eta_1 x}\left[C_{11}\cos(\eta_2 x) + C_{21}\sin(\eta_2 x)\right] - n_3\frac{d\tau(x)}{dx} \quad \text{for } \delta > 0 \tag{3.64}$$

$$\sigma(x) = C_3 e^{-\eta_3 x} + C_4 e^{-\eta_4 x} + C_{31}e^{\eta_3 x} + C_{41}e^{\eta_4 x} + n_8\frac{d\tau(x)}{dx} + n_9\frac{d^3\tau(x)}{dx^3} \text{ for } \delta < 0 \tag{3.65}$$

$$\sigma(x) = [C_5 + C_6 x]e^{-\eta_5 x} + [C_{51} + C_{61}x]e^{\eta_5 x} \text{ for } \delta = 0 \tag{3.66}$$

where C_1 to C_6 and C_{11} to C_{61} are constants of integration. They are to be determined from appropriate boundary conditions listed in Eq. 3.70 and

$$\eta_1 = 0.5\sqrt{\beta_1 + 2\sqrt{\beta_2}}\,; \qquad \eta_2 = \frac{\sqrt{\delta}}{4\eta_1}\,; \qquad \eta_3 = \sqrt{0.5(\beta_1 + \sqrt{-\delta})} \tag{3.66a}$$

$$\eta_4 = \sqrt{0.5(\beta_1 - \sqrt{-\delta})}\,; \qquad \eta_5 = \sqrt{0.5\beta_1}\,; \qquad n_3 = \frac{n_2}{(\eta_1^2 + \eta_2^2)^2} \tag{3.66b}$$

$$n_4 = \frac{2\eta_1\eta_2}{(\eta_1^2 - \eta_2^2 - \beta_1)(3\eta_1^2\eta_2 - \eta_2^3 - \eta_2\beta_1) + (3\eta_1\eta_2^2 - \eta_1^3 + \eta_1\beta_1)(2\eta_1\eta_2)} \tag{3.66c}$$

$$n_5 = \frac{1 - n_4(3\eta_1\eta_2^2 - \eta_1^3 + \eta_1\beta_1)}{\eta_1^2 - \eta_2^2 - \beta_1}\,; \qquad n_6 = \frac{n_4(\eta_1^2 - \eta_2^2 - \beta_1)}{2\eta_1\eta_2} \tag{3.66d}$$

$$n_7 = \frac{3\eta_1\eta_2^2 - \eta_1^3 + \eta_1\beta_1}{\eta_1^2 - \eta_2^2 - \beta_1}\,; \qquad n_8 = \frac{-n_2}{\eta_3^2\eta_4^2}\,; \qquad n_9 = n_8\left(\frac{1}{\eta_3^2} + \frac{1}{\eta_4^2}\right). \tag{3.66e}$$

Because $\sigma(x)\to 0$ for large values of x, C_{11} to C_{61} = 0 and Eqs 3.64-3.66 reduce to

$$\sigma(x) = e^{-\eta_1 x}\left[C_1\cos(\eta_2 x) + C_2\sin(\eta_2 x)\right] - n_3\frac{d\tau(x)}{dx} \text{ for } \delta > 0 \tag{3.67}$$

$$\sigma(x) = C_3 e^{-\eta_3 x} + C_4 e^{-\eta_4 x} + n_8\frac{d\tau(x)}{dx} + n_9\frac{d^3\tau(x)}{dx^3} \text{ for } \delta < 0 \tag{3.68}$$

$$\sigma(x) = [C_5 + C_6 x]e^{-\eta_5 x} \text{ for } \delta = 0 \tag{3.69}$$

3.5 Boundary Conditions in Case-3

The boundary conditions available in Case-3 are:

$$M_1(x)\big|_{x=0} = \frac{a}{L}[(L-a)V_{pl} - aV_{pr} + M_{pl} - M_{pr} + (N_{pl} - N_{pr})(\frac{L}{a}y_1 + y_2 + t_a)] = M_1(0) \tag{3.70a}$$

$$M_2(x)\big|_{x=0} = -M_{pl} \tag{3.70b}$$

$$N_1(x)\big|_{x=0} = N_{pl} - N_{pr} \tag{3.70c}$$

$$N_2(x)\big|_{x=0} = -N_{pl} \tag{3.70d}$$

$$V_1(x)\big|_{x=0} = V_T + V_{pl} - b_2 t_a \tau(x)\big|_{x=0} \tag{3.70e}$$

$$V_2(x)\big|_{x=0} = -V_{pl} \tag{3.70f}$$

$$M_1(x)\big|_{x=L_p} = \frac{a}{L}[aV_{pl} - (L-a)V_{pr} - M_{pl} + M_{pr} - (N_{pl} - N_{pr})(y_2 + t_a)] = M_1(L_p) \tag{3.70g}$$

$$M_2(x)\big|_{x=L_p} = -M_{pr} \tag{3.70h}$$

$$N_1(x)\big|_{x=L_p} = 0 \tag{3.70i}$$

$$N_2(x)\big|_{x=L_p} = -N_{pr} \tag{3.70j}$$

$$V_1(x)\big|_{x=L_p} = V_T + V_{pr} - b_2 t_a \tau(x)\big|_{x=L_p} \tag{3.70k}$$

$$V_2(x)\big|_{x=L_p} = -V_{pr} \tag{3.70l}$$

3.6 Application of Boundary Conditions

The constants of integration B_1 and B_2 in the general solution of interfacial shear stress (Eq. 3.56) and C_1 to C_6 in the general solution of interfacial normal stress (Eqs 3.67-3.69) are determined in this section from appropriate boundary conditions listed in Eq. 3.70.

3.6.1 Interfacial shear stress – Constants B_1 and B_2

Applying Eqs 3.70a-f into Eq. 3.54a gives

$$\left.\frac{d\tau(x)}{dx}\right|_{x=0} = \frac{G_a\alpha^2}{E_1}\left[-r_1M_1(0) + r_2M_{pl} - (r_3+r_4)N_{pl} + r_3N_{pr}\right] \tag{3.71}$$

The first derivative of Eq. 3.56 with respect to x at x=0 is

$$\left.\frac{d\tau(x)}{dx}\right|_{x=0} = B_2\lambda_n \tag{3.72}$$

From Eqs 3.71 and 3.72,

$$B_2 = \frac{G_a\alpha}{E_1\lambda}\left[-r_1M_1(0) + r_2M_{pl} - (r_3+r_4)N_{pl} + r_3N_{pr}\right] \tag{3.73}$$

Applying Eqs 3.70g-l into Eq. 3.54a gives

$$\left.\frac{d\tau(x)}{dx}\right|_{x=L_p} = \frac{G_a\alpha^2}{E_1}\left[-r_1M_1(L_p) + r_2M_{pr} - r_4N_{pr}\right] \tag{3.74}$$

The first derivative of Eq. 3.56 with respect to x at $x=L_p$ is

$$\left.\frac{d\tau(x)}{dx}\right|_{x=L_p} = \lambda_n[B_1\sinh(\lambda_nL_p) + B_2\cosh(\lambda_nL_p)] \tag{3.75}$$

From Eqs 3.74 and 3.75,

$$B_1 = -\frac{B_2}{\tanh(\lambda_nL_p)} + \frac{G_a\alpha^2}{E_1\lambda_n\sinh(\lambda_nL_p)}\left[-r_1M_1(L_p) + r_2M_{pr} - r_4N_{pr}\right] \tag{3.76}$$

It is found that λ_nL_p>10 for practical cases so $\tanh(\lambda_nL_p) \approx 1$ and $[1/\sinh(\lambda_nL_p)] \approx 0$. Therefore, Eq. 3.76 is reduced to

$$B_1 = -B_2 \tag{3.77}$$

3.6.2 Interfacial normal stress - Constants C_1 to C_6

Constants C_1 to C_2

Differentiating Eq. 3.57 twice with respect to x, substituting Eq. 3.58 into the resulting expression and then applying the boundary conditions in Eqs 3.70a-b gives

$$\left.\frac{d^2\sigma(x)}{dx^2}\right|_{x=0} = \frac{E_a}{t_aE_2I_2}[R_bM_1(0) + M_{pl}] + \beta_1\sigma(x)\big|_{x=0} \tag{3.78}$$

Setting x=0 in Eq. 3.67 and substituting in Eq. 3.78 gives

$$\left.\frac{d^2\sigma(x)}{dx^2}\right|_{x=0} = \frac{E_a}{t_aE_2I_2}[R_bM_1(0) + M_{pl}] + \beta_1C_1 - \beta_1n_3\left.\frac{d\tau(x)}{dx}\right|_{x=0} \tag{3.79}$$

Differentiating Eq. 3.67 twice with respect to x and setting x=0 into the resulting equation gives

$$\left.\frac{d^2\sigma(x)}{dx^2}\right|_{x=0} = (\eta_1^2 - \eta_2^2)C_1 - 2\eta_1\eta_2 C_2 - n_3 \left.\frac{d^3\tau(x)}{dx^3}\right|_{x=0} \tag{3.80}$$

From Eqs 3.79 and 3.80,

$$(\eta_1^2 - \eta_2^2 - \beta_1)C_1 - 2\eta_1\eta_2 C_2 = \frac{E_a}{t_a E_2 I_2}[R_b M_1(0) + M_{pl}] - n_3\left(\beta_1 \frac{d\tau(x)}{dx} - \frac{d^3\tau(x)}{dx^3}\right)\Bigg|_{x=0} \tag{3.81}$$

Differentiating Eq. 3.57 thrice with respect to *x*, substituting Eq. 3.60 into the resulting expression and then applying the boundary conditions in Eqs 3.70e-f gives

$$\left.\frac{d^3\sigma(x)}{dx^3}\right|_{x=0} = \frac{E_a}{t_a E_1 I_1} V_{Tm} - n_{2m}\tau(0) + \beta_1 \left.\frac{d\sigma(x)}{dx}\right|_{x=0} \tag{3.82a}$$

where

$$V_{Tm} = V_T + \left(\frac{1+R_b}{R_b}\right)V_{pl} \tag{3.82b}$$

$$n_{2m} = \frac{E_a b_2}{t_a}\left(\frac{y_1 + t_a}{E_1 I_1} - \frac{y_2}{E_2 I_2}\right) \tag{3.82c}$$

Differentiating Eq. 3.67 once with respect to *x*, setting $x=0$ and substituting the result into Eq. 3.82a gives

$$\left.\frac{d^3\sigma(x)}{dx^3}\right|_{x=0} = \frac{E_a}{t_a E_1 I_1} V_{Tm} - n_{2m}\tau(0) - \beta_1\eta_1 C_1 + \beta_1\eta_2 C_2 - \beta_1 n_3 \left.\frac{d^2\tau(x)}{dx^2}\right|_{x=0} \tag{3.83}$$

Differentiating Eq. 3.67 three times with respect to *x* and setting $x=0$ gives

$$\left.\frac{d^3\sigma(x)}{dx^3}\right|_{x=0} = [2\eta_1\eta_2^2 - \eta_1(\eta_1^2 - \eta_2^2)]C_1 + [2\eta_1^2\eta_2 + \eta_2(\eta_1^2 - \eta_2^2)]C_2 - n_3 \left.\frac{d^4\tau(x)}{dx^4}\right|_{x=0} \tag{3.84}$$

From Eqs 3.83 and 3.84,

$$(3\eta_1\eta_2^2 - \eta_1^3 + \eta_1\beta_1)C_1 + (3\eta_1^2\eta_2 - \eta_2^3 - \eta_2\beta_1)C_2 = \frac{E_a V_{Tm}}{t_a E_1 I_1} - n_{2m}\tau(0) - n_3\left(\beta_1 \frac{d^2\tau(0)}{dx^2} - \frac{d^4\tau(0)}{dx^4}\right) \tag{3.85}$$

C_1 and C_2 are obtained from Eqs 3.81 and 3.85 as

$$\begin{aligned} C_1 = {} & \frac{E_a}{t_a E_2 I_2}\left[R_b\left(n_4 V_{Tm} + n_5 M_1(0)\right) + n_5 M_{pl}\right] - n_{2m} n_4 \tau(0) \\ & - n_3 n_5\left(\beta_1 \frac{d\tau(0)}{dx} - \frac{d^3\tau(0)}{dx^3}\right) - n_3 n_4\left(\beta_1 \frac{d^2\tau(0)}{dx^2} - \frac{d^4\tau(0)}{dx^4}\right) \end{aligned} \tag{3.86}$$

$$\begin{aligned} C_2 = {} & \frac{E_a}{t_a E_2 I_2}\left[R_b\left(n_6 V_{Tm} - n_6 n_7 M_1(0)\right) - n_6 n_7 M_{pl}\right] - n_{2m} n_6 \tau(0) \\ & + n_3 n_6 n_7\left(\beta_1 \frac{d\tau(0)}{dx} - \frac{d^3\tau(0)}{dx^3}\right) - n_3 n_6\left(\beta_1 \frac{d^2\tau(0)}{dx^2} - \frac{d^4\tau(0)}{dx^4}\right) \end{aligned} \tag{3.87}$$

Constants C_3 and C_4

Setting x=0 in Eq. 3.68 and substituting in Eq. 3.78 gives

$$\left.\frac{d^2\sigma(x)}{dx^2}\right|_{x=0} = \frac{E_a}{t_a E_2 I_2}[R_b M_1(0) + M_{pl}] + \beta_1\left(C_3 + C_4 + n_8 \left.\frac{d\tau(x)}{dx}\right|_{x=0} + n_9 \left.\frac{d^3\tau(x)}{dx^3}\right|_{x=0} \right) \quad (3.88)$$

Differentiating Eq. 3.68 twice with respect to x and substituting x=0 into the resulting equation gives

$$\left.\frac{d^2\sigma(x)}{dx^2}\right|_{x=0} = \eta_3^2 C_3 + \eta_4^2 C_4 + n_8 \left.\frac{d^3\tau(x)}{dx^3}\right|_{x=0} \quad (3.89)$$

The fifth and higher derivatives of $\tau(x)$ are very small and hence neglected in this section.

From Eqs 3.88 and 3.89,

$$(\eta_3^2 - \beta_1)C_3 + (\eta_4^2 - \beta_1)C_4 = \frac{E_a}{t_a E_2 I_2}[R_b M_1(0) + M_{pl}] + n_8\beta_1 \frac{d\tau(0)}{dx} + (n_9\beta_1 - n_8)\frac{d^3\tau(0)}{dx^3} \quad (3.90)$$

Differentiating Eq. 3.68 once with respect to x, setting x=0 and substituting the result into Eq. 3.82 gives

$$\left.\frac{d^3\sigma(x)}{dx^3}\right|_{x=0} = \frac{E_a}{t_a E_1 I_1} V_{Tm} - n_{2m}\tau(0) - \beta_1\eta_3 C_3 - \beta_1\eta_4 C_4 + \beta_1\left(n_8 \frac{d^2\tau(x)}{dx^2} + n_9 \frac{d^4\tau(x)}{dx^4} \right)\Bigg|_{x=0} \quad (3.91)$$

Differentiating Eq. 3.68 three times with respect to x and setting x=0 gives

$$\left.\frac{d^3\sigma(x)}{dx^3}\right|_{x=0} = -\eta_3^3 C_3 - \eta_4^3 C_4 + n_8 \left.\frac{d^4\tau(x)}{dx^4}\right|_{x=0} \quad (3.92)$$

From Eqs 3.91 and 3.92,

$$-\eta_3(\eta_3^2 - \beta_1)C_3 - \eta_4(\eta_4^2 - \beta_1)C_4 = \frac{E_a V_{Tm}}{t_a E_1 I_1} - n_{2m}\tau(0) + n_8\beta_1 \frac{d^2\tau(0)}{dx^2} + (n_9\beta_1 - n_8)\frac{d^4\tau(0)}{dx^4} \quad (3.93)$$

C_3 and C_4 are obtained from Eqs 3.90 and 3.93 as

$$\begin{aligned} C_3 = {} & \frac{E_a n_{10}}{t_a E_2 I_2}\left(R_b[\frac{V_{Tm}}{\eta_4} + M_1(0)] + M_{pl} \right) - \frac{n_{2m} n_{10}}{\eta_4}\tau(0) + \\ & + n_8 n_{10}\beta_1\left(\frac{d\tau(0)}{dx} + \frac{1}{\eta_4}\frac{d^2\tau(0)}{dx^2} \right) + (n_9\beta_1 - n_8)n_{10}\left(\frac{d^3\tau(0)}{dx^3} + \frac{1}{\eta_4}\frac{d^4\tau(0)}{dx^4} \right) \end{aligned} \quad (3.94)$$

$$C_4 = \frac{E_a n_{11}}{t_a E_2 I_2}\left(R_b[\frac{V_{Tm}}{\eta_3} + M_1(0)] + M_{pl} \right) - \frac{n_{2m} n_{11}}{\eta_3}\tau(0) + \\ + n_8 n_{11}\beta_1\left(\frac{d\tau(0)}{dx} + \frac{1}{\eta_3}\frac{d^2\tau(0)}{dx^2} \right) + (n_9\beta_1 - n_8)n_{11}\left(\frac{d^3\tau(0)}{dx^3} + \frac{1}{\eta_3}\frac{d^4\tau(0)}{dx^4} \right) \quad (3.95)$$

where n_{10} and n_{11} are given as

$$n_{10} = \frac{\eta_4}{(\eta_4 - \eta_3)(\eta_3^2 - \beta_1)}; \qquad n_{11} = \frac{\eta_3}{(\eta_3 - \eta_4)(\eta_4^2 - \beta_1)} \quad (3.95a)$$

Constants C_5 and C_6

Setting x=0 in Eq. 3.69 and substituting in Eq. 3.78 gives

$$\left.\frac{d^2\sigma(x)}{dx^2}\right|_{x=0} = \frac{E_a}{t_a E_2 I_2}[R_b M_1(0) + M_{pl}] + \beta_1 C_5 \quad (3.96)$$

Differentiating Eq. 3.69 twice with respect to x and setting x=0 into the resulting equation gives

$$\left.\frac{d^2\sigma(x)}{dx^2}\right|_{x=0} = \eta_5(\eta_5 C_5 - 2C_6) \quad (3.97)$$

From Eqs 3.96 and 3.97,

$$(\eta_5^2 - \beta_1)C_5 - 2\eta_5 C_6 = \frac{E_a}{t_a E_2 I_2}[R_b M_1(0) + M_{pl}] \quad (3.98)$$

Differentiating Eq. 3.69 once with respect to x, setting x=0 and substituting the result into Eq. 3.82 gives

$$\left.\frac{d^3\sigma(x)}{dx^3}\right|_{x=0} = \frac{E_a}{t_a E_1 I_1} V_{Tm} - n_{2m}\tau(0) + \beta_1(C_6 - \eta_5 C_5) \quad (3.99)$$

Differentiating Eq. 3.69 three times with respect to x and setting x=0 gives

$$\left.\frac{d^3\sigma(x)}{dx^3}\right|_{x=0} = \eta_5^2(3C_6 - \eta_5 C_5) \quad (3.100)$$

From Eqs 3.99 and 3.100,

$$\eta_5(\eta_5^2 - \beta_1)C_5 - (3\eta_5^2 - \beta_1)C_6 = -\frac{E_a V_{Tm}}{t_a E_1 I_1} + n_{2m}\tau(0) \quad (3.101)$$

C_5 and C_6 are obtained from Eqs 3.98 and 3.101 as

$$C_5 = \frac{E_a n_{13}}{t_a E_2 I_2}\left(R_b[n_{12} V_{Tm} + M_1(0)] + M_{pl}\right) - n_{2m} n_{12} n_{13}\tau(0) \quad (3.102)$$

$$C_6 = \frac{(\eta_5^2 - \beta_1)}{2\eta_5} C_5 - \frac{E_a}{2\eta_5 t_a E_2 I_2} \left(R_b M_1(0) + M_{pl} \right) \tag{3.103}$$

where n_{12} and n_{13} are given as

$$n_{12} = \frac{2\eta_5}{(3\eta_5^2 - \beta_1)}; \qquad n_{13} = \frac{(3\eta_5^2 - \beta_1)}{(\eta_5^2 - \beta_1)^2} \tag{3.103a}$$

3.7 Solution for General Loading (Case-1)

The solutions from Case-2 and 3 are combined to get the solution for the original problem in Case-1. The interfacial shear stress is given by the summation of Eqs 3.15 and 3.56 as

$$\tau(x, y) = m_c(y) V_{Tc}(x) + B_1[\cosh(\lambda_n x) - \sinh(\lambda_n x)] + m_1 V_T \tag{3.104}$$

The interfacial normal stress is given by Eqs 3.67, 3.68 or 3.69 depending on δ in Eq. 3.63.

3.8 Comparison of Analytical Solutions

A comparison of the interfacial shear and normal stresses from the closed form solutions of Smith & Teng (2001), Narayanamurthy et al. (2010), Abdelouahed (2006) and the present solution are presented in this section. A steel plated RC beam of rectangular cross section subjected to a four point bending with two transverse loads each of 30kN as shown in Figure 3.4 is analysed here as a typical case. The material and geometric properties of this beam are given in Table 1 which are taken from an experimental study undertaken by Jones et al. (1988).

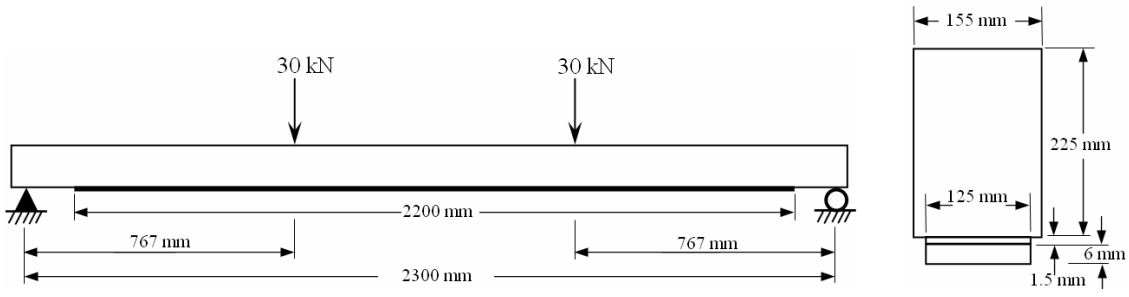

Figure 3.4. A steel plated RC beam subjected to 4 point bending

The interfacial stresses from the above analytical solutions are plotted in Figure 3.5. The solutions of Smith & Teng (2001) and Narayanamurthy et al. (2010) match closely but both solutions neglect the effect of shear deformation. The only difference between the present solution and Narayanamurthy et al. (2010) is the inclusion of the shear deformation in the adherends in the present solution. It is observed that the peak interfacial shear stress is reduced by 25% and the peak interfacial normal stress is increased by 29% in the present solution compared to Narayanamurthy et al. (2010). This is because the effect of shear deformation increases the transverse strain component and reduces the longitudinal strain in the adherends at the interface which in turn increases the peeling effect (interfacial normal stress) and reduces the interfacial shear stress respectively.

Table 3.1: Geometric and material properties of example plated beams

Component	Width (mm)	Depth (mm)	Length (mm)	Elastic modulus (GPa)	Transverse shear modulus (GPa)
RC beam	$b_1 = 155$	$t_1 = 225$	$L_1 = 2300$	$E_1 = 31$	$G_1 = 13.14$
Steel plate	$b_2 = 125$	$t_2 = 6$	$L_2 = 2200$	$E_2 = 200$	$G_2 = 76.92$
Adhesive layer	$b_a = 125$	$t_a = 1.5$	$L_a = 2200$	$E_a = 3^+$	$G_a = 1.11$
CFRP plate*	$b_2 = 125$	$t_2 = 6$	$L_2 = 2200$	$E_2 = 100$	$G_2 = 4.24$
GFRP plate*	$b_2 = 125$	$t_2 = 6$	$L_2 = 2200$	$E_2 = 50$	$G_2 = 3.50$

Note : * - used in parametric study; + - different from Jones et al. [21].

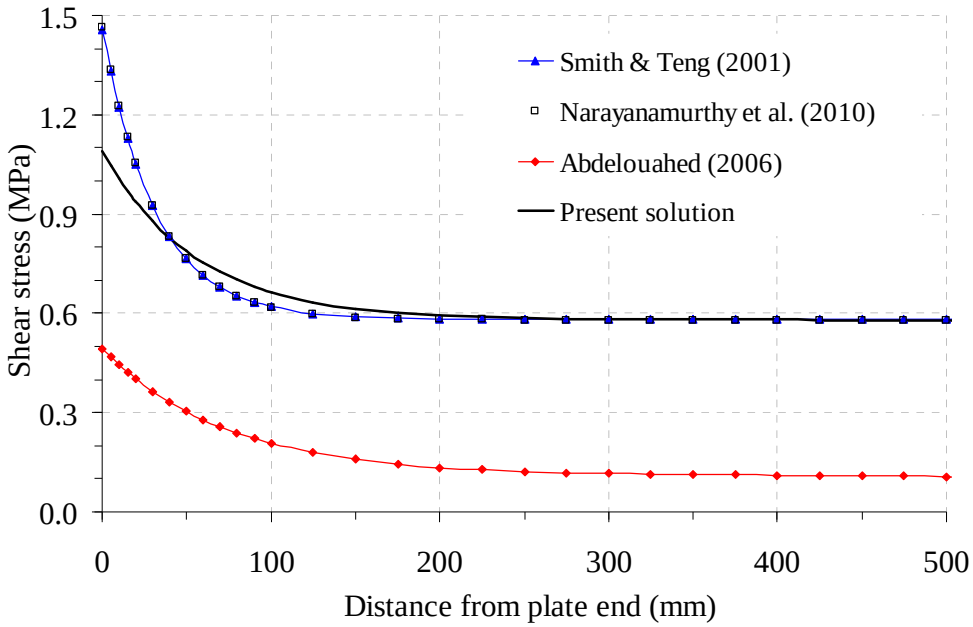

(a) Interfacial shear stress

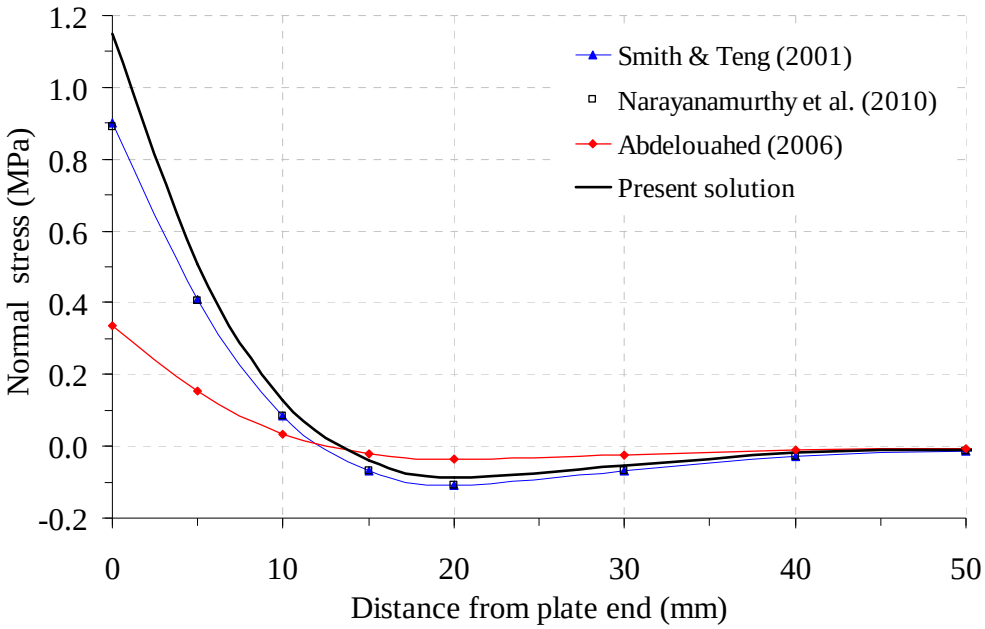

(b) Interfacial normal stress

Figure 3.5. Comparison of analytical solutions for interfacial stresses in a steel plated rectangular RC beam subjected to four point bending

Abdelouahed (2006) predicts much lower interfacial shear stress compared with all the other solutions. If the plane section assumption at the mid-span of the beam is satisfied, the tensile stress in the plate at the mid-span must be the same for all the solutions. Equilibrium requires that the integral of the interfacial shear stress from the plate end to mid-span of the beam (the area under the curve in Figure 3.5a) must be the same for all solutions and equal the tensile force in the plate at the mid-span. Abdelouahed's (2006) solution is erroneous probably due to the adopted assumption that shear stresses vary linearly through the depth of the adherends in a plated beam. Note that this assumption does not satisfy equilibrium.

It may be noted that the effect of shear deformations in the adherends are totally neglected in all the three previous solutions compared here in determining the interfacial normal stress. So only the present solution has captured this effect by a reasonable approximation in interfacial shear stress and accurately using Timoshenko's beam theory in interfacial normal stress in a closed-form, although the prediction of the former does influence the latter.

3.9 Parametric Study

The effects of various geometric and material parameters such as the elastic modulus of adhesive layer E_a, adhesive thickness t_a, plate material, its length L_p and thickness t_2 and beam thickness t_1 on the interfacial stresses are analysed. In this parametric study, only one of these parameters to be studied is varied while the applied load and all other parameters remain unchanged from those of the reference beam analysed in the preceding section. Figure 3.6 shows that the peak interfacial stresses are significantly affected by the magnitude of E_a: they are smaller for softer adhesives. Figure 3.7 depicts the peak interfacial shear stresses $\tau(x)$ and peak interfacial normal stresses $\sigma(x)$ predicted from Narayanamurthy et al. (2010), Smith and Teng (2001) and the present solution for different values of E_a. The predictions of the former two solutions agree well – they increase at a higher rate with E_a compared to the present solution. This may be explained as follows. The interfacial shear stress $\tau(x)$ is directly proportional to the integration constant B_1 (see Eq. 3.56). The effect of shear deformation in the adherends is reflected in α which reduces when E_a increases. On the other hand, the peak $\sigma(x)$ from the present solution is always higher than Narayanamurthy et al. (2010) and Smith and Teng (2001) and this difference reduces gradually with the increase in E_a.

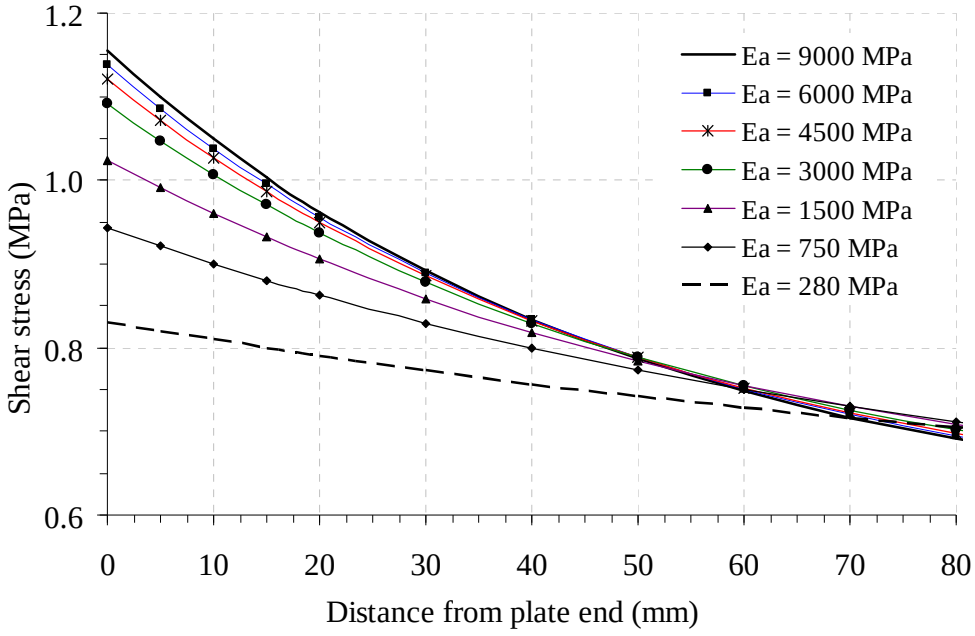

(a) Interfacial shear stress

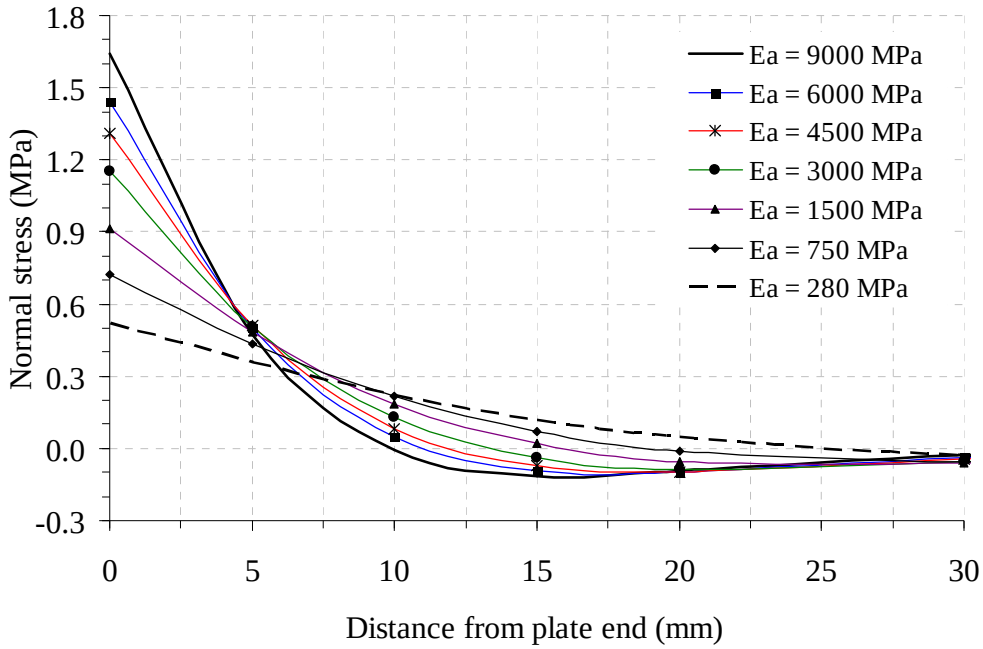

(b) Interfacial normal stress

Figure 3.6. Effect of elastic modulus of adhesive layer on interfacial stresses in steel plated RC beam subjected to four point bending

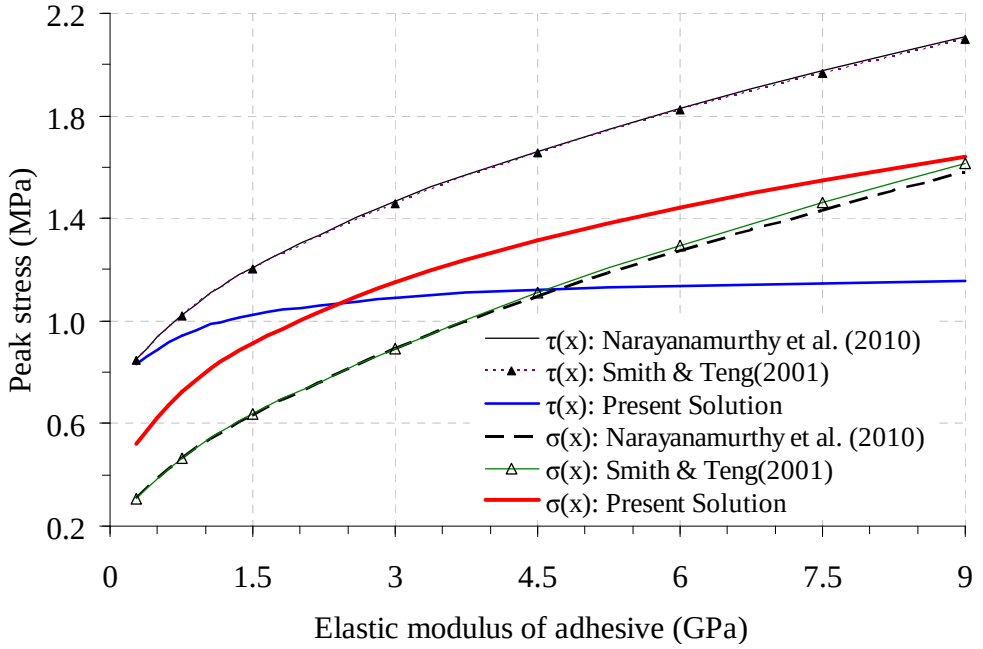

Figure 3.7. Effect of elastic modulus of adhesive layer on peak interfacial stresses in a steel plated RC beam subjected to four point bending

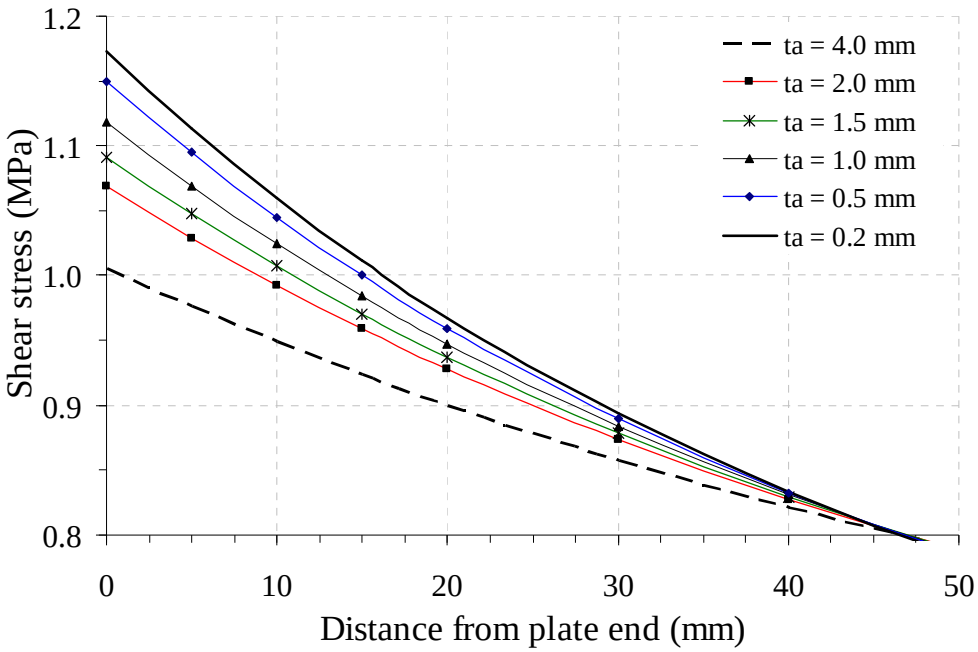

(a) Interfacial shear stress

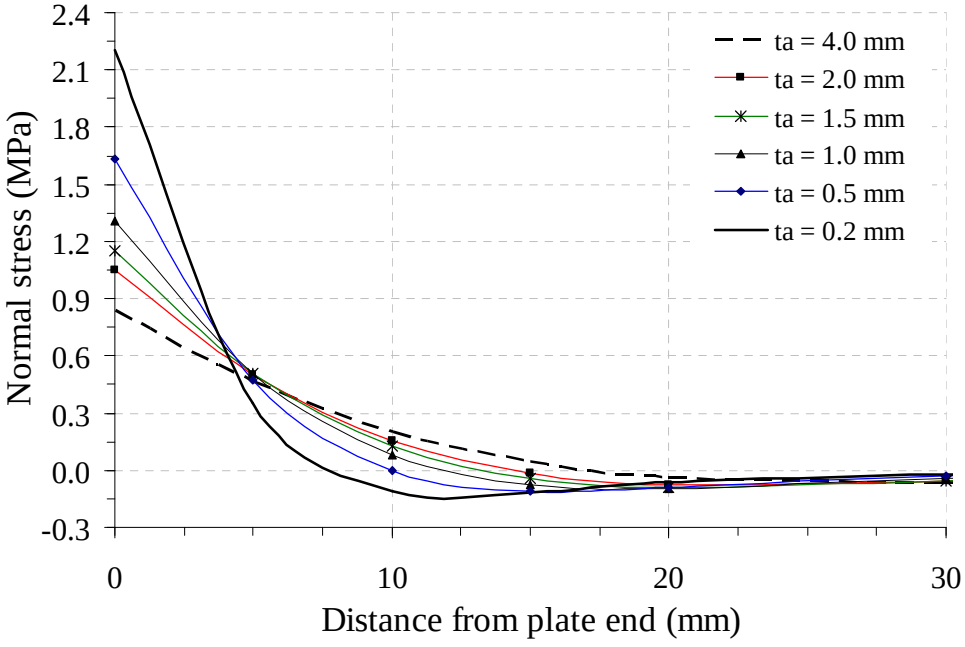

(b) Interfacial normal stress

Figure 3.8. Effect of adhesive thickness on interfacial stresses in a steel plated RC beam under four point bending

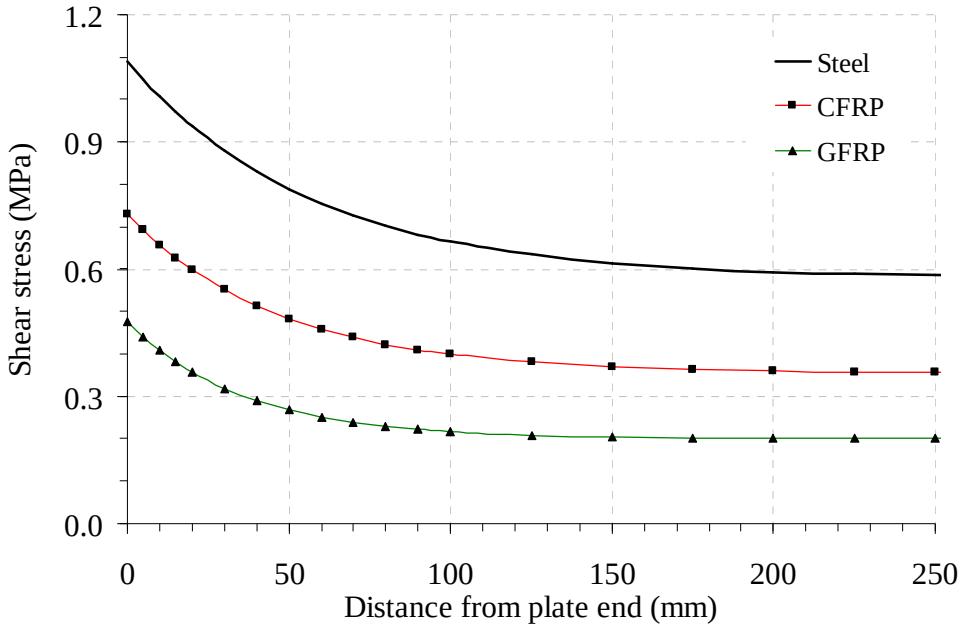

(a) Interfacial shear stress

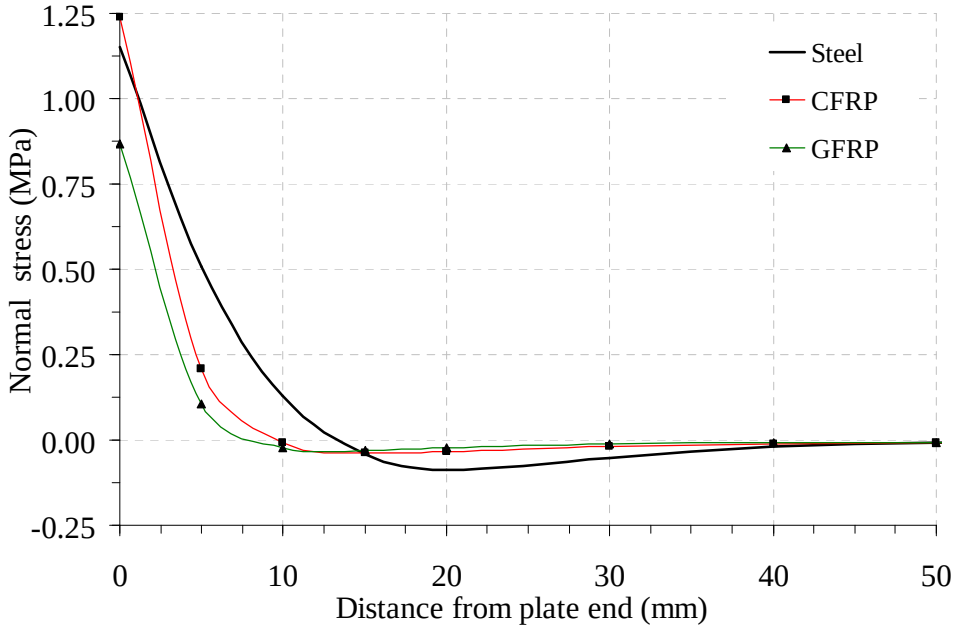

(b) Interfacial normal stress

Figure 3.9. Effect of plate material on interfacial stresses in a steel plated RC beam under four point bending

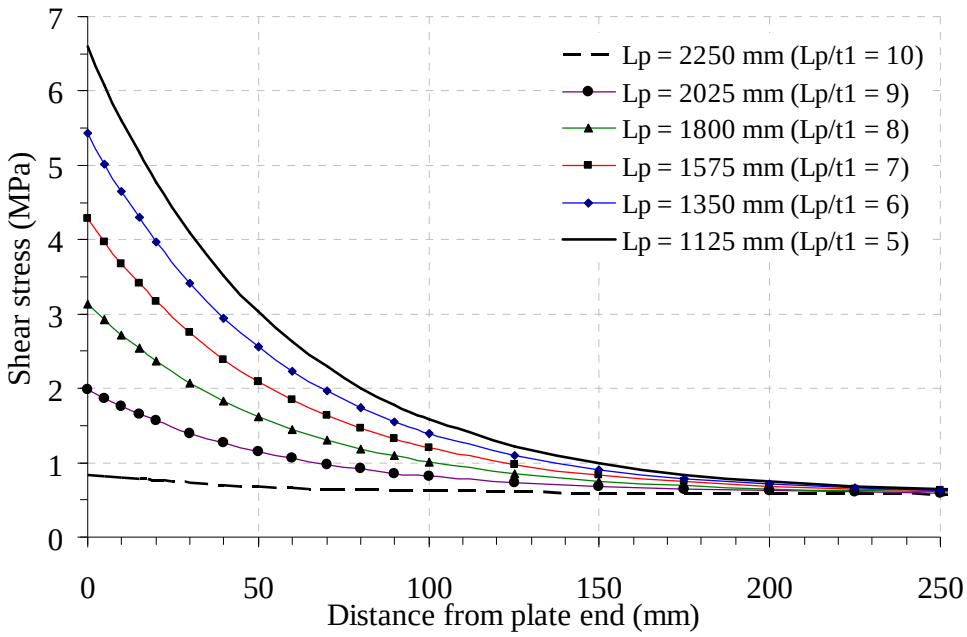

(a) Interfacial shear stress

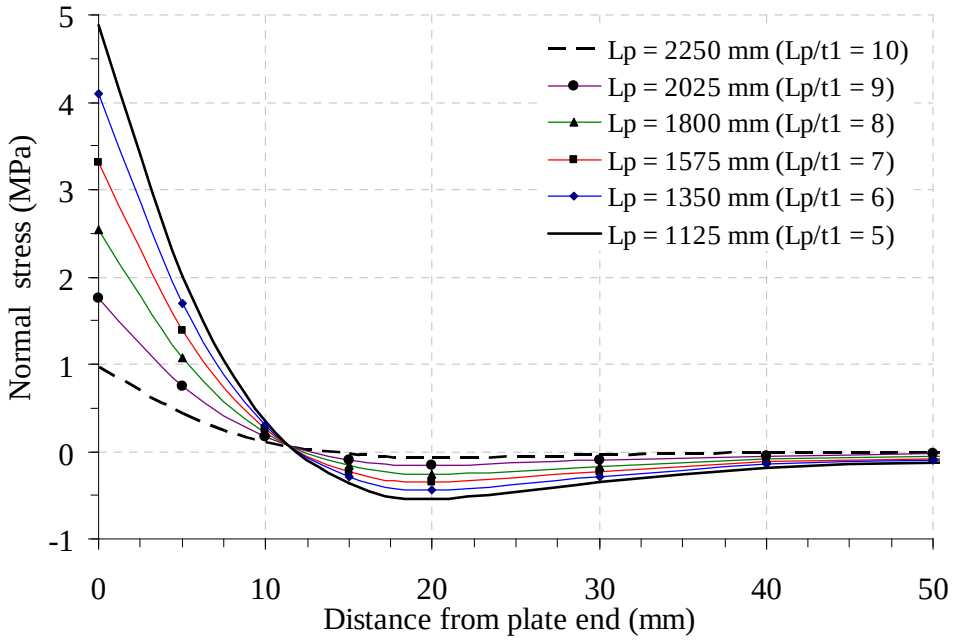

(b) Interfacial normal stress

Figure 3.10. Effect of plate length on interfacial stresses in a steel plated RC beam under four point bending

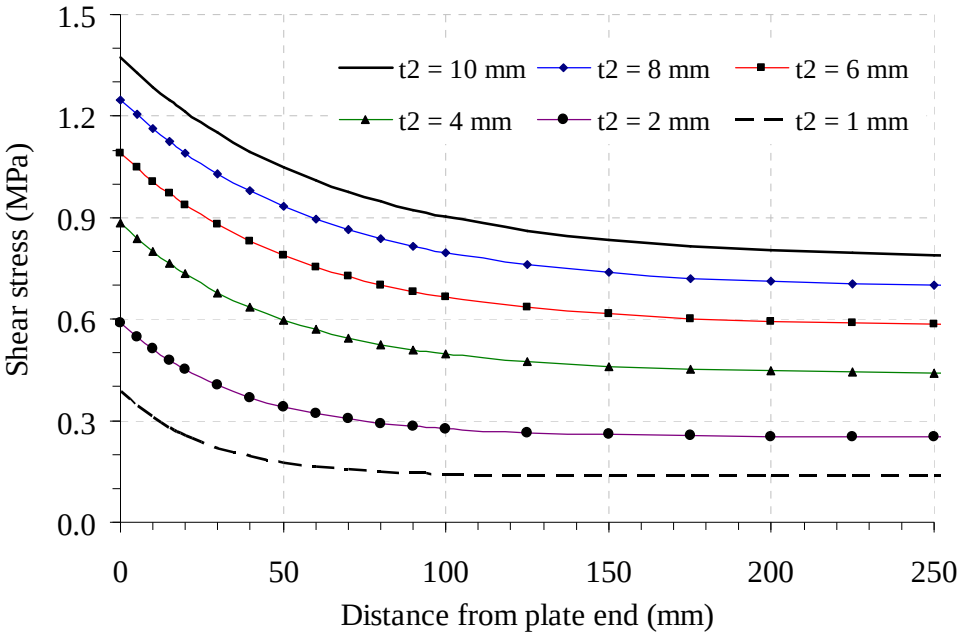

(a) Interfacial shear stress

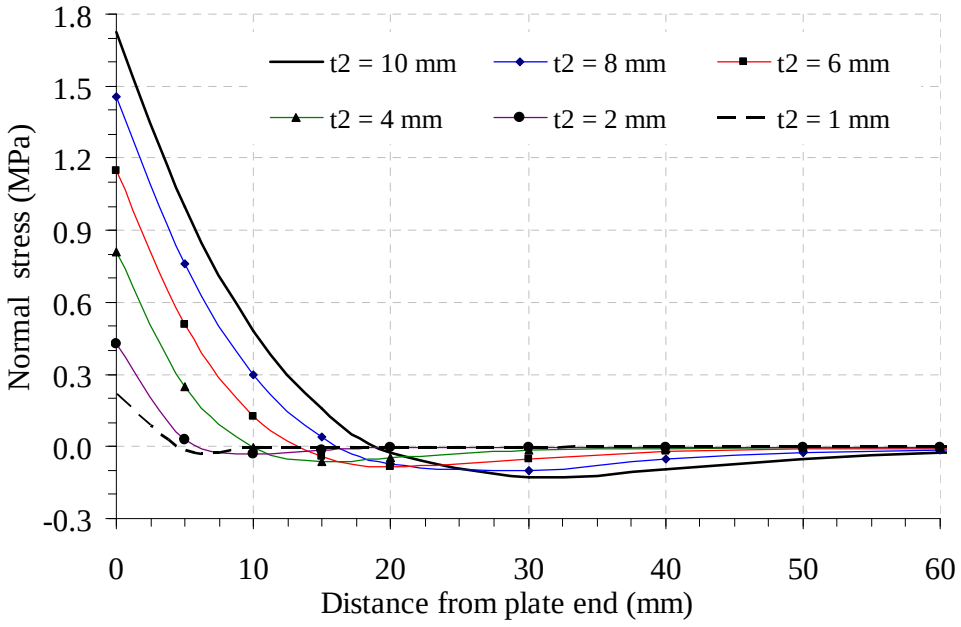

(b) Interfacial normal stress

Figure 3.11. Effect of plate thickness on interfacial stresses in a steel plated RC beam under four point bending

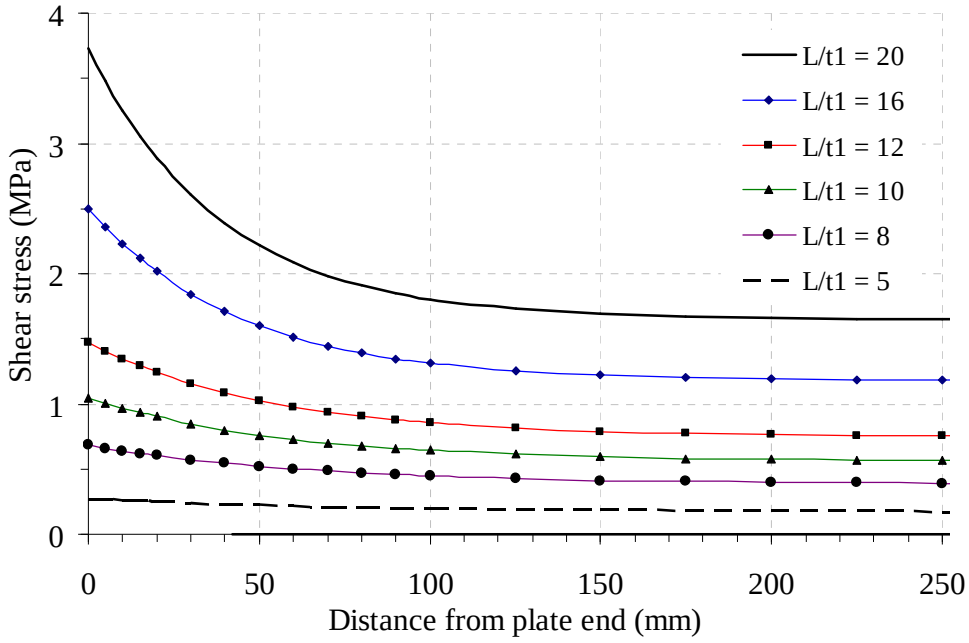

(a) Interfacial shear stress

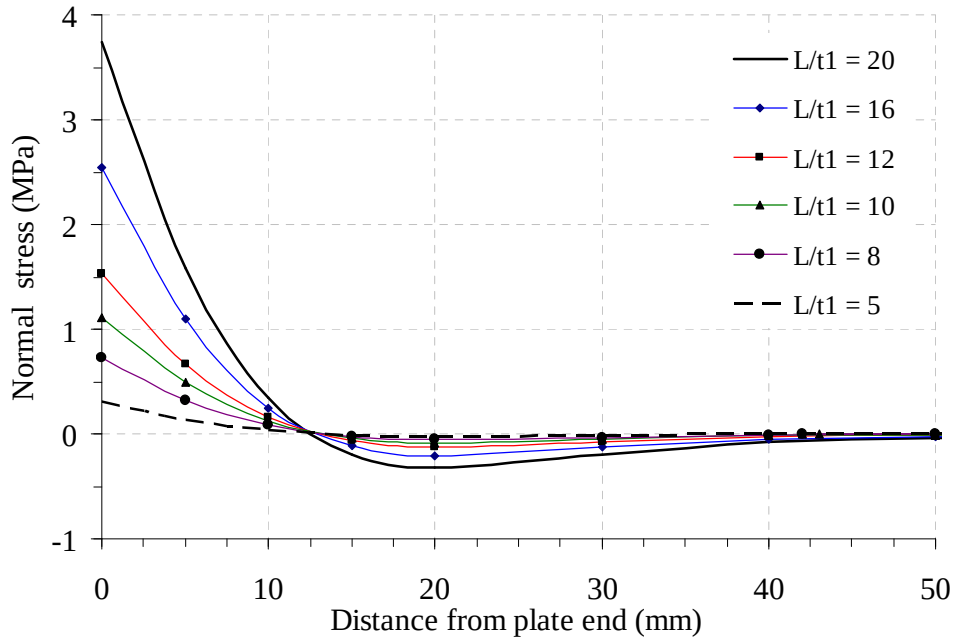

(b) Interfacial normal stress

Figure 3.12. Effect of span-to-depth ratio of beam on interfacial stresses in a steel plated RC beam under four point bending

Figure 3.8 shows the variation of interfacial stresses for different thicknesses of the adhesive layer. Higher interfacial stresses are found for a thinner adhesive layer. Figure 3.9 shows that typical GFRP, CFRP and steel plates produce interfacial shear stresses in

an increasing order. The peak interfacial normal stress in CFRP plated RC beam is higher than that in the steel and GFRP plated beams (Figure 3.9b). This is very different from the trends seen in their influence on the interfacial shear stress (Figure 3.9a) and is attributed to the influence of shear deformation in plates particularly with low shear modulus and higher elastic modulus. The termination position of the plate can significantly affect the interfacial stresses. When the plate is terminated far away from the support (with a smaller plate length-to-beam depth ratio L_p/t_1 in Figure 3.10), the interfacial stresses increase because of an increase of bending moment at the plate end section. The effect of soffit plate thickness on the interfacial stresses is shown in Figure 3.11. An increase in plate thickness increases the interfacial stresses. When the beam depth is reduced (the span-to-depth ratio L/t_1 is increased in Figure 3.12), the interfacial stresses increases because the relative stiffness of the plate to beam increases.

3.10 Conclusions

A closed-form plane stress solution for interfacial shear and normal stresses in plated beams including the effect of axial, bending and shear deformations in adherends has been presented in this chapter. The solution is based on the principle of superposition and deformation compatibility between the adherends considering invariant stresses through the thickness of the adhesive layer. The effect of shear deformations in the adherends on interfacial shear stress is included by assuming that shear stress varies in a parabolic manner through the depth of the beam and the plate. Its effect on interfacial normal stress is included through Timoshenko's beam theory. The present solution represents the first closed-form solution to consider the effect of shear deformation on both interfacial stresses applicable to plated beams made of any linear elastic structural material with any prismatic beam cross section under a general arbitrary loading arrangement. The results from an example plated beam have shown that the shear deformation in the adherends may significantly reduce the interfacial shear stress and increase the interfacial normal (peeling) stress at the plate ends. The parametric study shows the influence of different geometric and material properties of the plated beam on interfacial stresses. This study offers a more accurate and complete estimate of the interfacial normal and shear stress distribution in plated beams.

3.11 Notation

The following symbols are used in this chapter.

A = cross-sectional area of the adhesive or adherends;

b = width of the adhesive or adherends;

b_{1n} = width of beam section at its neutral axis;

E = modulus of elasticity of the adhesive or adherends;

G = shear modulus of the adhesive;

I = second moment of area of the adhesive or adherends about their centroidal axis;

I_{1c}, I_{ac}, I_{2c} = second moment of area of beam, adhesive and plate section respectively about the centroidal axis of the composite beam section;

I_e = second moment of area of the equivalent composite beam section about its centroidal axis;

L = length of the adhesive or adherends;

L_p = length of the plate;

M = bending moment in the adherends;

$M(0), M(L_p)$ = bending moment in plated beam at x=0 and x=L_p under original loading ignoring the effects of plate end loading (Case-2);

$M_1(0), M_1(L_p)$ = bending moment in beam at x=0 and x=L_p in Case-3 loading;

$M_T(x)$ = total applied bending moment at any section of the plated beam;

N = axial force in the adherends;

$N(x)$ = resultant axial force resisted by any section of the adherends;

$Q_e(x,y)$ = first moment of area of equivalent adhesive or plate section about the centroidal axis of the composite beam section;

$Q_i(x,y)$ = first moment of area of adherend's section about its centroidal axis;

R_a, R_b, R_{ab} = axial stiffness and bending stiffness ratio of plate to beam respectively;

R_{ab} = ratio between axial stiffness of plate and bending stiffness of beam;

R_{ma}, R_{m2} = modular ratio of adhesive and plate respectively to beam;

t = thickness of the adhesive or adherends;

u = longitudinal displacement of the adherends;

$u_{ib}(x)$ = longitudinal displacement of the adherents due to the bending moments;

$u_{im}(x)$ = longitudinal displacement of the adherents due to the membrane forces;

v = vertical displacement of the adherends;

$V(x)$ = shear force at any section of adherends;

$V_{Tc}(x)$ = total applied shear force at any section of the composite beam;

V_T = total shear force at any section of the plated beam in Case-3 loading;

y_c = vertical distance from top of the beam to the centroid of the composite beam section;

y_b = vertical distance from top of the beam to its centroid;

y_1, y_2 = vertical distance from bottom of the beam and top of the plate to their respective centroids respectively;

$_{pl,\, pr}$ = subscripts referring respectively to the left and right end of the plate;

$_{1,\, a,\, 2}$ = subscripts referring respectively to the beam, adhesive and plate;

κ_i = Timoshenko's shear coefficient;

$\sigma(x)$ = interfacial normal stress at any section of the plated beam;

$\sigma_i(x,y)$ = longitudinal normal stress in the adherends;

$\tau(x)$ = interfacial shear stress at any section of the plated beam;

$\tau_{in}(x)$ = shear stress at neutral axis of beam/plate section from beam theory;

γ_{xy} = engineering shear strain at the adhesive layer;

$\varepsilon_1(x), \varepsilon_2(x)$ = longitudinal strain at bottom layer of beam and at top layer of plate respectively;

$\varepsilon_{ib}(x)$ = strain induced in adherends due to the bending moments;

$\varepsilon_{im}(x)$ = strain induced in adherends due to the axial(membrane) forces; and

$m_c(y)$; r_1-r_7; λ_n, α, λ, m_1, r_8-r_9; β_1, β_2, n_2; δ; η_1-η_5, n_3-n_9; V_{Tm}, n_{2m}; n_{10}-n_{11}; and n_{12} -n_{13} = parameters defined respectively in Eqs 3.16; 3.54b-d; 3.55b-g; 3.62b-d; 3.63; 3.66a-e; 3.82b-c; 3.95a; and 3.103a.

Chapter 4

Rigorous Closed-Form Solution for Interfacial Stresses

Abstract

A significant increase in strength and performance of reinforced concrete (RC), timber and metallic beams may be achieved by adhesively bonding a fibre reinforced polymer (FRP) composite, or metallic such as steel plate to the tension face of a beam. One of the major failure modes in these plated beams is the debonding of the plate from the original beam in a brittle manner well before the flexural capacity of the plated beam is reached. This is commonly attributed to the interfacial shear and normal stresses between the adherends whose quantification has led to the development of many analytical solutions over the last two decades. The adherends are subjected to axial, bending and shear deformations under external loading in such plated beams. However, most analytical solutions have neglected the effect of the shear deformation of the adherends. For the few solutions which consider this effect in an approximate manner, they are limited to one or two specific loading conditions. This chapter presents a more rigorous analytical solution for predicting the interfacial stresses in plated beams under an arbitrary loading with the shear deformation of the adherends duly considered in closed form using Timoshenko's beam theory. The solution is general to arbitrary prismatic beam cross section linear elastic beams bonded with any thickness plate either symmetrically or asymmetrically to the beam and arbitrary loading.

4.1 Introduction

Reinforced concrete (RC), metallic or timber beams may be strengthened by adhesively bonding a fibre reinforced polymer (FRP) composite, steel or other metal soffit plate (Figure 4.1). Such a strengthened beam is commonly termed as a plated beam. This strengthening technique, especially the FRP strengthening technique, has become widely accepted in structural engineering for retrofitting and rehabilitation of existing structures. Under external loading, forces transfer between beam and plate, generating interfacial shear and normal stresses in the adhesive layer between the adherends. Their concentration is highest at the plate ends due to the presence of geometric discontinuity and their combination is believed to be responsible for the common brittle debonding failure well before the full flexural strength of the plated beam is reached.

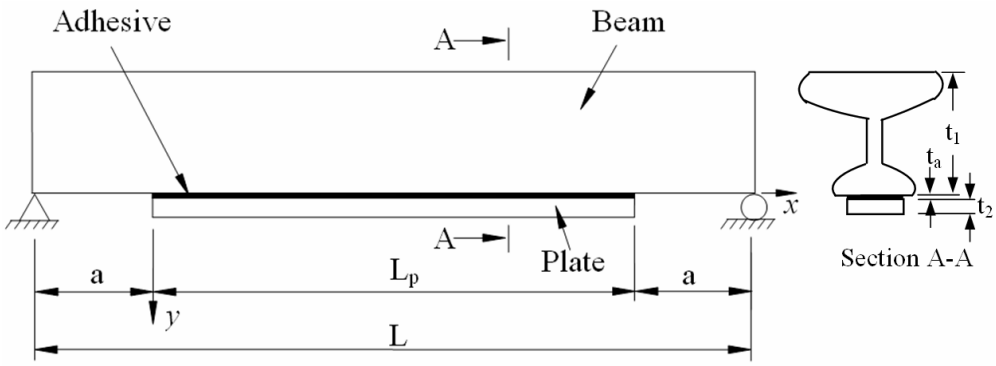

Figure 4.1. Plated beam

Consequently, the interfacial stresses between the plate and the original beam have attracted a great interest in the last two decades and many analytical solutions such as Vilnay (1988), Roberts (1989), Roberts and Haji-Kazemi (1989), Liu and Zhu (1994), Taljsten (1997), Malek et al. (1998), Rabinovich and Frostig (2000), Smith and Teng (2001), Shen et al. (2001), Deng et al. (2004), Yang et al. (2004, 2009), Stratford and Cadei (2006), De Lorenzis (2006), Abdelouahed (2006), Yang and Wu (2007), Narayanamurthy et al. (2010) and Zhang and Teng (2010a) have been developed to quantify them. All but a few (Rabinovich and Frostig, 2000; Shen et al., 2001; Yang et al., 2004, 2009) of these solutions assume invariant stresses through the thickness of the adhesive layer. Among them, Smith and Teng (2001) is simple, accurate and most popular. All solutions are applicable only for one or a few specific loading conditions except Narayanamurthy et al. (2010) and Zhang and Teng (2010a) which are applicable

for any loading arrangements and are simpler than and retain the accuracy of Smith and Teng (2001).

To the best knowledge of the author, only three solutions (Abdelouahed, 2006; Yang and Wu, (2007); and Narayanamurthy et al., 2009) included the effect of shear deformation of the adherends. Abdelouahed (2006) (applicable for UDL and single point loads) and Yang and Wu (2007) (applicable for UDL) included the shear deformation effect approximately only in the solution of interfacial shear stress. Their solutions suggest that the effect of shear deformation is more predominant on interfacial shear stress and negligible on interfacial normal stress but this is not necessarily correct in light of the present solution and finite element predictions. Narayanamurthy et al. (2009) (applicable for all loading arrangements) included the effect of shear deformation approximately on the interfacial shear stress and using Timoshenko's beam theory in deriving the interfacial normal stress. This is the first closed-form solution that includes the effects of adherend's shear deformation on both interfacial shear and normal stresses. Although the formulation for interfacial normal stress is accurate, its accuracy is compromised due to the approximation involved in interfacial shear stress. These three solutions adopted different approximate methods to overcome mathematical difficulties in arriving at the general solutions. The actual effect of adherend's shear deformation is not yet clearly understood.

The solution presented in this chapter is based on the principle of superposition and includes the simultaneous effect of axial, bending and shear deformation of the adherends on both interfacial shear and normal stresses in closed-form using Timoshenko's beam theory. The coupled governing differential equations of interfacial shear and normal stresses are solved and the general solutions are obtained by employing the appropriate conditions of plated beam. The solution is also general in nature, applicable to any linear elastic plated beams, with any prismatic beam cross sections, plate bonded symmetrically or asymmetrically over the span of the beam, and under any loading arrangements. The solution is compared with previous analytical solutions as well as finite element predictions for an example plated beam.

4.2 Assumptions

The following assumptions are employed in deriving the rigorous solution in this chapter:

a) the beam, adhesive and plate are linear elastic;
b) the shear and normal stresses through the thickness of the adhesive layer are constant although the shear stress variation is captured within the capability of the composite beam theory;
c) the curvature of the beam and the plate are the same when deriving the interfacial shear stress. This assumption is not used when deriving the interfacial normal stress;
d) there is no slip or separation between the beam and the adhesive and between the adhesive and the plate; and
e) the original beam and the plate are treated as two Timoshenko beams.

4.3 Methodology

Consider a simply supported beam symmetrically or asymmetrically strengthened with a soffit plate as in Figure 4.1. The plated beam under an arbitrary loading as shown in Case-1 (Figure 4.2) is decomposed into Case-2 and Case-3. Case-2 includes all the external loading in addition to an axial force, shear force and a bending moment at each end of the plate. The magnitude of these axial forces, shear forces and moments are determined from the deformation of the un-plated beam so that both ends of the plate deform compatibly with the un-plated beam under the external loading and the case can be analysed using the classical composite beam theory. Case-3 is the plated beam under the same but opposite plate end loading as in Case-2. The combined solution from Cases 2 and 3 gives the solution for the original problem in Case-1.

Let the axial and bending stiffness ratios of the plate to the beam be R_a and R_b respectively and the ratio between the axial stiffness of the plate and the bending stiffness of the beam be R_{ab} which are given as

$$R_a = \frac{E_2 A_2}{E_1 A_1}; \qquad R_b = \frac{E_2 I_2}{E_1 I_1}; \qquad R_{ab} = \frac{E_2 A_2}{E_1 I_1} \tag{4.1}$$

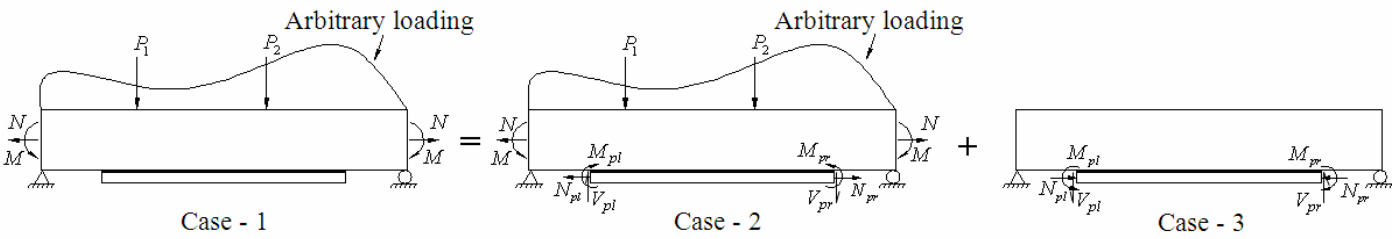

Figure 4.2. Principle of superposition in interfacial stress analysis of plated beam

The axial force N, shear force V and bending moment M at the plate ends for the composite beam in Case-2 (Figure 4.2) are given as:

$$N_{pl} = M(0)(y_1 + t_a + y_2)R_{ab} + NR_a \tag{4.2}$$

$$N_{pr} = M(L_p)(y_1 + t_a + y_2)R_{ab} + NR_a \tag{4.3}$$

$$V_{pl} = \frac{E_2 b_2 t_2^2[2t_2 + 3(t_1 + t_a - y_c)]}{6E_1 I_e} V(0) \tag{4.4}$$

$$V_{pr} = \frac{E_2 b_2 t_2^2[2t_2 + 3(t_1 + t_a - y_c)]}{6E_1 I_e} V(L_p) \tag{4.5}$$

$$M_{pl} = M(0)R_b \tag{4.6}$$

$$M_{pr} = M(L_p)R_b \tag{4.7}$$

where subscripts *pl* and *pr* refer respectively to the left and right plate ends; subscripts 1, *a* and 2 respectively refer to the original beam (adherend-1), adhesive and plate (adherend-2); $M(0)$, $M(L_p)$, $V(0)$ and $V(L_p)$ denote the bending moments and shear forces at $x=0$ and $x=L_p$ respectively on the beam under only the original loading; E, A, I, I_e, b and t refer to the elastic modulus, cross sectional area, second moment of area about the centroid of the concerned adherend, equivalent second moment of area of the composite beam section, breadth and thickness respectively; and y_1 and y_2 are the distances from the bottom of the adherend-1 (the original beam) and the top of the adherend-2 (the plate) to their respective centroids and y_c be the distance of the centroid of the composite beam section from the top surface.

4.4 Solution for the Composite Beam (Case-2)

As noted earlier the interfacial stresses in Case-2 can be obtained using the classical composite beam analysis. The equivalent second moment of area of the composite beam section is given by

$$I_e = I_{1c} + I_{ac} + I_{2c} \tag{4.8}$$

where I_{1c}, I_{ac} and I_{2c} are the equivalent second moment of area of the original beam, adhesive and plate sections respectively about the centroid of the composite beam section:

$$I_{1c} = I_1 + A_1\left[y_c - (t_1 - y_1)\right]^2 \tag{4.9}$$

$$I_{ac} = \left[\frac{b_a {t_a}^3}{12} + b_a t_a (t_1 + 0.5t_a - y_c)^2\right] R_{ma} \tag{4.10}$$

$$I_{2c} = \left[\frac{b_2 {t_2}^3}{12} + b_2 t_2 (t_1 + t_a + y_2 - y_c)^2\right] R_{m2} \tag{4.11}$$

in which y_c and the modular ratios R_{ma} and R_{m2} are given by

$$y_c = \frac{A_1(t_1 - y_1) + R_{ma} b_a t_a (t_1 + 0.5t_a) + R_{m2} b_2 t_2 (t_1 + t_a + y_2)}{A_1 + R_{ma} b_a t_a + R_{m2} b_2 t_2} \tag{4.12}$$

$$R_{ma} = \frac{E_a}{E_1}; \qquad R_{m2} = \frac{E_2}{E_1} \tag{4.13}$$

Considering a point in the adhesive layer with distance y from the beam to adhesive interface (so y ranges from 0 to t_a within the adhesive), the first moment of area of the equivalent plate and adhesive section below the considered position about the centroid of the composite beam section is given by

$$Q_e(y) = R_{m2} b_2 t_2 \left[t_1 + t_a + y_2 - y_c\right] + R_{ma} b_2 (t_a - y)\left[t_1 + 0.5(t_a + y) - y_c\right] \tag{4.14}$$

The shear stress at the considered position within the adhesive layer is thus

$$\tau(x, y) = m_c(y) V_{Tc}(x) \tag{4.15}$$

where $V_{Tc}(x)$ is the total shear force on the composite beam section at a distance x from the left plate end due to all the loading in Case-2 and

$$m_c(y) = \frac{Q_e(y)}{I_e b_2} \tag{4.16}$$

The interfacial normal stress from this theory is zero: $\sigma(x) \approx 0$.

4.5 Governing Differential Equations for Case-3

The governing differential equations for the interfacial shear and normal stresses between the adherends for the plated beam shown in Case-3 (Figure 4.2) are derived in this section.

4.5.1 Interfacial shear stress

The moment in the beam and the plate can be related assuming curvature compatibility between them:

$$R_b M_1(x) = M_2(x) \tag{4.17}$$

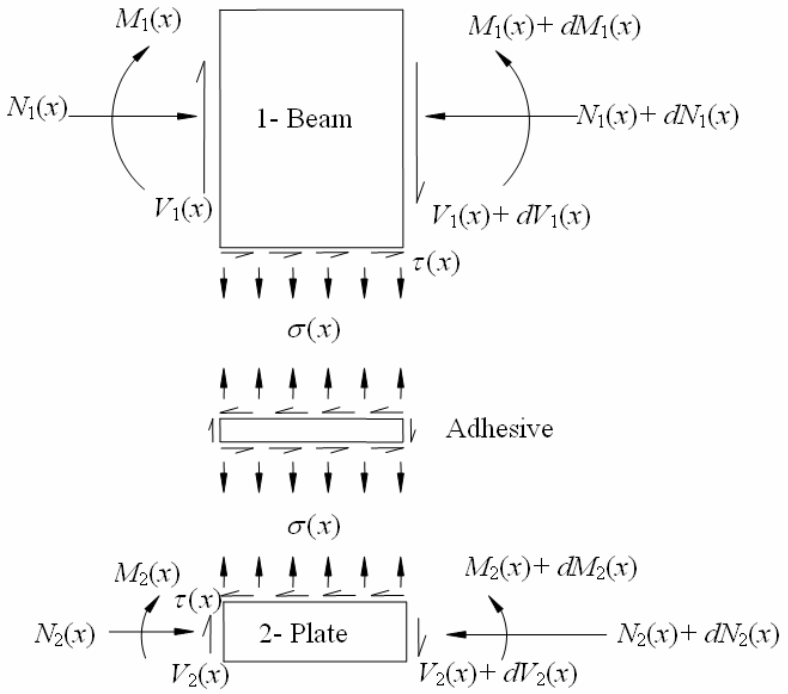

Figure 4.3. Differential segment of a plated beam

Longitudinal equilibrium of a differential segment of the plated beam as shown in Figure 4.3 gives

$$-\frac{dN_1(x)}{dx} = b_2\tau(x) = \frac{dN_2(x)}{dx} \tag{4.18}$$

where $\tau(x)$ is the interfacial shear stress between the adherends.

Eq. 4.18 and axial equilibrium of the left part of the structure gives

$$N_{pl} - N_{pr} - N_1(x) = b_2 \int_0^x \tau(x)dx = N_2(x) + N_{pl} \tag{4.19}$$

The total shear force $V_T(x)$ and total applied moment $M_T(x)$ at any section of the plated beam as obtained from plate end loadings in Figure 4.2 are

$$V_T(x) = \frac{1}{L}\left[M_{pl} - M_{pr} - (V_{pl} + V_{pr})a + (N_{pl} - N_{pr})(t_a + y_2)\right] = V_T \tag{4.20}$$

$$M_T(x) = V_{pl}a + V_T(a + x) - M_{pl} - N_{pl}(t_a + y_2) - N_{pr}(t_1 - y_c); \qquad 0 \le x \le L_p \tag{4.21}$$

$M_T(x)$ can also be expressed as a function of the adherend moments, interfacial shear stress and plate end axial forces and using Eq. 4.19 as

$$M_T(x) = M_1(x) + M_2(x) + (b_2 \int_0^x \tau(x)dx - N_{pl})(y_1 + t_a + y_2) + N_{pr}(y_c - t_1 + y_1) \tag{4.22}$$

From Eqs 4.17 and 4.22 the bending moment in each adherend can be found as

$$M_i(x) = \frac{E_i I_i}{E_1 I_1 + E_2 I_2}\left[M_T(x) - (b_2 \int_0^x \tau(x)dx - N_{pl})(y_1 + t_a + y_2) - N_{pr}(y_c - t_1 + y_1)\right] \tag{4.23}$$

where subscript i = 1, 2 refer respectively to adherend-1 and adherend-2.

The first derivative of Eq. 4.23 relates the bending moment in each adherend to the total shear force:

$$\frac{dM_i(x)}{dx} = \frac{E_i I_i}{E_1 I_1 + E_2 I_2}\left[V_T(x) - b_2(y_1 + t_a + y_2)\tau(x)\right]; \;\; i = 1, 2 \tag{4.24}$$

The longitudinal strain at the bottom of adherend-1 $\varepsilon_1(x)$ and at the top of adherend-2 $\varepsilon_2(x)$ are

$$\varepsilon_i(x) = \frac{du_i(x)}{dx} = (-1)^{i+1}\frac{y_i}{E_i I_i}M_i(x) + \frac{1}{E_i A_i}N_i(x) + \frac{y_i}{G_i A_i \kappa_i}b_2\sigma(x); \;\; i = 1, 2 \tag{4.25}$$

where κ is the Timoshenko's shear coefficient (κ = 5/6 for rectangular sections; 5/12 for hollow thin walled square sections, etc,), G is the transverse shear modulus of the adherends and $\sigma(x)$ is the interfacial normal stress.

Based on the theory of elasticity, the shear stress in the adhesive layer can be found from

$$\tau(x) = G_a\left[\frac{du(x,y)}{dy} + \frac{dv(x,y)}{dx}\right] \tag{4.26}$$

where G_a is the shear modulus of adhesive and $u(x,y)$ and $v(x,y)$ are the horizontal and vertical displacement in the adhesive layer.

The first derivative of Eq. 26 with respect to x (w.r.t.x) is

$$\frac{d\tau(x)}{dx} = G_a\left[\frac{d^2u(x,y)}{dxdy} + \frac{d^2v(x,y)}{dx^2}\right] \tag{4.27}$$

Applying the moment-curvature relation for a differential segment of the plated beam yields

$$\frac{d^2v(x,y)}{dx^2} = -\frac{1}{E_1 I_e} M_T(x) \tag{4.28}$$

The shear stress is assumed to be uniform through the thickness of the adhesive layer in Case-3. Hence, $u(x,y)$ varies linearly across t_a giving

$$\frac{du(x,y)}{dy} = \frac{1}{t_a}\left[u_2(x) - u_1(x)\right] \tag{4.29}$$

The first derivative of this equation w.r.t.x is

$$\frac{d^2u(x,y)}{dxdy} = \frac{1}{t_a}\left[\frac{du_2(x)}{dx} - \frac{du_1(x)}{dx}\right] \tag{4.30}$$

Substituting Eqs 4.28 and 4.30 into Eq. 4.27 gives

$$\frac{d\tau(x)}{dx} = \frac{G_a}{t_a}\left[\frac{du_2(x)}{dx} - \frac{du_1(x)}{dx}\right] - \frac{G_a}{E_1 I_e} M_T(x) \tag{4.31}$$

Substituting Eqs 4.22 and 4.25 into Eq. 4.31 yields

$$\frac{d\tau(x)}{dx} = \frac{G_a}{E_1}\left[-r_1 M_1(x) - r_2 M_2(x) - r_3 N_1(x) + r_4 N_2(x)\right] - \alpha_1 \sigma(x) \tag{4.32}$$

where

$$r_1 = \frac{y_1}{t_a I_1} + \frac{1}{I_e} \tag{4.32a}$$

$$r_2 = \frac{y_2}{t_a R_{m2} I_2} + \frac{1}{I_e} \tag{4.32b}$$

$$r_3 = \frac{1}{t_a A_1} - \frac{(y_c - t_1 + y_1)}{I_e} \tag{4.32c}$$

$$r_4 = \frac{1}{t_a R_{m2} A_2} - \frac{(t_1 + t_a + y_2 - y_c)}{I_e} \tag{4.32d}$$

$$\alpha_1 = \frac{G_a b_2}{t_a}\left[\frac{y_1}{G_1 A_1 \kappa_1} - \frac{y_2}{G_2 A_2 \kappa_2}\right] \tag{4.32e}$$

Differentiating Eq. 4.32 once w.r.t.*x* and substituting Eqs 4.18 and 4.24 into the resulting expression results in the governing differential equation for the interfacial shear stress:

$$\frac{d^2\tau(x)}{dx^2} - \lambda^2\tau(x) + m_1\lambda^2 V_T(x) + \alpha_1\frac{d\sigma(x)}{dx} = 0 \tag{4.33}$$

where

$$\lambda^2 = \frac{G_a b_2}{t_a}\left[\frac{(y_1+y_2)(y_1+t_a+y_2)}{(E_1I_1+E_2I_2)} + \frac{1}{E_1A_1} + \frac{1}{E_2A_2}\right] \tag{4.33a}$$

$$m_1 = \frac{G_a}{\lambda^2}\left[\frac{y_1+y_2}{t_a(E_1I_1+E_2I_2)} + \frac{1}{E_1I_e}\right] \tag{4.33b}$$

4.5.2 Interfacial normal stress

The interfacial normal stress exists between the adherends due to the existence of differential vertical displacement between them when the beam is loaded. Let the vertical displacements of adherends 1 and 2 be respectively $v_1(x)$ and $v_2(x)$, the interfacial normal stress $\sigma(x)$ can be found from

$$\sigma(x) = \frac{E_a}{t_a}[v_2(x) - v_1(x)] \tag{4.34}$$

The moment-curvature relation, moment and vertical equilibrium of the differential segment of adherends 1 and 2 (Figure 4.3) give the following relationships:

$$\frac{d^2v_i(x)}{dx^2} = -\frac{1}{E_iI_i}M_i(x) + (-1)^i\frac{b_2}{G_iA_i\kappa_i}\sigma(x); \qquad i = 1, 2 \tag{4.35}$$

$$\frac{dM_i(x)}{dx} = V_i(x) - b_2y_i\tau(x); \qquad i = 1, 2 \tag{4.36}$$

$$\frac{dV_i(x)}{dx} = (-1)^i b_2\sigma(x); \qquad i = 1, 2 \tag{4.37}$$

Differentiating Eq. 4.35 once w.r.t.*x* and substituting Eq. 4.36 into the resulting equation gives,

$$\frac{d^3v_i(x)}{dx^3} = -\frac{1}{E_iI_i}\left(V_i(x) - b_2y_i\tau(x)\right) + (-1)^i\frac{b_2}{G_iA_i\kappa_i}\frac{d\sigma(x)}{dx}; \qquad i = 1, 2 \tag{4.38}$$

Differentiating Eq. 4.38 once w.r.t.*x* and substituting Eq. 4.37 into the resulting equation gives,

$$\frac{d^4 v_i(x)}{dx^4} = (-1)^{i+1}\frac{b_2}{E_i I_i}\sigma(x) + (-1)^i \frac{b_2}{G_i A_i \kappa_i}\frac{d^2\sigma(x)}{dx^2} + \frac{b_2 y_i}{E_i I_i}\frac{d\tau(x)}{dx}; \qquad i = 1, 2 \tag{4.39}$$

Differentiating Eq. 4.34 four times w.r.t.*x* and substituting Eq. 4.39 into the resulting equation yields the following governing differential equation for the interfacial normal stress:

$$\frac{d^4\sigma(x)}{dx^4} - \beta_1\frac{d^2\sigma(x)}{dx^2} + \beta_2\sigma(x) + n_2\frac{d\tau(x)}{dx} = 0 \tag{4.40}$$

where

$$\beta_1 = \frac{E_a b_2}{t_a}\left[\frac{1}{G_1 A_1 \kappa_1} + \frac{1}{G_2 A_2 \kappa_2}\right] \tag{4.40a}$$

$$\beta_2 = \frac{E_a b_2}{t_a}\left[\frac{1}{E_1 I_1} + \frac{1}{E_2 I_2}\right] \tag{4.40b}$$

$$n_2 = \frac{E_a b_2}{t_a}\left[\frac{y_1}{E_1 I_1} - \frac{y_2}{E_2 I_2}\right] \tag{4.40c}$$

In Eq. 4.40, β_1 arose from Timoshenko's beam theory and reflects the effect of shear deformation. If $\beta_1 = 0$ it reduces to the governing equation for interfacial normal stress without considering shear deformation as in Narayanamurthy et al. (2010).

4.5.3 Uncoupling of governing differential equations

The governing differential equations for the interfacial shear and normal stresses [Eqs 4.33 and 4.40] are coupled and hence a general solution is not easily found. This coupling arises due to the introduction of the shear deformation effect in the adherends. To circumvent this difficulty, most previous researchers have neglected the shear deformation either from the beginning or at a late stage from the governing differential equations. A few others resorted to approximate methods or numerical techniques. A simple procedure is adopted here in uncoupling the governing equations which makes it possible to obtain closed-form solutions for the interfacial stresses.

Integrating Eq. 4.33 w.r.t.*x* gives,

$$\sigma(x) = \frac{1}{\alpha_1}\left(C - \frac{d\tau(x)}{dx} + \lambda^2\int\tau(x)dx - m_1\lambda^2\int V_T(x)dx\right) \tag{4.41}$$

where *C* is the constant of integration and vanishes in the subsequent operations.

Substituting the second and forth derivative of $\sigma(x)$ from Eq. 4.41 into Eq. 4.40 and differentiating the resulting expression once w.r.t.x yields an uncoupled GDE for the interfacial shear stress as

$$\frac{d^6\tau(x)}{dx^6} - \alpha_2 \frac{d^4\tau(x)}{dx^4} + \alpha_3 \frac{d^2\tau(x)}{dx^2} - \alpha_4\tau(x) + \alpha_5 V_T(x) = 0 \tag{4.42}$$

where

$$\alpha_2 = \beta_1 + \lambda^2 \tag{4.42a}$$

$$\alpha_3 = \beta_1\lambda^2 + \beta_2 - n_2\alpha_1 \tag{4.42b}$$

$$\alpha_4 = \beta_2\lambda^2 \tag{4.42c}$$

$$\alpha_5 = \beta_2 m_1\lambda^2 \tag{4.42d}$$

4.6 Boundary Conditions in Case-3

The boundary conditions available in Case-3 are:

$$M_1(x)\big|_{x=0} = \frac{a}{L}[(L-a)V_{pl} - aV_{pr} + M_{pl} - M_{pr} + (N_{pl} - N_{pr})(\frac{L}{a}y_1 + y_2 + t_a)] = M_1(0) \tag{4.43a}$$

$$M_2(x)\big|_{x=0} = -M_{pl} \tag{4.43b}$$

$$N_1(x)\big|_{x=0} = N_{pl} - N_{pr} \tag{4.43c}$$

$$N_2(x)\big|_{x=0} = -N_{pl} \tag{4.43d}$$

$$V_1(x)\big|_{x=0} = V_T + V_{pl} - b_2 t_a \tau(x)\big|_{x=0} \tag{4.43e}$$

$$V_2(x)\big|_{x=0} = -V_{pl} \tag{4.43f}$$

$$M_1(x)\big|_{x=L_p} = \frac{a}{L}[aV_{pl} - (L-a)V_{pr} - M_{pl} + M_{pr} - (N_{pl} - N_{pr})(y_2 + t_a)] = M_1(L_p) \tag{4.43g}$$

$$M_2(x)\big|_{x=L_p} = -M_{pr} \tag{4.43h}$$

$$N_1(x)\big|_{x=L_p} = 0 \tag{4.43i}$$

$$N_2(x)\big|_{x=L_p} = -N_{pr} \tag{4.43j}$$

$$V_1(x)\big|_{x=L_p} = V_T + V_{pr} - b_2 t_a \tau(x)\big|_{x=L_p} \tag{4.43k}$$

$$V_2(x)\big|_{x=L_p} = -V_{pr} \tag{4.43l}$$

4.7 General Solution for Interfacial Shear Stress for Case- 3

The governing equation for the interfacial shear stress given in Eq. 4.42 is a sixth order non-homogeneous ordinary differential equation and can be solved in closed-form. Its general solution can have the following two forms depending on the value of parameter Δ which depends on the material and geometric properties of the adherends and adhesive:

$$\Delta = \alpha_6^3 + \alpha_7^2 \tag{4.44}$$

$$\tau(x) = \left\{ \begin{array}{r} B_1 e^{\psi_1 x} + B_2 e^{-\psi_1 x} + e^{-\psi_2 x}\left(B_3 \cos(\psi_3 x) + B_4 \sin(\psi_3 x)\right) + \\ + e^{\psi_2 x}\left(B_5 \cos(\psi_3 x) + B_6 \sin(\psi_3 x)\right) + \alpha_{15} V_T \end{array} \right\} \quad \text{for } \Delta \geq 0 \tag{4.45}$$

$$\tau(x) = B_7 e^{\psi_4 x} + B_8 e^{-\psi_4 x} + B_9 e^{\psi_5 x} + B_{10} e^{-\psi_5 x} + B_{11} e^{\psi_6 x} + B_{12} e^{-\psi_6 x} + \alpha_{17} V_T \text{ for } \Delta < 0 \tag{4.46}$$

where B_1 to B_{12} are the constants of integration which can be determined from appropriate boundary conditions in Eq. 4.43. The expressions for α_6, α_7, ψ_1 to ψ_6 and other terms are given in Appendix A.

4.7.1 Determination of constants B_1 to B_{12}

The first three derivatives of Eq. 4.45 w.r.t.x are:

$$\frac{d\tau(x)}{dx} = \left\{ \begin{array}{l} \psi_1\left[B_1 e^{\psi_1 x} - B_2 e^{-\psi_1 x}\right] + \\ + e^{-\psi_2 x}\left[-(\psi_3 B_3 + \psi_2 B_4)\sin(\psi_3 x) + (\psi_3 B_4 - \psi_2 B_3)\cos(\psi_3 x)\right] + \\ + e^{\psi_2 x}\left[(\psi_2 B_6 - \psi_3 B_5)\sin(\psi_3 x) + (\psi_3 B_6 + \psi_2 B_5)\cos(\psi_3 x)\right] \end{array} \right\} \tag{4.47}$$

$$\frac{d^2\tau(x)}{dx^2} = \left\{ \begin{array}{l} \psi_1^2\left(B_1 e^{\psi_1 x} + B_2 e^{-\psi_1 x}\right) + e^{-\psi_2 x}\left(\begin{array}{l} [(\psi_2^2 - \psi_3^2)B_4 + 2\psi_2\psi_3 B_3]\sin(\psi_3 x) + \\ + [(\psi_2^2 - \psi_3^2)B_3 - 2\psi_2\psi_3 B_4]\cos(\psi_3 x) \end{array} \right) + \\ + e^{\psi_2 x}\left([(\psi_2^2 - \psi_3^2)B_6 - 2\psi_2\psi_3 B_5]\sin(\psi_3 x) + [(\psi_2^2 - \psi_3^2)B_5 + 2\psi_2\psi_3 B_6]\cos(\psi_3 x)\right) \end{array} \right\} \tag{4.48}$$

$$\frac{d^3\tau(x)}{dx^3} = \left\{ \begin{array}{l} \psi_1^3\left(B_1 e^{\psi_1 x} - B_2 e^{-\psi_1 x}\right) - e^{-\psi_2 x}\left(\begin{array}{l} [(3\psi_2^2 - \psi_3^2)\psi_3 \sin(\psi_3 x) - (3\psi_3^2 - \psi_2^2)\psi_2 \cos(\psi_3 x)]B_3 + \\ - [(3\psi_3^2 - \psi_2^2)\psi_2 \sin(\psi_3 x) + (3\psi_2^2 - \psi_3^2)\psi_3 \cos(\psi_3 x)]B_4 \end{array} \right) \\ - e^{\psi_2 x}\left(\begin{array}{l} [(3\psi_2^2 - \psi_3^2)\psi_3 \sin(\psi_3 x) + (3\psi_3^2 - \psi_2^2)\psi_2 \cos(\psi_3 x)]B_5 + \\ + [(3\psi_3^2 - \psi_2^2)\psi_2 \sin(\psi_3 x) - (3\psi_2^2 - \psi_3^2)\psi_3 \cos(\psi_3 x)]B_6 \end{array} \right) \end{array} \right\} \tag{4.49}$$

Differentiating Eq. 4.32 w.r.t.x and substituting Eqs 4.17, 4.18 and 4.24 into the resulting equation gives

$$\frac{d^2\tau(x)}{dx^2} = \frac{G_a}{E_1}\left[-m_2 V_T + m_3 b_2 \tau(x)\right] - \alpha_1 \frac{d\sigma(x)}{dx} \tag{4.50}$$

Differentiating Eq. 4.50 w.r.t.x gives

$$\frac{d^3\tau(x)}{dx^3} = \frac{G_a}{E_1} m_3 b_2 \frac{d\tau(x)}{dx} - \alpha_1 \frac{d^2\sigma(x)}{dx^2} \tag{4.51}$$

Applying Eqs 4.43a-4.43d and Eqs 4.43g-4.43j respectively to Eq. 4.32 provide

$$\left.\frac{d\tau(x)}{dx}\right|_{x=0} = \frac{G_a}{E_1}\left[-r_1 M_1(0) + r_2 M_{pl} - (r_3 + r_4) N_{pl} + r_3 N_{pr}\right] - \alpha_1 \sigma(0) \tag{4.52}$$

$$\left.\frac{d\tau(x)}{dx}\right|_{x=L_p} = \frac{G_a}{E_1}\left[-r_1 M_1(L_p) + r_2 M_{pl} - r_4 N_{pr}\right] - \alpha_1 \sigma(L_p) \tag{4.53}$$

Setting x=0 and x= L_p respectively in Eq. 4.47 and equating the results with Eqs 4.52 and 4.53 respectively yield

$$\psi_1(B_1 - B_2) - \psi_2(B_3 - B_5) + \psi_3(B_4 + B_6) = c_1 \tag{4.54}$$

$$m_9 B_1 - m_{10} B_2 - m_{11} B_3 + m_{12} B_4 + m_{13} B_5 + m_{14} B_6 = c_4 \tag{4.55}$$

Substituting Eq. 4.45 into Eq. 4.50, equating the result with Eq. 4.48 and setting x= 0 and x= L_p respectively give

$$m_4(B_1 + B_2) + m_5(B_3 + B_5) - 2\psi_2\psi_3(B_4 - B_6) = c_2 \tag{4.56}$$

$$m_{15} B_1 + m_{16} B_2 + m_{17} B_3 + m_{18} B_4 + m_{19} B_5 + m_{20} B_6 = c_5 \tag{4.57}$$

Substituting Eq. 4.47 into Eq. 4.51, equating the result with Eq. 4.49 and setting x= 0 and x= L_p respectively yield

$$m_6(B_1 - B_2) + m_7(B_3 - B_5) + m_8(B_4 + B_6) = c_3 \tag{4.58}$$

$$m_{21} B_1 - m_{22} B_2 - m_{23} B_3 + m_{24} B_4 - m_{25} B_5 - m_{26} B_6 = c_6 \tag{4.59}$$

Eqs 4.54-4.59 form a system of simultaneous equations as given below from which the integration constants B_1 to B_6 are determined:

$$\begin{bmatrix} \psi_1 & -\psi_1 & -\psi_2 & \psi_3 & \psi_2 & \psi_3 \\ m_4 & m_4 & m_5 & -2\psi_2\psi_3 & m_5 & 2\psi_2\psi_3 \\ m_6 & -m_6 & m_7 & m_8 & -m_7 & m_8 \\ m_9 & -m_{10} & -m_{11} & m_{12} & m_{13} & m_{14} \\ m_{15} & m_{16} & m_{17} & m_{18} & m_{19} & m_{20} \\ m_{21} & -m_{22} & -m_{23} & m_{24} & -m_{25} & -m_{26} \end{bmatrix} \begin{Bmatrix} B_1 \\ B_2 \\ B_3 \\ B_4 \\ B_5 \\ B_6 \end{Bmatrix} = \begin{Bmatrix} c_1 \\ c_2 \\ c_3 \\ c_4 \\ c_5 \\ c_6 \end{Bmatrix} \tag{4.60}$$

Adopting a similar procedure for Eq. 4.46 in consideration with Eqs 4.50-4.53 provides the following system of simultaneous equations from which the constants B_7 to B_{12} can be determined:

$$\begin{bmatrix} \psi_4 & -\psi_4 & \psi_5 & -\psi_5 & \psi_6 & -\psi_6 \\ p_1 & p_1 & p_2 & p_2 & p_3 & p_3 \\ \psi_4 p_1 & -\psi_4 p_1 & \psi_5 p_2 & -\psi_5 p_2 & \psi_6 p_3 & -\psi_6 p_3 \\ p_4 & -p_5 & p_6 & -p_7 & p_8 & -p_9 \\ p_{10} & p_{11} & p_{12} & p_{13} & p_{14} & p_{15} \\ \psi_4 p_{10} & -\psi_4 p_{11} & \psi_5 p_{12} & -\psi_5 p_{13} & \psi_6 p_{14} & -\psi_6 p_{15} \end{bmatrix} \begin{Bmatrix} B_7 \\ B_8 \\ B_9 \\ B_{10} \\ B_{11} \\ B_{12} \end{Bmatrix} = \begin{Bmatrix} c_1 \\ c_{2m} \\ c_3 \\ c_4 \\ c_{5m} \\ c_6 \end{Bmatrix} \tag{4.61}$$

Eqs 4.60 and 4.61 apply for all cases within the whole bond length of the plate. When only the interfacial stress near the plate end at x=0 is concerned, the positive exponential terms in Eqs 4.45 and 4.46 can be neglected for almost all practical plated beams so that $B_1 = B_5 = B_6 = B_7 = B_9 = B_{11} = 0$. This results in a simplified general solution from Eqs 4.45-4.46 as given by

$$\tau(x) = B_2 e^{-\psi_1 x} + e^{-\psi_2 x}\left(B_3 \cos(\psi_3 x) + B_4 \sin(\psi_3 x)\right) + \alpha_{15} V_T \qquad \text{for } \Delta \geq 0 \tag{4.62a}$$

$$\tau(x) = B_8 e^{-\psi_4 x} + B_{10} e^{-\psi_5 x} + B_{12} e^{-\psi_6 x} + \alpha_{17} V_T \qquad \text{for } \Delta < 0 \tag{4.62b}$$

This reduced solution can also be used to obtain the interfacial shear stress at the other plate end ($x = L$) by changing the horizontal coordinate so that it originates from that end. The coefficients in Eq. 4.62 can be obtained from the first three rows in Eqs 4.60 and 4.61 as

$$B_2 = \frac{1}{m_6}(m_7 B_3 + m_8 B_4 - c_3) \tag{4.63a}$$

$$B_3 = \frac{1}{m_{27}}(c_7 - m_{28} B_4) \tag{4.63b}$$

$$B_4 = \frac{m_{29}c_7 - m_{27}c_8}{m_{28}m_{29} - m_{27}m_{30}} \tag{4.63c}$$

$$B_8 = \frac{-1}{\psi_4 p_1}(\psi_5 p_2 B_{10} + \psi_6 p_3 B_{12} + c_3) \tag{4.63d}$$

$$B_{10} = \frac{1}{p_{16}}(c_9 - p_{17}B_{12}) \tag{4.63e}$$

$$B_{12} = \frac{p_{18}c_9 - p_{16}c_{10}}{p_{17}p_{18} - p_{16}p_{19}} \tag{4.63f}$$

The elements of the matrices in Eqs 4.60 and 4.61 and additional parameters in Eq. 4.63 are given in Appendix A in section 4.12.

4.8 General Solution for Interfacial Normal Stress for Case-3

The governing equation for the interfacial normal stress given in Eq. 4.40 is a fourth order non homogeneous ordinary differential equation. Its general solution can have the following three forms depending on the value of δ which is affected by the material and geometric properties of adherends and adhesive:

$$\delta = 4\beta_2 - \beta_1^2 \tag{4.64}$$

$$\sigma(x) = e^{-\eta_1 x}\left[C_1\cos(\eta_2 x) + C_2\sin(\eta_2 x)\right] + e^{\eta_1 x}\left[C_{11}\cos(\eta_2 x) + C_{21}\sin(\eta_2 x)\right] - n_3\frac{d\tau(x)}{dx}$$

$$\text{for } \delta > 0 \tag{4.65}$$

$$\sigma(x) = C_3 e^{-\eta_3 x} + C_4 e^{-\eta_4 x} + C_{31}e^{\eta_3 x} + C_{41}e^{\eta_4 x} + n_8\frac{d\tau(x)}{dx} + n_9\frac{d^3\tau(x)}{dx^3} \text{ for } \delta < 0 \tag{4.66}$$

$$\sigma(x) = [C_5 + C_6 x]e^{-\eta_5 x} + [C_{51} + C_{61}x]e^{\eta_5 x} \text{ for } \delta = 0 \tag{4.67}$$

where C_1 to C_6 and C_{11} to C_{61} are constants of integration to be determined from appropriate boundary conditions listed in Eq. 4.43. The expressions for n_3 to n_9 and η_1 to η_5 are given in Appendix B. Because $\sigma(x)\rightarrow 0$ for large values of x, C_{11} to C_{61} = 0 and Eqs 4.65-4.67 reduce to

$$\sigma(x) = e^{-\eta_1 x}\left[C_1\cos(\eta_2 x) + C_2\sin(\eta_2 x)\right] - n_3\frac{d\tau(x)}{dx} \text{ for } \delta > 0 \tag{4.68}$$

$$\sigma(x) = C_3 e^{-\eta_3 x} + C_4 e^{-\eta_4 x} + n_8\frac{d\tau(x)}{dx} + n_9\frac{d^3\tau(x)}{dx^3} \text{ for } \delta < 0 \tag{4.69}$$

$$\sigma(x) = [C_5 + C_6 x]e^{-\eta_5 x} \text{ for } \delta = 0 \tag{4.70}$$

4.8.1 Determination of constants C_1 to C_6

Differentiating Eq. 4.34 twice w.r.t.*x*, substituting Eq. 4.35 into the resulting expression and then applying the boundary condition of Eqs 4.43a-b gives

$$\left.\frac{d^2\sigma(x)}{dx^2}\right|_{x=0} = \frac{E_a}{t_a E_2 I_2}[R_b M_1(0) + M_{pl}] + \beta_1 \sigma(x)\big|_{x=0} \tag{4.71}$$

Setting x=0 in Eq. 4.68 and substituting in Eq. 4.71 gives

$$\left.\frac{d^2\sigma(x)}{dx^2}\right|_{x=0} = \frac{E_a}{t_a E_2 I_2}[R_b M_1(0) + M_{pl}] + \beta_1 C_1 - \beta_1 n_3 \left.\frac{d\tau(x)}{dx}\right|_{x=0} \tag{4.72}$$

Differentiating Eq. 4.68 twice w.r.t.x and setting x=0 into the resulting equation gives

$$\left.\frac{d^2\sigma(x)}{dx^2}\right|_{x=0} = (\eta_1^2 - \eta_2^2)C_1 - 2\eta_1\eta_2 C_2 - n_3 \left.\frac{d^3\tau(x)}{dx^3}\right|_{x=0} \tag{4.73}$$

From Eqs 4.72 and 4.73,

$$(\eta_1^2 - \eta_2^2 - \beta_1)C_1 - 2\eta_1\eta_2 C_2 = \frac{E_a}{t_a E_2 I_2}[R_b M_1(0) + M_{pl}] - n_3\left(\beta_1 \frac{d\tau(x)}{dx} - \frac{d^3\tau(x)}{dx^3}\right)\Bigg|_{x=0} \tag{4.74}$$

Differentiating Eq. 4.34 thrice w.r.t.*x*, substituting Eq. 4.38 into the resulting expression and then applying the boundary condition of Eq. 4.43e-f gives

$$\left.\frac{d^3\sigma(x)}{dx^3}\right|_{x=0} = \frac{E_a}{t_a E_1 I_1} V_{Tm} - n_{2m}\tau(0) + \beta_1 \left.\frac{d\sigma(x)}{dx}\right|_{x=0} \tag{4.75}$$

where

$$V_{Tm} = V_T + \left(\frac{1+R_b}{R_b}\right)V_{pl} \tag{4.75a}$$

Differentiating Eq. 4.68 once w.r.t.*x*, setting x=0 and substituting the result into Eq. 4.75 gives

$$\left.\frac{d^3\sigma(x)}{dx^3}\right|_{x=0} = \frac{E_a}{t_a E_1 I_1} V_{Tm} - n_{2m}\tau(0) - \beta_1\eta_1 C_1 + \beta_1\eta_2 C_2 - \beta_1 n_3 \left.\frac{d^2\tau(x)}{dx^2}\right|_{x=0} \tag{4.76}$$

Differentiating Eq. 4.68 thrice w.r.t.x and setting x=0 gives

$$\left.\frac{d^3\sigma(x)}{dx^3}\right|_{x=0} = [2\eta_1\eta_2^2 - \eta_1(\eta_1^2 - \eta_2^2)]C_1 + [2\eta_1^2\eta_2 + \eta_2(\eta_1^2 - \eta_2^2)]C_2 - n_3 \left.\frac{d^4\tau(x)}{dx^4}\right|_{x=0} \tag{4.77}$$

From Eqs 4.76 and 4.77,

$$(3\eta_1\eta_2^2-\eta_1^3+\eta_1\beta_1)C_1+(3\eta_1^2\eta_2-\eta_2^3-\eta_2\beta_1)C_2=\frac{E_aV_{Tm}}{t_aE_1I_1}-n_{2m}\tau(0)-n_3\left(\beta_1\frac{d^2\tau(0)}{dx^2}-\frac{d^4\tau(0)}{dx^4}\right) \tag{4.78}$$

C_1 and C_2 are obtained from Eqs 4.74 and 4.78 as

$$\begin{aligned}C_1=\frac{E_a}{t_aE_2I_2}\left[R_b\left(n_4V_{Tm}+n_5M_1(0)\right)+n_5M_{pl}\right]-n_{2m}n_4\tau(0)\\-n_3n_5\left(\beta_1\frac{d\tau(0)}{dx}-\frac{d^3\tau(0)}{dx^3}\right)-n_3n_4\left(\beta_1\frac{d^2\tau(0)}{dx^2}-\frac{d^4\tau(0)}{dx^4}\right)\end{aligned} \tag{4.79}$$

$$\begin{aligned}C_2=\frac{E_a}{t_aE_2I_2}\left[R_b\left(n_6V_{Tm}-n_6n_7M_1(0)\right)-n_6n_7M_{pl}\right]-n_{2m}n_6\tau(0)\\+n_3n_6n_7\left(\beta_1\frac{d\tau(0)}{dx}-\frac{d^3\tau(0)}{dx^3}\right)-n_3n_6\left(\beta_1\frac{d^2\tau(0)}{dx^2}-\frac{d^4\tau(0)}{dx^4}\right)\end{aligned} \tag{4.80}$$

Adopting a similar procedure individually to determine the coefficients for Eqs 4.69 and 4.70 in consideration of Eqs 4.71 and 4.75 provides the following expressions for constants C_3-C_6.

$$\begin{aligned}C_3=\frac{E_an_{10}}{t_aE_2I_2}\left(R_b[\frac{V_{Tm}}{\eta_4}+M_1(0)]+M_{pl}\right)-\frac{n_{2m}n_{10}}{\eta_4}\tau(0)+\\+n_8n_{10}\beta_1\left(\frac{d\tau(0)}{dx}+\frac{1}{\eta_4}\frac{d^2\tau(0)}{dx^2}\right)+(n_9\beta_1-n_8)n_{10}\left(\frac{d^3\tau(0)}{dx^3}+\frac{1}{\eta_4}\frac{d^4\tau(0)}{dx^4}\right)\end{aligned} \tag{4.81}$$

$$\begin{aligned}C_4=\frac{E_an_{11}}{t_aE_2I_2}\left(R_b[\frac{V_{Tm}}{\eta_3}+M_1(0)]+M_{pl}\right)-\frac{n_{2m}n_{11}}{\eta_3}\tau(0)+\\+n_8n_{11}\beta_1\left(\frac{d\tau(0)}{dx}+\frac{1}{\eta_3}\frac{d^2\tau(0)}{dx^2}\right)+(n_9\beta_1-n_8)n_{11}\left(\frac{d^3\tau(0)}{dx^3}+\frac{1}{\eta_3}\frac{d^4\tau(0)}{dx^4}\right)\end{aligned} \tag{4.82}$$

$$C_5=\frac{E_an_{13}}{t_aE_2I_2}\left(R_b[n_{12}V_{Tm}+M_1(0)]+M_{pl}\right)-n_{2m}n_{12}n_{13}\tau(0) \tag{4.83}$$

$$C_6=\frac{(\eta_5^2-\beta_1)}{2\eta_5}C_5-\frac{E_a}{2\eta_5t_aE_2I_2}\left(R_bM_1(0)+M_{pl}\right) \tag{4.84}$$

The expressions for n_{2m}, n_3 - n_{13} are given in Appendix B in section 4.13.

4.9 Solution for General Loading (Case-1)

The solutions from Case-2 and 3 are combined to get the solution for the original problem in Case-1. The interfacial shear stress is given by the combination of Eqs 4.15 and 4.45 or 4.46 as:

$$\tau(x,y) = m_c(y)V_{Tc}(x) + B_2 e^{-\psi_1 x} + e^{-\psi_2 x}\left[B_3\cos(\psi_3 x) + B_4\sin(\psi_3 x)\right] + \alpha_{15}V_T \quad \text{for } \Delta \geq 0 \tag{4.85}$$

$$\tau(x,y) = m_c(y)V_{Tc}(x) + B_8 e^{-\psi_4 x} + B_{10}e^{-\psi_5 x} + B_{12}e^{-\psi_6 x} + \alpha_{17}V_T \quad \text{for } \Delta < 0 \tag{4.86}$$

The interfacial normal stress is given by Eq. 4.68 or 4.69 or 4.70 depending on δ in Eq. 4.64.

4.10 Comparison of Interfacial Stress Solutions

4.10.1 Example beams, reference solutions and FEA

A comparison of the predicted interfacial shear and normal stresses from the closed-form solutions reviewed earlier is conducted in this section. A simply supported RC beam of rectangular cross section plated respectively with carbon-fibre-reinforced polymer (CFRP) composite and glass-fibre-reinforced polymer (GFRP) composite are taken as typical illustrative plated beam examples. The geometric and material properties of the example beam listed in Table 4.1 are taken from Smith & Teng (2001). Three different loading examples are considered: an UDL of 50 kN/m as in Figure 4.4a, a mid-point load of 150 kN as in Figure 4.4b and a complex loading arrangement as in Figure 4.4c.

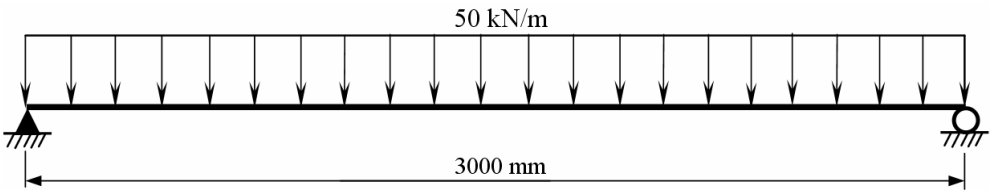

(a) Plated RC beam under UDL

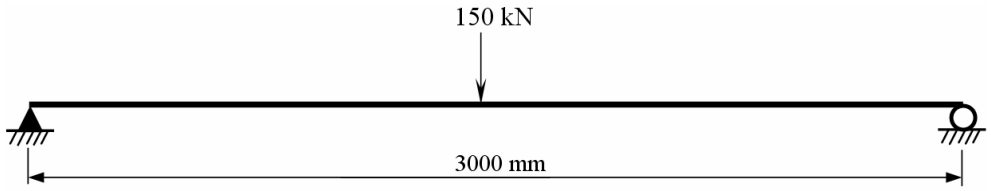

(b) Plated RC beam under mid-point load

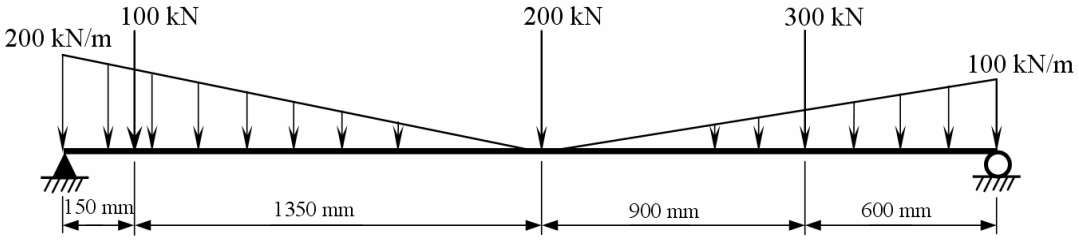

(c) Plated RC beam under complex load

Figure 4.4. Loading examples on plated beams

Table 4.1: Geometric and material properties of example plated beams

Component	Width (mm)	Depth (mm)	Length (mm)	Elastic Modulus (GPa)	Shear Modulus (GPa)
RC beam	$b_1 = 200$	$t_1 = 300$	$L_1 = 3000$	$E_1 = 30$	$G_1 = 12.82$
Adhesive layer	$b_a = 200$	$t_a = 2$	$L_a = 2400$	$E_a = 2$	$G_a = 0.74$
GFRP plate	$b_2 = 200$	$t_2 = 4$	$L_2 = 2400$	$E_2 = 50$	$G_2 = 3.50$
CFRP plate	$b_2 = 200$	$t_2 = 4$	$L_2 = 2400$	$E_2 = 100$	$G_2 = 4.24$

The interfacial shear and normal stresses computed using the present solution, reference solutions without shear deformation effect and previous solutions with shear deformation effect for the example beams are compared. Due to their accuracy and simplicity, the closed-form solutions of Smith & Teng (2001) and Narayanamurthy et al. (2010) are used as reference solutions for all solutions that have not considered the effect of shear deformation. The present solution is also compared with finite element analysis (FEA) results based on Euler-Bernoulli and Timoshenko beam elements and with previous three approximate solutions that have considered the effect of shear

deformation in adherends (Abdelouahed, 2006; Yang and Wu, 2007 and Narayanamurthy et al., 2009) for the UDL loading.

The FEA was carried out for the example plated beams under UDL in ANSYS 10.0 (2005). The plated beam was modelled as a beam-spring-beam (B-S-B) model as in Zhang and Teng (2010b). The beam and plate were modelled as beam elements using BEAM44, a uniaxial beam element which can function either as an Euler-Bernoulli or Timoshenko beam. The adhesive was modelled using COMBIN39, a non-linear unidirectional spring element which can be made to act as either a normal or shear elastic spring. Both normal and shear springs were used to model the adhesive and their stiffness represent that of the adhesive layer. This implies that interfacial shear and normal stresses are constant through the thickness of the adhesive layer. This B-S-B model reflects the assumptions employed in the reference and present solutions. The beam elements were located along the lower edge of the beam and the upper edge of the plate by appropriately offsetting the reference nodes in beam elements so that they can be connected directly by spring elements. An element size of 1mm was used in the model as recommended in Zhang and Teng (2010b) based on a convergence study. The interfacial stresses are converted from the discrete elastic spring forces by dividing the effective width (area) represented by the springs. This effective width equals the centre to centre spacing of two adjacent elements on the two sides of the spring for all springs except for the edge spring for which the effective width equals half width of the edge element.

4.10.2 Example beam under UDL

The peak interfacial stresses from various closed-form solutions considered here and from FEA for both CFRP and GFRP plated beams under UDL are provided in Table 4.2, while the distributions of the interfacial stresses near the plate end for the CFRP plated beam under UDL are shown in Figures 4.5a-d. The peak interfacial shear stresses from the present and the reference solutions are very slightly higher than those from FEA with and without shear deformation. Their differences reduce gradually away from the plate end and the predictions of all solutions are almost exactly the same 20 mm away from the plate end. The peak interfacial shear stress from the present solution (which includes the effect of shear deformation) is about 2.4% smaller than that from the reference solutions (which do not include the effect of shear deformation) for both

example beams (Figure 4.5a and Table 4.2). Similarly the results from FEA with shear deformation are smaller than those from without shear deformation by about 2.2% and 2.7% respectively for the CFRP and GFRP plated beams (Figure 4.5a and Table 4.2). It is seen from Figure 4.5a that the interfacial shear stress is not affected by the shear deformation of the adherends in any significant way.

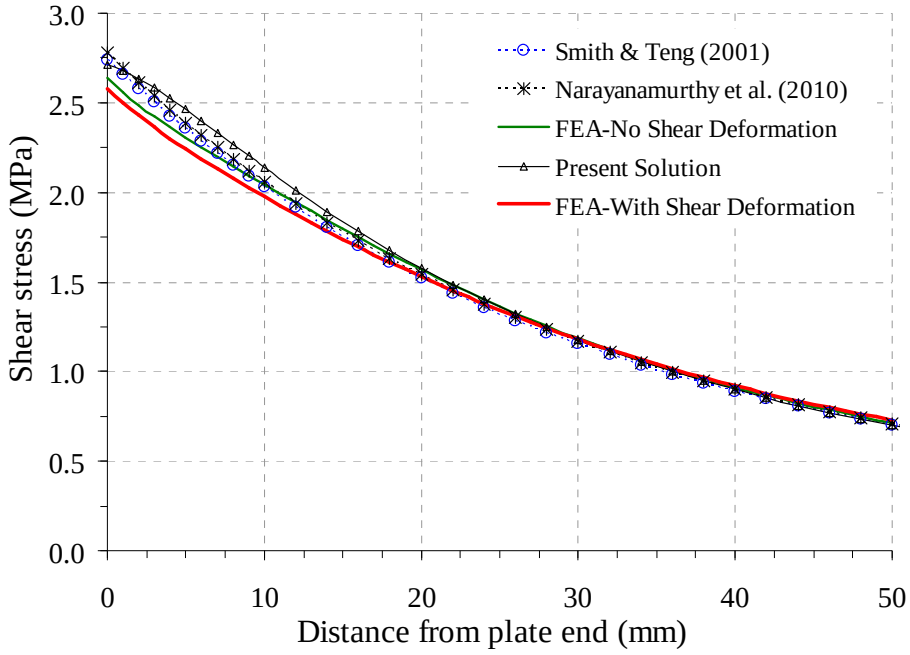

(a) Interfacial shear stress: present, FEA and reference solutions with no shear effect

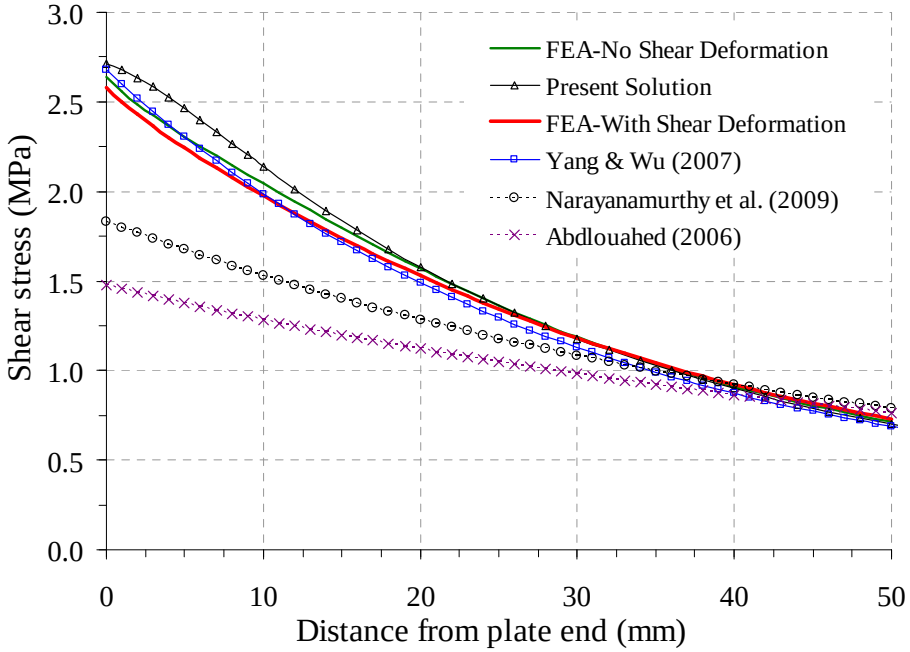

(b) Interfacial shear stress: present, FEA and previous solutions with shear effect

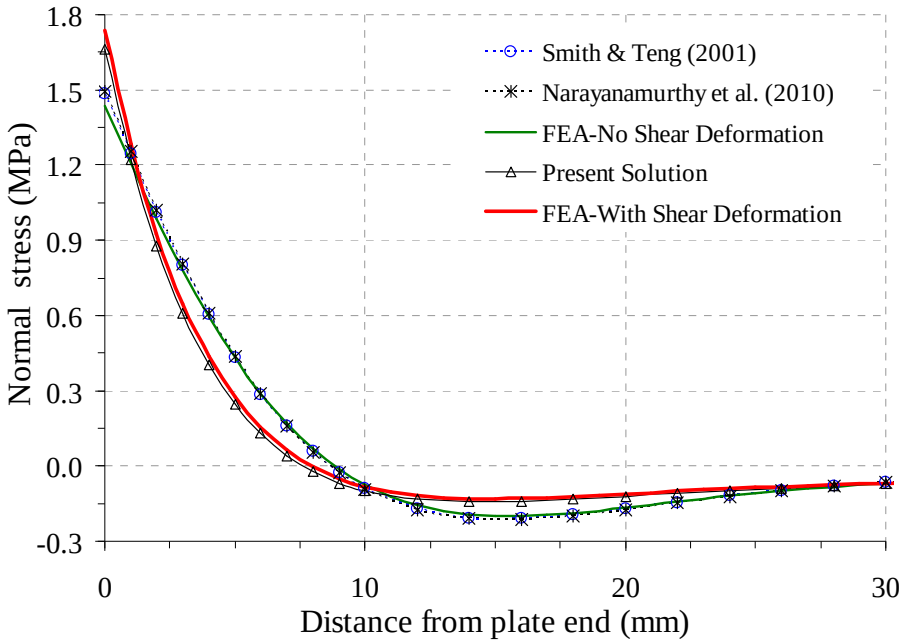

(c) Interfacial normal stress: present, FEA and reference solutions with no shear effect

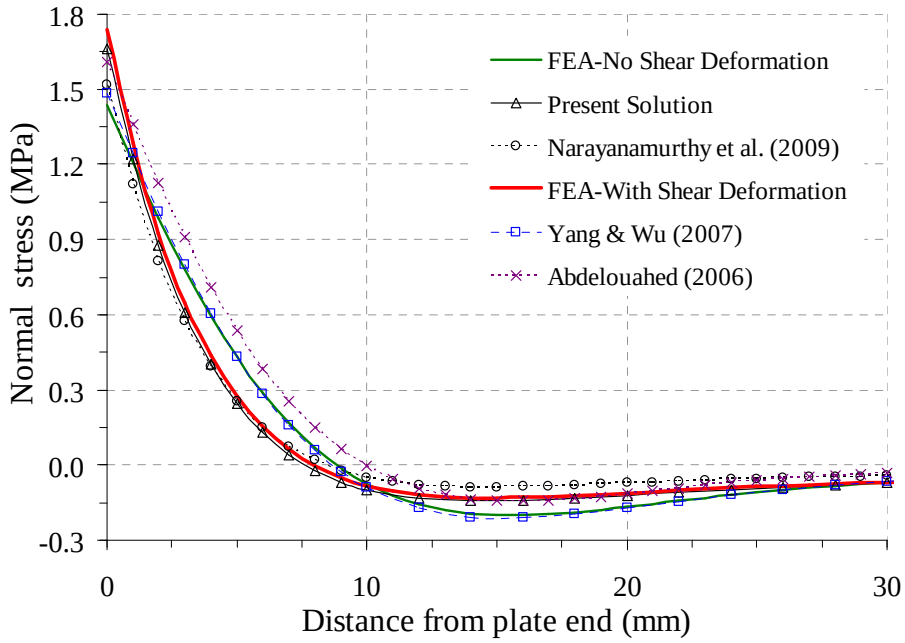

(d) Interfacial normal stress: present, FEA and previous solutions with shear effect

Figure 4.5 Comparison of present, FEA and previous solutions for interfacial stresses in a CFRP plated RC beam subjected to an UDL

All the three previous approximate solutions that considered the effect of shear deformation predict a reduction in the peak interfacial shear stress compared with the reference solution (Figure 4.5b and Table 4.2), but the two solutions that adopt approximate shear stress distribution in the adherends in considering the effect of shear deformation on interfacial shear stress (Abdelouahed, 2006 and Narayanamurthy et al.,

2009) predict huge reduction of the peak interfacial shear stress which does not conform to the present solution and FEA with shear deformation.

The interfacial normal stress predicted by the present solution is in very close agreement with the FEA prediction with shear deformation (Figure 4.5c). The two reference solutions are also in very close agreement with the FEA prediction without shear deformation, except a slightly lower peak value for the latter (Figure 4.5c). The shear deformation in the adherends increases the peak interfacial normal stress. The present solution predicts 11.1% and 3.9% higher than the reference solutions respectively for the CFRP and GFRP plated beams. Among the FEA results, FEA with shear deformation predicted 20.9% and 13.7% higher than FEA without shear deformation respectively for the two beams.

Among the three previous approximate solutions that considered the effect of shear deformation, Abdelouahed (2006) does not explicitly include the effect of adherends shear deformation on the interfacial normal stress term but its prediction does deviate slightly from the FEA without shear deformation because of the influence of its peak shear stress. Yang and Wu's (2007) prediction is almost the same as the FEA without shear deformation (and the reference solutions). Narayanamurthy et al.'s (2009) prediction is in good agreement with the FEA with shear deformation except within about 2-3mm from the plate end within which the prediction is lower than the latter.

Table 4.2: Peak interfacial stresses in plated RC beams under UDL (Fig. 4a), MPa

Theory	GFRP plated		CFRP plated	
	$\tau(x)$	$\sigma(x)$	$\tau(x)$	$\sigma(x)$
Roberts & Haji-Kazemi (Solution-1) (1989)	2.001	1.425	2.776	1.668
Roberts & Haji-Kazemi (Solution-2) (1989)	1.813	1.256	2.591	1.500
Roberts (1989)	1.945	1.386	2.604	1.567
Malek et al. (1998)	1.943	1.384	2.597	1.563
Smith & Teng (2001)	1.975	1.244	2.740	1.484
Narayanamurthy et al. (2010)	2.002	1.249	2.778	1.495
FEA- no shear deformation	1.867	1.185	2.638	1.437
Yang & Wu (2007)	1.955	1.227	2.684	1.472
Abdelouahed (2006)	1.042	1.366	1.475	1.606
Narayanamurthy et al. (2009)	1.298	1.184	1.834	1.518
Present	1.955	1.299	2.712	1.660
FEA- with shear deformation	1.818	1.347	2.580	1.738

Figures 4.6 and 4.7 illustrate the effect of shear deformation on the peak interfacial stresses for various elastic modulus of adhesive and plate thickness for the CFRP plated reference beam under UDL. The vertical coordinate represents the difference between the present solution and the reference solution of Narayanamurthy et al.'s (2010) with respect to the reference solution in percentage, so a positive number means an increase of the peak interfacial stress. Within the range of the parameters shown, the effect of the shear deformation is insignificant on the peak interfacial shear stress but it is significant and detrimental on the peak interfacial normal stress. The effect on the peak interfacial normal stress generally increases with a reduction of the elastic modulus of the adhesive and an increase of the plate thickness.

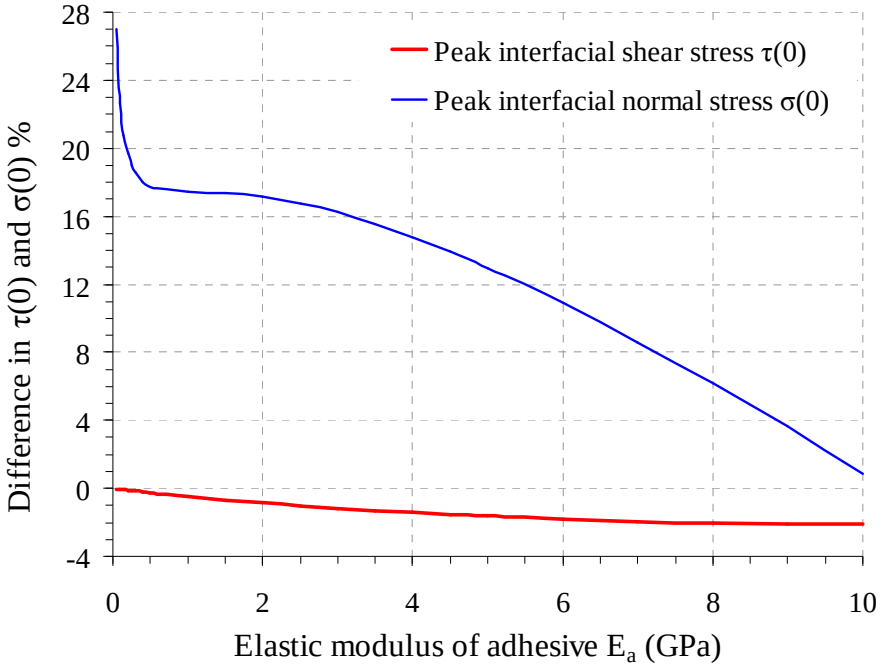

Figure 4.6. Effect of adherends shear deformation on peak interfacial stresses for various elastic modulus of adhesive

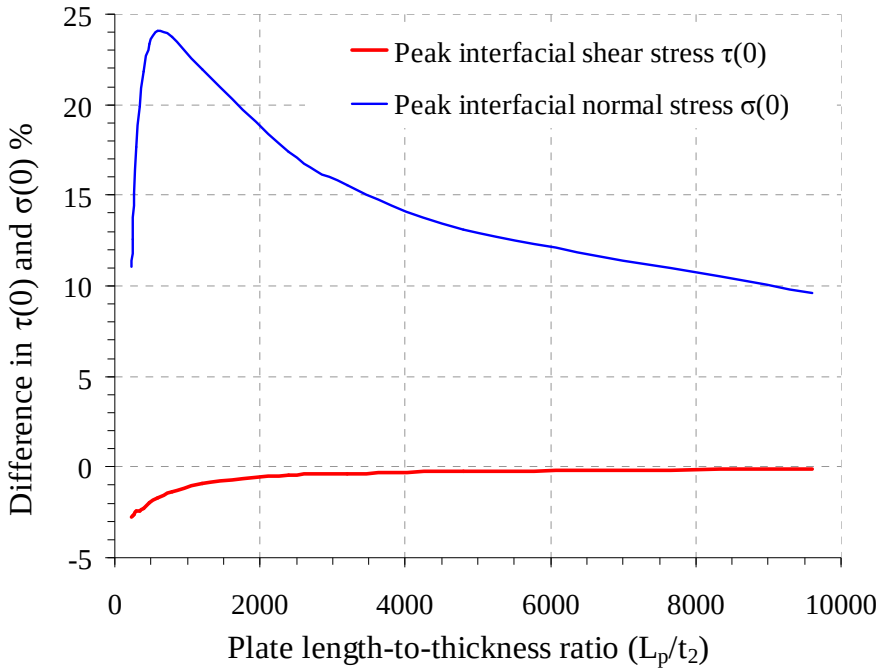

Figure 4.7. Effect of adherends shear deformation on peak interfacial stresses for various plate thicknesses

4.10.3 Example beam under other loading

The general conclusions drawn above on the effect of shear deformation also apply for the CFRP and GFRP plated beams under a mid point load (Figure 4.4b) and a complex loading arrangement (Figure 4.4c), with small variations in value. Taking Narayanamurthy et al.'s (2010) solution as the reference, the present solution predicts 2.7% and 2.6% lower peak shear stress and 4.6% and 2.8% higher peak normal stress respectively for the two loading arrangements for the GFRP plated beam. Similarly, the present prediction for the CFRP plated beam is lower by 2.5% in peak interfacial shear stress for both loading arrangements and is higher by 12% and 10% respectively in peak normal stresses (Figures 4.8-4.9 and Tables 4.3-4.4). This shows that this decrease in percentage between the present and reference solution is almost the same for the peak interfacial shear stress in both CFRP and GFRP plated beams in all the loading arrangements. The differences are also very close to those found between the two FEA predictions with and without shear deformation. The increase in percentage in the peak normal stress is much higher for the CFRP plated beam compared to the GFRP plated beam due to their differences in flexural stiffness.

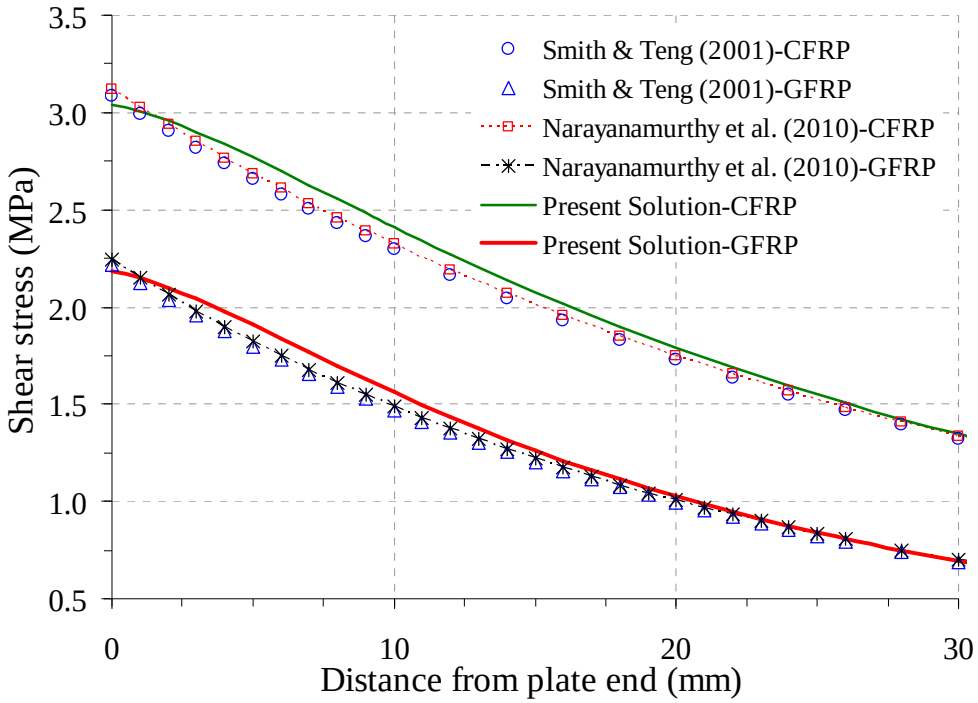

(a) Interfacial shear stress

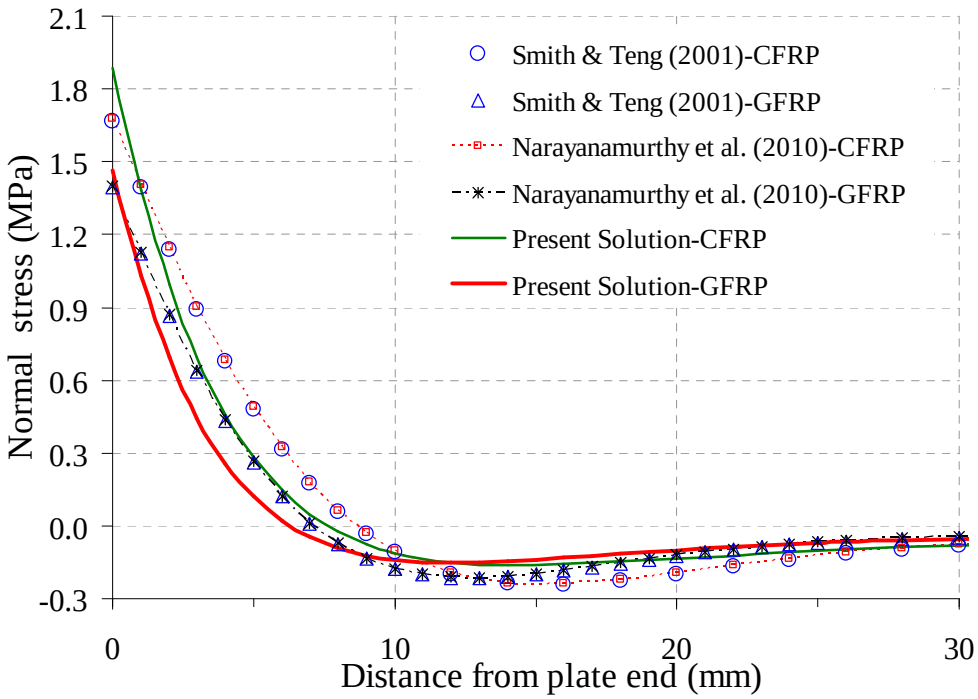

(b) Interfacial normal stress

Figure 4.8. Comparison present and reference solutions for interfacial stresses in GFRP and CFRP plated RC beam subjected to a mid point load

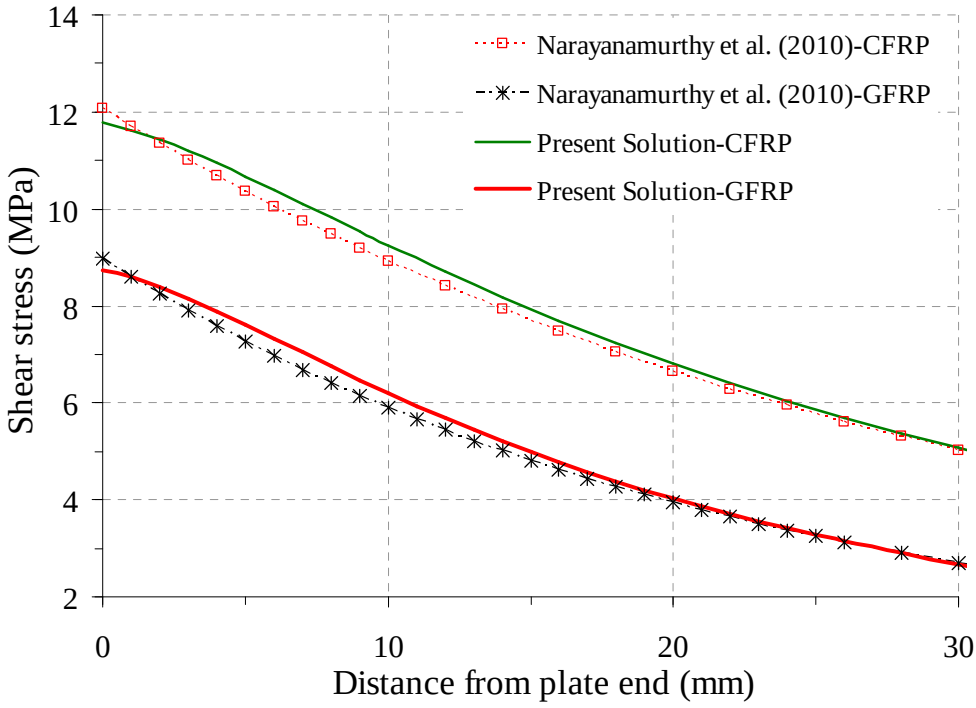

(a) Interfacial shear stress

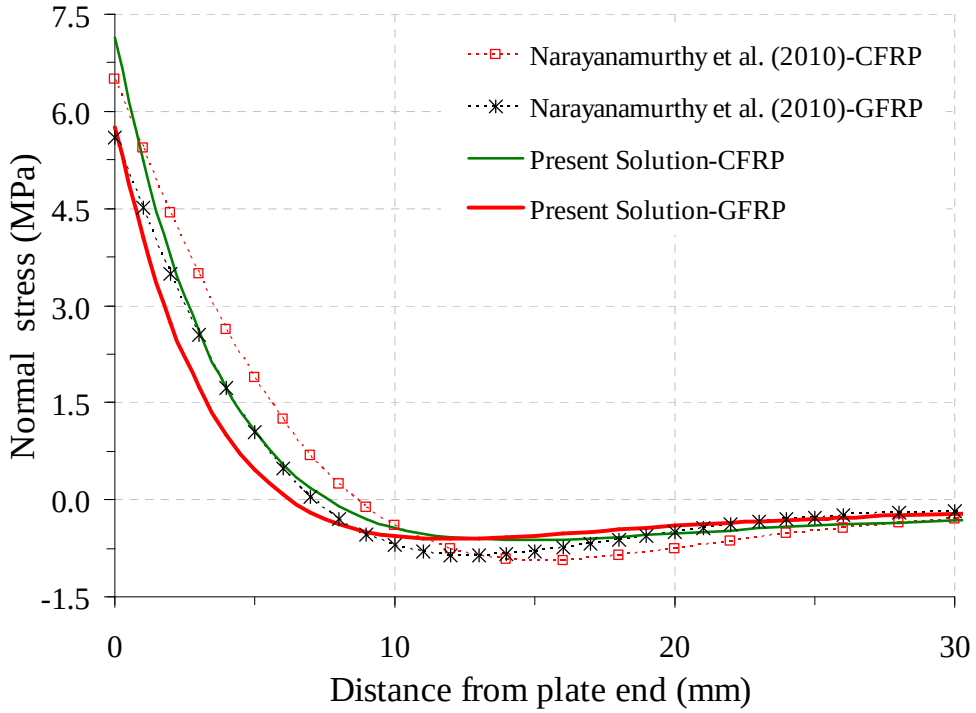

(b) Interfacial normal stress

Figure 4.9. Comparison of present and reference solutions for interfacial stresses in GFRP and CFRP plated RC beam subjected to a complex loading arrangement

Table 4.3: Peak interfacial stresses in plated RC beams under mid-point load (Figure 4.4b), MPa

Theory	GFRP plated		CFRP plated	
	$\tau(x)$	$\sigma(x)$	$\tau(x)$	$\sigma(x)$
Vilnay (1988)	2.240	1.381	3.152	1.669
Roberts (1989)	2.179	1.553	2.925	1.761
Taljsten (1997)	2.215	1.397	3.087	1.674
Malek et al. (1998)	2.179	1.553	2.925	1.761
Smith & Teng (2001)	2.214	1.396	3.083	1.671
Narayanamurthy et al. (2010)	2.242	1.400	3.119	1.679
Present	2.182	1.465	3.041	1.885

Table 4.4: Peak interfacial stresses in plated RC beams under complex loading (Figure 4.4c), MPa

Theory	GFRP plated		CFRP plated	
	$\tau(x)$	$\sigma(x)$	$\tau(x)$	$\sigma(x)$
Narayanamurthy et al. (2010)	8.977	5.599	12.070	6.493
Present	8.748	5.758	11.770	7.140

4.11 Conclusions

Concentration of interfacial stresses at the plate end is attributed to premature plate end debonding failures observed in plated beams. It is important to quantify these interfacial stresses correctly considering all deformations in adherends for the safe design of plated beams, but most previous solutions neglect the effect of shear deformations in adherends due to the complexity in the formulation. This chapter is concerned with the development of a first closed-form rigorous theoretical solution that includes the effect of axial, bending and shear deformations in adherends simultaneously to quantify these interfacial shear and normal stresses in plated beams. The solution has been developed by treating the plate and beam as two Timoshenko beams, and it is applicable for beams with any prismatic cross section bonded symmetrically or asymmetrically with a plate and under any loading arrangement. A comparison shows that the solution is in close agreement in both the interfacial shear and normal stress with finite element predictions. This study has shown that the effect of the shear deformation of the adherends is insignificant for the interfacial shear stress, but significant for the interfacial normal stress.

4.12 Appendix A. Terms Used in Solution of Interfacial Shear Stress

$$\alpha_6 = \frac{3\alpha_3 - \alpha_2^2}{9} \tag{4.A1}$$

$$\alpha_7 = \frac{-9\alpha_2\alpha_3 + 27\alpha_4 + 2\alpha_2^3}{54} \tag{4.A2}$$

$$\alpha_8 = \sqrt[3]{\alpha_7 + \sqrt{\Delta}} \tag{4.A3}$$

$$\alpha_9 = \sqrt[3]{\alpha_7 - \sqrt{\Delta}} \tag{4.A4}$$

$$\alpha_{10} = \frac{\alpha_2}{3} + \alpha_8 + \alpha_9 \tag{4.A5}$$

$$\alpha_{11} = \frac{\alpha_2}{3} - \frac{(\alpha_8 + \alpha_9)}{2} \tag{4.A6}$$

$$\alpha_{12} = \frac{\sqrt{3}}{2}(\alpha_8 - \alpha_9) \tag{4.A7}$$

$$\alpha_{13} = \psi_1^2[(\psi_1 + \psi_2)^2 + \psi_3^2][(\psi_1 - \psi_2)^2 + \psi_3^2] \tag{4.A8}$$

$$\alpha_{14} = (\psi_2^2 + \psi_3^2)[(\psi_1^2 - \psi_2^2)^2 + \psi_3^4 + 2\psi_3^2(\psi_1^2 + \psi_2^2)] \tag{4.A9}$$

$$\alpha_{15} = \frac{\alpha_5[\alpha_{13}(\psi_1^2 - 2\psi_2^2 + 2\psi_3^2) + \alpha_{14}]}{\alpha_{13}\alpha_{14}} \tag{4.A10}$$

$$\alpha_{16} = \sqrt{\alpha_7^2 - \Delta} \tag{4.A11}$$

$$\alpha_{17} = -\frac{\alpha_5[\psi_4^4(\psi_5^2 - \psi_6^2) + \psi_5^4(\psi_6^2 - \psi_4^2) + \psi_6^4(\psi_4^2 - \psi_5^2)]}{[(\psi_4^2 - \psi_5^2)(\psi_5^2 - \psi_6^2)(\psi_6^2 - \psi_4^2)(\psi_4^2\psi_5^2\psi_6^2)]} \tag{4.A12}$$

$$\theta = \frac{1}{3}\cos\left(\frac{\alpha_7}{\alpha_{16}}\right) \tag{4.A13}$$

$$\psi_1 = \sqrt{\alpha_{10}} \tag{4.A14}$$

$$\psi_2 = \sqrt{0.5(\sqrt{\alpha_{11}^2 + \alpha_{12}^2} + \alpha_{11})} \tag{4.A15}$$

$$\psi_3 = \frac{\alpha_{12}}{2\psi_2} \tag{4.A16}$$

$$\psi_4 = \sqrt{\frac{\alpha_2}{3} + 2\sqrt[3]{\alpha_{16}}\cos\theta} \tag{4.A17}$$

$$\psi_5 = \sqrt{\left|\frac{\alpha_2}{3} - \sqrt[3]{\alpha_{16}}(\cos\theta + \sqrt{3}\sin\theta)\right|} \tag{4.A18}$$

$$\psi_6 = \sqrt{\left|\frac{\alpha_2}{3} - \sqrt[3]{\alpha_{16}}(\cos\theta - \sqrt{3}\sin\theta)\right|} \tag{4.A19}$$

$$m_2 = \frac{r_1 + r_2 R_b}{1 + R_b} \tag{4.A20}$$

$$m_3 = \frac{(r_1 + r_2 R_b)(y_1 + y_2 + t_a)}{1 + R_b} + r_3 + r_4 \tag{4.A21}$$

$$m_4 = \psi_1^2 - \frac{G_a m_3 b_2}{E_1} \tag{4.A22}$$

$$m_5 = \psi_2^2 - \psi_3^2 - \frac{G_a m_3 b_2}{E_1} \tag{4.A23}$$

$$m_6 = \psi_1 m_4 \tag{4.A24}$$

$$m_7 = \psi_2(2\psi_3^2 - m_5) \tag{4.A25}$$

$$m_8 = \psi_3(2\psi_2^2 + m_5) \tag{4.A26}$$

$$m_i = \psi_1 e^{(-1)^{i+1}\psi_1 L_p} \quad ; \quad i = 9, 10 \tag{4.A27}$$

$$m_{11} = e^{-\psi_2 L_p}[\psi_3 \sin(\psi_3 L_p) + \psi_2 \cos(\psi_3 L_p)] \tag{4.A28}$$

$$m_{12} = e^{-\psi_2 L_p}[\psi_3 \cos(\psi_3 L_p) - \psi_2 \sin(\psi_3 L_p)] \tag{4.A29}$$

$$m_{13} = e^{\psi_2 L_p}[\psi_2 \cos(\psi_3 L_p) - \psi_3 \sin(\psi_3 L_p)] \tag{4.A30}$$

$$m_{14} = e^{\psi_2 L_p}[\psi_2 \sin(\psi_3 L_p) + \psi_3 \cos(\psi_3 L_p)] \tag{4.A31}$$

$$m_i = m_4 e^{(-1)^{i+1}\psi_1 L_p} \quad ; \quad i = 15, 16 \tag{4.A32}$$

$$m_{17} = e^{-\psi_2 L_p}[m_5 \cos(\psi_3 L_p) + 2\psi_2\psi_3 \sin(\psi_3 L_p)] \tag{4.A33}$$

$$m_{18} = e^{-\psi_2 L_p}[m_5 \sin(\psi_3 L_p) - 2\psi_2\psi_3 \cos(\psi_3 L_p)] \tag{4.A34}$$

$$m_{19} = e^{\psi_2 L_p}[m_5 \cos(\psi_3 L_p) - 2\psi_2\psi_3 \sin(\psi_3 L_p)] \tag{4.A35}$$

$$m_{20} = e^{\psi_2 L_p}[m_5 \sin(\psi_3 L_p) + 2\psi_2\psi_3 \cos(\psi_3 L_p)] \tag{4.A36}$$

$$m_{(21+i)} = \psi_1 m_{(15+i)} \quad ; \quad i = 0, 1 \tag{4.A37}$$

$$m_{23} = e^{-\psi_2 L_p}\left((3\psi_2^2 - \psi_3^2)\psi_3 \sin(\psi_3 L_p) - (3\psi_3^2 - \psi_2^2)\psi_2 \cos(\psi_3 L_p) - \frac{G_a m_3 b_2 m_{11}}{E_1}\right) \tag{4.A38}$$

$$m_{24} = e^{-\psi_2 L_p}\left((3\psi_3^2 - \psi_2^2)\psi_2 \sin(\psi_3 L_p) + (3\psi_2^2 - \psi_3^2)\psi_3 \cos(\psi_3 L_p) - \frac{G_a m_3 b_2 m_{12}}{E_1}\right) \tag{4.A39}$$

$$m_{25} = e^{\psi_2 L_p}\left((3\psi_2^2 - \psi_3^2)\psi_3 \sin(\psi_3 L_p) + (3\psi_3^2 - \psi_2^2)\psi_2 \cos(\psi_3 L_p) + \frac{G_a m_3 b_2 m_{13}}{E_1}\right) \tag{4.A40}$$

$$m_{26} = e^{\psi_2 L_p}\left((3\psi_3^2 - \psi_2^2)\psi_2 \sin(\psi_3 L_p) - (3\psi_2^2 - \psi_3^2)\psi_3 \cos(\psi_3 L_p) + \frac{G_a m_3 b_2 m_{14}}{E_1}\right) \quad (4.A41)$$

$$m_{27} = -\psi_2 - \frac{\psi_1 m_7}{m_6} \quad (4.A42)$$

$$m_{28} = \psi_3 - \frac{\psi_1 m_8}{m_6} \quad (4.A43)$$

$$m_{29} = \frac{m_4 m_7}{m_6} + m_5 \quad (4.A44)$$

$$m_{30} = \frac{m_4 m_8}{m_6} - 2\psi_2\psi_3 \quad (4.A45)$$

$$p_i = \psi_{(i+3)}^2 - \frac{G_a m_3 b_2}{E_1} \quad ; \quad i = 1, 2, 3 \quad (4.A46)$$

$$p_i = \psi_4 e^{(-1)^i \psi_4 L_p} \quad ; \quad i = 4, 5 \quad (4.A47)$$

$$p_i = \psi_5 e^{(-1)^i \psi_5 L_p} \quad ; \quad i = 6, 7 \quad (4.A48)$$

$$p_i = \psi_6 e^{(-1)^i \psi_6 L_p} \quad ; \quad i = 8, 9 \quad (4.A49)$$

$$p_i = p_1 e^{(-1)^i \psi_4 L_p} \quad ; \quad i = 10, 11 \quad (4.A50)$$

$$p_i = p_2 e^{(-1)^i \psi_5 L_p} \quad ; \quad i = 12, 13 \quad (4.A51)$$

$$p_i = p_3 e^{(-1)^i \psi_6 L_p} \quad ; \quad i = 14, 15 \quad (4.A52)$$

$$p_{16} = -\frac{\psi_5}{p_1}(p_1 - p_2) \quad (4.A53)$$

$$p_{17} = -\frac{\psi_6}{p_1}(p_1 - p_3) \quad (4.A54)$$

$$p_{18} = \frac{p_2}{\psi_4}(\psi_4 - \psi_5) \quad (4.A55)$$

$$p_{19} = \frac{p_3}{\psi_4}(\psi_4 - \psi_6) \quad (4.A56)$$

$$c_1 = \frac{G_a}{E_1}[-r_1 M_1(0) + r_2 M_{pl} - (r_3 + r_4) N_{pl} + r_3 N_{pr}] - \alpha_1 \sigma(0) \quad (4.A57)$$

$$c_2 = \frac{G_a}{E_1}(m_3 b_2 \alpha_{15} - m_2) V_T - \alpha_1 \sigma'(0) \quad (4.A58)$$

$$c_{2m} = \frac{G_a}{E_1}(m_3 b_2 \alpha_{17} - m_2) V_T - \alpha_1 \sigma'(0) \quad (4.A59)$$

$$c_3 = -\alpha_1 \sigma''(0) \quad (4.A60)$$

$$c_4 = \frac{G_a}{E_1}[-r_1 M_1(L_p) + r_2 M_{pl} - r_4 N_{pr}] - \alpha_1 \sigma(L_p) \tag{4.A61}$$

$$c_5 = \frac{G_a}{E_1}(m_3 b_2 \alpha_{15} - m_2) V_T - \alpha_1 \sigma'(L_p) \tag{4.A62}$$

$$c_{5m} = \frac{G_a}{E_1}(m_3 b_2 \alpha_{17} - m_2) V_T - \alpha_1 \sigma'(L_p) \tag{4.A63}$$

$$c_6 = -\alpha_1 \sigma''(L_p) \tag{4.A64}$$

$$c_7 = c_1 - \frac{\psi_1 c_3}{m_6} \tag{4.A65}$$

$$c_8 = c_2 + \frac{m_4 c_3}{m_6} \tag{4.A66}$$

$$c_9 = c_1 - \frac{c_3}{p_1} \tag{4.A67}$$

$$c_{10} = c_{2m} + \frac{c_3}{\psi_4} \tag{4.A68}$$

4.13 Appendix B. Terms Used in the Solution of Interfacial Normal Stress

$$\eta_1 = 0.5\sqrt{\beta_1 + 2\sqrt{\beta_2}} \tag{4.B1}$$

$$\eta_2 = \frac{\sqrt{\delta}}{4\eta_1} \tag{4.B2}$$

$$\eta_3 = \sqrt{0.5(\beta_1 + \sqrt{-\delta})} \tag{4.B3}$$

$$\eta_4 = \sqrt{0.5(\beta_1 - \sqrt{-\delta})} \tag{4.B4}$$

$$\eta_5 = \sqrt{0.5\beta_1} \tag{4.B5}$$

$$n_{2m} = \frac{E_a b_2}{t_a}\left(\frac{y_1 + t_a}{E_1 I_1} - \frac{y_2}{E_2 I_2}\right) \tag{4.B6}$$

$$n_3 = \frac{n_2}{(\eta_1^2 + \eta_2^2)^2} \tag{4.B7}$$

$$n_4 = \frac{2\eta_1\eta_2}{(\eta_1^2 - \eta_2^2 - \beta_1)(3\eta_1^2\eta_2 - \eta_2^3 - \eta_2\beta_1) + (3\eta_1\eta_2^2 - \eta_1^3 + \eta_1\beta_1)(2\eta_1\eta_2)} \tag{4.B8}$$

$$n_5 = \frac{1 - n_4(3\eta_1\eta_2^2 - \eta_1^3 + \eta_1\beta_1)}{\eta_1^2 - \eta_2^2 - \beta_1} \tag{4.B9}$$

$$n_6 = \frac{n_4(\eta_1^2 - \eta_2^2 - \beta_1)}{2\eta_1\eta_2} \tag{4.B10}$$

$$n_7 = \frac{3\eta_1\eta_2^2 - \eta_1^3 + \eta_1\beta_1}{\eta_1^2 - \eta_2^2 - \beta_1} \tag{4.B11}$$

$$n_8 = \frac{-n_2}{\eta_3^2\eta_4^2} \tag{4.B12}$$

$$n_9 = n_8\left(\frac{1}{\eta_3^2} + \frac{1}{\eta_4^2}\right) \tag{4.B13}$$

$$n_{10} = \frac{\eta_4}{(\eta_4 - \eta_3)(\eta_3^2 - \beta_1)} \tag{4.B14}$$

$$n_{11} = \frac{\eta_3}{(\eta_3 - \eta_4)(\eta_4^2 - \beta_1)} \tag{4.B15}$$

$$n_{12} = \frac{2\eta_5}{3\eta_5^2 - \beta_1} \tag{4.B16}$$

$$n_{13} = \frac{3\eta_5^2 - \beta_1}{(\eta_5^2 - \beta_1)^2} \tag{4.B17}$$

4.14 Notation

The following symbols are used in this chapter:

A = cross sectional area of the adhesive or adherends;

b = width of the adhesive or adherends;

E = modulus of elasticity of the adhesive or adherends;

G = shear modulus of the adhesive;

I = second moment of area of the adhesive or adherends about their centroidal axis;

I_{1c}, I_{ac}, I_{2c} = second moment of area of beam, adhesive and plate section about the centroidal axis of the composite beam section respectively;

I_e = second moment of area of the equivalent composite beam section about its centroidal axis;

L = length of the adhesive or adherends;

L_p = length of the plate;

M = bending moment in the adherends;

$M(0), M(L_p)$ = bending moment in plated beam at x=0 and x=L_p under original

loading ignoring the effects of plate end loading (Case-2);

$M_1(0), M_1(L_p)$ = bending moment in beam at $x=0$ and $x=L_p$ in Case-3 loading;

$M_T(x)$ = total applied bending moment at any section of the plated beam;

N = axial force in the adherends;

$N(x)$ = resultant axial force resisted by any section of the adherends;

$Q_e(x,y)$ = first moment of area of equivalent adhesive or plate section about the centroidal axis of the composite beam section;

t = thickness of the adhesive or adherends;

u = longitudinal displacement of the adherends;

v = vertical displacement of the adherends;

$V(x)$ = shear force at any section of adherends;

$V_{Tc}(x)$ = total applied shear force at any section of the composite beam;

V_T = total shear force at any section of the plated beam in Case-3 loading;

y_c = vertical distance from top of the beam to the centroid of the composite beam section;

y_1, y_2 = vertical distance from bottom of the beam and top of the plate to their respective centroids respectively;

$_{pl,\, pr}$ = subscripts referring respectively to the left and right end of the plate;

$_{1,\, a,\, 2}$ = subscripts referring respectively to the beam, adhesive and plate;

κ_i = Timoshenko's shear coefficient;

$\sigma(x)$ = interfacial normal stress at any section of the plated beam;

$\tau(x)$ = interfacial shear stress at any section of the plated beam;

γ_{xy} = engineering shear strain at the adhesive layer;

$\varepsilon_1(x), \varepsilon_2(x)$ = longitudinal strain at bottom layer of beam and at top layer of plate respectively;

ψ_1 - ψ_6 = roots for the governing differential equation of $\tau(x)$ in Case-3 loading;

η_1 - η_5 = roots for the governing differential equation of $\sigma(x)$ in Case-3 loading;

B_1 - B_{12} = integration constants in general solution of $\tau(x)$ in Case-3 loading; and

C_1 - C_6 = integration constants in general solution of $\sigma(x)$ in Case-3 loading.

Chapter 5

Interpretation of Interfacial Stresses from Experiments – A New Technique

Abstract

External bonding of fibre reinforced polymer (FRP) composite or steel plate is a popular technique for strengthening reinforced concrete or metallic beams. Debonding along the plate-beam interface due to high interfacial shear and normal stresses can lead to premature failure of this hybrid beam. Many analytical, numerical and experimental studies have been conducted during the last two decades to quantify these interfacial stresses. In almost all experimental studies, the strains measured on the bottom face of the plate are used to deduce the interfacial shear stresses near the plate end assuming that the plate is under pure tension. The peeling effect at the plate ends due to the flexural deformation of plate in such interpretation is ignored, resulting in errors in the interpreted interfacial shear stress and no interfacial normal stress.

This chapter presents a new technique to deduce the interfacial shear and normal stresses from the experimentally measured plate strains. The deduced interfacial stresses are compared with the traditional interpretation. The proposed technique is applicable for all the loading arrangements with any beam cross sections and offers high accuracy in the deduction of interfacial stresses. Additionally, the total plate strains from the interfacial stress solution of Narayanamurthy et al. (2010) and simple beam theory are compared with the experimental results; and the effect of plate thickness on the total, axial and bending strains in the plate and on the interfacial shear and normal stresses are studied and discussed in this chapter.

5.1 Introduction

The strength of a reinforced concrete (RC) or metal beam may be enhanced by bonding a fibre-reinforced polymer (FRP) composite or steel plate to its tension face. This method is now popularly adopted for the retrofitting of existing structures. Under external loading, stress transfer occurs between the bonded plate and the original beam leading to the development of high interfacial shear and normal stresses between the adherends at the plate end that may in turn cause a premature debonding failure along the plate-beam interface. Consequently, the interfacial stresses between the plate and the original beam have attracted a great interest in the last few decades. Thus many theoretical (as discussed in detail in Narayanamurthy et al., 2010, 2011) and experimental studies (Jones et al., 1988; Saadatmanesh and Ehsani, 1991; Spadea et al., 1998; Etman and Beeby, 2000; Rahimi and Hutchinson, 2001; Mukhopadhyaya and Swamy, 2001; Smith and Teng, 2002a, b; Brena and Macri, 2004; Pham and Mahaidi, 2006; and many more) have been conducted to quantify these interfacial stresses.

In almost all experimental studies to date, strains measured on the bottom face of the plate are used to deduce the interfacial shear stresses near the plate end assuming that the plate is under pure tension. This is usually carried out by considering horizontal equilibrium of the forces generated at the adherends interface due to interfacial shear stress and the axial forces calculated at the plate soffit through the measured plate strains. The peeling effect between the adherends is ignored to simplify the calculation procedure. So, the interfacial normal stresses cannot be calculated and the deduced interfacial shear stress from measured plate strains do not take into account the effect of interfacial normal stress. This leads to a major approximation or error in the reported interfacial shear stress. The analysis of axial and bending strains in the plate reveals that the bending effects are considerable near the plate ends.

In order to correctly deduce the interfacial shear and normal stresses from experiment, a new technique is developed in this chapter by extending the analytical approach of Narayanamurthy et al. (2010). The plate strains from experiments reported in Jones et al. (1988) for a plated beam shown in Figure 5.1 are used in deducing the interfacial stresses. These are compared with the traditional interpretation in Jones et al. (1988) and with the analytical solution of Narayanamurthy et al. (2010). This method is applicable for any loading arrangement with any beam cross section within the linear elastic

regime of the constituent materials. It offers high accuracy in the deduction of interfacial shear stress; additionally provides interfacial normal stress; and gives the freedom to discard one or two strain gauge readings if they are suspected for errors in measured strain due to installation or any other problems encountered during experiments.

Additionally, the total plate strains from the interfacial stress solution of Narayanamurthy et al. (2010) and simple beam theory are compared with the experimental results; and the effect of plate thickness on the total, axial and bending strains in the plate and on the interfacial shear and normal stresses are studied and critically discussed in this paper.

5.2 Plated Beam Test Specimen

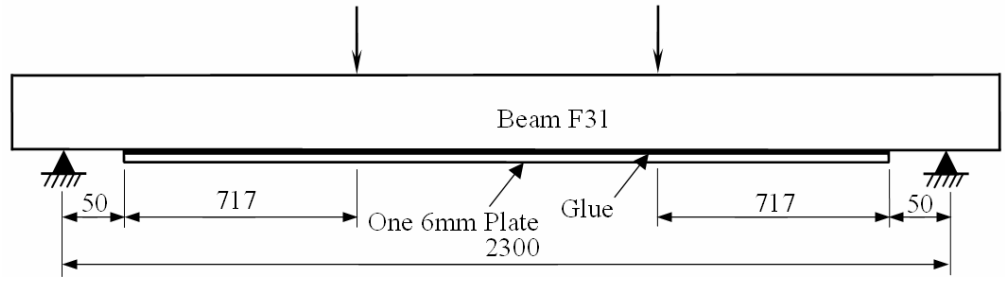

(a) RC beam bonded with one 6mm steel plate

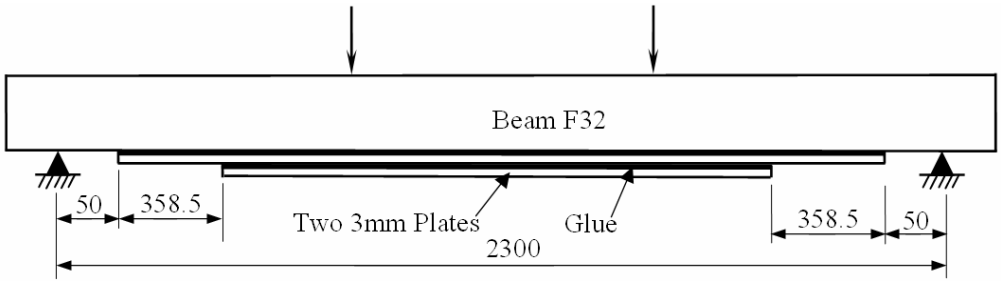

(b) RC beam bonded with two 3mm steel plates

Figure 5.1. Steel plated RC beams tested by Jones et al. (1988)

Jones et al. (1988) have conducted experiments on RC beams strengthened with different bonded plate configurations. The first two configurations shown in Figure 5.1 are considered as a typical case for the present study and analysis. The first one is the

RC beam plated with one single steel plate (F31 beam in Figure 5.1a) 6mm thick using an epoxy adhesive. The second one is the same RC beam plated with two steel plates each of 3mm thick bonded in a stepped configuration (F32 beam in Figure 5.1b). The thickness of the adhesive layer is 1.5 mm and is same in both configurations. The material and geometric properties of the above plated beam test specimens are given in Table 5.1. The measured plate strains and traditionally interpreted interfacial stresses from the experiments reported in their paper are used as a typical reference.

Table 5.1: Geometric and material properties of plated beam (Jones et al. 1988)

Component	Width (mm)	Depth (mm)	Length (mm)	Elastic Modulus (MPa)	Poisson's ratio
RC beam	$b_1 = 155$	$t_1 = 225$	$L = 2300$	$E_1 = 20\,000$	$\upsilon_1 = 0.17$
Adhesive layer	$b_a = 155$	$t_a = 1.5$	$L_a = 2200$	$E_a = 222$	$\upsilon_a = 0.35$
Steel plate	$b_2 = 155$	As shown in Figure 5.1		$E_2 = 200\,000$	$\upsilon_2 = 0.30$

5.3 Interfacial stresses from theoretical solution

Narayanamurthy et al.'s (2010) approach of interfacial stress analysis will be deployed in the interpretation of interfacial stresses from experiments, and is summarized here for ease of reference. This theoretical solution assumes a linear elastic material behaviour for the adherends and adhesive, with axial and bending deformations included for both the beam and the soffit plate. The adhesive layer is assumed to be subjected to stresses invariant across its thickness although part of the shear stress variation is captured within the capability of the composite beam theory. Compatibility of adherends deformations and the principle of superposition are adopted in the analysis. The solution for the original plated beam under external loading (Case-1) is obtained as the superposition of the composite beam solution having all the external loadings plus additional plate end loads (Case-2) and the plated beam solution subjected to only the opposite plate end loads (Case-3).

The general solution for the interfacial shear stress is given by

$$\tau(x,y) = m_c(y)V_{Tc}(x) + B_1\left[\cosh(\lambda x) - \sinh(\lambda x)\right] + m_1 V_T \tag{5.1}$$

where

$$m_c(y) = \frac{Q_e(y)}{I_e b_2} \tag{5.2}$$

$$B_1 = \frac{G_a}{E_1 \lambda}\left[r_1 M_1(0) - r_2 M_{pl} + (r_3 + r_4) N_{pl} - r_3 N_{pr}\right] \tag{5.3}$$

$$r_1 = \frac{y_1}{t_a I_1} + \frac{1}{I_e} \tag{5.4}$$

$$r_2 = \frac{y_2}{t_a R_{m2} I_2} + \frac{1}{I_e} \tag{5.5}$$

$$r_3 = \frac{1}{t_a A_1} - \frac{(y_c - t_1 + y_1)}{I_e} \tag{5.6}$$

$$r_4 = \frac{1}{t_a R_{m2} A_2} - \frac{(t_1 + t_a + y_2 - y_c)}{I_e} \tag{5.7}$$

$$M_1(0) = \frac{a}{L}\left[M_{pl} - M_{pr} + \left(N_{pl} - N_{pr}\right)\left(\frac{L}{a} y_1 + y_2 + t_a\right)\right] \tag{5.8}$$

$$N_{pl} = M(0)(y_1 + t_a + y_2) R_{ab} + N R_a \tag{5.9}$$

$$N_{pr} = M(L_p)(y_1 + t_a + y_2) R_{ab} + N R_a \tag{5.10}$$

$$M_{pl} = M(0) R_b \tag{5.11}$$

$$M_{pr} = M(L_p) R_b \tag{5.12}$$

$$\lambda^2 = \frac{G_a b_2}{t_a}\left[\frac{(y_1 + y_2)(y_1 + t_a + y_2)}{(E_1 I_1 + E_2 I_2)} + \frac{1}{E_1 A_1} + \frac{1}{E_2 A_2}\right] \tag{5.13}$$

$$m_1 = \frac{G_a}{\lambda^2}\left[\frac{y_1 + y_2}{t_a (E_1 I_1 + E_2 I_2)} + \frac{1}{E_1 I_e}\right] \tag{5.14}$$

$$V_T = \frac{1}{L}\left[M_{pl} - M_{pr} + (N_{pl} - N_{pr})(t_a + y_2)\right] \tag{5.15}$$

in which $Q_e(y)$ is the first moment of area of the equivalent plate and adhesive section below the considered position in the adhesive layer about the centroid of the composite beam section; I_e is the equivalent second moment of area of the composite beam section; $V_{Tc}(x)$ is the total shear force on the composite beam section at a distance of x from the plate end due to all the external loading (including the contribution from plate end loadings); y_1 and y_2 are the distances from the bottom of the adherend-1 (the original beam) and the top of the adherend-2 (the plate) to their respective centroids; y_c is the distance of the centroid of the composite beam section from the top surface; N_{pl}, N_{pr} and M_{pl}, M_{pr} refer to the axial forces and bending moments at the left and right plate ends respectively; $M(0)$ and $M(L_p)$ denote the bending moment at x=0 and x=L_p respectively on the beam under the original loading ignoring the plate end loads; N is the external axial load acting at the centroidal axis of the beam; G, E, A, I, b and t refer

to the shear modulus, elastic modulus, cross sectional area, second moment of area about the centroid of the concerned adherend (i.e. beam or plate), breadth and thickness respectively; subscripts 1, *a* and 2 respectively refer to the original beam, adhesive and plate; *a* is the distance between the plate curtailment and the nearest support of the beam; L_p is the plate length; L is the span of the plated beam; R_a is the axial stiffness ratio of the plate to the beam; R_b is the bending stiffness ratio of the plate to the beam; and R_{ab} is the ratio between the axial stiffness of the plate and the bending stiffness of the beam.

The general solution for the interfacial normal stress is given by

$$\sigma(x) = e^{-\beta x}\left[C_1 \cos(\beta x) + C_2 \sin(\beta x)\right] - n_1 \frac{d\tau(x)}{dx} \tag{5.16}$$

where

$$\beta = \left[\frac{E_a b_2}{4t_a}\left(\frac{1}{E_1 I_1} + \frac{1}{E_2 I_2}\right)\right]^{(0.25)} \tag{5.17}$$

$$n_1 = \frac{y_1 E_2 I_2 - y_2 E_1 I_1}{E_1 I_1 + E_2 I_2} \tag{5.18}$$

$$C_1 = \frac{E_a}{2\beta^3 t_a E_2 I_2}\left[R_b\left(V_T + \beta M_1(0)\right) + \beta M_{pl}\right] - \frac{n_2}{2\beta^3}\tau(0) + \frac{B_1 n_1 \lambda^3}{2\beta^3}\left(\lambda - \beta\right) \tag{5.19}$$

$$C_2 = \frac{B_1 n_1 \lambda^3}{2\beta^2} - \frac{E_a}{2\beta^2 t_a E_2 I_2}\left(R_b M_1(0) + M_{pl}\right) \tag{5.20}$$

5.4 A new interpretation of interfacial stresses from experiments

The interfacial stresses cannot be measured directly and can only be interpreted from the experimentally measured strains at the soffit of the plate. In order to overcome the limitation discussed in the traditional interpretation, a new technique has been developed as detailed below where the measured plate strains are expressed in terms of the plate end axial forces from which the interfacial stresses can be computed.

Consider only Case-3 of the plated beam subjected only to the plate end loads given in Narayanamurthy et al. (2010). The axial forces and moments in the bonded plate are given as

$$N_2(x) = b_2 \int_0^x \tau(x)dx - N_{pl} \tag{5.21}$$

$$M_2(x) = \frac{R_b}{1+R_b}\left[V_T x - [(N_2(x) + N_{pl})(y_1 + t_a + y_2)]\right] - M_{pl} \tag{5.22}$$

The longitudinal strain at the soffit of the plate is:

$$\varepsilon_{p3}(x) = \frac{y_2}{E_2 I_2} M_2(x) + \frac{1}{E_2 A_2} N_2(x) \tag{5.23}$$

Substituting Eq. 5.22 in to Eq. 5.23 yields

$$\varepsilon_{p3}(x) = w_2 V_T x - w_4 N_2(x) - w_3 N_{pl} - w_1 M_{pl} \tag{5.24}$$

where

$$w_1 = \frac{y_2}{E_2 I_2} \tag{5.25}$$

$$w_2 = \left(\frac{R_b}{1+R_b}\right) w_1 \tag{5.26}$$

$$w_3 = (y_1 + t_a + y_2) w_2 \tag{5.27}$$

$$w_4 = w_3 - \frac{1}{E_2 A_2} \tag{5.28}$$

Let,

$$w_5 = w_5(x) = (w_2 - w_4 b_2 m_1)x \tag{5.29}$$

$$w_6 = w_6(x) = \frac{G_a w_4 b_2}{E_1 \lambda^2}\left[\sinh(\lambda x) - \cosh(\lambda x) + 1\right] \tag{5.30}$$

Substituting Eqs 5.15 and 5.21 in to Eq. 5.24 provides

$$\varepsilon_{p3}(x) = w_7(x) M_{pl} + w_8(x) M_{pr} + w_9(x) N_{pl} + w_{10}(x) N_{pr} \tag{5.31}$$

where

$$w_7(x) = \frac{w_5(x)}{L} - w_1 + \left(r_2 - \frac{r_1 a}{L}\right) w_6(x) \tag{5.32}$$

$$w_8(x) = \frac{1}{L}\left(r_1 a w_6(x) - w_5(x)\right) \tag{5.33}$$

$$w_9(x) = \frac{w_5(x)}{L}(t_a + y_2) - w_3 + w_4 - \left[r_3 + r_4 + r_1 \frac{a}{L}\left(\frac{L}{a} y_1 + t_a + y_2\right)\right] w_6(x) \tag{5.34}$$

$$w_{10}(x) = \left[r_3 + r_1 \frac{a}{L}\left(\frac{L}{a} y_1 + t_a + y_2\right)\right] w_6(x) - \frac{w_5(x)}{L}(t_a + y_2) \tag{5.35}$$

The bending moments at the plate ends can be re-written from Eqs 5.9-5.12 as:

$$M_{pl} = (N_{pl} - NR_a)\frac{R_b}{R_{ab}(y_1 + t_a + y_2)} \tag{5.36}$$

$$M_{pr} = (N_{pr} - NR_a)\frac{R_b}{R_{ab}(y_1 + t_a + y_2)} \tag{5.37}$$

The plate strains can be expressed in terms of the plate end axial forces by substituting Eqs 5.36-5.37 in to Eq. 5.31 as

$$\varepsilon_{p3}(x) = w_{11}(x)N_{pl} + w_{12}(x)N_{pr} - w_{12a} \tag{5.38}$$

where

$$w_{11}(x) = \frac{R_b w_7(x)}{R_{ab}(y_1 + t_a + y_2)} + w_9(x) \tag{5.39}$$

$$w_{12}(x) = \frac{R_b w_8(x)}{R_{ab}(y_1 + t_a + y_2)} + w_{10}(x) \tag{5.40}$$

$$w_{12a} = \frac{NR_a R_b}{R_{ab}(y_1 + t_a + y_2)}\big(w_7(x) + w_8(x)\big) \tag{5.41}$$

Now consider Case-2 of the plated beam subjected to the external loading and plate end loads as given in Narayanamurthy et al. (2010).

The longitudinal strain at the soffit of the plate is:

$$\varepsilon_{p2}(x) = \frac{(t_1 + t_a + t_2 - y_c)}{E_1 I_e} M_{Tc}(x) \tag{5.42}$$

where I_e is the equivalent second moment of area of the composite beam section and $M_{Tc}(x)$ is the total bending moment at any section of the plated beam due to all external loading including the contribution from the plate end loadings. $M_{Tc}(x)$ depends on the type of loading on the plated beam. The loading arrangement considered in this study is the four point bending on the steel plated RC beam as shown in Fig.1 for which $M_{Tc}(x)$ can be written as:

$$M_{Tc}(x) = \begin{cases} R_{1y}(a + x) + N_{pr}(t_1 - y_c) + M_{pl} + N_{pl}(t_a + y_2); & 0 \le x < (l_1 - a) \\ R_{1y}(a + x) - P(a + x - l_1) + N_{pr}(t_1 - y_c) + M_{pl} + N_{pl}(t_a + y_2); & (l_1 - a) \le x \le 0.5L_p \end{cases} \tag{5.43}$$

where

$$R_{1y} = \frac{1}{L}\left[P(2L - l_1 - l_2) - (N_{pl} - N_{pr})(t_a + y_2) - M_{pl} + M_{pl}\right] \tag{5.44}$$

in which l_1 and l_2 are respectively the distances from the left support to the two concentrated loads (P) applied on the plated beam under four point bending arrangement.

Substituting Eq. 5.43 in to Eq. 5.42 and applying Eqs 5.36-5.37 in to the resulting expression yields

$$\varepsilon_{p2}(x) = \begin{Bmatrix} w_{13a}(x) + w_{18}(x)N_{pl} + w_{19}(x)N_{pr} & ; & 0 \le x < (l_1 - a) \\ w_{13b}(x) + w_{18}(x)N_{pl} + w_{19}(x)N_{pr} & ; & (l_1 - a) \le x \le 0.5L_p \end{Bmatrix} \tag{5.45}$$

where

$$w_{13a}(x) = \frac{P(a+x)(2L - l_1 - l_2)(t_1 + t_a + t_2 - y_c)}{E_1 I_e L} - w_{19a}(x) \tag{5.46}$$

$$w_{13b}(x) = \frac{P[(a+x)(2L - l_1 - l_2) - L(a + x - l_1)](t_1 + t_a + t_2 - y_c)}{E_1 I_e L} - w_{19a}(x) \tag{5.47}$$

$$w_{14}(x) = \frac{(L - a - x)(y_2 + t_a)(t_1 + t_a + t_2 - y_c)}{E_1 I_e L} \tag{5.48}$$

$$w_{15}(x) = \frac{[(a+x)(y_2 + t_a) + L(t_1 - y_c)](t_1 + t_a + t_2 - y_c)}{E_1 I_e L} \tag{5.49}$$

$$w_{16}(x) = \frac{w_{14}(x)}{(y_2 + t_a)} \tag{5.50}$$

$$w_{17}(x) = \frac{(a+x)(t_1 + t_a + t_2 - y_c)}{E_1 I_e L} \tag{5.51}$$

$$w_{18}(x) = w_{14}(x) + \frac{R_b w_{16}(x)}{R_{ab}(y_1 + t_a + y_2)} \tag{5.52}$$

$$w_{19}(x) = w_{15}(x) + \frac{R_b w_{17}(x)}{R_{ab}(y_1 + t_a + y_2)} \tag{5.53}$$

$$w_{19a}(x) = \frac{NR_a R_b[w_{16}(x) + w_{17}(x)]}{R_{ab}(y_1 + t_a + y_2)} \tag{5.54}$$

Let us now consider the original plated beam subjected to the external loading which is mentioned as a Case-1 in Narayanamurthy et al. (2010). The total longitudinal strain at

the soffit of the bonded plate is obtained as the summation of the plate strains given in Eqs 5.38 and 5.45 as given below.

$$\varepsilon_p(x) = \varepsilon_{p2}(x) + \varepsilon_{p3}(x) \tag{5.55}$$

$$\varepsilon_p(x) = \begin{Bmatrix} w_{13c}(x) + w_{20}(x)N_{pl} + w_{21}(x)N_{pr} & ; & 0 \le x < (l_1 - a) \\ w_{13d}(x) + w_{20}(x)N_{pl} + w_{21}(x)N_{pr} & ; & (l_1 - a) \le x \le 0.5L_p \end{Bmatrix} \tag{5.56}$$

where

$$w_{13c}(x) = w_{13a}(x) - w_{12a}(x) \tag{5.57}$$

$$w_{13d}(x) = w_{13b}(x) - w_{12a}(x) \tag{5.58}$$

$$w_{20}(x) = w_{11}(x) + w_{18}(x) \tag{5.59}$$

$$w_{21}(x) = w_{12}(x) + w_{19}(x) \tag{5.60}$$

Thus, the plate strain at a given (measurement) location is expressed in terms of the two unknown plate end axial forces (Eq. 5.55). If strain measurements at two locations are made, the two plate end axial forces can be obtained by solving the resultant pair of simultaneous equations. Once the two plate end axial forces are known, all other parameters can be computed and the interfacial shear and normal stresses can be obtained from Eqs 5.1 and 5.16 respectively.

In practical experiments, usually more than two strain gauges are used to measure the plate strain at different locations along the plate length. This leads to more equations than required, but more accurate results can be obtained by making use of all the measurements by determining the plate end axial forces using the least squares method. This technique gives the possibility to discard even one or two strain gauge readings if they are suspected for any errors in measured strain due to mounting, installation or any other problems encountered during experiments.

5.5 Comparison of interfacial stresses

The experimentally measured plate strains reported in Jones et al. (1988) for the steel plated RC beam (plated beam specimens F31 and F32 shown in Figure 5.1) are used for the computation of interfacial stresses using the technique detailed in the previous section. The deduced interfacial shear and normal stresses are compared (Figures 5.2-

5.7) with the theoretical solution of Narayanamurthy et al. (2010) and the interfacial shear stress is compared with the traditional interpretations by Jones et al. (1988). The prediction of interfacial normal stress which could not be obtained directly from plate strain measurements in experiments is an added advantage of the new technique

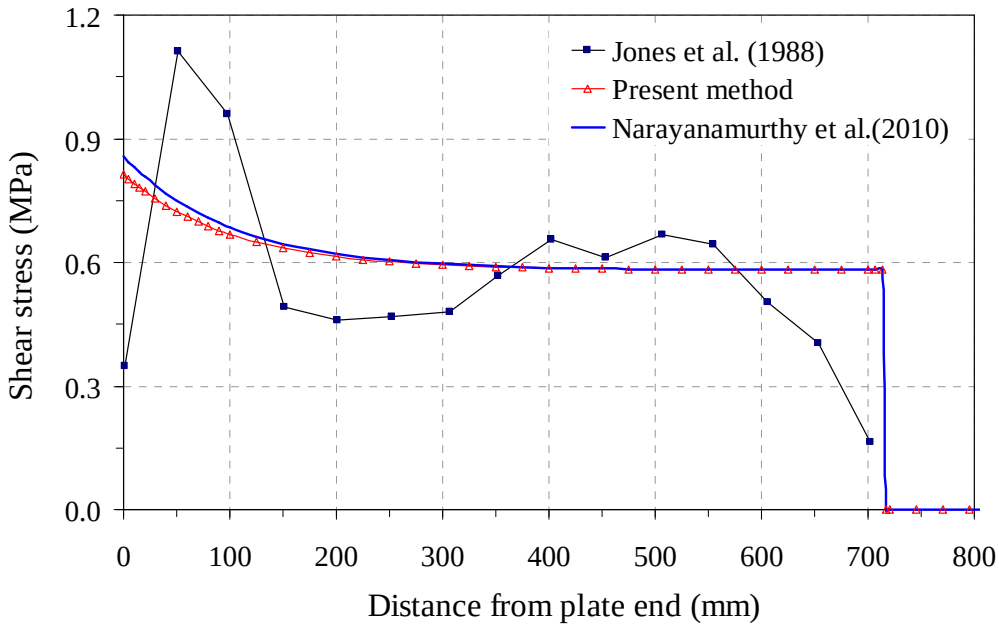

(a) Interfacial shear stress

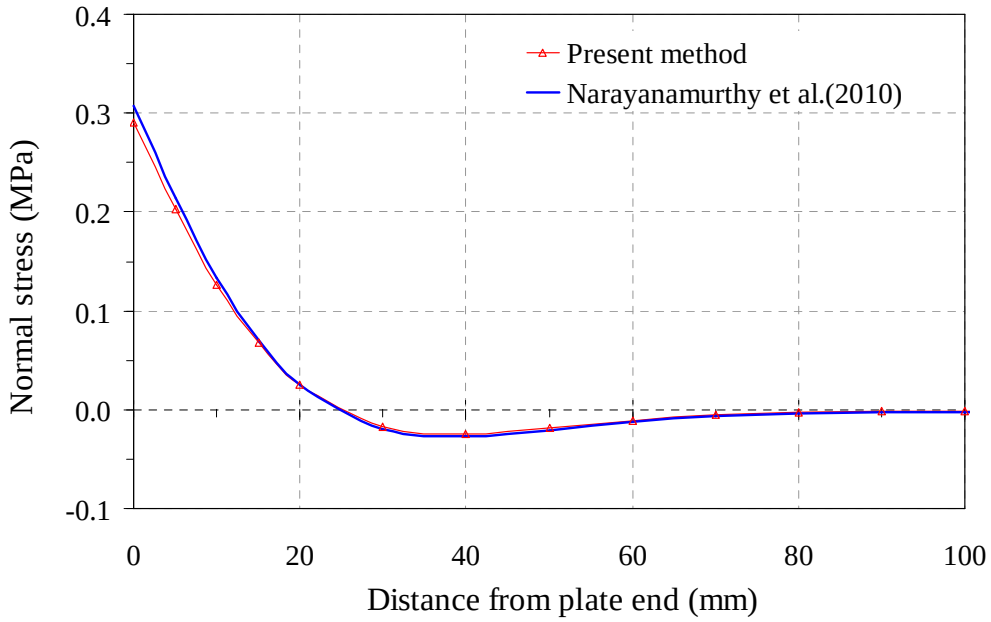

(b) Interfacial normal stress

Figure 5.2. Interfacial stresses in F31 beam at 60 kN (nearer to SLS) from present method, traditional interpretation and theoretical solution

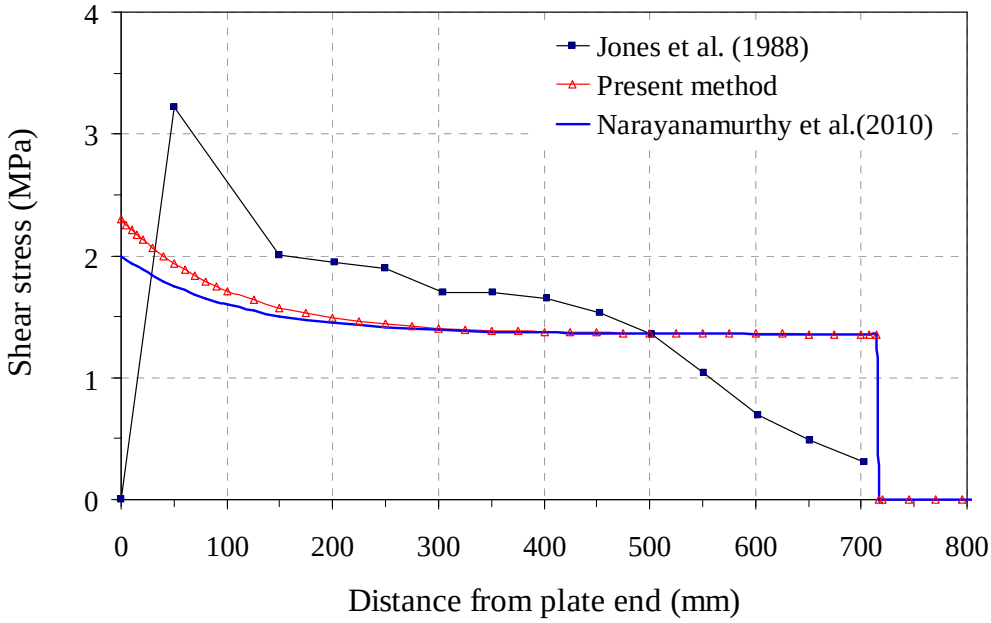

(a) Interfacial shear stress

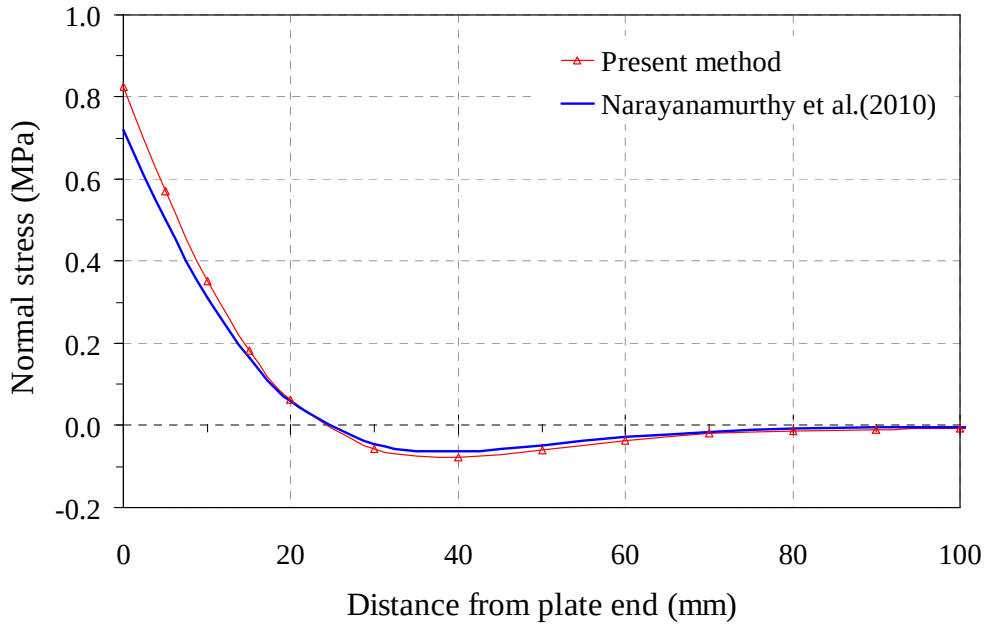

(b) Interfacial normal stress

Figure 5.3. Interfacial stresses in F31 beam at 140 kN (above SLS) from present method, traditional interpretation and theoretical solution

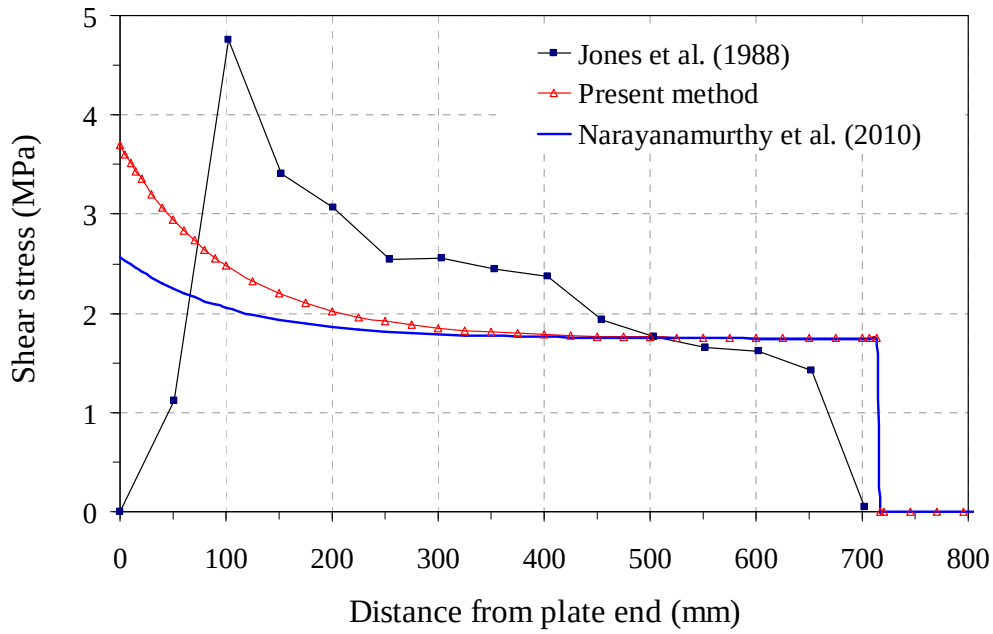

(a) Interfacial shear stress

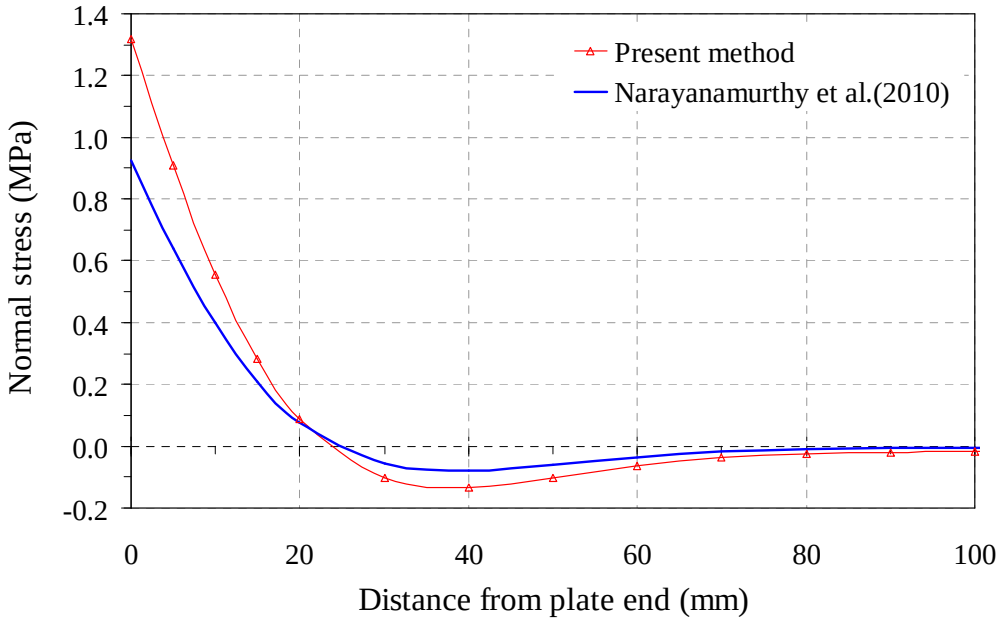

(b) Interfacial normal stress

Figure 5.4. Interfacial stresses in F31 beam at 180 kN (close to ULS) from present method, traditional interpretation and theoretical solution

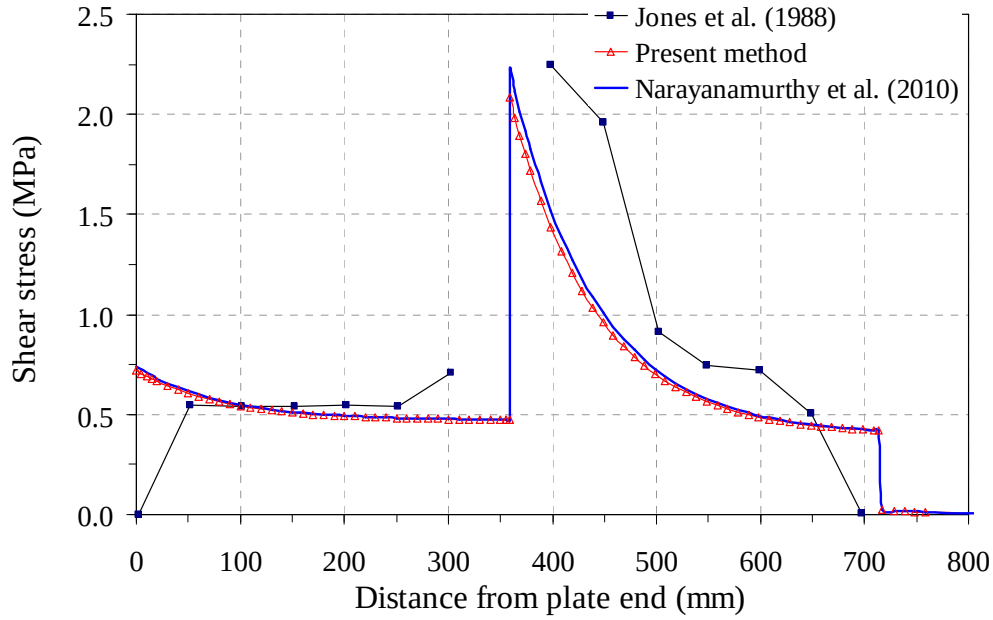

(a) Interfacial shear stress

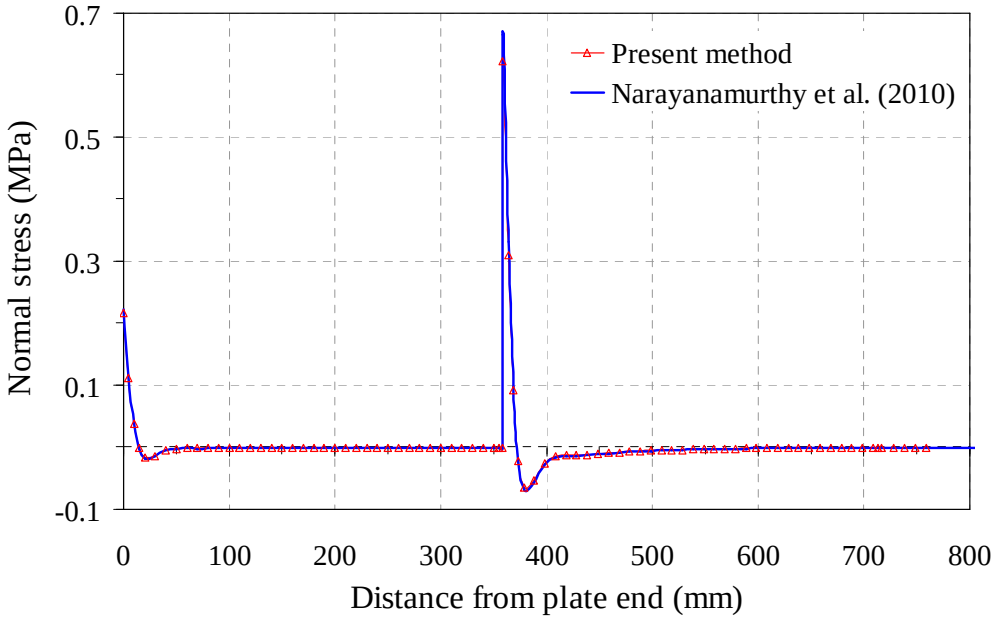

(b) Interfacial normal stress

Figure 5.5. Interfacial stresses in F32 beam at 80 kN (nearer to SLS) from present method, traditional interpretation and theoretical solution

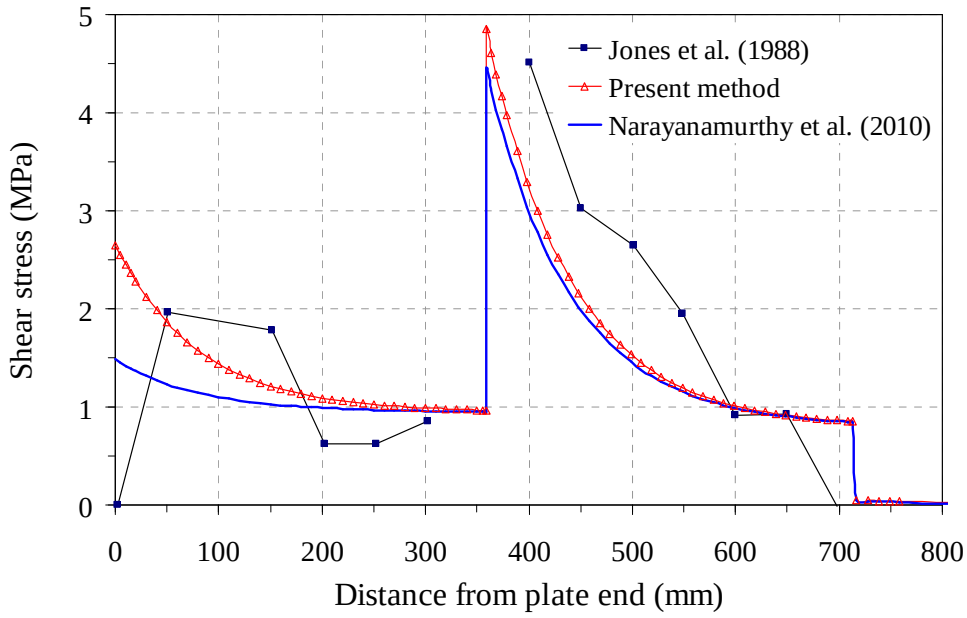

(a) Interfacial shear stress

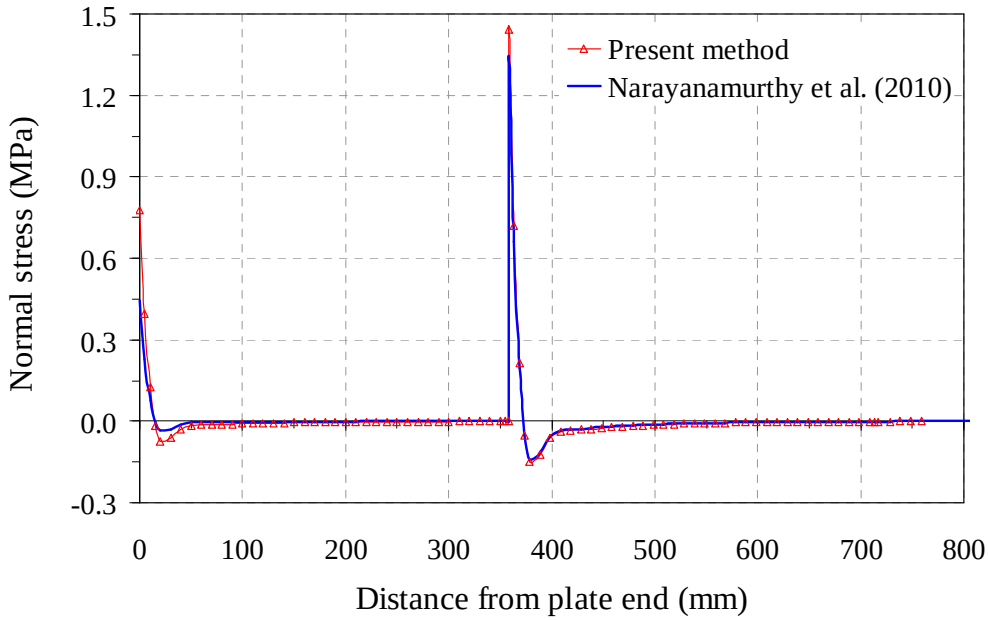

(b) Interfacial normal stress

Figure 5.6. Interfacial stresses in F32 beam at 160 kN (above SLS) from present method, traditional interpretation and theoretical solution

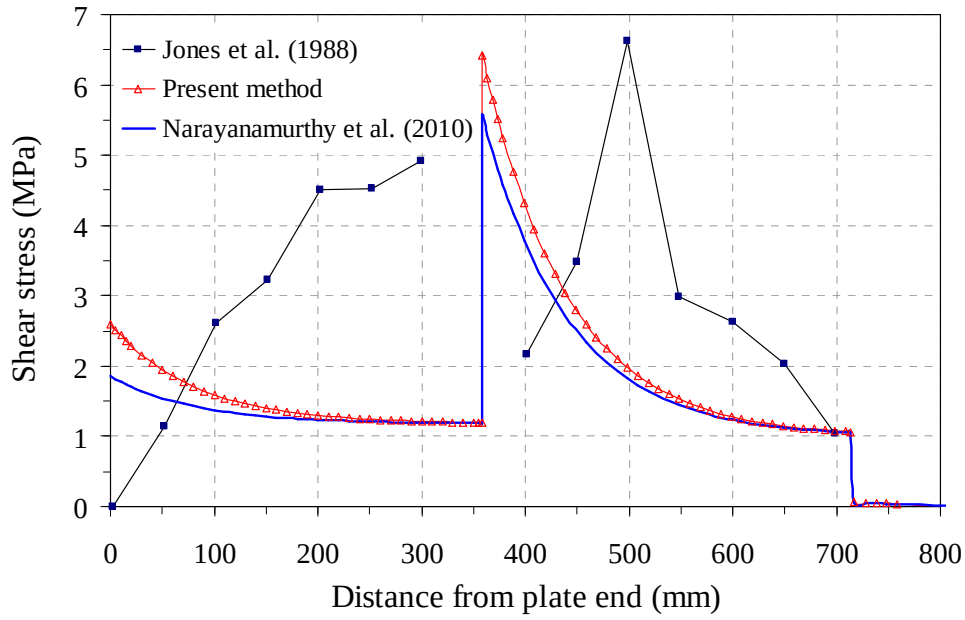

(a) Interfacial shear stress

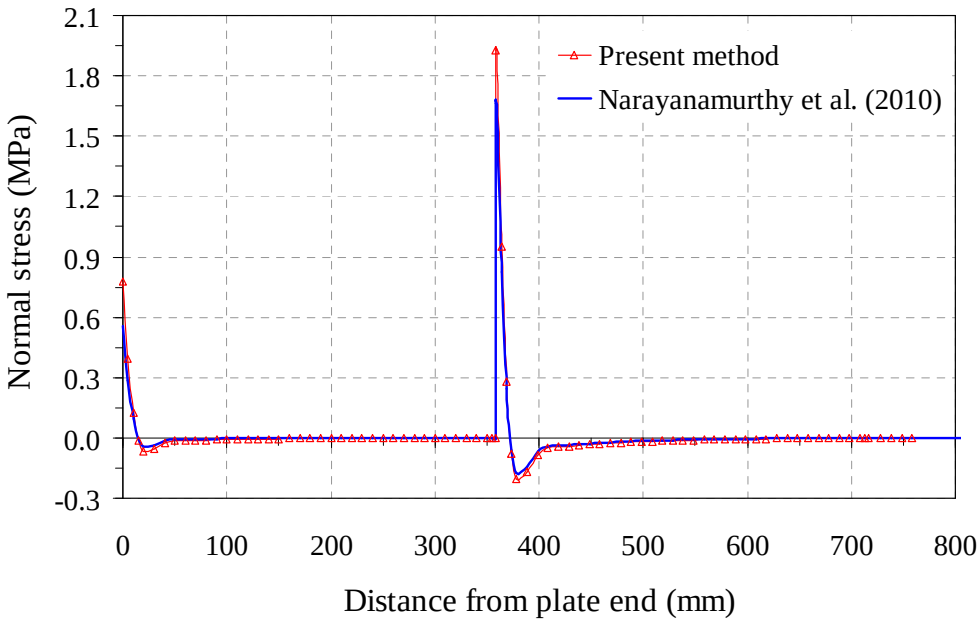

(b) Interfacial normal stress

Figure 5.7. Interfacial stresses in F32 beam at 200 kN (close to ULS) from present method, traditional interpretation and theoretical solution

The failure of F31 beam was by plate separation at a load of 182 kN (Jones et al., 1988). The interpreted interfacial stresses from experiments are closer to the theoretical predictions of Narayanamurthy et al. (2010) at a notional service load of 60 kN as shown in Figure 5.2. The experimental interpretations are found to increase on the

higher side than the theoretical predictions for higher loads of 140 kN and 180 kN (Figures 5.3-5.4). This can be justified as Narayanamurthy et al. (2010) gives correct results for the plated beam in elastic stage that may exist up to service load, beyond which materials non-linearity begins to play a more significant role.

The interfacial stresses between the plates for the F32 beam with stepped steel plates bonded to the RC beam are found by treating the RC beam and the upper plate as a composite section, with the lower plate as the strengthening. A similar approach has already been adopted in Stratford and Cadei (2006). The failure of F32 beam was by inner plate separation and the failure load was 208 kN (Jones et al., 1988). Similar to F31 beam, the deduced interfacial stresses from experiments are very close (Figure 5.5) to Narayanamurthy et al. (2010) for a load of 80 kN which is near to service load. The experimental interpretations are higher than the theoretical predictions for higher loads of 160 kN and 200 kN (Figures 5.6-5.7). In all the above cases, the interfacial shear stresses deduced by Jones et al. (1988) is far away from the newly interpreted stresses and theoretical predictions due to the limitations in the traditional interpretation method.

5.6 Comparison of plate strains

The longitudinal strain measured at the soffit of the plate for F31 and F32 beams (Jones et al., 1988) is compared with the theoretically predicted strains from Narayanamurthy et al. (2010) and with simple beam theory. The axial and bending strains in the plates are also computed and discussed in this section. The longitudinal strain at the soffit of the plate in Narayanamurthy et al.'s (2010) solution is obtained as the summation of Eqs 5.23 and 5.42 as:

$$\varepsilon_p(x) = \frac{(t_1 + t_a + t_2 - y_c)}{E_1 I_e} M_{Tc}(x) + \frac{y_2}{E_2 I_2} M_2(x) + \frac{1}{E_2 A_2} N_2(x) \tag{5.61}$$

The plate strain predicted from simple beam theory is

$$\varepsilon_p(x) = \frac{(t_1 + t_a + t_2 - y_c)}{E_1 I_e} M(x) \tag{5.62}$$

where $M(x)$ is the bending moment in the beam due to external loading alone. The predictions of Narayanamurthy et al. (2010) agree well with the experimentally measured plate strains for 60 kN on F31 beam. The simple beam theory predictions are reasonably close to the others except at the plate end which is an important location for initiation of plate end debonding failures, as shown in Figure 5.8. The measured plate strains are higher than the theoretical predictions as the load increases close to failure i.e at 140 kN and 180 kN as shown in Figures 5.9-5.10. The predictions from Narayanamurthy et al. are closer to the measured strains from the beginning of the stepped plate for F32 beam as compared to the simple beam theory at the loads of 80 kN, 160 kN and 200 kN as shown in Figures 5.11-5.13. Just ahead of the stepped plate termination, the theoretical predictions are much lower than the measured strains at all the above three loads, with their difference increasing as the loads increase towards failure.

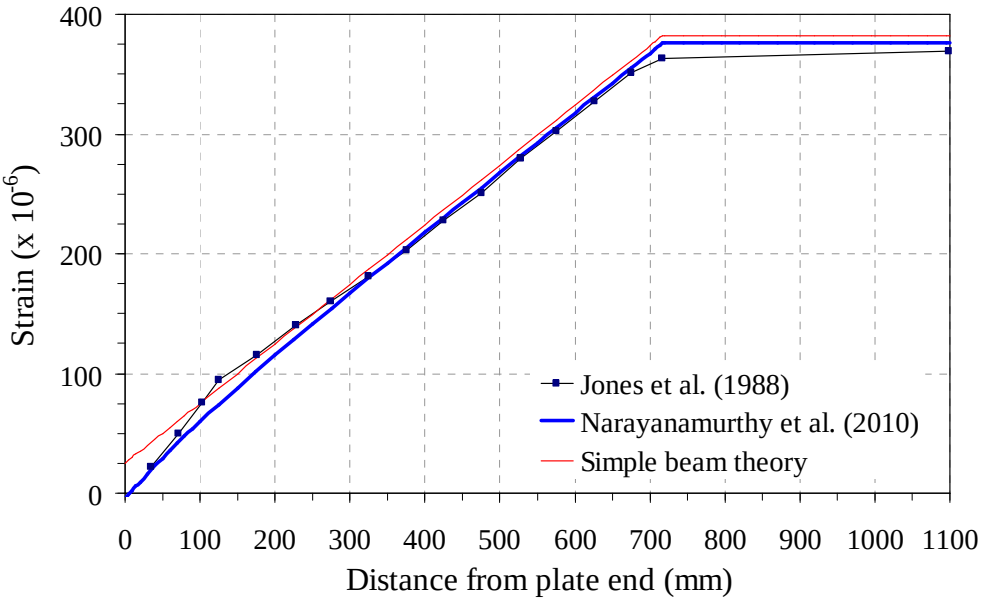

Figure 5.8. Total plate strain in F31 beam at 60 kN (nearer to SLS) from experiment and theory

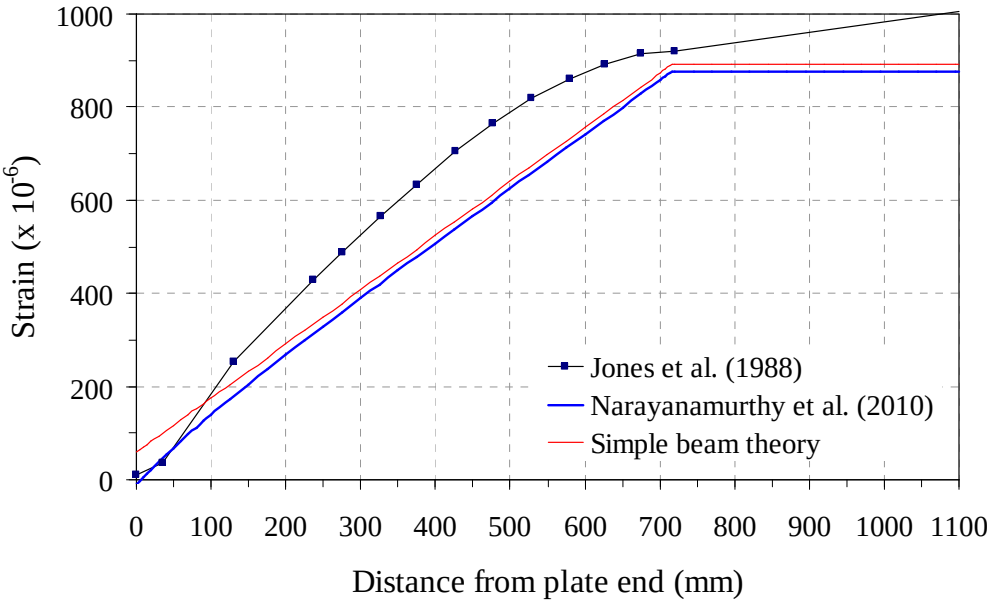

Figure 5.9. Total plate strain in F31 beam at 140 kN (above SLS) from experiment and theory

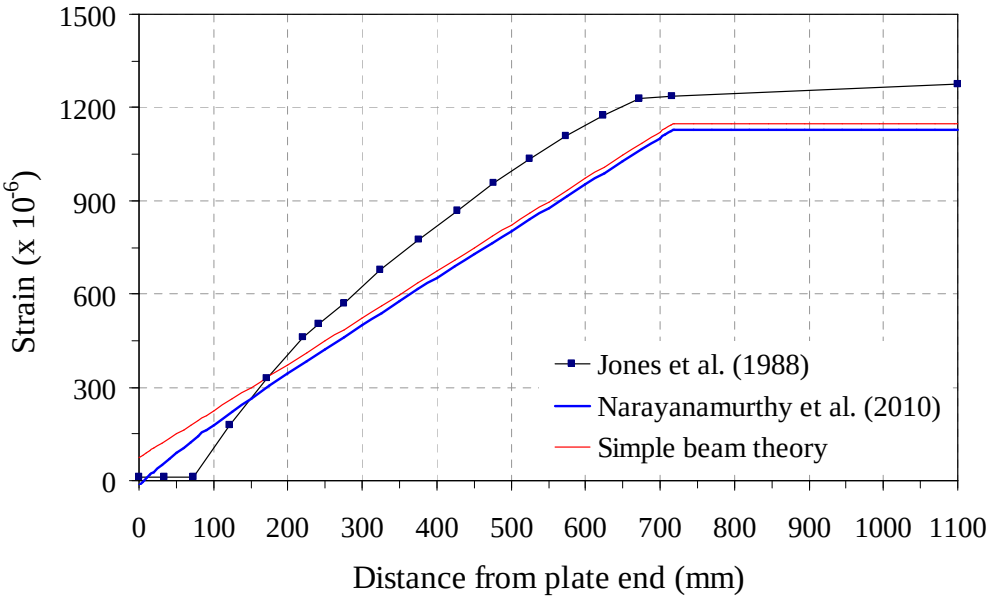

Figure 5.10. Total plate strain in F31 beam at 180 kN (close to ULS) from experiment and theory

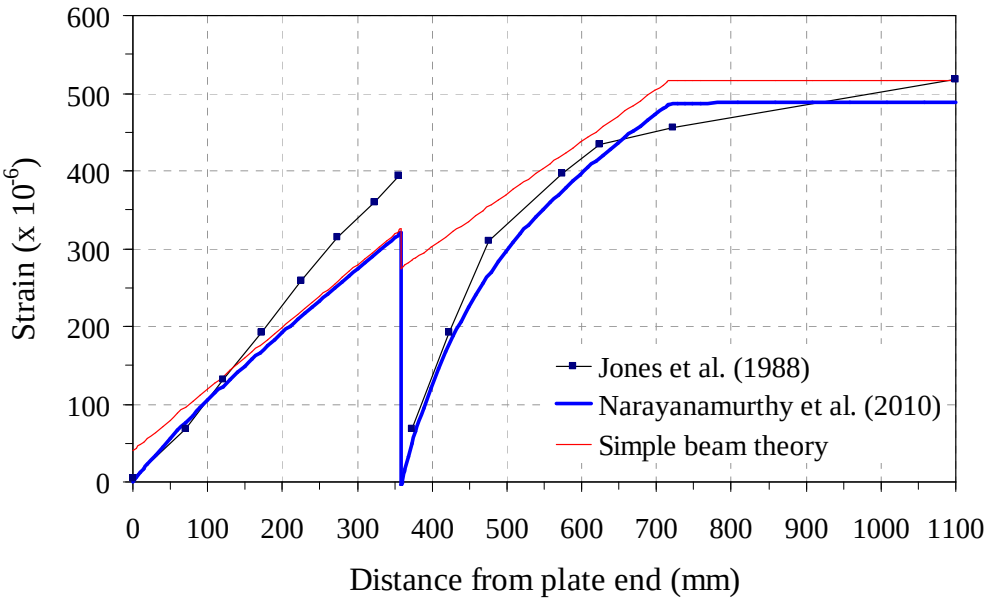

Figure 5.11. Total plate strain in F32 beam at 80 kN (nearer to SLS) from experiment and theory

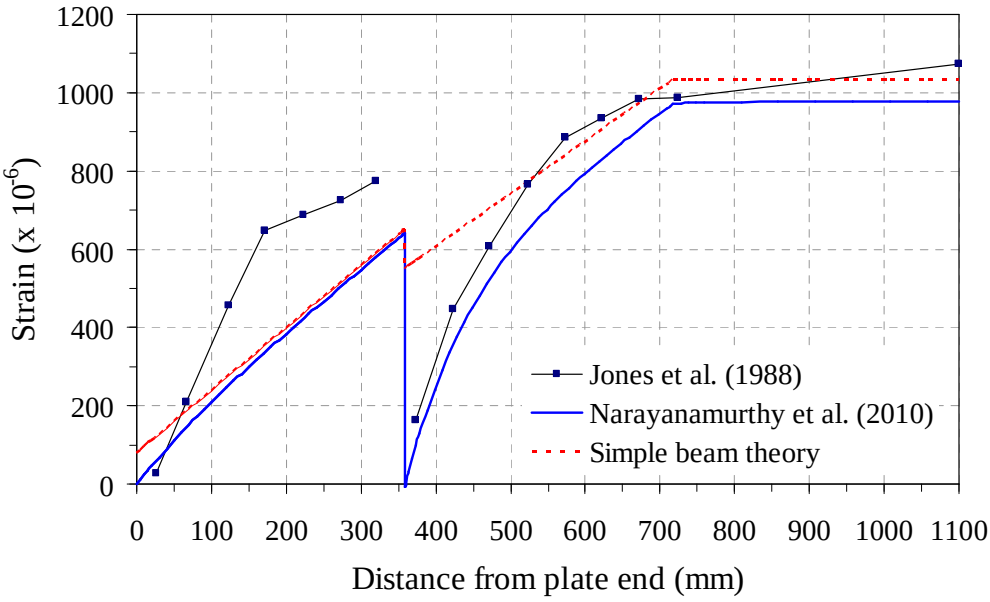

Figure 5.12. Total plate strain in F32 beam at 160 kN (above SLS) from experiment and theory

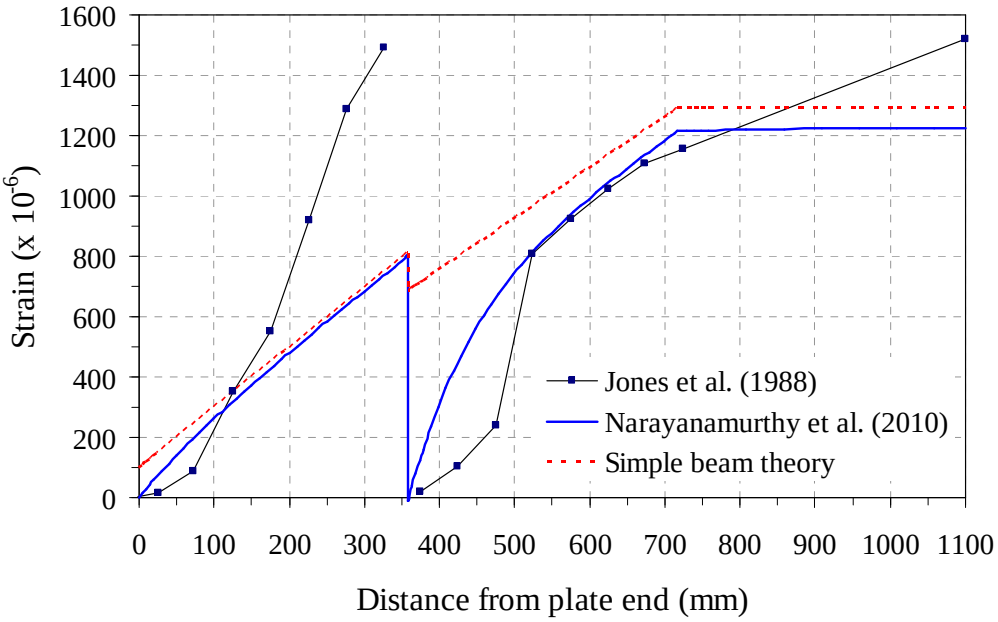

Figure 5.13. Total plate strain in F32 beam at 200 kN (close to ULS) from experiment and theory

The plate strains from simple beam theory are significantly higher at the plate ends and slightly higher at the remaining locations. This is because the simple beam theory cannot capture the stress concentration caused by the geometric discontinuity at the plate ends and also it assumes that there are no relative longitudinal or vertical displacements between the two adherends at the adhesive interface.

5.7 Parametric study

A parametric study has been conducted to understand the effect of plate thickness on the predicted total, axial and bending strain components and on the interfacial shear and normal stresses for beam F31 subjected to a load of 60 kN, based on Narayanamurthy et al. (2010). The geometric and material properties of the F31 beam remain as given in Table 5.1 except for the variation in plate thickness. Figure 5.14a shows the variation of total longitudinal strain at the soffit of the plate for a plate thickness ranging from 1 to 12mm. The predicted strain is non linear and is found to increase for decreasing plate thickness. The predicted axial strain shows a similar trend (Figure 5.14b). Unlike axial strains, the magnitudes of the bending strains (Figure 5.14c) are far lower and are found to increase for increasing thickness of the plate. The magnitude of bending strains increases from 1- 32% of the axial strains as the plate thickness increases from 1-12 mm (Figure 5.14d). An increase in plate thickness increases both the predicted interfacial

shear and normal stresses (Figures 5.15a-b). The normal stresses are always less than the interfacial shear stresses and, unlike interfacial shear stress, tend to reach zero within a short distance from the plate termination.

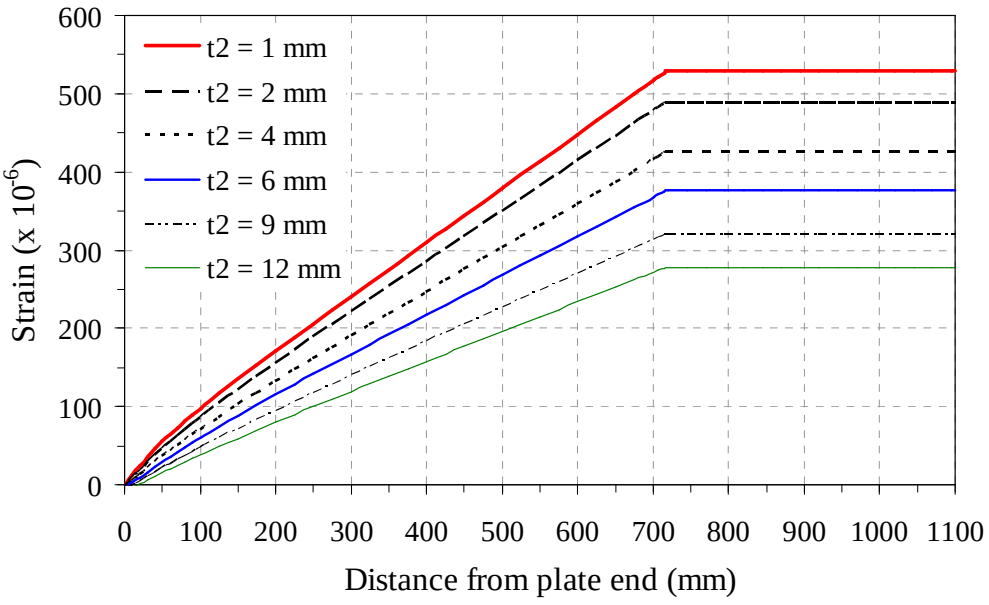

(a) Total Strain

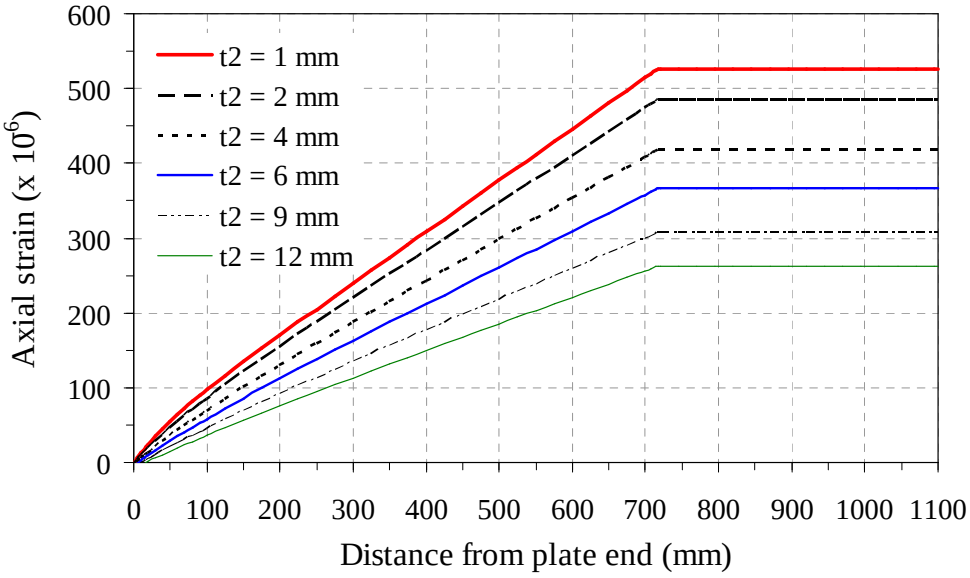

(b) Axial Strain

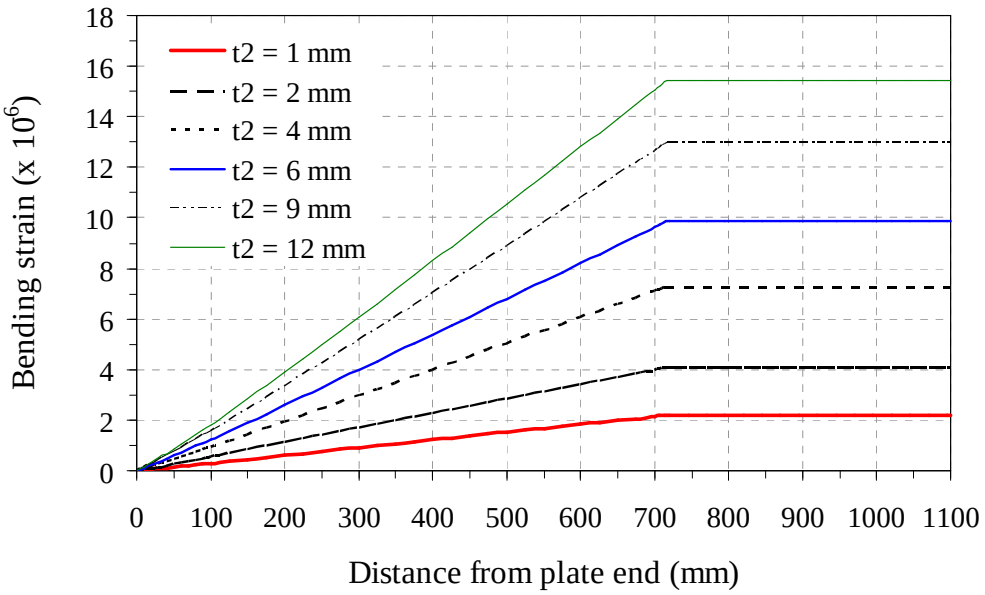

(c) Bending Strain

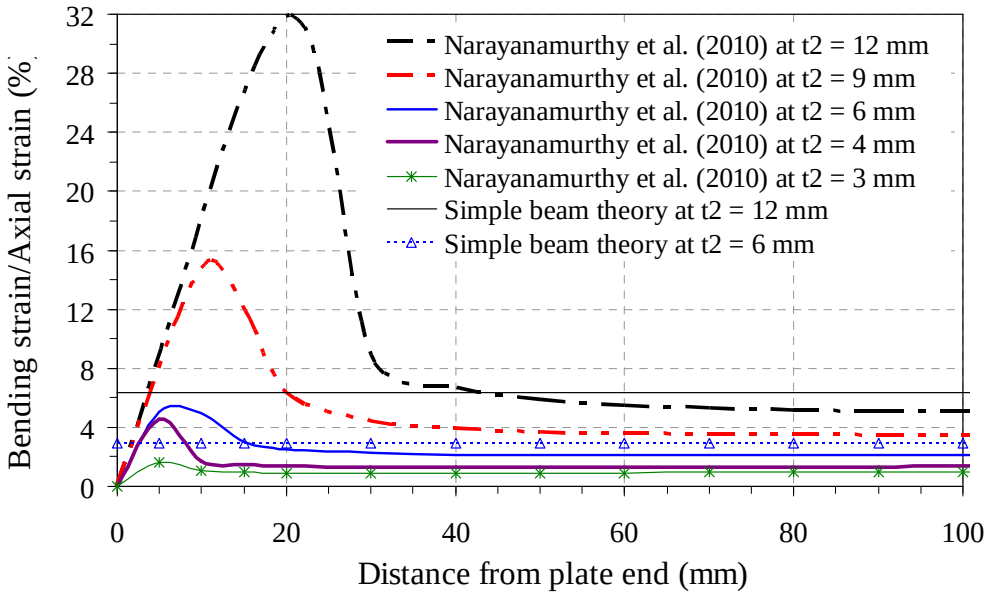

(d) Ratio of bending strain-to-axial strain (%)

Figure 5.14. Effect of plate thickness on predicted plate strain in F31 beam at 60 kN

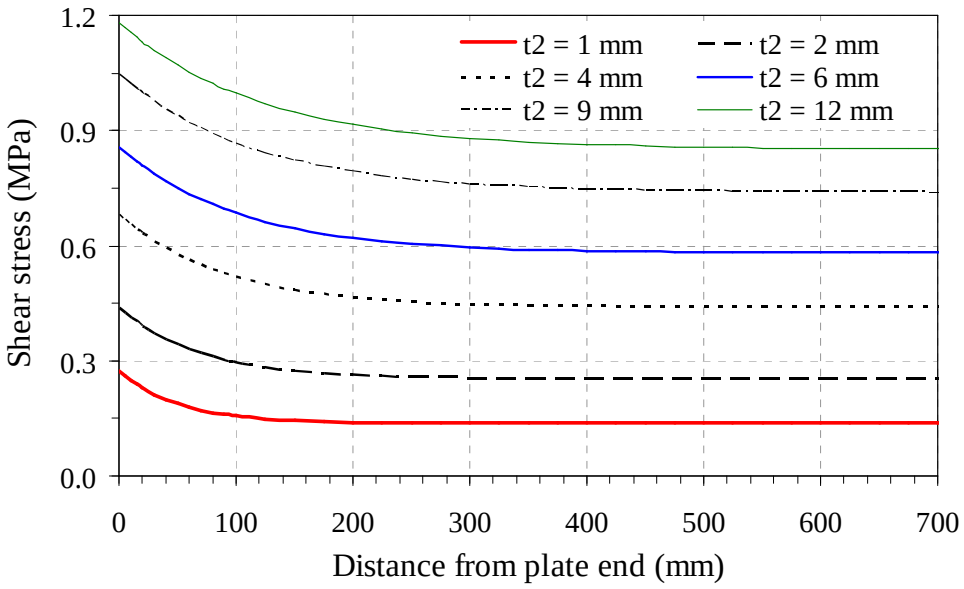

(a) Interfacial shear stress

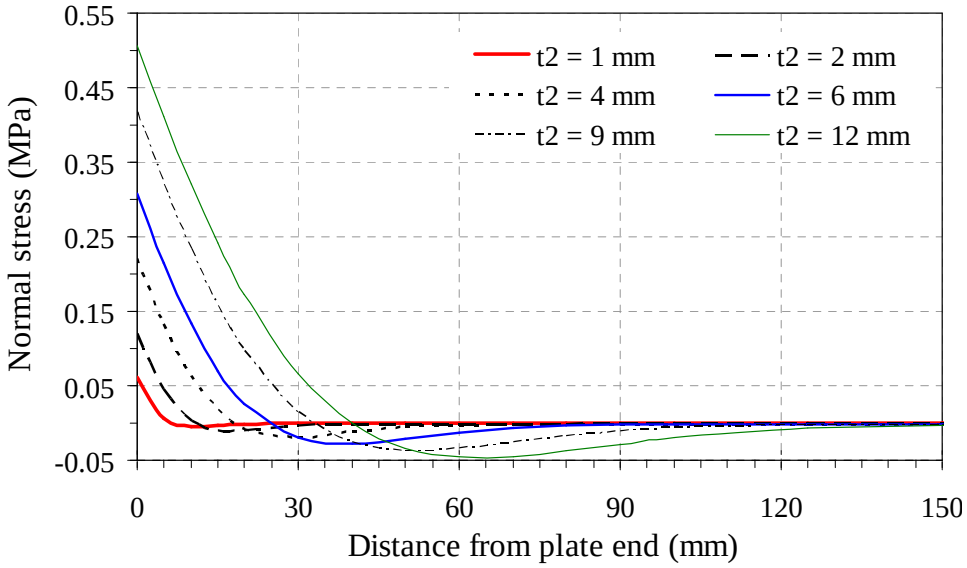

(b) Interfacial normal stress

Figure 15. Effect of plate thickness on predicted interfacial stresses in F31 beam at 60 kN

5.8 Conclusions

Concentration of higher interfacial shear and normal stresses at the plate ends are responsible for plate end interfacial debonding failures in plated beams. Hence, it is important to quantify these interfacial stresses for the safe design of plated beams. In all the experimental studies, the interfacial shear stress is deduced traditionally from the measured plate strains assuming that the plate is under pure tension. The peeling effect at the interface of the adherends is neglected, leading to severe approximations in the interpreted interfacial shear stress. It is also not possible to directly compute the interfacial normal stresses from the strain measurements along the plate soffit. The new technique developed and demonstrated in this chapter overcomes these limitations and helps in the accurate interpretation of interfacial shear and normal stresses from experiments besides offering flexibility in selection of the measured strain readings. The variation in the components of plate strain and interfacial stresses for different plate thickness is illustrated through the parametric study that highlights that the peeling effects due to bending strains are significant at the plate end.

Chapter 6

Plate End Flexural Debonding Models for Plated Beams

Abstract

Reinforced concrete (RC) beams flexurally strengthened by adhesively bonding fibre reinforced polymer (FRP) or steel plate at their tension face are susceptible to premature plate end debonding failures. Safe design of such a strengthened RC beam demands a reliable and predictive debonding strength model. There are two special cases of plate end debonding failures: flexural debonding for the case when the plate terminates within a constant bending moment zone (CMR) and shear debonding for the case when the plate terminates at places where the shear force is large but the bending moment is minimal. An interaction equation is usually used to model a general plate end debonding case. This chapter is concerned with flexural debonding. A brief review of existing models is presented before the plate end interfacial stresses are examined. Three new models with different levels of accuracy are then developed: the first ever theoretical model based on a simplified interfacial fracture mechanics analysis; a semi-empirical model; and an empirical model. These three models together with two existing models are assessed with a carefully constructed test database containing 67 test data from an extensive literature survey.

6.1 Introduction

RC beams strengthened in flexure by adhesive bonding of an FRP or steel plate to their tension (soffit) face are vulnerable to various debonding failures. There are many different classifications of these debonding failures, but they may be broadly classified into two types: plate end debonding (PED) and intermediate crack induced debonding (ICD) (Teng and Chen 2009). Several ICD strength models are now available, either based on extensive finite element analysis (FEA) (Lu et al., 2005b) or rigorous mechanics analysis (Teng et al., 2003; Chen et al., 2006; Teng et al., 2006; Chen et al. 2007). In contrast, all existing PED strength models are either empirical or semi-empirical.

The PED failure initiates at or near the plate ends. It appears in different modes (Teng and Chen 2009): (1) concrete cover separation; (2) interfacial debonding at the adhesive interface; (3) mixed mode with a combination of (1) and (2); (4) critical diagonal crack (CDC) initiated concrete cover separation; and (5) critical diagonal crack (CDC) initiated interfacial debonding. The first three types of PED failure are observed in RC beams with plates terminated in constant bending moment region (CMR) or where bending deformation is dominant. These debonding failures are brittle in nature and occur usually well before the full flexural capacity of the plated section is achieved. Many empirical or semi-empirical models have been developed for predicting PED strength. A thorough review and classification of all debonding strength models priori to 2002 can be found in Smith and Teng (2002a, b).

Oehlers (1992) introduced a methodology to develop a PED strength model in three stages based on the location where the plate terminates: (1) a flexural debonding model that caters for the case where the plate terminates in CMR; (2) a shear debonding model that caters for the case where plate terminates in a pure shear or high shear region with zero or low bending moment; and (3) an interaction model based on these above two special models that caters for any region in between the above two cases (shear-moment region). This methodology was subsequently adopted by Smith and Teng (2003) where an interaction model was proposed fully based on limited test data. The debonding shear capacity model of Smith and Teng (2002b) was used in this interaction model. More recently, Teng and Yao (2007) developed a more accurate interaction model following Oehlers' (1992) strategy.

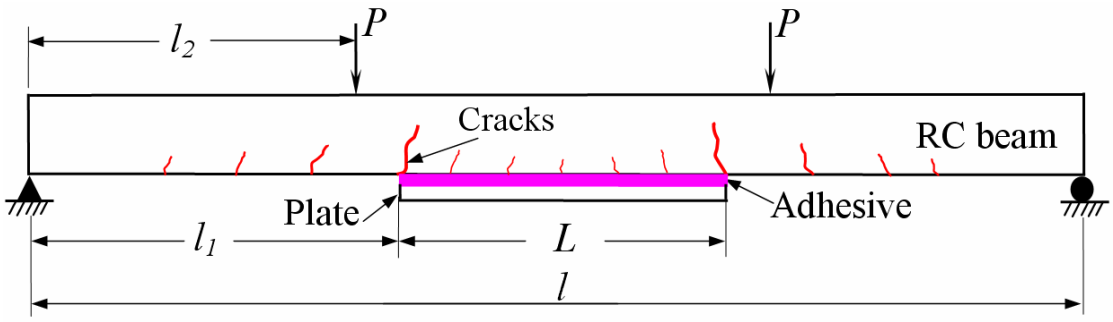

Figure 6.1. Flexural-strengthened RC beam with plate terminated in CMR

Based on the above discussion, PED in a CMR does not only represent a special case of PED, but more importantly, its corresponding flexural debonding strength model often forms the basis of a general model for predicting PED. However, very limited research is concerned with PED in a CMR and only two flexural debonding models have been developed (Oehlers and Moran, 1990; Teng and Yao, 2007). Oehlers and Moran's (1990) model is a semi-theoretical one calibrated with 43 steel plated beams and its accuracy was found to be poorer by Teng and Yao (2007) when applied to FRP plated beams. Teng and Yao's (2007) empirical model was developed based on the test results of 16 FRP and steel plated beams: there is a need for its accuracy and reliability to be assessed with a large test database.

This chapter is concerned with flexural debonding strength model for the special case of RC beams with the plate terminated in CMR, such as the one illustrated in Figure 6.1. The existing two models are introduced first before the plate end interfacial stresses are examined. Three new models with different levels of accuracy are then developed. These three models together with the two existing models are assessed with a carefully constructed test database containing 67 test data from an extensive literature survey.

6.2 Existing Flexural Debonding Models

To the best knowledge of the authors, only two flexural debonding models are available in the open literature. They are summarized as follows.

6.2.1 Oehlers and Moran's (1990) model

Based on an approximate elastic analysis, FEA and subsequent calibration with test results of 43 steel plated beams, Oehlers and Moran (1990) proposed the following semi-empirical flexural debonding model:

$$M_{Oeh} = \frac{(EI)_{c,p}\, f_t}{0.901 E_2 t_2} \tag{6.1}$$

where M_{Oeh} is the predicted debonding moment from Eq. 6.1; $(EI)_{c,p}$ is the flexural rigidity of the cracked tensile reinforced plated beam section; f_t is the splitting tensile strength of the concrete; E and t are respectively the elastic modulus and thickness; and subscripts *1* and *2* denote the beam and plate respectively.

6.2.2 Teng and Yao's (2007) model

Teng and Yao (2007) developed an empirical model based on the test results of 4 steel plated and 12 FRP plated RC beams to predict the debonding moment $M_{T\text{-}Y}$:

$$M_{T-Y} = \frac{0.488 M_{u,0}}{(\alpha_a \alpha_f \alpha_w)^{(1/9)}} \le M_{u,0} \tag{6.2a}$$

where $M_{u,0}$ is the moment capacity of the un-plated beam. The plate to beam axial stiffness ratio α_a, flexural stiffness enhancement ratio α_f, and the beam to plate width ratio α_w are

$$\alpha_a = \frac{E_2 t_2}{E_1 d_e}; \qquad \alpha_f = \frac{(EI)_{c,p} - (EI)_{c,0}}{(EI)_{c,0}}; \qquad \alpha_w = \frac{b_1}{b_2} \le 3 \tag{6.2b}$$

in which b and I are respectively the breadth and second moment of area; d_e is the effective depth of the beam; and $(EI)_{c,0}$ is the flexural rigidity of the cracked tensile reinforced un-plated beam section.

6.3 Assessment of Peeling and Shear Effect from Adhesion Analysis

The adherends undergo longitudinal and vertical displacements relative to each other when the beam is loaded. The former introduces interfacial shear stresses whilst the latter is responsible for the peeling effect between the adherends. These two effects are termed Mode-2 and Mode-1 respectively in fracture mechanics. The PED failure is usually a combination of these two modes, but their relative significance depends on the

geometry, material and loading of the plated beam. A simplistic assessment of their relative significance for the concerned case with the plate terminated in the CMR is attempted here based on the elastic adhesion analysis but much more rigorous further research is obviously required.

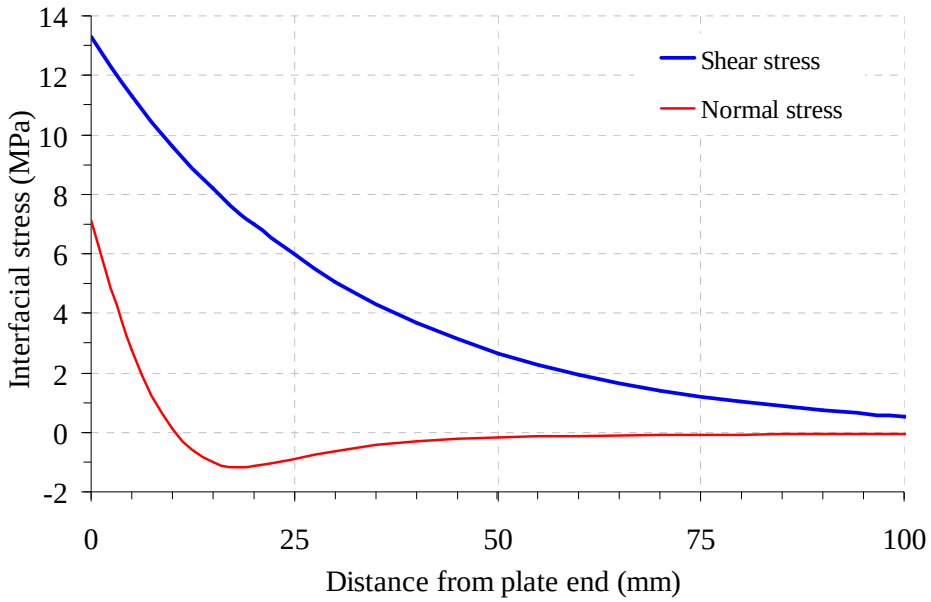

Figure 6.2. Interfacial stresses in a typical steel plated RC beam with plate terminated in CMR

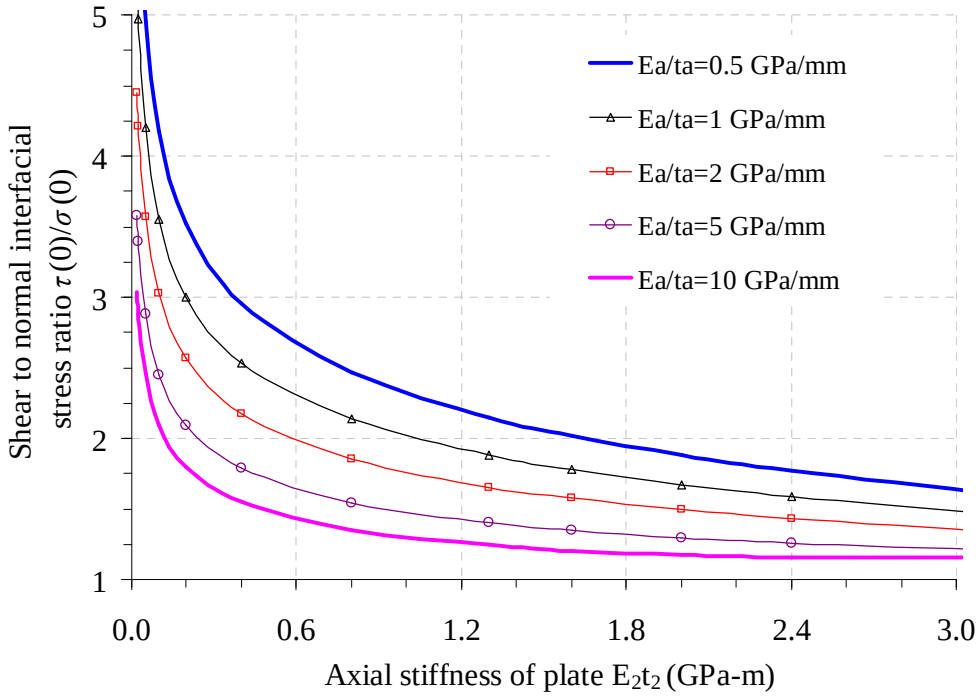

Figure 6.3. Interfacial shear versus normal stress at plate end in a plated beam with plates terminated in CMR

Figure 6.2 shows the interfacial shear stress $\tau(x)$ and normal stress $\sigma(x)$ found from Narayanamurthy et al.'s (2010) solution for a test steel plated RC beam (S13/20 in Oehlers and Moran (1990), see Tables 6.1-6.2) with plates terminated in CMR. The adhesive was assumed to have an elastic modulus of 3GPa in the calculation. Peak interfacial shear stress is about 85% higher than the interfacial normal (peeling) stress. These interfacial stresses are mostly influenced by the shear stiffness of adhesive and the axial stiffness of the plate. Figure 6.3 shows that within a wide range of these two parameters, the peak interfacial shear stress is predominant as compared to the peak interfacial normal stress. For practical values of adhesive and plate stiffnesses, the peak shear stress can be greater than the peak normal stress by about 50-500%. Therefore, it may be reasonable to assume that the Mode-2 fracture dominates in the concerned flexural debonding and Mode-1 fracture is neglected in the following analysis for simplicity.

6.4 Interfacial Shear Behaviour

The interfacial shear behaviour is modelled in this section that can lead to the development of a theoretical flexural debonding model in plated beams.

6.4.1 Bonded joint model

Consider a simply supported RC beam with a span of l and under four point bending (Figure 6.1). It is strengthened in flexure by adhesive bonding of an FRP or steel plate of length L within the CMR. The PED in this beam may be considered by investigating the plated beam segment between the two major flexural cracks at the two plate end locations. Cracks between the two ends of the plate are neglected but their effects on the axial and flexural stiffness can be easily taken into consideration by using values of the cracked section. This plated beam segment between two cracks is idealised as a bonded joint and is subjected to identical axial forces and bending moments on both sides as shown in Figure 6.4. The plate ends are unstressed. The adhesive is assumed to have a constant thickness and the bond stress is assumed to be constant through its thickness.

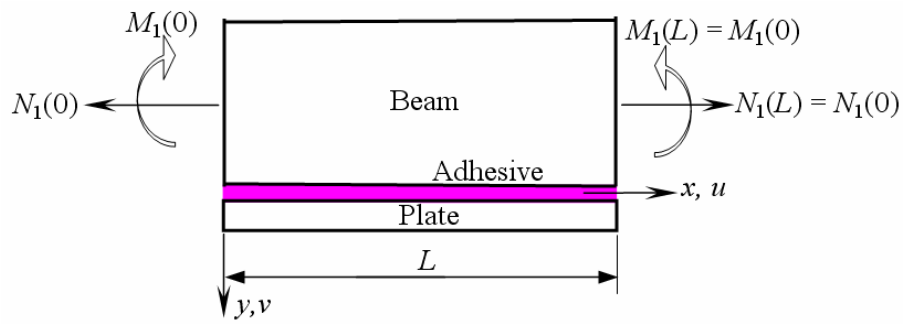

Figure 6.4. Idealised bond model

The interfacial shear behaviour of the idealised joint is investigated in this section, considering the deformations in the adherends due to axial forces, transverse shear forces and bending moments. Note that transverse shear forces are present in the adherends that acts against each other due to the transfer of forces between them, despite the total shear force on the plated section being zero in the CMR. The adherends are assumed to behave linearly although the effect of cracking on their stiffnesses may be considered as noted above. The curvature of the adherends are assumed to be the same in relating the bending moments of the adherends

6.4.2 Governing equations

The equilibrium, constitutive relations and the interface compatibility requirements for a differential segment of the plated beam between two flexural cracks as shown in Figure 6.5 are used to derive the governing differential equations to analyse the initiation and propagation of plate end debonding in a flexurally strengthened plated beam. Longitudinal, vertical and moment equilibrium gives

$$\frac{dN_i(x)}{dx} = (-1)^i b_2 \tau(x); \qquad i = 1, 2 \tag{6.3}$$

$$\frac{dV_i(x)}{dx} = (-1)^i b_2 \sigma(x); \qquad i = 1, 2 \tag{6.4}$$

$$\frac{dM_i(x)}{dx} = V_i(x) - b_2 y_i \tau(x); \qquad i = 1, 2 \tag{6.5}$$

where $N_i(x)$, $V_i(x)$ and $M_i(x)$ refer respectively to axial force, transverse shear force and bending moment in the adherend; y_1 and y_2 are the distances from the bottom of beam and top of plate to their respective centroids.

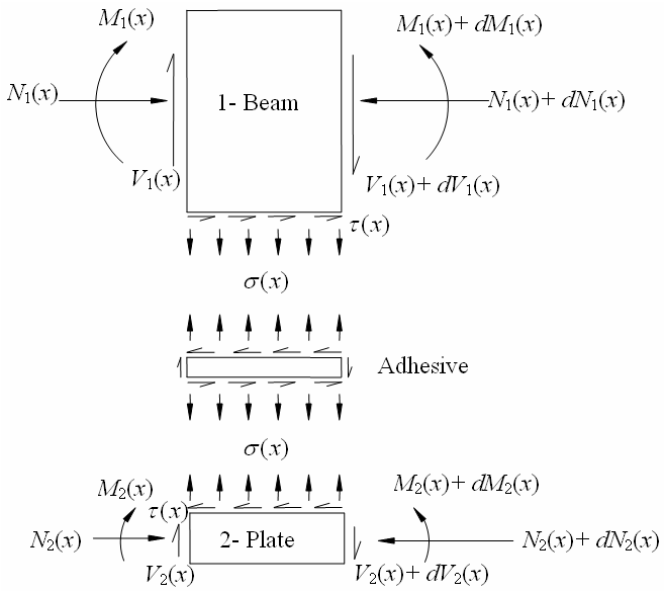

Figure 6.5. Differential segment in a bonded joint model

The total axial force, shear force and moment at any section of the plated beam are

$$N_T(x) = N_1(x) + N_2(x) \tag{6.6}$$

$$V_T(x) = V_1(x) + V_2(x) + b_2 t_a \tau(x) \tag{6.7}$$

$$M_T(x) = M_1(x) + M_2(x) + N_2(x)\left[t_1 + t_a + y_2 - y_c\right] - N_1(x)\left[y_c - (t_1 - y_1)\right] \tag{6.8}$$

where y_c is the distance of the centroid of the plated section from the top surface of the beam and t_a is the thickness of the adhesive layer.

From the constitutive relationship for the adherends, the longitudinal strain at the bottom of adherend-1 $\varepsilon_1(x)$ and at the top of adherend-2 $\varepsilon_2(x)$ are:

$$\varepsilon_i(x) = \frac{du_i(x)}{dx} = (-1)^{i+1}\frac{y_i}{E_i I_i}M_i(x) + \frac{1}{E_i A_i}N_i(x); \qquad i = 1, 2 \tag{6.9}$$

where $u(x)$ is the longitudinal displacement of the adherends.

The moment in the beam and the plate can be related by assuming curvature compatibility:

$$R_b M_1(x) = M_2(x) \tag{6.10}$$

where R_b is the ratio between the flexural stiffness (EI) of the plate and the beam.

The relative longitudinal displacement at the interface between the beam and the plate is the interfacial slip $\delta(x)$ given by

$$\delta(x) = u_2(x) - u_1(x) \tag{6.11}$$

Taking the first derivative of Eq. 6.11 with respect to *x* and substituting Eqs 6.3 and 6.8-6.10 into the resulting expression provides the relationship between $N_2(x)$ and $\delta(x)$ as

$$N_2(x) = \left(\frac{(y_1 + y_2)(y_1 + t_a + y_2)}{E_1 I_1 + E_2 I_2} + \frac{1}{E_1 A_1} + \frac{1}{E_2 A_2} \right)^{-1} \left[\frac{d\delta}{dx} + \frac{(y_1 + y_2)}{E_1 I_1 + E_2 I_2} M_T(x) \right] \tag{6.12a}$$

Assuming that the local bond-slip relationship is bi-linear, the interfacial fracture energy $G_f = \tau_f \delta_f / 2$ where τ_f is the local bond strength and δ_f is the interfacial slip at initiation of debonding is introduced into Eq. 6.12a that yields

$$N_2(x) = \frac{\tau_f^2 b_2}{2 G_f \lambda^2} \left(\frac{d\delta(x)}{dx} + m\lambda^2 M_T(x) \right) \tag{6.12b}$$

where

$$\lambda^2 = \frac{\tau_f^2 b_2}{2 G_f} \left[\frac{(y_1 + y_2)(y_1 + t_a + y_2)}{E_1 I_1 + E_2 I_2} + \frac{1}{E_1 A_1} + \frac{1}{E_2 A_2} \right] \tag{6.12c}$$

$$m = \frac{1}{\lambda^2} \left[\frac{y_1 + y_2}{(E_1 I_1 + E_2 I_2)} \right] \tag{6.12d}$$

Differentiating Eq. 6.12b once with respect to *x*, substituting Eq. 6.3 into the resulting equation and replacing $\tau(x)$ by $f(\delta)$ yield the governing differential equation for the bonded joint as

$$\frac{d^2\delta(x)}{dx^2} - \frac{2 G_f \lambda^2}{\tau_f^2} f(\delta) + m\lambda^2 V_T(x) = 0 \tag{6.13}$$

In a constant moment region $V_T(x) = 0$, so, Eq. 6.13 is reduced to

$$\frac{d^2\delta(x)}{dx^2} - \frac{2 G_f \lambda^2}{\tau_f^2} f(\delta) = 0 \tag{6.14}$$

The Eq. 6.14 can be solved if the local bond slip model relating the local interfacial bond stress to the local interfacial slip represented by $f(\delta)$ is established.

6.4.3 Local deformation (bond-slip) model

Previous experimental (Sebastian, 2001; Chajes et al., 1995, 1996; Bizindavyi and Neale, 1999; Dai et al., 2005; Yao et al., 2005a, b) and analytical (Yuan et al., 2004; Lu et al., 2005a, b; Teng et al., 2006; Wang, 2006a, b) studies have shown that the bond-slip relationship at the interface between the adherends is nonlinear where a bilinear model with a linearly ascending branch (linear elastic stage) followed by a linearly descending branch (softening stage) represents a close approximation to the bond-slip

behaviour of the bonded joint. In this bilinear model, the local interfacial shear stress increases linearly with the increases in the interfacial slip until it reaches the peak shear

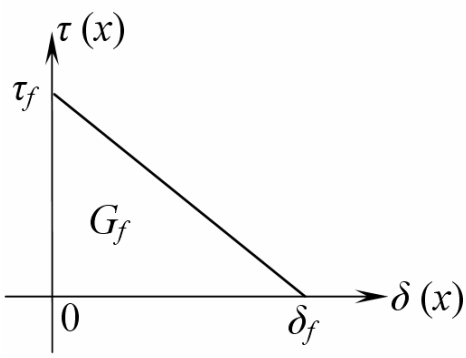

Figure 6.6. Linearly softening local bond-slip model

stress (bond strength) τ_f which is followed by initiation of interfacial softening (micro-cracking). This is accompanied by decreases in the interfacial shear stress and increases in the interfacial slip until the shear stress reaches zero at an ultimate slip of δ_f which initiates macro cracking or debonding. Experimental studies have shown that the elastic deformation δ_1 at τ_f is much smaller than the δ_f so it is neglected and a linearly softening bond-slip model as shown in Figure 6.6 is adopted in this study. This simplification has an insignificant effect on the final predictions (Chen et al. 2007). This bond-slip model can be described mathematically as:

$$\tau(x) = f(\delta) = \begin{cases} 0 & \text{when } \delta(x) = 0 \\ \dfrac{\tau_f}{\delta_f}[\delta_f - \delta(x)] & \text{when } 0 < \delta(x) \le \delta_f \end{cases} \tag{6.15}$$

The governing equation (Eq. 6.14) can be solved using the cohesive model in Eq. 6.15 to find the distributions of the interfacial shear stress and interfacial slip along the interface and load-displacement response in the bonded joint.

6.4.4 Failure process and solution for different states of interface

Figure 6.7 shows the interfacial shear stress distribution and the sequence of debonding propagation for a typical failure process for the bonded joint shown in Figure 6.4. Under loading, a point of the interface can be in a rigid, softening, or debonded state. Letters R (rigid), S (softening) and D (debonding) are used to describe the states of the interface from the left to the right. The entire interface is initially rigid because the adopted local bond–slip model neglects any elastic deformation. Softening initiates at the plate ends as soon as any loading is applied resulting in micro-cracking and interfacial slip. The

softening length a of the interface increases with increases in loading and reaches a_d when debonding (macro-cracking) initiates. The interface ahead of the softening front remains rigid and has no interfacial stresses in the present analysis (Figure 6.7a-c), which makes the softening front abrupt whereas when a bilinear bond-slip model is used the actual stress distribution would be smooth ahead of the softening front throughout the whole loading process (Teng et al. 2006).

Because β=1 in the CMR, the interface during the failure process is symmetrical about the middle of the bonded joint so only half of the interface (from x = 0 to 0.5L) needs to be considered in this analysis. Assuming that the bond length is sufficiently large so that $L > 2a_d$, (if $L \leq 2a_d$ no debonding state exists), the interface experiences progressively the following states during the loading process:

1) softening–rigid (S–R) state (Figure 6.7a);
2) debonding–softening–rigid (D–S–R) state (Figure 6.7b,c); and
3) debonding–softening (D–S) state (Figure 6.7d,e).

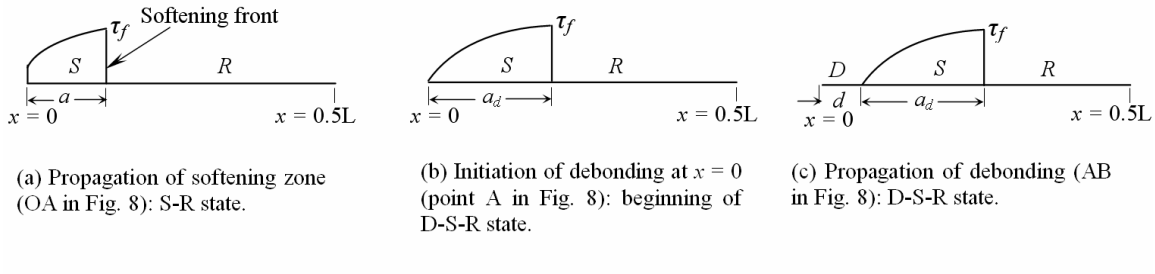

(a) Propagation of softening zone (OA in Fig. 8): S-R state.

(b) Initiation of debonding at x = 0 (point A in Fig. 8): beginning of D-S-R state.

(c) Propagation of debonding (AB in Fig. 8): D-S-R state.

(d) Softening front reaches x = 0.5L; disappearance of R zone (point B in Fig. 8): beginning of D-S state.

(e) Propagation of debonding till failure (B onwards in Fig. 8): D-S

Figure 6.7 Failure process and distribution of interfacial shear stress at different states of interface in the bonded joint

The solutions for the different interface states described above are deduced as follows. Substituting Eq. 6.15 for the case of $0 < \delta(x) \leq \delta_f$ into Eq. 6.14 yields the governing equation for the softening interface as:

$$\frac{d^2\delta(x)}{dx^2} + \lambda^2\delta(x) = \lambda^2\delta_f \tag{6.16}$$

The interfacial slip, the interfacial shear stress and the axial force in the plate for the softening region can be found by solving Eq. 6.16.

Softening–rigid (S–R) interface

The interface remains in S–R state as shown in Figure 6.7a until the debonding bending moment M_{Td} is reached at the left plate end (x = 0) when the loads are increased gradually from zero. The general solution for the softening region of the interface ($0 \le x \le a$) with $0 < \delta(x) \le \delta_f$ is given by

$$\delta(x) = A_1 \sin[\lambda(x-a)] + B_1 \cos[\lambda(x-a)] + \delta_f \tag{6.17a}$$

$$\tau(x) = -\frac{\tau_f}{\delta_f}\left(A_1 \sin[\lambda(x-a)] + B_1 \cos[\lambda(x-a)]\right) \tag{6.17b}$$

$$N_2(x) = m_1\left(A_1\lambda \cos[\lambda(x-a)] - B_1\lambda \sin[\lambda(x-a)] + m\lambda^2 M_T(x)\right). \tag{6.17c}$$

where

$$m_1 = \frac{\tau_f^2 b_2}{2G_f\lambda^2} \tag{6.17d}$$

The boundary and continuity conditions at the softening region of the interface are:

$N_2(x) = 0$ at $x = 0$ (6.18a)

$N_2(x)$ is continuous at $x = a$ (6.18b)

$\delta(x) = 0$ at $x = a$ (6.18c)

The constants of integration A_1 and B_1 and the softening length a are obtained by applying Eqs 6.18a-c to Eqs 6.17a-c as given below.

$$A_1 = 0; \qquad B_1 = -\delta_f \tag{6.19}$$

$$\delta_f \sin(\lambda a) = m\lambda M_T \tag{6.20}$$

The softening length a increases gradually with the applied loading. The relative displacements between the adherends at left end referred to as Δ_0 can be obtained from Eq. 6.17a as:

$$\Delta_0 = \delta_f[1 - \cos(\lambda a)] \tag{6.21}$$

Debonding–softening–rigid (D–S–R) interface

An S–R interface becomes a D–S–R interface (Figure 6.7b) when Δ_0 reaches δ_f. From Eq. 6.21 this gives

$$a_d = \frac{\pi}{2\lambda} \tag{6.22}$$

The applied bending moment at the initiation of debonding M_{Td} can be obtained from Eq. 6.20 as:

$$M_{Td} = \frac{\delta_f}{m\lambda} \tag{6.23}$$

The shape and length of the softening regions and the applied loading remains constant until the rigid region of the interface ahead of the softening front vanishes as debonding propagates. This is achieved by the movement of the softening front steadily towards the mid-length of the bonded joint ($x = 0.5L$) as shown in Figure 6.7c-d. In this process, the debonded length d at the left end of the interface increases from 0 to ($0.5L–a_d$).

Solutions given in Eqs 6.17–6.20 are valid if x is replaced by [x-(0.5L–d)] and a by a_d. The axial plate force within the debonded zone is zero. Considering Eq. 6.12b, the slip or the relative displacement at x = 0 during D–S–R state of interface can be obtained as

$$\Delta_0 = \delta_f + m\lambda^2 M_{Td} d \tag{6.24}$$

Alternatively, a direct elastic analysis gives the following expression which is the same as Eq. 6.24:

$$\Delta_0 = \delta_f + \frac{M_{Td}}{E_1 I_1} y_1 d \tag{6.25}$$

Debonding–softening (D–S) interface

A D–S–R interface becomes a D–S interface when the length of the rigid region ahead of the softening front reduces to zero and $d = (0.5L - a_d)$ as shown in Figure 6.7d. The general solutions in Eqs 6.17a–c are valid if (x–a) is replaced by [x – (0.5L – a)] and the constants of integration A_1 and B_1 are replaced by A_2 and B_2, which can be determined from the following boundary and symmetric conditions for the softening region of the interface:

$N_2(x) = 0$ at $x = (0.5L–a)$ (6.26a)

$\delta(x) = \delta_f$ at $x = (0.5L–a)$ (6.26b)

$\delta(x) = 0$ at $x = 0.5L$ (6.26c)

Application of Eqs 6.26a-c to the modified general solutions from Eqs 6.17a–c as described above provide the following expressions for the softening length a and the integration constants A_2 and B_2.

$$A_2 = -m\lambda M_T; \qquad B_2 = 0 \tag{6.27}$$

$$\sin(\lambda a) = \frac{\delta_f}{m\lambda M_T} \tag{6.28}$$

Any further increase in applied loading is accompanied by the decrease in the softening length a as per Eq. 6.28. The relative displacement at $x = 0$ during the debonding process can be obtained from Eq. 6.24. The distribution of interfacial stress is shown in Figure 6.7e for this state which notionally ends when $a = 0$.

Mathematically complete debonding occurs only when $a \rightarrow 0$ and $M_T \rightarrow \infty$ (Eq. 6.28) but this is not practical and is a result of the assumed static behaviour. If dynamic behaviour during the debonding process is considered, any increase of the loading during this stage is unlikely to be experienced in practice. What is significant from this analysis is the debonding initiation moment (Eq. 6.23).

Load–displacement response

Figure 6.8 shows the load-displacement (plate end slip) response predicted using the above formulations (Eqs 6.20-6.25 and 6.28) for the test steel plated RC beam specimen S13/20 reported in Oehlers and Moran (1990). The bond-slip parameters calculated using Lu et al.'s (2005b) bi-linear bond-slip model are: $\delta_f = 0.16$ mm; $\tau_f = 3.5$ MPa; and $G_f = 0.28$ N/mm. These parameters may also be obtained using other models such as Seracino et al. (2007) although the former is used through out this chapter. Note that the elastic deformation in this model is neglected but the interfacial fracture energy (the area under the bond-slip curve) is preserved in calculating the parameters for the linearly softening bond-slip model. Characteristic points in the load-displacement response are marked as O, A and B in Figure 6.8. The curve OA represents the S–R state of the interface, with point A representing the initiation of debonding. The plateau AB represents the D–S–R state, with point B representing the end of the D-S-R

interface and when the softening front reaches the mid-span. The curve starting from B onwards (dotted line in Figure 6.8) refers to D–S state of interface which has little practical significance as discussed above.

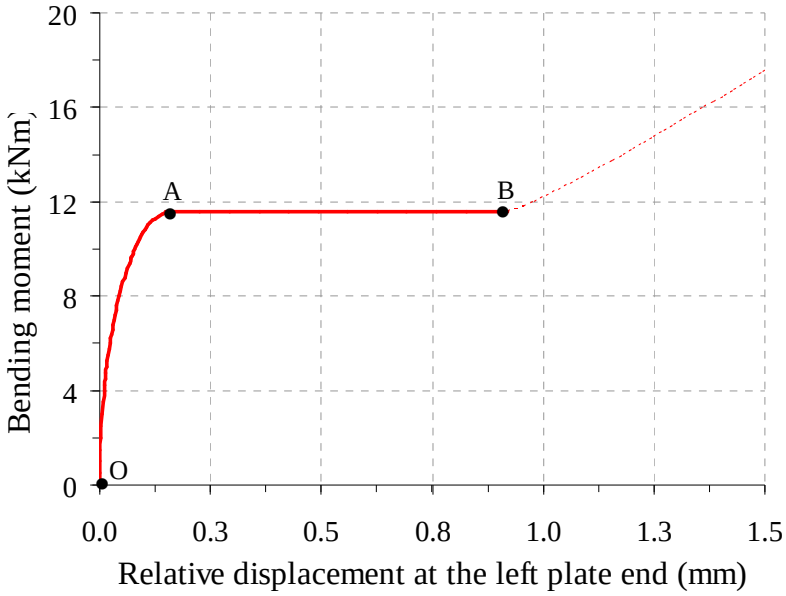

Figure 6.8. Load-displacement response of the bonded joint in CMR

6.5 Flexural Debonding Test Database

6.5.1 General description and consideration

An extensive literature survey has resulted in the largest ever database containing 67 RC beams with the flexural strengthening plate terminated in CMR and failed due to flexural debonding. It includes 54 steel plated beams, 9 CFRP plated beams, 2 GFRP plated beams and 2 C-GFRP plated beams. In all the tests, the bonded plate was not subjected to any prestress or anchorage in any form and the beam was not preloaded before being loaded to debonding failure. All the beams failed due to flexural PED failure either by concrete cover separation or interfacial failure or a combination of these two modes. The geometric and material parameters of these test beams are given in Tables 6.1 and 6.2 and their test results in Table 6.3. In Table 6.2, l_1 and l_2 denote the distance of the plate end and the applied transverse load P respectively from the left support; f_2 is the tensile yield strength of steel plate or tensile rupture strength of the FRP plate; and E_s, A_s and f_y refer respectively to the elastic modulus, cross sectional area and tensile yield strength of the internal tension steel reinforcement. It is seen that

these tests cover a wide range of important parameters: (1) elastic modulus of plate E_2 = 8.8-257 GPa; (2) nominal thickness of plate t_2 = 0.165-32 mm; (3) cubic strength of the concrete f_{cu} = 25-59 MPa; (4) splitting tensile strength of the concrete f_t = 2.55-4.9 MPa; (5) elastic modulus of concrete E_1 = 20-32 GPa; (6) axial stiffness of plate per unit width E_2t_2 = 3.76-315 (x10^4) N/mm; (7) effective axial stiffness of beam per unit width E_1d_e = 2.4-7.1 (x10^6) N/mm; (8) flexural rigidity of the cracked plated RC beam section $(EI)_{c,p}$ = 0.85-9.3 (x10^{12}) Nmm^2; (9) flexural rigidity of the cracked un-plated RC beam section $(EI)_{c,0}$ = 0.37-5.8 (x10^{12}) Nmm^2; (10) width ratio of beam to plate α_w = 1.0-4.8; (11) internal tensile reinforcement steel ratio ρ_s = 0.44-5.40 %; (12) interfacial fracture energy G_f = 0.25-0.88 Nmm/mm^2; and (13) interfacial bond strength τ_f = 2.7-6.8 N/mm^2.

The adhesive thickness t_a was not available for most of the 67 test beams. In such cases it is assumed that t_a = 2 mm for steel and pultruded FRP plates; t_a = total thickness of FRP plate including adhesive t_{pa} – nominal thickness of all FRP sheets t_2; and only for few cases where t_{pa} was also not available, it is calculated by assuming the thickness of adhesive layer between each FRP layer as 0.42mm following Smith and Teng (2002b). This methodology in t_a calculation is adopted to make best use of the available test data without rejecting any merely for the non availability of t_a. Also, accurate measurement of t_a is not possible in many cases, especially for wet lay-up FRP systems. Experiments have also shown that these adhesive parameters have a limited effect on debonding test results (Swamy et al., 1987; Quantrill et al., 1996; Oehlers and Ali, 1998). Therefore, it is desirable that debonding models for practical design use should be insensitive to or avoid the adhesive parameters. The formulation of the proposed theoretical model does include t_a, but the results with and without (i.e. setting t_a =0) including it have little difference. The predictions from the proposed models presented in the rest of the chapter do not include the effect of adhesive parameters.

Not all concrete properties such as f_t, f_{cu} and cylinder strength f_c were available for many test beams. In such cases, the following relationships are used to calculate the missing properties from the known ones:

$$f_c = 0.79 f_{cu} \qquad \text{(BS 8110, 1997)} \qquad (6.29a)$$

$$f_t = 0.53\sqrt{f_c} \qquad \text{(ACI 318-02, 2002)} \qquad (6.29b)$$

$$E_1 = 4730\sqrt{f_c} \qquad \text{(ACI 318-02, 2002)} \qquad (6.29c)$$

Table 6.1: Flexural debonding test database: details of RC beams

Reference	Specimen	b_1 (mm)	t_1 (mm)	d_e (mm)	l (mm)	f_c (MPa)	f_{cu} (MPa)	f_t (MPa)	E_1 (GPa)
Oehlers & Moran (1990)	S1/1, 2	125	150	112	2100	37.9	48.0	3.80	28.0
	S2/1, 2	125	150	122	2100	26.9	34.0	2.90	25.0
	S3/1, 2	125	150	122	2100	22.1	28.0	2.80	28.0
	S3/3, 4	125	150	122	2100	22.1	28.0	2.90	28.0
	S4/1, 2	125	150	122	2100	35.6	45.0	4.10	25.0
	S4/3, 4	125	150	122	2100	34.8	44.0	4.20	26.0
	S5/1, 2	125	150	122	2100	34.8	44.0	3.50	30.0
	S5/3, 4	125	150	122	2100	34.0	43.0	3.30	27.0
	S6/1, 2	125	150	122	2100	28.4	36.0	3.10	29.0
	S6/3, 4	125	150	122	2100	28.4	36.0	3.30	23.0
	S9/1, 2	125	150	122	2100	30.0	38.0	3.20	23.0
	S9/3, 4	125	150	122	2100	22.9	29.0	3.20	23.0
	S10/1, 2	120	180	152	1650	26.1	33.0	3.80	26.0
	S10/3, 4	120	180	152	1650	29.2	37.0	3.50	23.0
	S11/1, 2	120	180	152	1650	26.9	34.0	3.30	26.0
	S11/3, 4	120	180	152	1650	28.4	36.0	4.10	32.0
	S12/1, 2	120	180	152	1650	23.7	30.0	3.40	23.0
	S12/3, 4	120	180	152	1650	28.4	36.0	3.70	32.0
	S13/6	120	200	182	2500	33.2	42.0	3.30	21.0
	S13/7	120	240	222	2500	32.4	41.0	3.50	22.0
	S13/9, 10	120	160	142	1800	36.3	46.0	4.60	25.0
	S13/11	120	160	142	1800	27.7	35.0	4.90	26.0
	S13/13, 14	120	160	122	1800	29.2	37.0	3.40	20.0
	S13/15, 16	120	160	120	1800	26.1	33.0	3.20	22.0
	S13/17, 18	120	160	102	1800	34.0	43.0	3.20	24.0
	S13/19, 20	120	160	124	1800	34.0	43.0	3.30	21.0
Oehlers (1992)	7/2/*	130	175	147	3000	46.6	59.0	4.60	32.0
	8/2/*	130	175	147	2325	37.1	47.0	3.90	27.0
Yao & Teng (2007)	CS-A	150	253	217	1500	24.3	30.7	3.11	25.3
	CS-L1-A	150	253	214	1500	28.8	36.4	3.41	24.4
	CS-L3-A	151	253	217	1500	26.0	32.9	3.51	27.2
	CS-W50-A	151	255	218	1500	31.2	39.5	3.21	26.0
	CS-W100-A	151	254	214	1500	29.9	37.8	3.27	24.3
	CP-A	151	253	218	1500	29.2	37.0	3.83	27.4
	SP-A	151	253	214	1500	28.0	35.4	3.72	26.5
	GS-A	151	252	213	1500	30.7	38.9	4.31	28.8
	CS-C10-A	151	253	236	1500	21.6	27.3	4.01	30.0
	CS-C50-A	151	253	196	1500	30.7	38.8	2.68	29.3
Smith & Teng (2003)	6-A	151	250	215	-	28.6	36.1	2.85	29.4
Mohomed Ali et. al. (2001)	FP-S-5, FP-C-8.5, FP-CG2-16, FP-G-32, FP-CG-16	150	250	190	2800	19.8	21.6	2.55	30.1

Table 6.2: Flexural debonding test database: details of soffit plate, internal tensile reinforcement and loading

Reference	Specimen	b_2 (mm)	t_2 (mm)	E_2 (GPa)	f_2 (MPa)	E_s (GPa)	f_y (MPa)	A_s (mm^2)	l_1 (mm)	l_2 (mm)
Oehlers	S1/1, 2	125	3	210.0	272	210	444	402	600	450
& Moran (1990)	S2/1, 2	125	5	210.0	272	210	444	402	600	450
	S3/1, 2	125	3	210.0	272	210	444	402	600	450
	S3/3, 4	125	3	210.0	272	210	444	402	600	450
	S4/1, 2	125	5	210.0	272	210	444	402	600	450
	S4/3, 4	125	5	210.0	272	210	444	402	600	450
	S5/1, 2	125	5	210.0	272	210	444	402	600	450
	S5/3, 4	125	5	210.0	272	210	444	402	600	450
	S6/1, 2	125	5	210.0	272	210	444	402	600	450
	S6/3, 4	125	5	210.0	272	210	444	402	600	450
	S9/1, 2	125	3	210.0	272	210	444	402	600	450
	S9/3, 4	125	3	210.0	272	210	444	402	600	450
	S10/1, 2	120	10	210.0	272	210	444	402	535	385
	S10/3, 4	120	6.5	210.0	272	210	444	402	535	385
	S11/1, 2	120	3	210.0	272	210	444	402	535	385
	S11/3, 4	120	15	210.0	273	210	444	402	535	385
	S12/1	100	10	210.0	272	210	444	402	535	385
	S12/2	50	11	210.0	273	210	445	402	535	385
	S12/3	25	10	210.0	272	210	444	402	535	385
	S12/4	75	11	210.0	273	210	445	402	535	385
	S13/6, 7	120	5	210.0	272	210	444	402	900	550
	S13/9, 10	120	2	210.0	272	210	444	402	550	350
	S13/11	120	5	210.0	272	210	444	402	500	350
	S13/13, 14	120	2, 5	210.0	272	210	444	402	550	400
	S13/15, 16	120	2, 5	210.0	272	210	390	629	550	400
	S13/17, 18	120	6, 2	210.0	272	210	444	402	550	400
	S13/19, 20	120	2, 5	210.0	272	210	500	226	550	400
Oehlers (1992)	7/2/*	130	5	210.0	272	210	444	402	1150	1000
	8/2/*	130	5	210.0	272	210	444	402	900	775
Yao & Teng (2007)	CS-A	148	0.33	256.0	4114	199	536	157	600	500
	CS-L1-A	148	0.165	256.0	4114	199	536	157	600	500
	CS-L3-A	148	0.495	256.0	4114	199	536	157	600	500
	CS-W50-A	50	0.33	256.0	4114	199	536	157	600	500
	CS-W100-A	100	0.33	256.0	4114	199	536	157	600	500
	CP-A	148	1.2	165.0	2800	199	536	157	600	500
	SP-A	148	2	174.0	158	199	536	157	600	500
	GS-A	148	1.67	22.5	159	199	536	157	600	500
	CS-C10-A	148	0.33	256.0	4114	199	536	157	600	500
	CS-C50-A	148	0.33	256.0	4114	200	524	157	600	500
Smith & Teng (2003)	6-A	145	0.33	257.0	4114	207	524	157	-	-
Mohomed Ali	FP-S-5	150	5	200.0	272	200	433	1571	1100	800
et. al. (2001)	FP-C-8.5	150	7.4	130.6	2800	200	433	1571	1100	800
	FP-CG2-16	150	16	42.1	1000	200	433	1571	1100	800
	FP-G-32	150	32	10.2	350	200	433	1571	1100	800
	FP-CG-16	150	16	8.8	1000	200	433	1571	1100	800

6.5.2 Theoretical ultimate moment and flexural rigidity

Theoretical ultimate moment of the un-plated section $M_{u,0}$ is evaluated in accordance with ACI 318-02 (2002). Compression reinforcement is ignored in all calculations. Careful attention needs to be paid in applying the right procedure for over-reinforced and under-reinforced un-plated beam sections. Failing to consider this procedure carefully resulted in different values of $M_{u,0}$ for the test beams of Mohammed Ali et al. (2001) reported in Teng and Yao (2007). The procedure in Teng et al. (2002a) is adopted in computing the flexural rigidity of a plated section $(EI)_{c,p}$ with a careful observation on the strain level in tension steel reinforcement to distinguish under- and over- reinforced plated sections.

6.6 New Flexural Debonding Strength Models

Three new models with different levels of accuracy are developed in this section for predicting the PED failure in RC beams strengthened with a tension face plate which terminates in the CMR, based on the above interfacial shear analysis and the database.

6.6.1 Model-1: theoretical model

The first model directly employs the theoretical debonding moment $M_{p\text{-}1}$ (Eq. 6.23) from the interfacial shear analysis, i.e.

$$M_{p-1} = \phi_1 \frac{\delta_f}{m\lambda} \tag{6.30a}$$

where λ and m are given in Eqs 6.12b-c in which the parameters A_1; y_1; and I_1 shall be replaced respectively by $A_{c,e}$; y_1; and $I_{c,e}$, the elastic sectional properties of the cracked unplated beam section. For a rectangular RC section, these properties can be expressed as (Figure 6.9)

$$A_{c,e} = b_1 y_{c,0} + m_s A_s \tag{6.30b}$$

$$y_{c,e} = \frac{0.5 b_1 y_{c,0}^2 + m_s A_s d_e}{A_{c,e}} \tag{6.30c}$$

$$y_1 = t_1 - y_{c,e} \tag{6.30d}$$

$$I_{c,e} = \frac{b_1 y_{c,0}^3}{12} + b_1 y_{c,0} (y_{c,e} - y_{c,0})^2 + m_s A_s (d_e - y_{c,e})^2 \tag{6.30e}$$

where m_s is the modular ratio of internal tension steel to concrete and $y_{c,0}$ is the neutral axis depth of unplated beam at $M_{u,0}$.

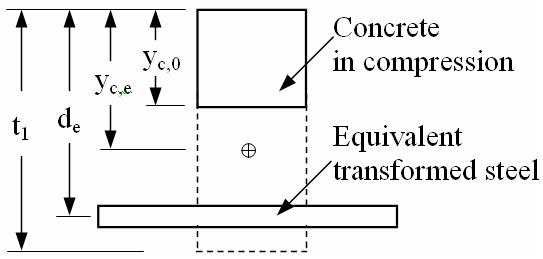

Figure 6.9. A cracked rectangular RC beam section

The values of $M_{p\text{-}1}$ (Eq. 6.30a) listed in Table 6.3 were calculated by using the bond properties δ_f; τ_f and G_f based on Lu et al.'s (2005b) bilinear bond-slip model. Other models may also be used. The statistical results for the proposed model-1 and model-2 using Seracino et al.'s (2007) bond properties are also given in Table 6.4, which give similar accuracy to Lu et al.'s (2005b) model.

In Eq. 6.30a, the coefficient ϕ_1 = 1 for prediction and ϕ_1 = 0.786 to make it a 95 percentile (1.645 × standard deviation) lower bound model suitable for design.

6.6.2 Model-2: semi-empirical model

A detailed analysis of the effects of different parameters shows that the accuracy of the above theoretical model (Eq. 6.30a) can be improved by calibrating it with the test database (Tables 6.1 and 6.2), leading to the development of an accurate semi-empirical model:

$$M_{p-2} = \phi_2 \frac{\delta_f}{m\lambda}\left(17.03\alpha^3 - 23.20\alpha^2 + 7.43\alpha + 0.74\right) \tag{6.31a}$$

where α is the axial stiffness enhancement ratio given as

$$\alpha = \frac{E_2 A_2}{E_1 A_1 + E_s A_s} \tag{6.31b}$$

and the coefficient ϕ_2 = 1 for prediction and ϕ_2 = 0.758 to make it a 95 percentile lower bound model suitable for design.

6.6.3 Model-3: empirical model

Without the restraint of the theoretical model (Eq. 6.30), a thorough study of the test database shows that the flexural debonding failure is mainly controlled by two parameters: the first yield moment $M_{y,0}$ of the cracked un-plated beam section (which should take the ultimate moment capacity $M_{u,0}$ for over-reinforced beam sections); and contribution of the bonded plate to the flexural rigidity of the cracked tensile reinforced concrete section in terms of α_f (Eq. 6.2b). The chief factor is the first yield moment $M_{y,0,}$ which if considered alone (in the form of $M_p = M_{y,0}$) provides an average test to prediction debonding moment ratio of 0.773, with a coefficient of variation (CoV) of 0.280 in comparison with 67 test results. This suggests that the yielding of the tension steel reinforcement plays a crucial role in initiating the flexural plate end debonding.

The inclusion of α_f and calibration with test results (in the form of $M_p = 1.3e^{-0.56\sqrt{\alpha_f}} M_{y,0}$) can improve the average ratio to 1.018 with a much reduced CoV of 0.187. Further including the effect of the width ratio factor between the bonded plate and the original beam β_w (as in Chen and Teng's 2001 pull-off bond strength model) as follows can very marginally improve the average ratio and CoV to 1.001 and 0.179 respectively. A simple empirical model with slightly lower accuracy than model-2 may thus be proposed:

$$M_{p-3} = \phi_3 e^{-0.8\beta_w\sqrt{\alpha_f}} M_{y,0} \le M_{u,0} \tag{6.32a}$$

where

$$\beta_w = \sqrt{\frac{2b_1 - b_2}{b_1 + b_2}} \tag{6.32b}$$

and the coefficient ϕ_3 = 1.332 for prediction and ϕ_3 = 1.004 to make it a 95 percentile lower bound model suitable for design.

Alternatively, the ultimate moment capacity of the un-plated section $M_{u,0}$ may be used instead of the first yield moment in Eq. 6.32a:

$$M_{p-3} = \phi_3 e^{-0.8\beta_w\sqrt{\alpha_f}} M_{u,0} \le M_{u,0} \tag{6.32c}$$

Equation 6.32c has almost the same accuracy as Eq. 6.32a (with an average ratio of 0.997 and CoV of 0.182).

6.7 Comparison of Flexural Debonding Models with Test Database

The test flexural debonding moment and the predicted values from the proposed three models (Eqs 6.30-6.32) as well as those of Oehlers and Moran's (1990) model (Eq. 6.1) and Teng and Yao's (2007) model (Eq. 6.2) are listed in Table 6.3. The statistical performance of the test to predicted moment ratio is shown in Table 6.4. The proposed theoretical model (model-1) does not rely on experimental test results and is fully based on the interfacial fracture mechanics. Its prediction (Figure 6.10a) is conservative for 53 out of the 67 test data. The proposed semi-empirical model (model-2) improves the accuracy of the theoretical model (Table 6.4 and Figure 6.10b) to a large extent with significantly reduced variations. Its predictions ranged from 75%-125% for 62 out of the 67 test data. The proposed empirical model (model-3) is simpler with slightly lower accuracy than model-2 (Table 6.4 and Figure 6.10c) and is more accurate than model-1.

Oehlers and Moran's (1990) is the first ever model for flexural debonding but it is over conservative for most of test data and too un-conservative for around 10 data reported by Teng and Yao (2007) as shown in Figure 6.10d. Its statistical performance is significantly worse than other models. Teng and Yao's (2007) empirical model is reasonably accurate with its statistical performance slightly worse than the proposed models 2 and 3 but better than the proposed model-1 and Oehlers and Moran's (1990) (Table 6.4). It is conservative for almost 90% of the test data (Figure 6.10e).

The statistical performance of the natural logarithm of test-to-predicted debonding moment ratios of the five models are also provided in Table 6.5. The distribution of the simple test-to-prediction ratio is skewed but the distribution of the logarithm of test-to-predicted debonding moment ratio should be close to normal, better suited for deriving design coefficients. The design coefficients in Eqs 6.30-6.32 were derived from this distribution. The average, maximum and minimum should be close to zero; and the standard deviation should be small for a good model. The positive and negative sign in average, maximum and minimum can be considered as a representation of the conservative and unconservative predictions respectively.

Table 6.3: Test and predicted flexural debonding moment

Reference	S. No	Specimen	M_e (kNm)	ε_e (με)	M_{p-1} (kNm)	M_{p-2} (kNm)	M_{p-3} (kNm)	M_{Oeh} (kNm)	M_{T-Y} (kNm)
Oehlers &	1	S1/N1	9.2	618	7.9	10.8	11.3	7.1	9.1
Moran (1990)	2	S1/N2	9.9	639	7.9	10.8	11.3	7.1	9.1
	3	S2/N1	12.2	502	7.9	11.3	11.7	4.3	8.7
	4	S2/N2	11.5	491	7.9	11.3	11.7	4.3	8.7
	5	S3/N1	11.3	606	8.8	12.1	11.9	6.0	8.5
	6	S3/N2	10.8	546	8.8	12.1	11.9	6.0	8.5
	7	S3/N3	12.6	588	8.9	12.2	11.9	6.2	8.5
	8	S3/N4	13.5	748	8.9	12.2	11.9	6.2	8.5
	9	S4/N1	12.6	512	8.6	12.3	11.8	5.9	9.3
	10	S4/N2	14.0	562	8.6	12.3	11.8	5.9	9.3
	11	S4/N3	13.5	543	8.6	12.5	11.7	6.1	9.3
	12	S4/N4	14.4	588	8.6	12.5	11.7	6.1	9.3
	13	S5/N1	11.5	603	8.4	12.2	11.6	5.5	9.4
	14	S5/N2	15.1	717	8.4	12.2	11.6	5.5	9.4
	15	S5/N3	11.5	615	8.2	11.9	11.6	4.9	9.2
	16	S5/N4	9.9	639	8.2	11.9	11.6	4.9	9.2
	17	S6/N1	16.0	617	8.2	11.9	11.7	5.0	9.0
	18	S6/N2	12.6	551	8.2	11.9	11.7	5.0	9.0
	19	S6/N3	12.6	536	8.0	11.4	11.6	4.6	8.8
	20	S6/N4	14.2	558	8.0	11.4	11.6	4.6	8.8
	21	S9/N1	16.7	1103	8.7	12.2	13.2	5.9	9.8
	22	S9/N2	14.0	999	8.7	12.2	13.2	5.9	9.8
	23	S9/N3	13.5	825	8.7	12.4	12.0	6.0	8.5
	24	S9/N4	15.3	1109	8.7	12.4	12.0	6.0	8.5
	25	S10/N1	12.3	244	9.9	11.3	11.9	6.7	10.1
	26	S10/N2	10.8	231	9.9	11.3	11.9	6.7	10.1
	27	S10/N3	11.2	348	10.1	14.0	14.3	6.5	11.3
	28	S10/N4	11.7	305	10.1	14.0	14.3	6.5	11.3
	29	S11/N1	12.3	573	11.6	15.5	17.4	10.0	13.2
	30	S11/N2	13.1	498	11.6	15.5	17.4	10.0	13.2
	31	S11/N3	7.9	128	10.0	8.4	10.1	6.8	9.7
	32	S11/N4	9.2	174	10.0	8.4	10.1	6.8	9.7
	33	S12/N1	10.4	261	10.0	12.1	11.6	5.2	9.8
	34	S12/N2	12.7	403	10.3	14.9	12.2	3.5	9.7
	35	S12/N3	16.4	1004	10.4	12.0	13.5	3.3	10.3
	36	S12/N4	10.6	268	11.0	15.9	11.0	5.6	10.4
	37	S13/N6	24.4	682	13.6	19.7	21.5	9.2	15.9
	38	S13/N7	23.9	682	17.6	25.3	27.2	15.7	20.6
	39	S13/N9	17.6	971	13.6	17.0	18.8	14.2	14.1
	40	S13/N10	16.1	938	13.6	17.0	18.8	14.2	14.1
	41	S13/N11	13.1	461	11.1	16.2	14.7	9.0	11.0
	42	S13/N13	12.6	765	8.7	11.4	13.6	8.1	10.1
	43	S13/N14	9.0	425	7.4	10.4	10.9	4.7	8.4
	44	S13/N15	15.3	870	10.8	13.5	15.0	8.4	10.5
	45	S13/N16	11.4	472	8.7	12.7	12.0	4.9	8.5
	46	S13/N17	6.3	214	5.5	7.6	6.8	4.3	6.3
	47	S13/N18	7.9	629	6.3	7.9	9.7	7.1	7.9
	48	S13/N19	10.6	618	6.7	8.8	8.7	7.4	7.2
	49	S13/N20	10.2	395	5.9	8.3	6.7	4.7	6.0

Table 6.3 (Contd.): Test and predicted flexural debonding moment

Reference	S. No	Specimen	M_e (kNm)	ε_e (με)	M_{p-1} (kNm)	M_{p-2} (kNm)	M_{p-3} (kNm)	M_{Oeh} (kNm)	M_{T-Y} (kNm)
Oehlers (1992)	50	7/2/*	13.5	-	11.9	17.1	15.9	11.3	13.0
	51	8/2/*	12.9	-	11.1	16.1	15.3	8.9	12.3
Yao & Teng (2007)	52	CS-A	12.5	1158	16.5	13.9	15.6	62.8	14.7
	53	CS-L1-A	17.0	2425	21.2	16.9	18.2	111.6	18.0
	54	CS-L3-A	13.5	919	15.2	13.3	14.2	56.6	13.5
	55	CS-W50-A	13.8	1689	22.9	17.9	18.3	52.3	16.5
	56	CS-W100-A	13.3	1038	19.1	15.5	16.2	56.7	15.1
	57	CP-A	11.4	404	14.1	13.2	13.0	48.4	12.5
	58	SP-A	11.5	215	12.2	13.0	10.5	35.5	10.6
	59	GS-A	19.1	2924	23.5	18.5	18.1	158.8	18.5
	60	CS-C10-A	18.9	1540	20.9	17.3	16.8	97.8	16.3
	61	CS-C50-A	11.9	1211	13.4	11.1	13.4	48.5	13.0
Smith & Teng (2003)	62	6-A	17.0	-	17.0	14.1	15.6	58.2	14.9
Mohomed Ali	63	FP-S-5	26.3	325	28.1	36.5	32.1	23.7	22.5
et. al. (2001)	64	FP-C-8.5	28.1	342	28.3	36.4	30.9	26.1	22.1
	65	FP-CG2-16	28.0	455	30.8	35.9	32.6	34.3	23.7
	66	FP-G-32	40.4	809	38.0	37.2	35.9	61.3	27.5
	67	FP-CG-16	62.1	1775	56.1	48.0	40.3	124.4	34.4

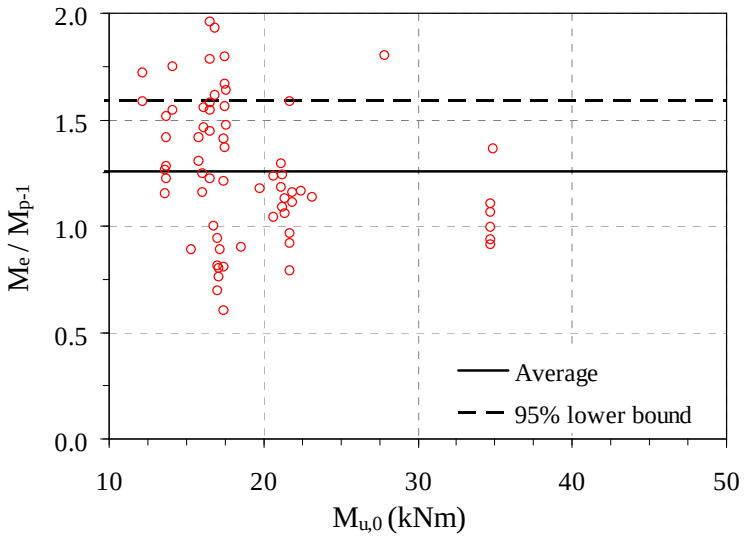

(a) Present model-1(Theoretical model)

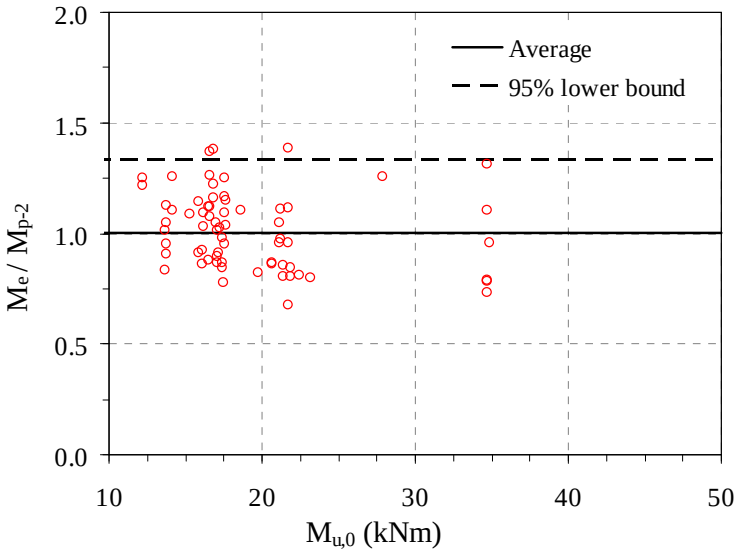

(b) Present model-2(Semi-empirical model)

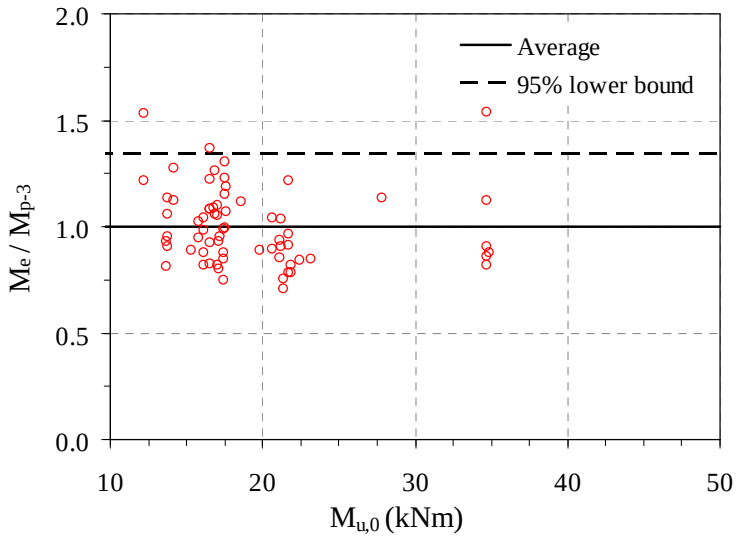

(c) Present model-3(Empirical model)

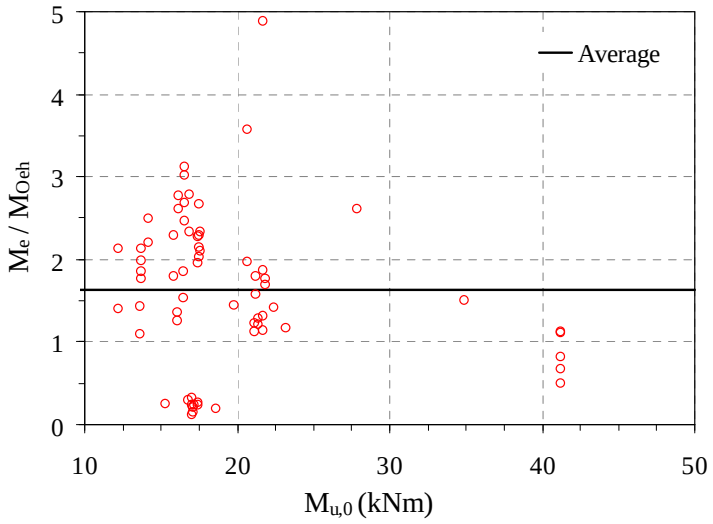

(d) Oehlers and Moran's (1990) model

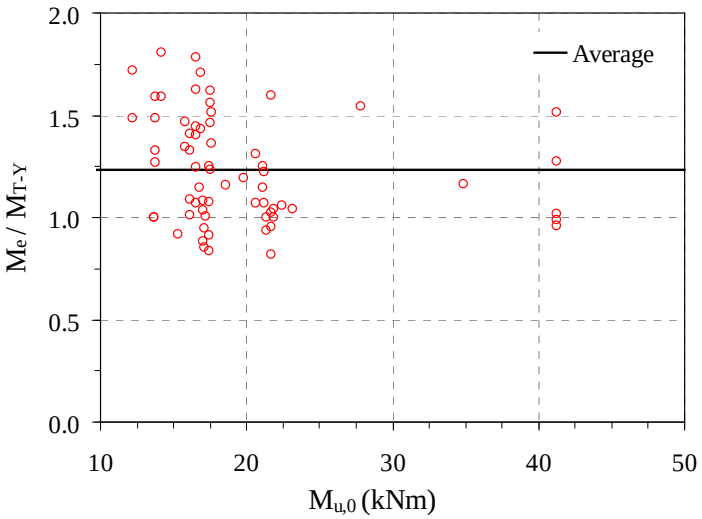

(e) Teng and Yao's (2007) model

Figure 6.10. Comparison of flexural debonding models with test data

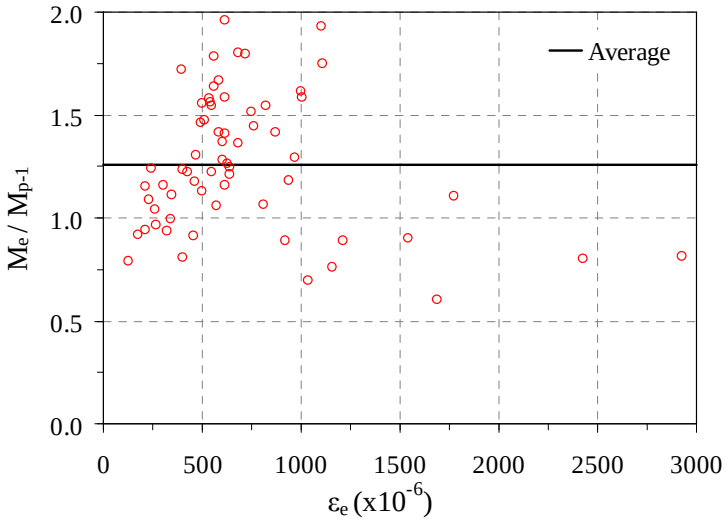

(a) Present model-1(Theoretical model)

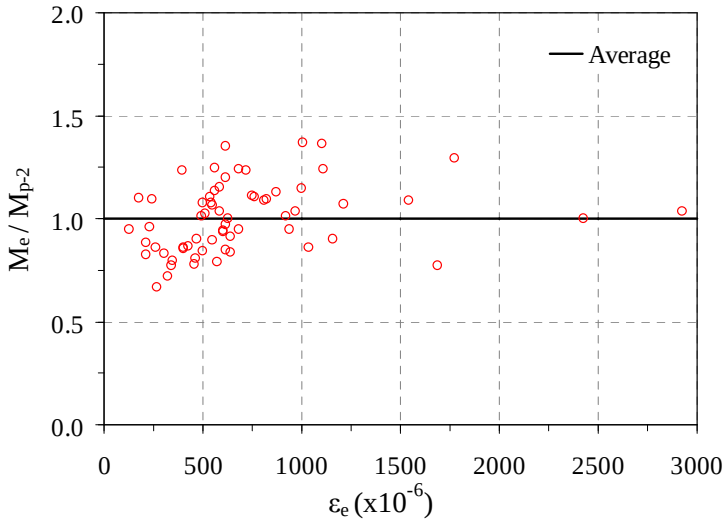

(b) Present model-2(Semi-empirical model)

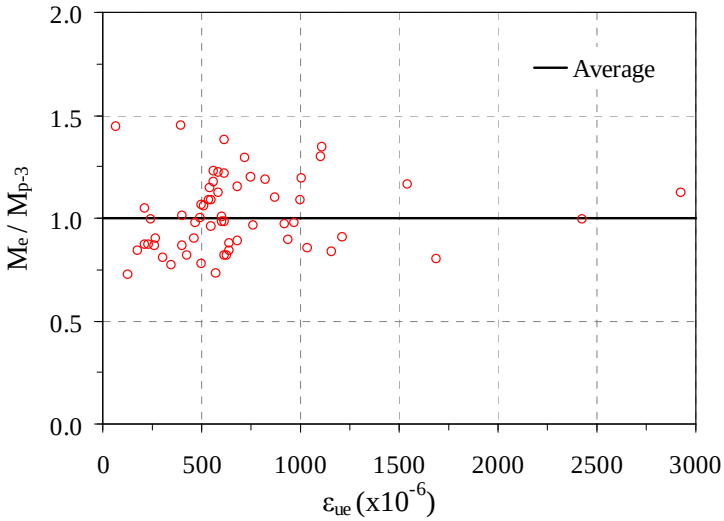

(c) Present model-3(Empirical model)

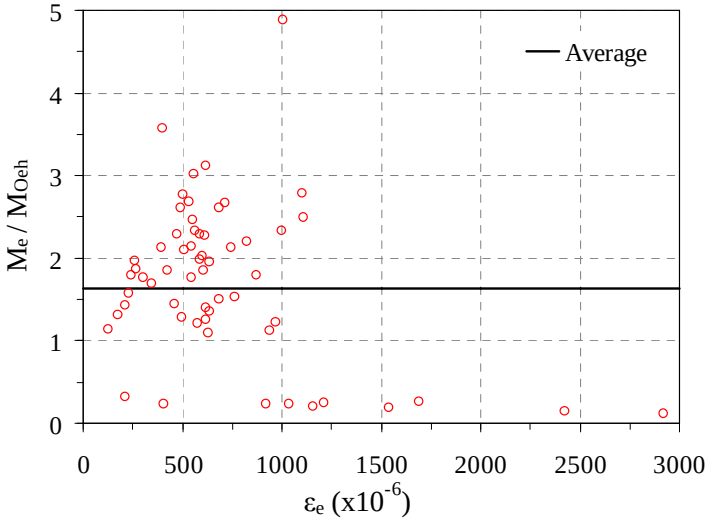

(d) Oehlers and Moran's (1990) model

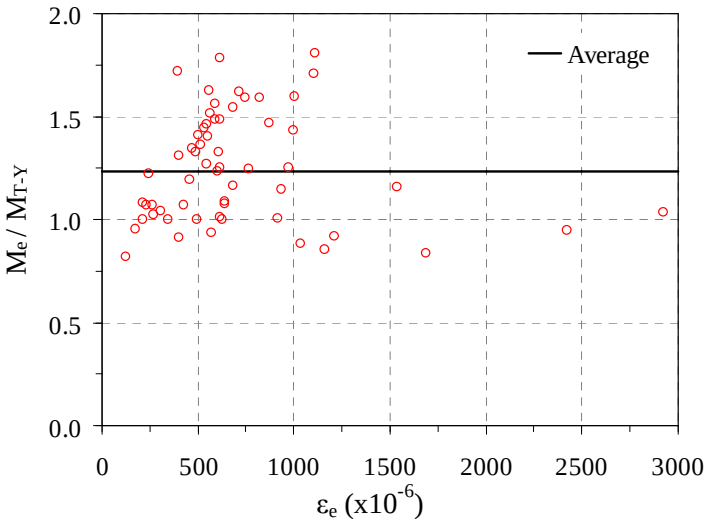

(e) Teng and Yao's (2007) model

Figure 6.11. Flexural debonding moment: tests-to-predictions against plate strain

Table 6.4: Statistics of test-to-predicted debonding moment ratio (M_e/M_p)

Model	Average	CoV	Maximum	Minimum
Model-1 (with Lu et al.'s (2005b) bond model)	1.258	0.255	1.961	0.600
Model-1 (with Seracino et al.'s (2007) bond model)	1.150	0.244	1.811	0.653
Model-2 (with Lu et al.'s (2005b) bond model)	1.001	0.168	1.368	0.665
Model-2 (with Seracino et al.'s (2007) bond model)	0.920	0.184	1.405	0.630
Model-3	1.001	0.179	1.539	0.709
Oehlers & Moran (1990)	1.662	0.576	4.940	0.120
Teng & Yao (2007)	1.246	0.211	1.807	0.816

Table 6.5: Statistics of test-to-predicted debonding strength ratio $\ln(M_e/M_p)$

Model	Average	Standard Deviation	Maximum	Minimum
Model-1 (with Lu et al.'s (2005b) bond model)	0.196	0.266	0.673	-0.510
Model-1 (with Seracino et al.'s (2007) bond model)	0.110	0.249	0.594	-0.427
Model-2 (with Lu et al.'s (2005b) bond model)	-0.013	0.169	0.313	-0.407
Model-2 (with Seracino et al.'s (2007) bond model)	-0.099	0.179	0.340	-0.462
Model-3	-0.014	0.171	0.431	-0.344
Oehlers & Moran (1990)	0.240	0.879	1.597	-2.118
Teng & Yao (2007)	0.199	0.209	0.592	-0.203

Thus it can be concluded that the proposed model-2 is the most accurate model followed by model-3, Teng and Yao (2007), model-1 and finally Oehlers and Moran (1990) but the proposed model-1 is the simplest in form and the only one which is solely based on a theoretical analysis.

The debonding moment from test-to-predictions against measured plate strains at mid-span ε_e during debonding failure for 64 out of 67 test results are plotted in Figure 6.11a-e. These plots show that the debonding plate strain is spread over a wide range so that a cap on axial plate strain limit can not be imposed to prevent debonding failure (ACI 440 model).

6.8 Conclusions

This chapter has presented an investigation on the plate end debonding behaviour of flexurally strengthened RC beams with the bonded plate terminated in the constant bending region (CMR), or the so called flexural debonding behaviour. A simple assessment of the interfacial stresses near the plate end suggests that the interfacial shear behaviour, rather than the peeling behaviour dominates in this case which may appear counter intuitive. Based on an interfacial shear analysis between the bonded plate and the RC beam, and a test database constructed from an extensive literature survey, three new models with different levels of accuracy have been developed for predicting the flexural debonding moment: the first theoretical model based on an interfacial fracture mechanics analysis (model-1); a semi-empirical model based on model-1 with much improved accuracy; and a simple empirical model with slightly less accuracy than model-2. These three models together with two existing models are assessed with the test database containing 67 test data.

The theoretical model is the simplest of all models and provides a reasonable accuracy with a conservative prediction for 79% of the test data. This further confirms that the interfacial shear behaviour dominates in the flexural debonding failure mode. The assessment shows that the proposed models 2 and 3 offer a very good accuracy, but the former is slightly complex in form. The proposed model-2 is the most accurate model to date followed closely by model-3 and both are suitable for incorporation in design codes and guidelines as a reliable predictive debonding strength model. From the development of model-3, it is suggested that the yielding of the tension steel reinforcement in the RC beam plays a crucial role in initiating the flexural plate end debonding.

6.9 Notation

The following symbols are used in this Chapter:

a = softening length of the interface;

a_d = softening length of the interface at initiation of debonding;

A = cross-sectional area;

b = width;

CoV = coefficient of variation;

d_e = effective depth of RC beam;

E = modulus of elasticity;

$(EI)_{c,0}$ = cracked section flexural rigidity of un-plated RC beam;

$(EI)_{c,p}$ = cracked section flexural rigidity of plated RC beam;

f_2 = tensile yield strength of steel plate or tensile strength of FRP plate;

f_c = cylinder compressive strength of concrete;

f_{cu} = cubic compressive strength of concrete;

f_t = tensile strength of concrete;

f_y = yield strength of steel reinforcement;

G_f = interfacial fracture energy (area under the local bond-slip curve);

I = second moment of area;

L = length of a bonded joint;

l = effective span of the plated beam;

l_1 = distance from nearest support to the plate end;

l_2 = distance from nearest support to the loading point (shear span);

$M(x)$ = bending moment;

M_e = debonding moment from experiment;

$M_{p\text{-}1}, M_{p\text{-}2}, M_{p\text{-}3}$ = debonding moment from proposed models 1, 2 and 3 respectively;

M_{Oeh} = debonding moment from Oehlers and Moran's (1990) model;

$M_{T\text{-}Y}$ = debonding moment from Teng and Yao's (2007) model;

$M_T(x)$ = total bending moment at a section of the plated beam;

M_{Td} = total bending moment at initiation of debonding;

$M_{u,0}$ = ultimate moment capacity of the un-plated beam section;

$N(x)$ = axial force;

$N_T(x)$ = total axial force at a section of the plated beam;

P = applied transverse load;

R_b = bending stiffness ratio of plate to beam;

t = thickness;

u = longitudinal displacement;

v = vertical displacement;

$V(x)$ = shear force;

$V_T(x)$ = total shear force at a section of the plated beam;

y_1, y_2 = vertical distance from bottom of the beam and top of the plate to their respective centroids;

α = axial stiffness ratio between plate and original beam including steel tension reinforcement;

$\alpha_w, \alpha_a, \alpha_f$ = width ratio, and axial and flexural rigidity ratio respectively;

β = ratio between moments at left and right adjacent cracks;

β_w = width ratio parameter used in proposed model-3;

$\delta(x)$ = interfacial slip;

δ_1 = slip corresponding to the attainment of τ_f;

δ_f = maximum slip at initiation of debonding;

λ, m, m_1 = parameters defined respectively by Eqs 12b, 12c and 17d;

ρ = reinforcement ratio;

$\phi_1; \phi_2; \phi_3$ = coefficients in proposed models 1, 2 and 3 respectively;

ε_e = plate strain at mid-span;

$\sigma(x)$ = interfacial normal stress;

$\tau(x)$ = interfacial shear stress;

τ_f = bond strength; and

$_{1; a; 2; s}$ = subscripts referring respectively to the beam; adhesive; plate and tension steel reinforcement.

Chapter 7

Strength Model for Plate End Debonding in FRP and Steel Plated Beams

Abstract

RC beams strengthened in flexure by adhesive bonded FRP or steel plates on their tension face are prone to common and premature plate end debonding failures. Safe design of such a strengthened RC beam demands a reliable and predictive debonding strength model. Initially, flexural debonding strength models for a plate end located in a pure bending region and shear debonding strength models for a plate end located in a high shear-zero (or low) moment region are briefly reviewed, followed by providing a simple and an explicit shear debonding strength model. The general case of a plate end under combined shear and bending is treated as an interaction of these two extreme boundary conditions whose debonding strength can be predicted with an interaction model. The proposed and existing shear and shear-bending interaction debonding strength models are assessed with a carefully constructed large test database of plated RC beams reported to have failed by plate end debonding, to demonstrate the simplicity and the accuracy of the proposed models that can easily be incorporated in any design codes and guidelines.

7.1 Introduction

RC beams strengthened in flexure by adhesive bonding of an FRP or steel plate to their tension (soffit) face (Figure 7.1) are vulnerable to common and premature plate end debonding failures. This plate end debonding failures that initiate at or near the plate ends are found to appear in different modes (Teng and Chen 2009): (1) concrete cover separation; (2) interfacial debonding at the adhesive interface; (3) mixed mode debonding with a combination of (1) and (2); (4) critical diagonal crack (CDC) initiated concrete cover separation; and (5) CDC initiated interfacial debonding. The first three types (1-3) of plate end debonding failures are observed in RC beams with plates terminated in constant bending moment region (CMR) while all types are observed for plates terminated in pure shear or shear-bending interaction regions. These debonding failures are brittle in nature and occur well below the full flexural capacity of the plated section. Debonding failures should be prevented to make best use of the full strength of the plated beam in service. This demands a sound debonding model that can predict the debonding strength accurately and reliably.

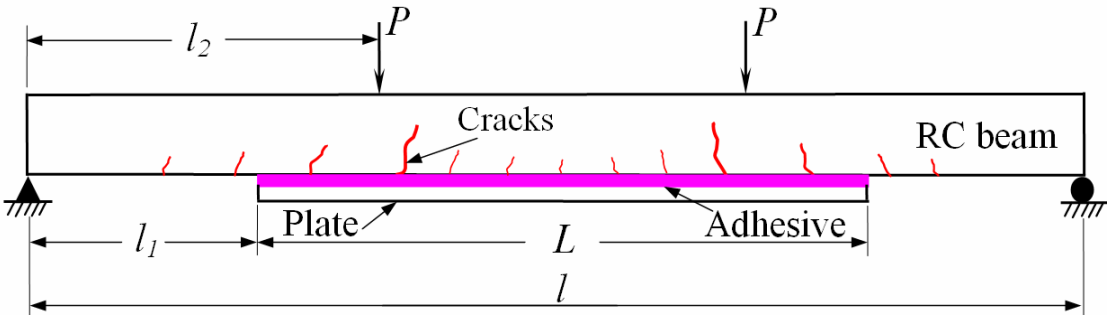

Figure 7.1. A general flexural-strengthened RC beam

Narayanamurthy et al. (2011) reviewed all flexural debonding models applicable to plates terminated in CMR, and additionally proposed three models (model-1, 2 and 3) amongst which the models 2 and 3 were shown to be more accurate than the best existing model (Teng and Yao, 2007). It was also shown that the model-3 is slightly less accurate but simpler than model-2. The objective of this Chapter is to make use of this flexural debonding model-3; to independently develop a simple and an explicit shear debonding model for plates terminated in a high shear and (zero) or low moment region; and to finally propose a shear-bending interaction debonding strength model with improved accuracy combining these two models applicable for plates terminated in any shear-bending interaction region. The proposed model is applicable to all types of plate

end debonding failures in FRP and steel plated RC beams. In this chapter, all flexural, shear and shear-bending interaction debonding models are reviewed; new shear and shear-bending interaction debonding strength models are proposed; databases containing the test results of 67, 68 and 91 plated RC beams reported to have failed by plate end debonding respectively in CMR, pure shear and shear-bending interaction regions are compiled from existing literature; and the proposed and the existing models are then assessed against the test results from these databases to demonstrate the accuracy and the simplicity of the proposed models.

7.2 Flexural Debonding

There are five flexural debonding strength models for predicting the plate end debonding failure in the special case of an RC beam with flexural-strengthening plate terminated in CMR. These are the three recent models of Narayanamurthy et al. (2011): model-1(theoretical model); model-2(semi-empirical model) and model-3(empirical model) and two other existing models of Teng and Yao (2007) and Oehlers and Moran (1990). These models have been assessed in Narayanamurthy et al. (2011) in detail based on 67 test results of FRP and steel plated beams reported to have failed by plate end debonding in CMR. This assessment has shown model-2 as the most accurate model followed closely by model-3 and then by Teng and Yao's (2007), model-1 and Oehlers and Moran's (1990). These debonding strength models are briefly summarised in this section.

7.2.1 Existing models

Model-1 (Theoretical model)

Behaviour of the plate-RC interface is dominated by interfacial shear stress. Considering only mode-II effect of interfacial deformation and using a linearly softening bond-slip model, the theoretical debonding moment $M_{p\text{-}1}$ was formulated as:

$$M_{p-1} = \phi_1 \frac{\delta_f}{m\lambda} \tag{7.1a}$$

where

$$\lambda^2 = \frac{\tau_f^2 b_2}{2G_f}\left[\frac{(y_1+y_2)(y_1+t_a+y_2)}{(E_1I_1+E_2I_2)}+\frac{1}{E_1A_1}+\frac{1}{E_2A_2}\right] \quad (7.1b)$$

$$m = \frac{1}{\lambda^2}\left[\frac{y_1+y_2}{E_1I_1+E_2I_2}\right] \quad (7.1c)$$

in which δ_f, τ_f and G_f refer to the ultimate slip that initiates macro cracking or debonding of the local bond element, local bond strength and interfacial fracture energy respectively. These bond slip parameters can be determined from Lu et al.'s (2005) bi-linear bond-slip model for any material and geometric properties of the plated beam. The parameters *E*, *A*, *I*, *t*, and *b* refer respectively to the elastic modulus, cross-sectional area, second moment of area, thickness and breadth; subscripts *1*, *2* and *a* denote the beam, plate and adhesive respectively; and y_1 and y_2 are the distances from the bottom of the beam and top of the plate to their respective centroids.

The parameters A_1, y_1 and E_1 in Eq. 7.1b-c shall be replaced respectively by $A_{c,e}$, y_1 and $I_{c,e}$ which are the elastic sectional properties of the cracked unplated beam section. For a rectangular RC section, these properties can be expressed as

$$A_{c,e} = b_1 y_{c,0} + m_s A_s \quad (7.1d)$$

$$y_{c,e} = \frac{0.5 b_1 y_{c,0}^2 + m_s A_s d_e}{A_{c,e}} \quad (7.1e)$$

$$y_1 = t_1 - y_{c,e} \quad (7.1f)$$

$$I_{c,e} = \frac{b_1 y_{c,0}^3}{12} + b_1 y_{c,0}(y_{c,e}-y_{c,0})^2 + m_s A_s (d_e - y_{c,e})^2 \quad (7.1g)$$

where m_s is the modular ratio of internal tension steel to concrete and $y_{c,0}$ is the neutral axis depth of unplated beam at its ultimate moment $M_{u,0}$.

In Eq. 7.1a, the coefficient ϕ_1 = 1 for prediction and ϕ_1 = 0.786 to make it a 95 percentile lower bound model suitable for design.

Model-2: semi-empirical model

A semi-empirical model is developed by calibrating the theoretical model (Eq. 7.1a) with the 67 flexural debonding test results and shown to be the most accurate of all the existing and proposed flexural debonding models. The debonding moment is given as

$$M_{p-2} = \phi_2 \frac{\delta_f}{m\lambda}\left(17.25\alpha^3 - 23.51\alpha^2 + 7.53\alpha + 0.75\right) \tag{7.2a}$$

where α is the axial stiffness enhancement ratio given as

$$\alpha = \frac{E_2 A_2}{E_1 A_1 + E_s A_s} \tag{7.2b}$$

The coefficient ϕ_2 is taken as 1.0 for mean strength prediction and 0.758 for 95 percentile lower bound suitable for design. The subscript *s* refers to the steel tension reinforcement.

Model-3 (Empirical model)

A thorough study on the effect of various individual factors that contribute to the flexural debonding failure in comparison with 67 debonding test results resulted in the development of an empirical model influenced by three important governing parameters. The debonding moment in model-3 is expressed as:

$$M_{p-3} = \phi_3 e^{-0.8\beta_w\sqrt{\alpha_f}} M_{y,0} \le M_{u,0} \tag{7.3a}$$

where

$$\alpha_f = \frac{(EI)_{c,p} - (EI)_{c,0}}{(EI)_{c,0}}; \qquad \beta_w = \sqrt{\frac{2b_1 - b_2}{b_1 + b_2}} \tag{7.3b}$$

in which $M_{y,0}$ refer to the first yield moment of the cracked un-plated beam section (which should take the ultimate moment capacity $M_{u,0}$ for over-reinforced beam sections); α_f and β_w refer to the contribution of the bonded plate to the flexural rigidity of the cracked tensile reinforced concrete section and the effect of the width ratio factor between the bonded plate and the original beam; $(EI)_{c,p}$ and $(EI)_{c,0}$ denote the flexural rigidity of the cracked tensile reinforced plated and un-plated concrete beam section respectively; and the coefficient ϕ_3 = 1.332 for mean debonding strength predictions and ϕ_3 = 1.004 for 95 percentile lower bound model for design purposes.

Teng and Yao's (2007) model

Teng and Yao (2007) proposed an empirical model based on 16 flexural debonding test results from 4 steel plated and 12 FRP plated beams to predict the debonding moment. The debonding moment from this model is as given below.

$$M_{T-Y} = \frac{0.488M_{u,0}}{(\alpha_a \alpha_f \alpha_w)^{(1/9)}} \leq M_{u,0} \tag{7.4a}$$

where

$$\alpha_a = \frac{E_2 t_2}{E_1 d_e}; \qquad \alpha_w = \frac{b_1}{b_2} \leq 3 \tag{7.4b}$$

in which α_a denotes axial stiffness ratio; d_e refers to the effective depth of the beam; and α_w the width ratio.

Oehlers and Moran's (1990) model

Based on an approximate elastic theoretical and finite element analyses and subsequent calibration with 43 test results of steel plated beams with plates terminated in the CMR, Oehlers and Moran (1990) proposed a semi-theoretical flexural debonding model where the debonding moment is given as:

$$M_{Oeh} = \frac{(EI)_{c,p} f_t}{0.901 E_2 t_2} \tag{7.5}$$

where f_t refers to the splitting tensile strength of concrete.

7.2.2 Flexural debonding test database

The database containing the test results of 67 RC beams with the bonded plate terminated in C.M.R. and reported to have failed by plate end debonding is briefly reviewed here as it will be used later in assessing the shear-bending interaction model. The geometric and material parameters of these test beams are given in Tables 1 and 2 and their test results in Table 3 in Narayanamurthy et al. (2011). These tests include 54 steel plated beams, 9 CFRP plated beams, 2 GFRP plated beams and 2 C-GFRP plated beams. In all these tests the bonded plate was not subjected to any prestress or anchorage in any form and the beam was not preloaded before being loaded to debonding failure. These beams have experienced flexural plate end debonding failure either by concrete cover separation or interfacial failure or combination of these two modes. These tests cover a wide range of important parameters: (1) elastic modulus of plate E_2 = 8.8-257 GPa; (2) nominal thickness of plate t_2 = 0.165-32 mm; (3) cubic strength of the concrete f_{cu} = 25-59 MPa; (4) splitting tensile strength of the concrete f_t = 2.55-4.9 MPa; (5) elastic modulus of concrete E_1 = 20-32 GPa; (6) axial stiffness of plate per unit width E_2t_2 = 3.76-315 (x10^4) N/mm; (7) effective axial stiffness of beam

per unit width $E_1 d_e$ = 2.44-7.07 (x10^6) N/mm; (8) flexural rigidity of the cracked plated RC beam section $(EI)_{c,p}$ = 0.853-9.293 (x10^{12}) Nmm^2; (9) flexural rigidity of the cracked un-plated RC beam section $(EI)_{c,0}$ = 0.372-5.794 (x10^{12}) Nmm^2; (10) width ratio of beam to plate α_w = 1.0-4.8; (11) internal tensile reinforcement steel ratio ρ_s = 0.44-5.40 %; (12) mode-2 interfacial fracture energy G_f = 0.246-0.879 Nmm/mm^2; and (13) interfacial bond strength τ_f = 2.705-6.758 N/mm^2.

7.3 Shear Debonding

Shear debonding is the plate end debonding failure initiated by high shear force with very low or zero bending moment at the plate end. This occurs in another special case of an RC beam where the bonded plate is terminated at or very close to the support or the point of contraflexure. Many shear debonding models exist in literature. All models have their own advantages and limitations in terms of accounting for shear reinforcement, accuracy and simplicity. A few models are simpler but relatively inaccurate, while a few others are better but rather too complex for design use. Only the shear debonding models reported to be best in previous review by Smith and Teng (2002a, b) and Teng and Yao (2007) and other models that are found to be good in this study are briefly reviewed and discussed here. This is followed by a proposal for a new shear debonding strength model of comparable accuracy which includes the effect of shear reinforcements in addition to providing an explicit expression for the shear debonding capacity. A test database of 68 RC beams with plates terminated within 50mm from the support and reported to have failed by plate end debonding is used for assessing the performance of the proposed and other existing models in this section.

7.3.1 Existing shear debonding strength models

Oehlers' (1992) model

Based on experimental observations, Oehlers (1992) proposed that the plate end debonding occurs when the shear force at the plate end $V_{Oeh\text{-}1}$ reaches the shear capacity of the concrete in the RC beam V_{uc} omitting any contribution from shear links. This is given as:

$$V_{Oeh-1} = V_{uc} = \left(1.4 - \frac{d_e}{2000}\right) b_1 d_e (\rho_s f_c)^{1/3} \tag{7.6a}$$

where ρ_s is the tension steel reinforcement ratio given by

$$\rho_s = \frac{A_s}{b_1 d_e} \tag{7.6b}$$

and f_c is the cylinder compressive strength of the concrete. The above equation for V_{uc} is that given by Australian concrete code (1988) and it is a requirement that [1.4-(d_e/2000)] $\geq$ 1.1.

Smith and Teng's (2002) model

A comprehensive review and assessment of all debonding models in comparison with a large test database of 67 test results of plated beams with plates terminated in any region of bending and shear was used by Smith and Teng (2002) to propose a shear debonding model by slightly modifying Oehlers' (1992) model. The debonding shear force $V_{S\text{-}T}$ is given by

$$V_{S-T} = 1.5 V_{uc} \qquad \text{subject to the condition} \qquad M(0) \leq 0.67 M_{u,0} \tag{7.7}$$

where $M(0)$ is the bending moment at the plate end and $M_{u,0}$ is the ultimate moment capacity of the unplated beam.

Oehlers et al.'s (2004) model

Oehlers et al (2004) proposed a passive prestress model to predict the shear debonding strength of plated RC beams that fail by critical diagonal crack (CDC) debonding. This is basically an extension of Zhang's (1997) approach that the concrete component of the shear capacity depends on the shear to cause a diagonal crack V_{crack} and the shear to cause sliding along the diagonal crack V_{slide}. They treated the additional axial force in the plate as the passive prestressing force that acts after a diagonal crack is formed which in turn increases the shear capacity. Debonding strength is found as the shear resistance of the prestressed beam without the internal steel shear reinforcement. Debonding shear force $V_{Oeh\text{-}2}$ is given by V_{crack} or V_{slide} when V_{crack} = V_{slide} and is obtained by an iterative procedure. The expressions are:

$$V_{crack} l_2 = (x^2 + t_1^2)\left(\frac{b_1 f_{tef}}{2} + \frac{f_t m_p A_2}{t_1}\right) + (F_{ps} d_{ps}) \tag{7.8a}$$

$$V_{slide} = 0.4 f_c b_1 t_1 \left(1 + 2\frac{F_{ps} + P_{axial}}{f_c b_1 t_1}\right)\left[\sqrt{1 + \left(\frac{x}{t_1}\right)^2} - \frac{x}{t_1}\right] f_1(f_c).f_2(t_1).f_3(\rho_s) \quad (7.8b)$$

where l_2 is the shear span; x is the horizontal projection of CDC on tension face; f_{tef} is the effective tensile strength of the concrete; f_t is the tensile strength of the concrete; m_p is the modular ratio of plate-to-beam material; F_{ps} is the tendon prestressing force; d_{ps} is the tendon prestressing force position; P_{axial} is the maximum axial force in the plate which is limited by the IC debonding resistance or the ultimate axial capacity of the plate; and f_1, f_2 and f_3 are the parameters that are functions of f_c, t_1 and ρ_s respectively.

Oehlers et al.'s (2005) model

The Iterative approach of Oehlers et al. (2004) model is cumbersome for design use. So, a simpler code based approach was proposed by Oehlers et al. (2005) for the debonding shear strength V_{Oeh-3} as:

$$V_{Oeh-3} = (V_{u,0})_{code} + 0.15 P_{axial} \quad (7.9)$$

where $V_{u,0}$ is the shear capacity of the prestressed or unprestressed concrete beam neglecting internal steel shear reinforcement from Eurocode (1992). For non-prestressed beams $V_{u,0} = V_{uc}$ from any design code.

Teng and Yao's (2007) model

Teng and Yao (2007) added the contribution of internal steel shear reinforcement to the Oehlers et al.'s (2004) model and proposed a new debonding strength model as:

$$V_{T-Y} = (V_{con} + V_{pl}) + \varepsilon_{v,e} V_{st} \quad (7.10a)$$

where

$$(V_{con} + V_{pl}) = V_{Oeh-2} \quad (7.10b)$$

$$\varepsilon_{v,e} = \frac{10^{-5}}{\sqrt{\alpha_f \alpha_E \alpha_t \alpha_w}} \quad (7.10c)$$

$$\alpha_E = m_p; \qquad \alpha_t = \left(\frac{t_2}{d_e}\right)^{1.3} \quad (7.10d)$$

$$V_{st} = \frac{A_{sv} E_{sv} d_e}{s_v} \quad (7.10e)$$

in which A_{sv}, E_{sv} and s_v refer to the cross-sectional area of the two legs of each vertical stirrup, the elastic modulus and the longitudinal spacing of the steel shear stirrups respectively. Note that the expression for the effective strain in stirrups $\varepsilon_{v,e}$ in Eq. 7.10c is the corrected expression as there is a typographical error in the versions published by Teng and Yao (2007) and Teng and Chen (2009). The expression in Eq. 7.10c is the best fit for $\varepsilon_{v,e}$ from 8 test results from this research group for the RC beams without shear reinforcement and with plates terminated within 50 mm from the support.

Collotti et al.'s (2004) model

Collotti et al. (2004) proposed a model based on truss analogy to predict the debonding strength and failure modes of plated RC beams. Four different expressions are provided for four corresponding failure modes: (1) plate-debonding failure; (2) shear failure; (3) tension/concrete crushing failure; and (4) plate rupture. The actual failure load or the load carrying capacity of the plated beam is found as the minimum of the values from the four expressions.

Gao et al.'s (2005) model

Gao et al.'s model predicts the load carrying capacity of plated RC beams that fail by concrete cover separation. This model predicts that the interfacial stresses between the concrete cover and the tension steel reinforcement are inversely proportional to cover thickness.

Casas and Pascual's (2007) model

Casas and Pascual (2007) developed a single model to predict the debonding strength of plated RC beams that fail either by plate end debonding or by IC debonding. Their model is very sensitive to adhesive parameters, many of which are not available during the construction of the test database and any assumed value under estimates its accuracy. So, this model will not be used in further comparisons.

The models of Collotti et al. (2004) and Gao et al. (2005) will not be used in these comparisons due to their limitations as described in Teng and Yao (2007).

7.3.2 Proposed shear debonding strength model

The detailed analysis of all the better performing shear debonding strength models in comparison with the shear debonding test database of 68 plated RC beams reveals that the major contribution to the shear debonding strength comes from the concrete component of the shear capacity neglecting shear reinforcement V_{uc} and to a small extent from the shear reinforcement and the bonded plate. So the debonding shear strength contributed by the vertical stirrups-shear reinforcement and the soffit plate are combined and added to V_{uc} to provide a better debonding strength model as given below.

$$V_p = 0.593\left[V_{uc} + \left(\frac{A_{sv} f_{yv} d_e / s_v + A_2 f_2}{1000}\right)^{0.573}\right]^{1.142} \tag{7.11}$$

where V_p is the predicted debonding strength in kN from the proposed model and f_2 = yield strength for steel plate and ultimate strength for FRP plate. V_{uc} in kN can be calculated from any design codes or guidelines. It has been demonstrated by Oehlers (1992) through experiments on steel plated RC beams that the effect of shear reinforcement stirrups does not significantly alter the shear debonding strength of plated RC beams but they influence the type of plate end debonding failure (such as concrete cover separation or plate end interfacial debonding or a combination of these two modes or such failures initiated from CDC). This is also evidenced from the test results of Teng and Yao (2007) from FRP plated RC beams where minimal changes are observed in the experimental shear debonding strength due to the presence of vertical stirrups. However, their inclusion helps to improve the accuracy of the proposed model. Similar observations are found with the contribution of bonded plate to the shear debonding capacity which can also be understood from Oehlers et al. (2004) and Teng and Yao (2007).

7.3.3 Shear debonding test database

The database comprises test results for 68 RC beams with the bonded plate terminated within 0-50 mm from the support so that they experience high shear with zero or low bending moment from 21 existing studies in published literature. The geometric and material parameters and the results of these beams are given in Tables 7.1a-c and 7.2a-c. They include 12 steel plated beams, 48 CFRP plated beams (32 with pultruded and 16

with wet lay-up plates) and 8 GFRP plated beams (7 with pultruded and 1 with wet lay-up plates). In all cases the bonded plate was not subjected to any prestress, not tapered or anchored in any form, nor preloaded before loading. These beams have experienced shear plate end debonding failure either by concrete cover separation or interfacial failure or by combination of these two modes that initiated from CDC. These tests cover a wide range of influencing parameters: (1) elastic modulus of plate E_2 = 10.3-300 GPa; (2) nominal thickness of plate t_2 = 0.33-12 mm; (3) cubic strength of the concrete f_{cu} = 20-78.6 MPa; (4) splitting tensile strength of the concrete f_t = 2.1-4.5 MPa; (5) elastic modulus of concrete E_1 = 19-40 GPa; (6) axial stiffness of plate per unit width E_2t_2 = 4.33-252 (x10^4) N/mm; (7) effective axial stiffness of beam per unit width E_1d_e = 2.29-13.57 (x10^6) N/mm; (8) flexural rigidity of the cracked plated RC beam section $(EI)_{c,p}$ = 9.65-4150 (x10^{10}) Nmm^2; (9) flexural rigidity of the cracked un-plated RC beam section $(EI)_{c,0}$ = 9.41-1680 (x10^{10}) Nmm^2; (10) width ratio of beam to plate α_w = 1.0-3.33; (11) internal tensile reinforcement steel ratio ρ_s = 0.075-3.202 %; (12) mode-2 interfacial fracture energy G_f = 0.250-0.754 Nmm/mm^2; and (13) interfacial bond strength τ_f = 2.639-6.514 N/mm^2.

Tables 7.1a-c give the details of RC beams and adhesive while Tables 7.2a-c give the details of plate, loading and shear debonding tests together with predictions from the various shear debonding strength models. In Tables 7.2a-c, V_e refers to the debonding shear force from the test result; 4PB = four point bending; 3PB = three point bending; UDL = uniformly distributed load. The adhesive thickness t_a was not available in most of the 68 test database. In such cases the following values are used: t_a = 2 mm for steel and pultruded FRP plates; and t_a = [total thickness of FRP plate including adhesive t_{pa} – nominal thickness of all FRP sheets t_2]. For the few cases where t_{pa} was not available, it was calculated by assuming the thickness of adhesive layer between each FRP layer as 0.42mm. This methodology and assumptions adopted in t_a calculation are very similar to the approach adopted by Smith and Teng (2002b) to make best use of the available test database without rejecting them merely for the non availability of t_a. Also accurate measurement of t_a is not always possible in many cases particularly for wet lay-up FRP plates and a best debonding model for design use should be least sensitive to the adhesive material and geometric parameters. The proposed and the existing models compared here are only marginally influenced by adhesive thickness and are independent of adhesive material properties. Where only some concrete material

properties such as f_t, f_{cu} and cylinder strength f_c were available, others have been determined using the following relationships

$$f_c = 0.79 f_{cu} \quad \text{(BS 8110, 1997)} \quad (7.12a)$$

$$f_t = 0.53\sqrt{f_c} \quad \text{(ACI 318-02, 2002)} \quad (7.12b)$$

$$E_1 = 4730\sqrt{f_c} \quad \text{(ACI 318-02, 2002)} \quad (7.12c)$$

in which f_c and f_{cu} are in MPa.

7.3.4 Comparison of shear debonding strength models

The proposed shear debonding model (Eq. 7.11) and the first five existing models reviewed earlier such as: (1) Oehlers' (1992); (2) Oehlers et al.'s (2004); (3) Oehlers et al.'s (2005); (4) Smith and Teng's (2002); and (5) Teng and Yao's (2007) provided in Eqs 7.6 – 7.10 are assessed (Figures 7.2a-f) against 68 test results from the shear debonding test database. The predictions from different models are compared with measured strength V_e in Tables 7.2a-c and their statistical performances are summarised in Tables 7.3a-b.

It can be seen from this comparison that the Oehlers et al.'s (2004) shows the least scatter among all existing models with the lowest CoV, and it provides conservative predictions for 80% of test results. However, this model is very cumbersome due to the iterative solution procedure and it is therefore unsuitable for routine design use. The proposed model offers better accuracy than that of Oehlers et al.'s (2004) but with slightly higher CoV. Only 10% of the test data have their test-to-prediction ratio between 0.5-0.75 and 50% of its predictions are conservative with a maximum test-to-prediction ratio reaching 1.6. Oehlers' (1992) model under-predicts the test results and is highly conservative. Smith and Teng's (2002) model which is an extension of Oehlers' (1992) also under-predicts 95% of the test results. But its under-prediction is reasonable and lesser than that of Oehlers' (1992) model. Oehlers et al.'s (2005) predictions are similar to that of Oehlers (1992) and its maximum conservative predictions lies between that of Smith and Teng's (2002) and Oehelers' (1992). The predictions of Teng and Yao's (2007) are conservative for about 95% of the test data but this model offers same level of difficulty for design use as it is an extension of Oehlers et al.'s (2004) model.

Table 7.1a: Shear debonding test database-RC beam; internal tension and shear reinforcement; and adhesive details

Reference	S.No.	Specimen	b_1 (mm)	t_1 (mm)	d_e (mm)	l (mm)	f_c (MPa)	f_{cu} (MPa)	f_t (MPa)	E_1 (GPa)	E_s (GPa)	f_y (MPa)	A_s (mm^2)	E_{sv} (GPa)	f_{yv} (MPa)	A_{sv} (mm^2)	s_v (mm)	E_a (GPa)	t_a (mm)
Ritchie et al. (1991)	1	G	152	305	251	2438	43.0	53.8	3.5	25.5	200	414	253	200	414	99	102	8.50	2.00
	2	M	152	305	251	2438	43.0	53.8	3.5	25.5	200	414	253	200	414	99	102	8.50	2.00
Quantrill et al. (1996a)	3	B2	100	100	84	900	42.4	53.0	3.5	34.0	215	350	85	215	350	14	50	11.56	2.00
	4	B3	100	100	84	900	42.4	53.0	3.5	34.0	215	350	85	215	350	14	50	11.56	2.00
	5	B4	100	100	84	900	42.4	53.0	3.5	34.0	215	350	85	215	350	14	50	11.56	2.00
	6	B6	100	100	84	900	42.4	53.0	3.5	34.0	215	350	85	215	350	14	50	11.56	2.00
Quantrill et al. (1996b)	7	A1c	100	100	84	900	55.3	70.0	3.9	35.2	215	350	85	215	350	14	100	11.56	2.00
	8	A2b	100	100	84	900	33.2	42.0	3.1	27.2	215	350	85	215	350	14	100	11.56	2.00
	9	A2c	100	100	84	900	33.2	42.0	3.1	27.2	215	350	85	215	350	14	100	11.56	2.00
Garden et al. (1997)	10	$1A_u$	100	100	84	900	47.3	59.1	4.2	39.9	215	350	85	215	350	14	51	11.56	2.00
	11	$1B_u$	100	100	84	900	47.3	59.1	4.2	39.9	215	350	85	215	350	14	51	11.56	2.00
	12	$1B_{2u}$	100	100	84	900	47.3	59.1	4.2	39.9	215	350	85	215	350	14	51	11.56	2.00
	13	$1C_u$	100	100	84	900	47.3	59.1	4.2	39.9	215	350	85	215	350	14	51	11.56	2.00
	14	$2A_u$	100	100	84	900	47.3	59.1	4.2	39.9	215	350	85	215	350	14	50	11.56	2.00
	15	$2B_u$	100	100	84	900	47.3	59.1	4.2	39.9	215	350	85	215	350	14	51	11.56	2.00
	16	$2C_u$	100	100	84	900	47.3	59.1	4.2	39.9	215	350	85	215	350	14	51	11.56	2.00
	17	$3A_u$	100	100	84	900	47.3	59.1	4.2	39.9	215	350	85	215	350	14	50	11.56	2.00
	18	$3B_u$	100	100	84	900	47.3	59.1	4.2	39.9	215	350	85	215	350	14	50	11.56	2.00
	19	$3C_u$	100	100	84	900	47.3	59.1	4.2	39.9	215	350	85	215	350	14	50	11.56	2.00
Garden et al. (1998)	20	B1u,1.0	100	100	84	900	43.2	54.0	3.5	31.1	215	350	85	215	350	14	51	8.60	2.00
	21	B2u,1.0	100	100	84	900	43.2	54.0	3.5	31.1	215	350	85	215	350	14	51	8.60	2.00
	22	B1u,2.3	130	230	206	2200	37.6	47.0	3.2	29.0	220	556	236	220	350	57	150	8.60	2.00
Ahmed & van Gemert (1999a)	23	DF.2	125	225	193	1500	46.0	57.5	3.6	30.0	185	568	151	185	553	57	100	7.20	-
	24	DF.3	125	225	193	1500	46.0	57.5	3.6	30.0	185	568	151	185	553	57	100	7.20	-
	25	DF.4	125	225	193	1500	46.0	57.5	3.6	30.0	185	568	151	185	553	57	100	7.20	-
Tumialan et al. (1999)	26	A3	150	300	250	2130	51.7	64.6	3.8	34.0	207	427	792	207	427	143	125	2.00	-
	27	A8	150	300	250	2130	51.7	64.6	3.8	34.0	207	427	792	207	427	143	125	2.00	-
	28	C2	150	300	250	2130	51.7	64.6	3.8	34.0	207	427	792	207	427	143	250	2.00	-
Juvandes et al. (1998)	29	B7	75	150	250	1500	37.0	46.3	3.2	28.8	200	190	14	200	190	14	60	10.25	2.50
Hau (1999)	30	5	150	250	205	1500	40.6	50.8	3.4	30.2	231	537	157	231	537	157	100	3.26	0.37

Table 7.1b: Shear debonding test database-RC beam; internal tension and shear reinforcement; and adhesive details

Reference	S.No.	Specimen	b_1 (mm)	t_1 (mm)	d_e (mm)	l (mm)	f_c (MPa)	f_{cu} (MPa)	f_t (MPa)	E_1 (GPa)	E_s (GPa)	f_y (MPa)	A_s (mm^2)	E_{sv} (GPa)	f_{yv} (MPa)	A_{sv} (mm^2)	s_v (mm)	E_a (GPa)	t_a (mm)
Ross et al. (1999)	31	1B	200	200	152	2742	54.8	68.5	3.9	34.5	200	410	396	200	410	143	102	8.50	2.00
	32	1C	200	200	152	2742	54.8	68.5	3.9	34.5	200	410	396	200	410	143	102	8.50	2.00
	33	2B	200	200	152	2742	54.8	68.5	3.9	34.5	200	410	396	200	410	143	102	8.50	2.00
	34	2C	200	200	152	2742	54.8	68.5	3.9	34.5	200	410	396	200	410	143	102	8.50	2.00
	35	2D	200	200	152	2742	54.8	68.5	3.9	34.5	200	410	396	200	410	143	102	8.50	2.00
	36	3B	200	200	152	2742	54.8	68.5	3.9	34.5	200	410	396	200	410	143	102	8.50	2.00
	37	3C	200	200	152	2742	54.8	68.5	3.9	34.5	200	410	396	200	410	143	102	8.50	2.00
	38	3D	200	200	152	2742	54.8	68.5	3.9	34.5	200	410	396	200	410	143	102	8.50	2.00
Oehlers (1992)	39	1/4/S	130	175	147	1650	42.0	52.5	3.2	22.0	200	444	402	210	568	25	500	8.50	2.00
Gao et al. (2004)	40	1T6LN	150	200	162	1500	47.8	60.5	3.7	32.5	200	460	157	200	250	101	75	8.50	-
	41	2T6LN	150	200	162	1500	62.1	78.6	4.2	37.1	200	460	157	200	250	101	75	8.50	-
	42	2T4LN	150	200	162	1500	62.1	78.6	4.2	37.1	200	460	157	200	250	101	75	8.50	-
Valcuende et al. (2003)	43	A-S1	100	150	128	1000	39.5	49.9	3.3	29.7	200	500	157	200	500	57	100	8.50	2.00
	44	A-S2	100	150	128	1000	39.5	49.9	3.3	29.7	200	500	157	200	500	57	100	8.50	2.00
	45	B-S1	100	150	128	1000	41.6	52.6	3.4	30.5	200	500	157	200	500	57	100	8.50	2.00
	46	B-S2	100	150	128	1000	41.6	52.6	3.4	30.5	200	500	157	200	500	57	100	8.50	2.00
Smith & Teng (2003)	47	1B	154	250	215	1500	31.1	39.4	2.4	23.3	207	506	157	207	506	157	100	8.50	-
	48	3B	151	250	215	1500	44.7	56.6	3.2	29.0	207	506	157	207	506	157	100	8.50	-
Ahmed et al. (2001)	49	AF4	125	225	193	1500	41.0	51.9	2.8	30.0	185	568	101	185	553	57	71	8.50	-
Rahimi & Hutchinson (2001)	50	A10	200	150	120	2100	48.6	61.5	3.0	25.0	210	575	157	200	250	57	150	8.50	2.00
	51	A11	200	150	120	2100	48.6	61.5	3.0	25.0	210	575	157	200	250	57	150	8.50	2.00
Mohammed Ali (2001)	52	SP01	200	370	340	2300	48.9	61.1	4.5	39.9	210	444	942	0	0	0	1	8.50	2.00
	53	SP-T6	200	370	340	2400	35.3	44.1	3.6	34.3	210	444	1257	210	500	157	100	8.50	2.00
	54	SP-T12	200	370	340	2400	35.3	44.1	3.6	34.3	210	444	1257	210	500	157	100	8.50	2.00
Luo (1993)	55	FP/B2/L	130	180	150	1000	38.1	47.6	3.6	34.2	210	444	402	0	0	0	1	8.50	2.00
	56	FP/B2/R	130	180	150	1000	39.1	48.9	3.6	34.2	210	444	402	0	0	0	1	8.50	2.00
	57	FP/B3/L	130	180	150	1000	40.1	50.1	3.6	34.2	210	444	402	0	0	0	1	8.50	2.00
	58	FP/B3/R	130	180	150	1000	41.1	51.4	3.6	34.2	210	444	402	0	0	0	1	8.50	2.00
	59	FP/B4/L	130	180	150	1000	42.1	52.6	3.6	34.2	210	444	402	0	0	0	1	8.50	2.00
	60	FP/B4/R	130	180	150	1000	42.1	52.6	3.6	34.2	210	444	402	0	0	0	1	8.50	2.00

Table 7.1c: Shear debonding test database-RC beam; internal tension and shear reinforcement; and adhesive details

Reference	S.No.	Specimen	b_1 (mm)	t_1 (mm)	d_e (mm)	l (mm)	f_c (MPa)	f_{cu} (MPa)	f_t (MPa)	E_1 (GPa)	E_s (GPa)	f_y (MPa)	A_s (mm^2)	E_{sv} (GPa)	f_{yv} (MPa)	A_{sv} (mm^2)	s_v (mm)	E_a (GPa)	t_a (mm)
Yao & Teng (2007)	61	CS-B	150	253	217	1500	24.6	30.7	3.1	25.3	199	536	157	199	536	157	100	8.50	1.41
	62	CS-L3-B	151	253	217	1500	26.3	32.9	3.5	27.2	199	536	157	199	536	157	100	8.50	2.14
	63	CS-W100-B	151	254	214	1500	30.2	37.8	3.3	24.3	199	536	157	199	536	157	100	8.50	1.62
	64	CP-B	151	253	218	1500	29.6	37.0	3.8	27.4	199	536	157	199	536	157	100	8.50	2.00
	65	SP-B	151	253	214	1500	28.3	35.4	3.7	26.5	199	536	157	199	536	157	100	8.50	2.00
	66	CS-C10-B	151	253	236	1500	21.8	27.3	4.0	30.0	199	536	157	199	536	157	750	8.50	1.53
Aprile & Feo (2007)	67	SB4/01/0.95	150	250	210	2000	16.0	20.0	2.1	6.9	210	515	942	210	515	57	200	8.50	2.00
Jones et al. (1988)	68	F31	155	225	190	2300	42.9	53.6	3.6	31.0	200	430	943	200	324	57	75	0.28	1.50

Table 7.2a: Shear debonding test database-Plate and loading details; shear debonding model- tests versus predictions

Reference	S.No.	Specimen	b_2 (mm)	t_2 (mm)	E_2 (GPa)	f_2 (GPa)	Type	l_1 (mm)	l_2 (mm)	Load	V_e (kN)	V_p (kN)	V_{Oeh-1} (kN)	V_{Oeh-2} (kN)	V_{Oeh-3} (kN)	V_{S-T} (kN)	V_{T-Y} (kN)
Ritchie et al. (1991)	1	G	152	4.19	10.3	0.18	G-P	0	914	4PB	62.9	56.2	32.0	52.7	35.7	48.0	186.1
	2	M	152	1.27	117.9	1.49	C-P	0	914	4PB	72.1	66.5	32.0	54.6	38.8	48.0	68.5
Quantrill et al. (1996a)	3	B2	80	1.20	49	1.08	G-P	20	300	4PB	17.0	21.8	8.6	17.7	11.0	12.9	20.0
	4	B3	30	1.20	49	1.08	G-P	20	300	4PB	12.3	15.8	8.6	17.2	9.9	12.9	19.0
	5	B4	60	1.60	49	1.08	G-P	20	300	4PB	17.5	21.8	8.6	17.7	10.8	12.9	19.3
	6	B6	80	1.20	118.5	0.99	C-P	20	300	4PB	20.4	21.1	8.6	18.3	11.5	12.9	18.9
Quantrill et al. (1996b)	7	A1c	80	1.20	49	1.08	G-P	20	300	4PB	22.0	22.3	9.4	20.4	12.1	14.1	22.0
	8	A2b	80	1.20	49	1.08	G-P	20	300	4PB	18.4	20.8	7.9	15.6	10.1	11.9	16.6
	9	A2c	80	1.20	49	1.08	G-P	20	300	4PB	18.7	20.8	7.9	15.6	10.1	11.9	16.6
Garden et al. (1997)	10	$1A_u$	90	0.50	111	1.27	C-P	20	300	4PB	19.8	18.0	8.9	18.8	11.5	13.4	21.4
	11	$1B_u$	65	0.70	111	1.27	C-P	20	300	4PB	18.3	18.1	8.9	18.8	11.4	13.4	20.5
	12	$1B_{2u}$	65	0.70	111	1.27	C-P	20	300	4PB	18.2	18.1	8.9	18.8	11.4	13.4	20.5
	13	$1C_u$	45	1.00	111	1.27	C-P	20	300	4PB	16.0	18.0	8.9	18.7	11.0	13.4	19.8
	14	$2A_u$	90	0.50	111	1.27	C-P	20	340	4PB	19.3	18.0	8.9	18.0	11.6	13.4	20.7
	15	$2B_u$	65	0.70	111	1.27	C-P	20	340	4PB	17.0	18.1	8.9	18.1	11.7	13.4	19.8
	16	$2C_u$	45	1.00	111	1.27	C-P	20	340	4PB	17.8	18.0	8.9	18.0	11.4	13.4	19.1
	17	$3A_u$	90	0.50	111	1.27	C-P	20	400	4PB	19.5	18.0	8.9	17.0	11.6	13.4	19.7
	18	$3B_u$	65	0.70	111	1.27	C-P	20	400	4PB	17.3	18.1	8.9	17.1	11.7	13.4	18.8
	19	$3C_u$	45	1.00	111	1.27	C-P	20	400	4PB	15.4	18.0	8.9	17.0	11.5	13.4	18.2
Garden et al. (1998)	20	B1u,1.0	67	0.82	111	1.41	C-P	20	300	4PB	18.3	19.6	8.7	18.1	11.1	13.0	19.4
	21	B2u,1.0	67	0.82	111	1.41	C-P	20	300	4PB	16.0	19.6	8.7	18.1	11.1	13.0	19.4
	22	B1u,2.3	90	1.28	115	1.28	C-P	40	844	4PB	50.2	43.8	24.0	34.4	28.8	36.1	39.5
Ahmed & van Gemert (1999a)	23	DF.2	75	0.334	240	3.50	C-W	50	500	4PB	60.3	38.0	20.8	40.8	23.3	31.1	51.1
	24	DF.3	75	0.501	240	3.50	C-W	50	500	4PB	60.0	41.2	20.8	41.1	23.5	31.1	46.9
	25	DF.4	75	0.668	240	3.50	C-W	50	500	4PB	62.8	44.2	20.8	41.4	23.7	31.1	45.3
Tumialan et al. (1999)	26	A3	150	0.495	230	3.40	C-W	0	1065	3PB	86.1	87.1	49.2	63.7	55.4	73.9	183.7
	27	A8	75	0.990	230	3.40	C-W	0	1065	3PB	98.2	87.1	49.2	63.7	55.4	73.9	118.0
	28	C2	150	0.495	230	3.40	C-W	0	1065	3PB	79.3	83.5	49.2	63.7	55.4	73.9	123.7
Juvandes et al. (1998)	29	B7	50	1.20	150	2.40	C-P	10	650	4PB	12.5	23.6	7.2	13.1	10.2	10.8	14.8
Hau (1999)	30	5	150	2.64	19.7	0.26	G-W	50	500	4PB	79.4	50.0	23.6	50.0	26.1	35.4	95.7

Note: V_e is debonding strength from experiment and V_p; V_{Oeh-1}; V_{Oeh-2}; V_{Oeh-3}; V_{S-T}; and V_{T-Y} are debonding strength predictions from Eqs 7.11; 7.6; 7.8; 7.9; 7.7; and 7.10 respectively.

Table 7.2b: Shear debonding test database-Plate and loading details; shear debonding model- tests versus predictions

Reference	S.No.	Specimen	b_2 (mm)	t_2 (mm)	E_2 (GPa)	f_2 (GPa)	Type	l_1 (mm)	l_2 (mm)	Load	V_e (kN)	V_p (kN)	V_{Oeh-1} (kN)	V_{Oeh-2} (kN)	V_{Oeh-3} (kN)	V_{S-T} (kN)	V_{T-Y} (kN)
Ross et al. (1999)	31	1B	200	0.45	138	2.21	C-P	1	914	4PB	40.1	65.4	36.0	55.2	42.1	54.0	99.6
	32	1C	200	0.45	138	2.21	C-P	1	914	4PB	35.6	65.4	36.0	55.2	42.1	54.0	99.6
	33	2B	200	0.45	138	2.21	C-P	1	914	4PB	49.0	65.4	36.0	55.2	42.1	54.0	99.6
	34	2C	200	0.45	138	2.21	C-P	1	914	4PB	35.6	65.4	36.0	55.2	42.1	54.0	99.6
	35	2D	200	0.45	138	2.21	C-P	1	914	4PB	40.1	65.4	36.0	55.2	42.1	54.0	99.6
	36	3B	200	0.45	138	2.21	C-P	1	914	4PB	54.5	65.4	36.0	55.2	42.1	54.0	99.6
	37	3C	200	0.45	138	2.21	C-P	1	914	4PB	54.1	65.4	36.0	55.2	42.1	54.0	99.6
	38	3D	200	0.45	138	2.21	C-P	1	914	4PB	54.3	65.4	36.0	55.2	42.1	54.0	99.6
Oehlers (1992)	39	1/4/S	130	5.00	210	0.27	S	50	550	4PB	41.0	44.6	24.3	48.8	34.9	36.5	48.9
Gao et al. (2004)	40	1T6LN	150	0.66	235	4.20	C-W	20	500	4PB	58.1	58.3	21.7	46.3	28.4	32.5	53.6
	41	2T6LN	150	0.66	235	4.20	C-W	20	500	4PB	68.0	60.6	23.6	53.0	31.1	35.5	61.0
	42	2T4LN	150	0.44	235	4.20	C-W	20	500	4PB	66.7	53.3	23.6	52.2	29.8	35.5	65.6
Valcuende et al. (2003)	43	A-S1	50	1.20	165	2.60	C-P	50	400	4PB	39.3	33.0	13.4	23.6	15.2	20.2	25.4
	44	A-S2	50	1.20	165	2.60	C-P	50	400	4PB	42.1	33.0	13.4	23.6	15.2	20.2	25.4
	45	B-S1	50	1.20	165	2.60	C-P	50	400	4PB	35.1	33.2	13.7	24.3	15.5	20.5	26.2
	46	B-S2	50	1.20	165	2.60	C-P	50	400	4PB	37.8	33.2	13.7	24.3	15.5	20.5	26.2
Smith & Teng (2003)	47	1B	150	0.33	271	3.72	C-W	25	500	4PB	66.8	53.4	22.6	45.0	25.9	33.9	71.5
	48	3B	147	0.33	257	4.52	C-W	50	500	4PB	65.3	58.4	25.2	53.5	28.2	37.8	87.1
Ahmed et al. (2001)	49	AF4	75	0.334	240	3.50	C-W	50	500	4PB	55.5	36.1	17.4	37.3	20.0	26.2	47.5
Rahimi & Hutchinson (2001)	50	A10	150	0.80	127	1.53	C-P	0	750	4PB	33.8	42.8	22.0	39.7	28.8	32.9	41.2
	51	A11	150	0.80	127	1.53	C-P	0	750	4PB	34.7	42.8	22.0	39.7	28.8	32.9	41.2
Mohammed Ali (2001)	52	SP01	200	10.00	210	0.33	S	50	1150	3PB	140.0	133.2	73.5	123.0	107.4	110.2	123.0
	53	SP-T6	200	6.00	210	0.37	S	50	1200	3PB	113.0	134.1	72.5	100.3	97.2	108.8	107.2
	54	SP-T12	200	12.00	210	0.31	S	50	1200	3PB	113.0	146.8	72.5	115.6	105.7	108.8	118.9
Luo (1993)	55	FP/B2/L	130	3.00	210	0.32	S	0	500	3PB	46.8	39.7	23.8	42.7	32.0	35.8	42.7
	56	FP/B2/R	130	3.00	210	0.32	S	0	500	3PB	50.0	40.0	24.0	43.2	32.3	36.1	43.2
	57	FP/B3/L	130	5.00	210	0.32	S	0	500	3PB	64.2	46.2	24.2	47.5	34.1	36.4	47.5
	58	FP/B3/R	130	5.00	210	0.32	S	0	500	3PB	70.8	46.5	24.4	48.0	34.4	36.7	48.0
	59	FP/B4/L	130	10.00	210	0.29	S	0	500	3PB	85.0	57.2	24.6	56.5	37.3	37.0	56.5
	60	FP/B4/R	130	10.00	210	0.29	S	0	500	3PB	78.7	57.2	24.6	56.5	37.3	37.0	56.5

Note: V_e is debonding strength from experiment and V_p; V_{Oeh-1}; V_{Oeh-2}; V_{Oeh-3}; V_{S-T}; and V_{T-Y} are debonding strength predictions from Eqs 7.11; 7.6; 7.8; 7.9; 7.7; and 7.10 respectively.

Table 7.2c: Shear debonding test database-Plate and loading details; shear debonding model- tests versus predictions

Reference	S.No.	Specimen	b_2 (mm)	t_2 (mm)	E_2 (GPa)	f_2 (GPa)	Type	l_1 (mm)	l_2 (mm)	Load	V_e (kN)	V_p (kN)	V_{Oeh-1} (kN)	V_{Oeh-2} (kN)	V_{Oeh-3} (kN)	V_{S-T} (kN)	V_{T-Y} (kN)
Yao & Teng (2007)	61	CS-B	148	0.33	256	4.11	C-W	50	500	3PB	54.3	52.6	20.7	38.8	22.2	31.0	61.4
	62	CS-L3-B	148	0.495	256	4.11	C-W	50	500	3PB	52.3	58.4	21.2	41.3	23.3	31.9	55.5
	63	CS-W100-B	100	0.33	256	4.11	C-W	50	500	3PB	53.9	50.4	22.0	43.4	23.5	33.0	69.2
	64	CP-B	148	1.20	165	2.80	C-P	50	500	3PB	50.7	68.5	22.1	45.2	25.0	33.2	53.5
	65	SP-B	148	2.00	174	0.16	S	50	500	3PB	45.5	44.5	21.6	46.7	25.4	32.4	50.8
	66	CS-C10-B	148	0.33	256	4.11	C-W	50	500	3PB	66.3	43.8	20.9	36.7	22.4	31.4	40.4
Aprile & Feo (2007)	67	SB4/01/0.95	50	1.40	300	1.45	C-P	50	696	UDL	49.3	49.6	31.9	35.9	33.7	47.9	37.6
Jones et al. (1988)	68	F31	125	6.00	200	0.25	S	50	767	4PB	91.0	70.0	42.7	67.9	57.1	64.1	69.0

Note: V_e is debonding strength from experiment and V_p; V_{Oeh-1}; V_{Oeh-2}; V_{Oeh-3}; V_{S-T}; and V_{T-Y} are debonding strength predictions from Eqs 7.11; 7.6; 7.8; 7.9; 7.7; and 7.10 respectively.

Table 7.3a: Shear debonding model- test-to-predicted debonding strength ratios

Model	Average	Coefficient of variation	Maximum	Minimum
Proposed model: (V_e/V_p)	1.032	0.251	1.589	0.530
Oehlers (1992): (V_e/V_{Oeh-1})	2.174	0.278	3.449	0.990
Oehlers et al. (2004): (V_e/V_{Oeh-2})	1.169	0.234	1.805	0.645
Oehlers et al. (2005): (V_e/V_{Oeh-3})	1.773	0.303	3.038	0.845
Smith & Teng (2002): (V_e/V_{S-T})	1.449	0.278	2.299	0.660
Teng & Yao (2007): (V_e/V_{T-Y})	0.965	0.328	1.657	0.338

Table 7.3b: Shear debonding model-natural logarithm of test-to-predicted debonding strength ratios

Model	Average	Standard deviation	Maximum	Minimum
Proposed model: $\ln(V_e/V_p)$	0.000	0.258	0.463	-0.636
Oehlers (1992): $\ln(V_e/V_{Oeh-1})$	0.736	0.294	1.238	-0.010
Oehlers et al. (2004): $\ln(V_e/V_{Oeh-2})$	0.128	0.241	0.591	-0.439
Oehlers et al. (2005): $\ln(V_e/V_{Oeh-3})$	0.527	0.308	1.111	-0.168
Smith & Teng (2002): $\ln(V_e/V_{S-T})$	0.330	0.294	0.833	-0.416
Teng & Yao (2007): $\ln(V_e/V_{T-Y})$	-0.097	0.375	0.505	-1.085

The statistical performance of the natural logarithm of test-to-predicted debonding strength ratios of the five models are provided in Table 7.3b. Ideally, the average, maximum and minimum should be nearer to zero; and the standard deviation should be less for any good debonding model. The positive and negative sign in average, maximum and minimum can be considered as a representation of the extent of conservative and unconservative predictions respectively. Based on the above comparisons, it is found that only the present model offers good accuracy with reasonable conservatism and is easy to incorporate in any design codes.

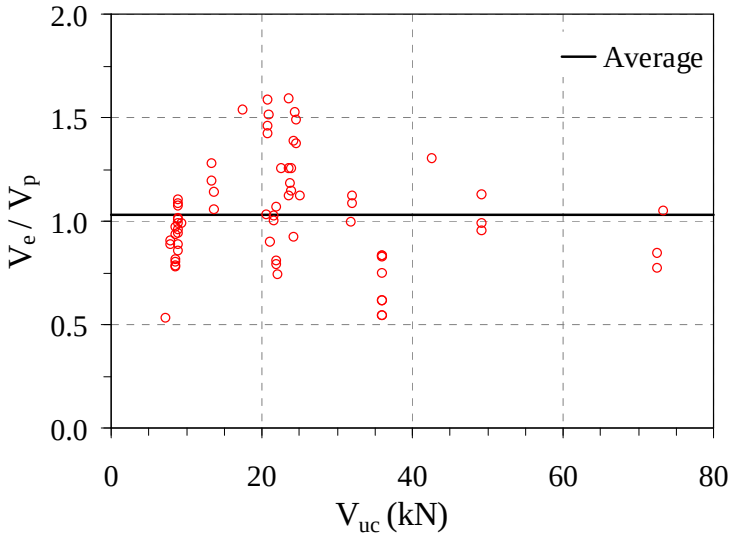

(a) Proposed model

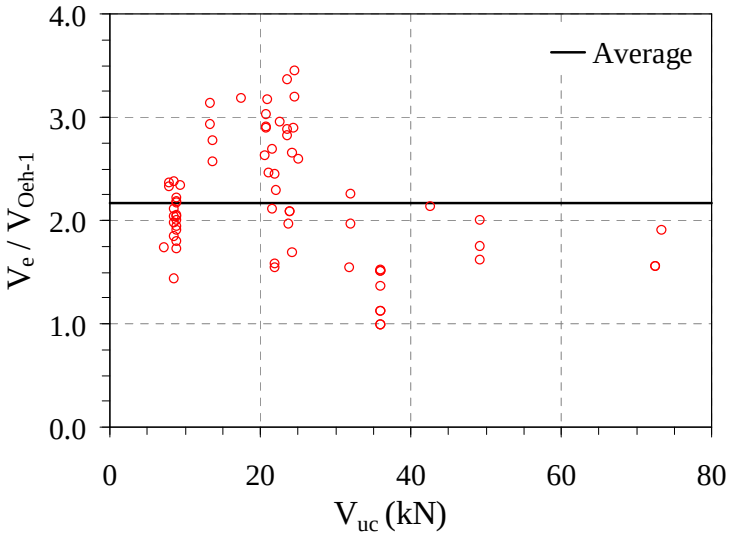

(b) Oehlers' (1992) model

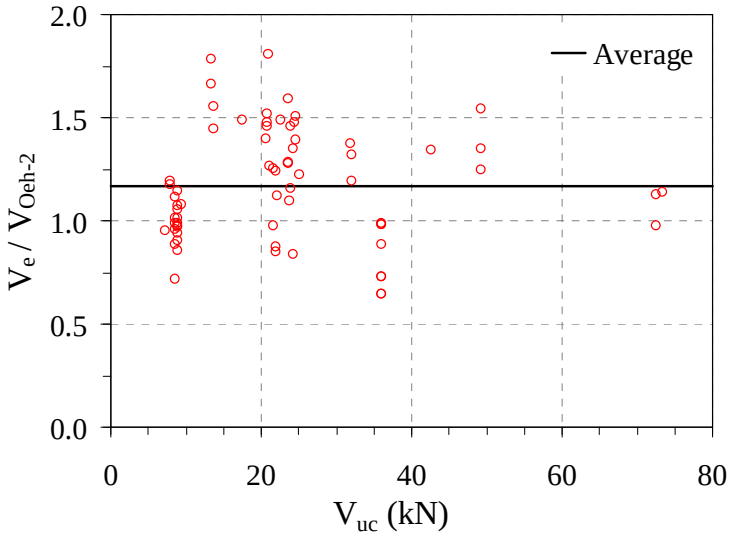

(c) Oehlers et al.'s (2004) model

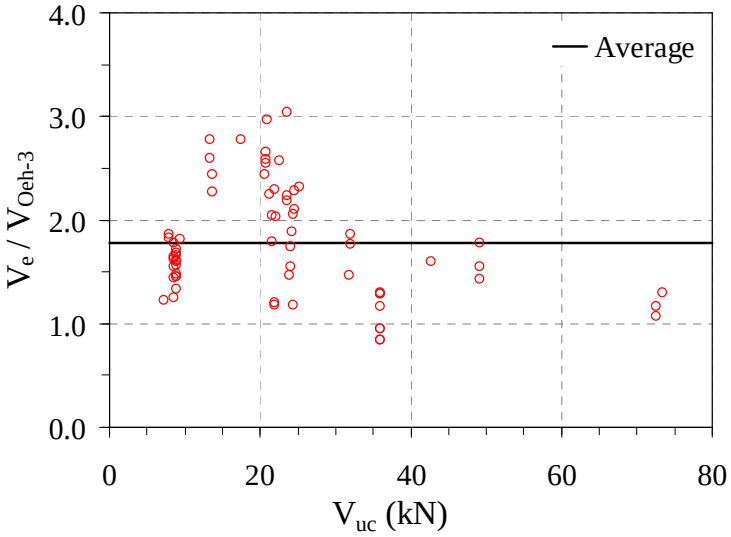

(d) Oehlers et al.'s (2005) model

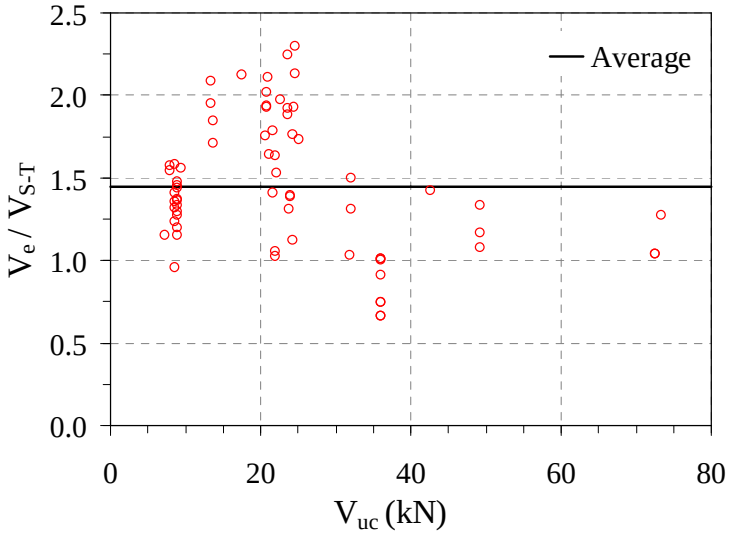

(e) Smith and Teng's (2002) model

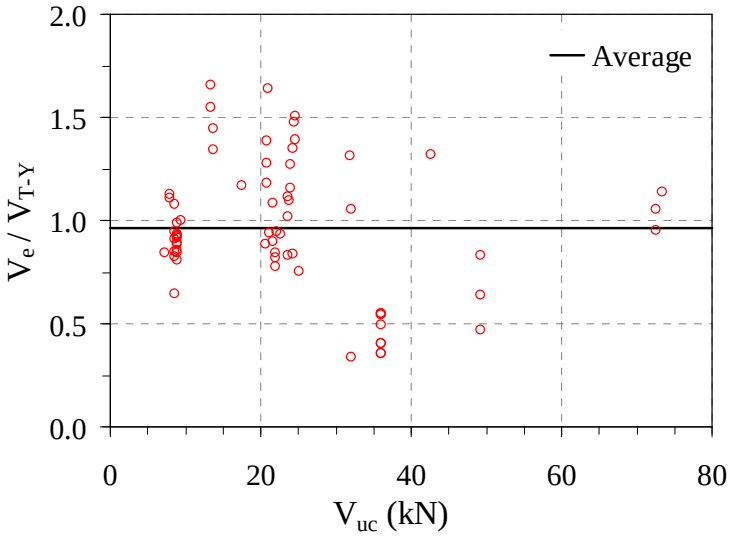

(e) Teng and Yao's (2007) model

Figure 7.2. Comparison of shear debonding models: tests versus predictions

7.4 Shear-Bending Interaction Debonding Model

Debonding models applicable to two extreme cases of bending moment (M) or shear force (V) in the beam at the plate end locations have been discussed in preceding sections. This has shown that debonding occurs at $M = M_{prediction}$ when $V \rightarrow 0$; and $V = V_{prediction}$ when $M \rightarrow 0$, respectively for beams with plates terminated in CMR and nearer to support. The plate end debonding in any general case of a plated beam is due to the combination of both M and V. The interfacial stresses on either the adhesive-concrete or in tension reinforcement-composite plate (the bonded plate and concrete cover impregnated with adhesive behave as a composite plate located just below tension reinforcement); and the shear forces causing crack growth and sliding in concrete that are believed and proven by previous studies to be responsible for plate end debonding failures are influenced by both the applied moment and the shear force at the plate end. A strong interaction between bending moment and shear force exists at the plate end in any general case of a plated RC beam. The debonding load in such situations can be estimated from an interaction debonding model. Three such interaction models existing in literature are from Oehlers (1992), Smith and Teng (2003) and Teng and Yao (2007). These models have been developed from the models pertinent to the two extreme cases of M (flexural debonding) and V (shear debonding). The accuracy, simplicity and the adaptability of the final interaction model obviously depends on the two constituent

models for the extreme situations. The limitations in the existing extreme debonding models discussed previously demands the development of a new interaction model. This section presents a brief review of existing interaction models followed by the proposed new interaction model, shear-bending interaction debonding test database and the comparison of all the studied interaction models.

7.4.1 Existing shear-bending interaction debonding strength models

Oehlers' (1992) model

Based on Oehlers and Moran's (1990) flexural debonding model and Oehlers's (1992) shear debonding strength model in combination with experimental observations, Oehlers (1992) proposed a first shear-bending interaction model to predict the debonding load in any general case of a plated RC beam as given below.

$$\frac{V_e}{V_{Oeh-1}} + \frac{M_e}{M_{Oeh}} \leq 1.17 \tag{7.13}$$

where $V_{\text{Oeh-1}}$ and M_{Oeh} are the debonding shear and bending strengths predicted from Eqs 7.5 and 7.6a respectively and subscript *e* to *V* and *M* refers to such values obtained from experiments. This model over-predicts the debonding strength in extreme cases of plate termination i.e in CMR and pure shear region where *V* and *M* are respectively zero.

Smith and Teng's (2003) model

Smith and Teng (2003) proposed an interaction model for an FRP plated RC beam fully based on their shear debonding model given in Eq. 7 and limited test results as:

$$\frac{V_e}{V_{S-T}} + 0.4\frac{M_e}{M_{prediction}} = 1.0, \qquad \text{if } V_e \geq 0.6V_{S-T} \tag{7.14a}$$

$$M_{prediction} = M_e \qquad \text{if } V_e < 0.6V_{S-T} \tag{7.14b}$$

Teng and Yao's (2007) model

Based on their flexural and shear debonding models and the shear-bending interaction test database with 23 test results, Teng and Yao (2007) proposed an interaction model given by

$$\left(\frac{V_e}{V_{T-Y}}\right)^2+\left(\frac{M_e}{M_{T-Y}}\right)^2=1.0. \tag{7.15}$$

where $M_{\text{T-Y}}$ and $V_{\text{T-Y}}$ are the predicted bending moment and shear force at debonding from the Teng and Yao's (2007) models given in Eqs 7.4 and 7.10.

7.4.2 Proposed new shear-bending interaction debonding strength model

A new shear-bending interaction model that can use the simple, accurate and explicit predictive models given in Eqs 7.3 and 7.11 is developed based on a detailed analysis with the largest debonding test database containing the test results of 226 FRP and steel plated RC beams constructed from 91 test results in shear-bending interaction region discussed in next section together with the 68 shear debonding and 67 flexural debonding test databases discussed previously. This circular interaction debonding model is given by

$$\left(\frac{V_e}{V_p}\right)^2+\left(\frac{M_e}{M_p}\right)^2=1.0. \tag{7.16}$$

where $M_{\text{p}} = M_{\text{p-3}}$ and V_{p} are the predicted bending moment and shear force at debonding from the models given in Eqs 7.3 and 7.11.

7.4.3 Shear-bending interaction debonding test database

The database comprises the test results of 91 common RC beams with the bonded plate terminated in region of shear and bending interaction. This is constructed from 17 experimental studies in literature. The geometric and material parameters and the test results of these test beams are given in Tables 7.4a-c and 7.5a-c. These tests include 37 steel plated beams, 46 CFRP plated beams (30 with pultruded and 16 with wet lay-up plates) and 8 GFRP plated beams (4 with pultruded and 4 with wet lay-up plates). In all these tests, the plate termination lies within 50mm < l_1 < l_2, where l_1 is the distances from the support to the plate end and l_2 is the shear span. The selection criterion for the bonded plate and RC beam remained the same as that of previous two databases. These tests cover a wide range of important parameters: (1) elastic modulus of plate E_2 = 11.7-300 GPa; (2) nominal thickness of plate t_2 = 0.17-6.00 mm; (3) cubic strength of the concrete f_{cu} = 20-101.3 MPa; (4) splitting tensile strength of the concrete f_{t} = 2.1-5.0 MPa; (5) elastic modulus of concrete E_1 = 18.9-39.2 GPa; (6) axial stiffness of plate per

unit width E_2t_2 = 2.6-105.0 (x10^4) N/mm; (7) effective axial stiffness of beam per unit width E_1d_e = 2.04-11319 (x10^6) N/mm; (8) flexural rigidity of the cracked plated RC beam section $(EI)_{c,p}$ = 10.51-2235 (x10^{10}) Nmm^2; (9) flexural rigidity of the cracked un-plated RC beam section $(EI)_{c,0}$ = 8.27-2052 (x10^{10}) Nmm^2; (10) width ratio of beam to plate α_w = 1.0-3.0; (11) internal tensile reinforcement steel ratio ρ_s = 0.4-4.4 %; (12) mode-2 interfacial fracture energy G_f = 0.250-0.616 Nmm/mm^2; and (13) interfacial bond strength τ_f = 2.639-6.234 N/mm^2.

Tables 7.4a-c give the details of RC beams and adhesives. Tables 7.5a-c give the details of plate, loading and shear force and bending moments during debonding from tests versus predictions from two existing and proposed shear-bending interaction debonding strength models. All tests were conducted on simply supported beams, and in Tables 5a-c, P_e refer to the applied transverse load (= R for 4PB; 2R for 3PB; and load 2R for UDL; if R = a support reaction) during debonding from the test result. The procedures adopted in the absence of data for concrete properties and adhesive follow those outlined earlier

Table 7.4a: Shear-bending interaction debonding test database-RC beam; internal tension and shear reinforcement; and adhesive details

Reference	S.No.	Specimen	b_1 (mm)	t_1 (mm)	d_e (mm)	l (mm)	f_c (MPa)	f_{cu} (MPa)	f_t (MPa)	E_1 (GPa)	E_s (GPa)	f_y (MPa)	A_s (mm^2)	E_{sv} (GPa)	f_{yv} (MPa)	A_{sv} (mm^2)	s_v (mm)	E_a (GPa)	t_a (mm)
Ritchie et al. (1991)	1	C	152	305	251	2438	39.8	49.8	3.30	22.8	200	414	253	200	414	99	102	8.5	2.00
	2	D	152	305	251	2438	39.8	49.8	3.30	22.8	200	414	253	200	414	99	102	8.5	2.00
	3	I	152	305	251	2438	39.8	49.8	3.30	22.8	200	414	253	200	414	99	102	8.5	2.00
Beber et al. (1999)	4	VR5	120	250	214	2350	33.6	42.0	3.10	27.4	200	565	157	200	738	57	110	8.5	-
	5	VR6	120	250	214	2350	33.6	42.0	3.10	27.4	200	565	157	200	738	57	110	8.5	-
	6	VR7	120	250	214	2350	33.6	42.0	3.10	27.4	200	565	157	200	738	57	110	8.5	-
	7	VR8	120	250	214	2350	33.6	42.0	3.10	27.4	200	565	157	200	738	57	110	8.5	-
	8	VR9	120	250	214	2350	33.6	42.0	3.10	27.4	200	565	157	200	738	57	110	8.5	-
	9	VR10	120	250	214	2350	33.6	42.0	3.10	27.4	200	565	157	200	738	57	110	8.5	-
David et al. (1999)	10	P_2	150	300	257	2800	40.0	50.0	3.40	29.9	200	500	308	200	500	57	140	8.5	1.00
	11	P_3	150	300	257	2800	40.0	50.0	3.40	29.9	200	500	308	200	500	57	140	8.5	1.00
	12	P_4	150	300	257	2800	40.0	50.0	3.40	29.9	200	500	308	200	500	57	140	8.5	1.00
	13	P_5	150	300	257	2800	40.0	50.0	3.40	29.9	200	500	308	200	500	57	140	8.5	1.00
Hau KM (1999)	14	2	150	250	205	1500	35.4	44.3	3.20	28.2	231	537	157	231	537	157	100	3.26	0.37
	15	4	150	250	205	1500	36.2	45.3	3.45	28.5	231	537	157	231	537	157	100	3.26	0.37
	16	6	150	250	205	1500	39.9	49.9	3.30	29.9	231	537	157	231	537	157	100	3.26	0.37
	17	7	150	250	205	1500	37.6	47.0	3.20	29.0	231	537	157	231	537	157	100	3.26	0.37
Nguyen et al. (2001)	18	A950	120	150	120	1330	25.7	32.1	2.70	24.0	200	384	236	200	400	57	50	12.8	1.50
	19	A1100	120	150	120	1330	25.7	32.1	2.70	24.0	200	384	236	200	400	57	50	12.8	1.50
	20	A1150	120	150	120	1330	25.7	32.1	2.70	24.0	200	384	236	200	400	57	50	12.8	1.50
	21	B2	120	150	120	1330	35.7	44.6	3.20	28.3	200	466	628	200	400	57	50	12.8	1.50
Sadatmanesh & Ehsani (1991)	22	B	205	455	400	4575	35.0	43.8	3.10	28.0	200	456	1013	200	456	253	150	8.5	1.50
Taljsten (1999)	23	SB1	200	300	252	3600	51.2	64.0	3.80	33.8	200	527	402	200	527	157	75	8.5	2.10
	24	SB2	200	300	252	3600	52.0	65.0	3.80	34.1	200	527	402	200	527	157	75	8.5	2.40
	25	SB3	200	300	252	3600	52.0	65.0	3.80	34.1	200	527	402	200	527	157	75	8.5	3.00
	26	MB1	200	300	252	3600	56.0	70.0	4.00	35.4	200	527	402	200	527	157	75	8.5	2.40
	27	HB1	200	300	252	3600	56.0	70.0	4.00	35.4	200	527	402	200	527	157	75	8.5	2.10
	28	FB1	200	300	252	3600	51.2	64.0	3.80	33.8	200	527	402	200	527	157	75	8.5	0.40
Ahmed & van	29	AF3	125	225	193	1500	46.0	57.5	3.60	30.0	185	568	101	195	553	57	71	7.2	-
Gemert (1999b)	30	CF2-1	125	225	193	1500	46.0	57.5	3.60	30.0	185	568	129	195	553	57	71	7.2	-
	31	CF3-1	125	225	193	1500	46.0	57.5	3.60	30.0	185	568	151	195	553	57	71	7.2	-
	32	CF4-1	125	225	193	1500	46.0	57.5	3.60	30.0	183	586	207	195	553	57	71	7.2	-

Table 7.4b: Shear-bending interaction debonding test database-RC beam; internal tension and shear reinforcement; and adhesive details

Reference	S.No.	Specimen	b_1 (mm)	t_1 (mm)	d_e (mm)	l (mm)	f_c (MPa)	f_{cu} (MPa)	f_t (MPa)	E_1 (GPa)	E_s (GPa)	f_y (MPa)	A_s (mm^2)	E_{sv} (GPa)	f_{yv} (MPa)	A_{sv} (mm^2)	s_v (mm)	E_a (GPa)	t_a (mm)
Smith & Teng (2003)	33	6B	151	250	215	1500	40.4	51.2	2.85	29.4	207	506	157	207	506	157	100	8.5	-
	34	2B	151	250	215	1500	48.0	60.7	3.59	28.8	207	506	157	207	506	157	100	8.5	-
	35	3A	151	250	215	1500	44.7	56.6	3.24	29.0	207	506	157	207	506	157	100	8.5	-
	36	1A	154	250	215	1500	31.1	39.4	2.44	23.3	207	506	157	207	506	157	100	8.5	-
	37	2A	151	250	215	1500	48.0	60.7	3.59	28.8	207	506	157	207	506	157	100	8.5	-
Aprile & Feo (2007)	38	SB4/02/0.85	150	250	210	2000	16.0	20.0	2.12	18.9	210	515	942	210	515	57	200	8.5	2.00
	39	SB4/03/0.75	150	250	210	2000	16.0	20.0	2.12	18.9	210	515	942	210	515	57	200	8.5	2.00
	40	SB4/04/0.65	150	250	210	2000	16.0	20.0	2.12	18.9	210	515	942	210	515	57	200	8.5	2.00
Ceroni et al.(2001)	41	A2	150	100	80	1800	29.0	36.7	2.85	25.5	200	590	101	200	250	57	750	8.5	2.00
	42	A3	150	100	80	1800	29.0	36.7	2.85	25.5	200	590	101	200	250	57	750	8.5	2.00
	43	C2	100	150	125	1800	29.0	36.7	2.85	25.5	200	590	101	200	250	57	750	8.5	2.00
	44	C3	100	150	125	1800	29.0	36.7	2.85	25.5	200	590	101	200	250	57	750	8.5	2.00
Pornpongsaroj &	45	A-420-P3	120	220	176	2000	44.0	55.7	3.52	31.4	200	480	628	200	399	57	50	8.5	2.00
Pimanmas (2003)	46	B-200-P4	120	220	176	2000	44.0	55.7	3.52	31.4	200	554	628	200	399	57	50	8.5	2.00
Fanning & kelly (2001)	47	F5	155	240	203	2800	80.0	101.3	5.00	39.2	204	532	339	197.5	306	57	125	8.5	2.00
	48	F6	155	240	203	2800	80.0	101.3	5.00	39.2	204	532	339	197.5	306	57	125	8.5	2.00
	49	F7	155	240	203	2800	80.0	101.3	5.00	39.2	204	532	339	197.5	306	57	125	8.5	2.00
	50	F8	155	240	203	2800	80.0	101.3	5.00	39.2	204	532	339	197.5	306	57	125	8.5	2.00
	51	F9	155	240	203	2800	80.0	101.3	5.00	39.2	204	532	339	197.5	306	57	125	8.5	2.00
	52	F10	155	240	203	2800	80.0	101.3	5.00	39.2	204	532	339	197.5	306	57	125	8.5	2.00
Rahimi &	53	A8*	200	150	120	2100	48.6	61.5	3.00	25.0	210	575	157	200	250	57	150	8.5	2.00
Hutchinson (2001)	54	A9*	200	150	120	2100	48.6	61.5	3.00	25.0	210	575	157	200	250	57	150	8.5	2.00
Luo (1993)	55	SP/S1/L	130	180	150	1000	35.1	43.9	3.60	34.2	210	444	402	-	-	-	-	8.5	2.00
	56	SP/S2/L	130	180	150	1000	35.1	43.9	3.60	34.2	210	444	402	-	-	-	-	8.5	2.00
	57	SP/S5/L	130	180	150	1000	35.1	43.9	3.60	34.2	210	444	402	-	-	-	-	8.5	2.00
	58	SP/S6/L	130	180	150	1000	35.1	43.9	3.60	34.2	210	444	402	-	-	-	-	8.5	2.00
	59	SP/S7/L	130	180	150	1000	35.1	43.9	3.60	34.2	210	444	402	-	-	-	-	8.5	2.00
	60	SP/S8/L	130	180	150	1000	35.1	43.9	3.60	34.2	210	444	402	-	-	-	-	8.5	2.00
	61	SP/S9/L	130	180	150	1000	35.1	43.9	3.60	34.2	210	444	402	-	-	-	-	8.5	2.00

Table 7.4c: Shear-bending interaction debonding test database-RC beam; internal tension and shear reinforcement; and adhesive details

Reference	S.No.	Specimen	b_1 (mm)	t_1 (mm)	d_e (mm)	l (mm)	f_c (MPa)	f_{cu} (MPa)	f_t (MPa)	E_1 (GPa)	E_s (GPa)	f_y (MPa)	A_s (mm^2)	E_{sv} (GPa)	f_{yv} (MPa)	A_{sv} (mm^2)	s_v (mm)	E_a (GPa)	t_a (mm)
Oehlers (1992)	62	1/2/S	130	175	147	-	42.0	52.5	3.20	22.0	210	444	402	210	568	25	500	8.5	2.00
	63	1/2/N	130	175	147	-	42.0	52.5	3.20	22.0	210	444	402	210	568	25	500	8.5	2.00
	64	1/3/S	130	175	147	-	42.0	52.5	3.20	22.0	210	444	402	210	568	25	500	8.5	2.00
	65	1/3/N	130	175	147	-	42.0	52.5	3.20	22.0	210	444	402	210	568	25	500	8.5	2.00
	66	2/1/N	130	175	147	-	45.6	57.0	4.30	29.0	210	444	402	210	568	25	500	8.5	2.00
	67	2/1/S	130	175	147	-	45.6	57.0	4.30	29.0	210	444	402	210	568	25	500	8.5	2.00
	68	2/2/N	130	175	147	-	45.6	57.0	4.30	29.0	210	444	402	210	568	25	75	8.5	2.00
	69	2/2/S	130	175	147	-	45.6	57.0	4.30	29.0	210	444	402	210	568	25	75	8.5	2.00
	70	2/3/N	130	175	147	-	45.6	57.0	4.30	29.0	210	444	402	210	511	57	75	8.5	2.00
	71	2/3/S	130	175	147	-	45.6	57.0	4.30	29.0	210	444	402	210	511	57	75	8.5	2.00
	72	2/4/N	130	175	147	-	45.6	57.0	4.30	29.0	210	444	402	210	511	57	45	8.5	2.00
	73	2/4/S	130	175	147	-	45.6	57.0	4.30	29.0	210	444	402	210	511	57	45	8.5	2.00
	74	5/1/N	130	175	147	-	47.2	59.0	4.70	29.0	210	444	402	210	511	57	45	8.5	2.00
	75	5/1/S	130	175	147	-	47.2	59.0	4.70	29.0	210	444	402	210	511	57	45	8.5	2.00
	76	6/1/-	130	175	147	-	50.4	63.0	4.30	30.0	210	444	402	210	568	25	875	8.5	2.00
	77	6/2/-	130	175	147	-	50.4	63.0	4.30	30.0	210	444	402	210	568	25	875	8.5	2.00
	78	6/3/-	130	175	147	-	50.4	63.0	4.30	30.0	210	444	402	210	568	25	1075	8.5	2.00
	79	6/4/-	130	175	147	-	50.4	63.0	4.30	30.0	210	444	402	210	568	25	1075	8.5	2.00
	80	7/1/N	130	175	147	-	47.2	59.0	4.60	32.0	210	444	402	210	568	25	1350	8.5	2.00
	81	7/1/S	130	175	147	-	47.2	59.0	4.60	32.0	210	444	402	210	568	25	1350	8.5	2.00
	82	8/1/N	130	175	147	-	37.6	47.0	3.90	27.0	210	444	402	210	568	25	1650	8.5	2.00
	83	8/1/S	130	175	147	-	37.6	47.0	3.90	27.0	210	444	402	210	568	25	1650	8.5	2.00
Oehlers & Moran (1990)	84	S7/N1	120	200	172	1650	28.0	35.0	3.10	33.0	210	444	402	210	511	57	50	8.5	2.00
	85	S7/N2	120	200	172	1650	28.0	35.0	3.10	33.0	210	444	402	210	511	57	50	8.5	2.00
	86	S7/N3	120	200	172	1650	27.2	34.0	3.20	28.0	210	444	402	210	511	57	50	8.5	2.00
	87	S7/N4	120	200	172	1650	27.2	34.0	3.20	28.0	210	444	402	210	511	57	50	8.5	2.00
	88	S8/N1	120	200	172	1650	29.6	37.0	3.00	37.0	210	444	402	210	511	57	50	8.5	2.00
	89	S8/N2	120	200	172	1650	29.6	37.0	3.00	37.0	210	444	402	210	511	57	50	8.5	2.00
	90	S8/N3	120	200	172	1650	28.0	35.0	2.70	24.0	210	444	402	210	511	57	50	8.5	2.00
	91	S8/N4	120	200	172	1650	28.0	35.0	2.70	24.0	210	444	402	210	511	57	50	8.5	2.00

Table 7.5a: Shear-bending interaction debonding test database-plate and loading details; debonding model- tests versus predictions

Reference	S.No.	Specimen	b_2 (mm)	t_2 (mm)	E_2 (GPa)	f_2 (GPa)	Type	l_1 (mm)	l_2 (mm)	Load	V_e (kN)	M_e (kNm)	P_e (kN)	V_p (kN)	P_p (kN)	V_{Oeh-1} (kN)	P_{Oeh} (kN)	V_{T-Y} (kN)	P_{T-Y} (kN)
Ritchie et al. (1991)	1	C	152	4.76	11.7	0.16	G-P	203	914	4PB	55.4	11.2	55.4	55.2	51.8	31.2	35.2	98.1	81.6
	2	D	151	4.76	11.7	0.16	G-P	203	914	4PB	59.6	12.1	59.6	55.1	51.8	31.2	35.2	98.4	81.8
	3	I	150	4.06	27.6	0.32	C/G-P	203	914	4PB	50.6	10.3	50.6	60.2	54.9	31.2	34.3	68.3	58.8
Beber et al. (1999)	4	VR5	120	0.44	230	3.40	C-W	75	783	4PB	51.1	3.8	51.1	44.4	43.6	19.6	22.2	39.6	38.9
	5	VR6	120	0.44	230	3.40	C-W	75	783	4PB	50.3	3.8	50.3	44.4	43.6	19.6	22.2	39.6	38.9
	6	VR7	120	0.77	230	3.40	C-W	75	783	4PB	62.1	4.7	62.1	52.0	50.4	19.6	22.0	36.8	36.0
	7	VR8	120	0.77	230	3.40	C-W	75	783	4PB	62.0	4.7	62.0	52.0	50.4	19.6	22.0	36.8	36.0
	8	VR9	120	1.10	230	3.40	C-W	75	783	4PB	64.8	4.9	64.8	58.7	55.9	19.6	21.8	36.3	35.5
	9	VR10	120	1.10	230	3.40	C-W	75	783	4PB	68.5	5.1	68.5	58.7	55.9	19.6	21.8	36.3	35.5
David et al. (1999)	10	P_2	100	1.20	150	2.40	C-P	200	933	4PB	68.0	13.6	68.0	65.6	61.9	33.5	36.0	56.9	53.6
	11	P_3	100	1.20	150	2.40	C-P	200	933	4PB	71.1	14.2	71.1	65.6	61.9	33.5	36.0	56.9	53.6
	12	P_4	100	2.40	150	2.40	C-P	200	933	4PB	78.0	15.6	78.0	80.2	71.2	33.5	34.3	54.7	50.6
	13	P_5	100	2.40	150	2.40	C-P	200	933	4PB	79.5	15.9	79.5	80.2	71.2	33.5	34.3	54.7	50.6
Hau KM (1999)	14	2	150	1.32	19.7	0.26	G-W	350	500	4PB	53.0	18.6	53.0	45.5	35.6	22.6	25.2	172.9	57.5
	15	4	150	1.32	19.7	0.26	G-W	200	500	4PB	65.4	13.1	65.4	45.7	41.6	22.7	26.0	175.9	91.6
	16	6	150	1.32	19.7	0.26	G-W	200	500	4PB	63.1	12.6	63.1	46.6	42.3	23.5	26.8	189.5	94.9
	17	7	150	1.32	19.7	0.26	G-W	350	500	4PB	53.9	18.9	53.9	46.0	36.0	23.0	25.7	181.0	58.5
Nguyen et al. (2001)	18	A950	80	1.20	181	3.14	C-P	190	440	4PB	28.1	5.3	28.1	43.9	28.7	14.5	12.5	24.4	19.5
	19	A1100	80	1.20	181	3.14	C-P	115	440	4PB	28.7	3.3	28.7	43.9	36.0	14.5	14.0	24.7	22.4
	20	A1150	80	1.20	181	3.14	C-P	90	440	4PB	29.5	2.7	29.5	43.9	38.5	14.5	14.5	25.0	23.5
	21	B2	80	1.20	181	3.14	C-P	115	440	4PB	65.1	7.5	65.1	53.2	50.9	22.4	22.2	37.6	36.3
Sadatmanesh & Ehsani (1991)	22	B	152	6.00	37.2	0.40	G-P	155	1983	4PB	125.0	19.4	125.0	135.1	134.2	74.4	84.2	132.5	131.4
Taljsten (1999)	23	SB1	120	1.40	155	2.40	C-P	150	1300	4PB	71.4	10.7	71.4	100.5	96.1	47.6	51.8	93.9	89.1
	24	SB2	120	1.40	155	2.40	C-P	200	1300	4PB	75.5	15.1	75.5	100.8	93.3	47.9	50.8	94.7	86.4
	25	SB3	120	1.40	155	2.40	C-P	300	1300	4PB	73.9	22.2	73.9	100.8	85.9	47.9	48.6	94.7	78.6
	26	MB1	120	1.40	210	2.00	C-P	150	1300	4PB	79.6	11.9	79.6	99.2	94.4	49.1	52.6	91.0	86.0
	27	HB1	100	1.40	300	1.40	C-P	150	1300	3PB	80.1	12.0	80.1	92.3	87.7	49.1	51.1	85.6	80.7
	28	FB1	150	2.40	95	1.80	C-W	150	1300	3PB	74.4	11.2	74.4	110.9	104.6	47.6	51.9	90.1	85.6
Ahmed & van	29	AF3	75	0.33	240	3.50	C-W	100	500	3PB	50.2	5.0	50.2	36.9	34.7	18.2	20.2	50.4	44.4
Gemert (1999b)	30	CF2-1	75	0.33	240	3.50	C-W	100	500	4PB	48.3	4.8	48.3	38.7	37.2	19.7	22.0	53.3	49.0
	31	CF3-1	75	0.33	240	3.50	C-W	100	500	4PB	52.4	5.2	52.4	39.9	38.8	20.8	23.2	55.5	52.0
	32	CF4-1	75	0.33	240	3.50	C-W	100	500	4PB	59.1	5.9	59.1	42.5	41.9	23.1	25.9	59.1	57.0

Note: V_e & M_e = measured debonding strength; V_p; V_{Oeh-1}; & V_{T-Y} = prediction from Eqs 7.11; 7.6; & 7.10 respectively; P_p; P_{Oeh}; & P_{T-Y} = calculated load from Eqs 7.16; 7.13; & 7.15 respectively

Table 7.5b: Shear-bending interaction debonding test database-plate and loading details; debonding model- tests versus predictions

Reference	S.No.	Specimen	b_2 (mm)	t_2 (mm)	E_2 (GPa)	f_2 (GPa)	Type	l_1 (mm)	l_2 (mm)	Load	V_e (kN)	M_e (kNm)	P_e (kN)	V_p (kN)	P_p (kN)	V_{Oeh-1} (kN)	P_{Oeh} (kN)	V_{T-Y} (kN)	P_{T-Y} (kN)
Smith & Teng (2003)	33	6B	145	0.33	257	4.52	C-W	75	500	4PB	60.2	4.5	60.2	57.2	55.4	24.4	27.6	82.8	76.7
	34	2B	148	0.33	271	3.72	C-W	125	500	4PB	57.6	7.2	57.6	57.0	52.6	25.8	28.9	86.8	70.7
	35	3A	147	0.33	257	4.52	C-W	175	500	4PB	53.3	9.3	53.3	58.4	50.1	25.2	27.6	86.3	61.6
	36	1A	150	0.33	271	3.72	C-W	250	500	4PB	39.8	10.0	39.8	53.4	41.4	22.6	23.6	70.5	44.6
	37	2A	148	0.33	271	3.72	C-W	375	500	4PB	32.1	12.0	32.1	57.0	35.5	25.8	26.6	86.8	36.8
Aprile & Feo (2007)	38	SB4/02/0.85	50	1.40	300	1.45	C-P	150	696	UDL	46.3	7.5	108.8	49.6	114.4	31.9	72.5	36.7	84.4
	39	SB4/03/0.75	50	1.40	300	1.45	C-P	250	696	UDL	39.3	11.5	104.8	49.6	124.3	31.9	72.2	36.7	91.3
	40	SB4/04/0.65	50	1.40	300	1.45	C-P	350	696	UDL	37.9	16.8	116.5	49.6	133.4	31.9	72.8	36.7	97.3
Ceroni et al.(2001)	41	A2	110	0.17	230	3.43	C-P	150	750	4PB	9.3	1.4	9.3	19.2	15.6	10.2	10.1	15.6	13.1
	42	A3	110	0.17	230	3.43	C-P	300	750	4PB	9.6	2.9	9.6	19.2	11.0	10.2	8.8	15.6	9.6
	43	C2	80	0.17	230	3.43	C-P	400	750	4PB	9.0	3.6	9.0	17.5	12.4	10.3	10.0	15.5	11.2
	44	C3	80	0.17	230	3.43	C-P	500	750	4PB	8.1	4.0	8.1	17.5	10.9	10.3	9.5	15.5	9.9
Pornpongsaroj &	45	A-420-P3	100	1.20	150	2.20	C-P	420	1000	3PB	47.8	20.1	95.6	61.9	105.4	30.3	56.4	45.4	79.7
Pimanmas (2003)	46	B-200-P4	100	1.20	150	2.20	C-P	200	700	4PB	52.8	10.6	52.8	61.9	60.1	30.3	31.6	51.7	50.1
Fanning & kelly (2001)	47	F5	120	1.20	155	2.40	C-P	385	1100	4PB	50.0	19.3	50.0	74.1	58.8	38.9	38.2	65.8	51.3
	48	F6	120	1.20	155	2.40	C-P	385	1100	4PB	51.5	19.8	51.5	74.1	58.8	38.9	38.2	65.8	51.3
	49	F7	120	1.20	155	2.40	C-P	462	1100	4PB	48.8	22.5	48.8	74.1	54.5	38.9	37.0	65.6	47.3
	50	F8	120	1.20	155	2.40	C-P	462	1100	4PB	32.0	14.8	32.0	74.1	54.5	38.9	37.0	65.6	47.3
	51	F9	120	1.20	155	2.40	C-P	550	1100	4PB	31.0	17.1	31.0	74.1	49.9	38.9	35.7	64.6	42.9
	52	F10	120	1.20	155	2.40	C-P	550	1100	4PB	41.0	22.6	41.0	74.1	49.9	38.9	35.7	64.6	42.9
Rahimi &	53	A8*	150	0.80	127	1.53	C-P	85	750	4PB	32.6	2.8	32.6	42.8	40.0	22.0	23.1	41.2	37.8
Hutchinson (2001)	54	A9*	150	0.80	127	1.53	C-P	85	750	4PB	32.0	2.7	32.0	42.8	40.0	22.0	23.1	41.2	37.8
Luo (1993)	55	SP/S1/L	130	5.00	210	0.32	S	150	500	3PB	33.4	5.0	66.8	45.0	81.9	23.2	40.4	42.3	75.4
	56	SP/S2/L	130	5.00	210	0.32	S	150	500	3PB	26.4	4.0	52.8	45.0	81.9	23.2	40.4	42.3	75.4
	57	SP/S5/L	130	5.00	210	0.32	S	70	500	3PB	27.9	2.0	55.8	45.0	88.1	23.2	46.8	43.8	85.1
	58	SP/S6/L	130	5.00	210	0.32	S	70	500	3PB	33.1	2.3	66.2	45.0	88.1	23.2	46.8	43.8	85.1
	59	SP/S7/L	130	5.00	210	0.32	S	70	500	3PB	33.0	2.3	66.0	45.0	88.1	23.2	46.8	43.8	85.1
	60	SP/S8/L	130	5.00	210	0.32	S	70	500	3PB	33.0	2.3	66.0	45.0	88.1	23.2	46.8	43.8	85.1
	61	SP/S9/L	130	5.00	210	0.32	S	70	500	3PB	31.5	2.2	63.0	45.0	88.1	23.2	46.8	43.8	85.1

Note: V_e & M_e = measured debonding strength; V_p; V_{Oeh-1}; & V_{T-Y} = prediction from Eqs 7.11; 7.6; & 7.10 respectively; P_p; P_{Oeh}; & P_{T-Y} = calculated load from Eqs 7.16; 7.13; & 7.15 respectively

Table 7.5c: Shear-bending interaction debonding test database-plate and loading details; debonding model- tests versus predictions

Reference	S.No.	Specimen	b_2 (mm)	t_2 (mm)	E_2 (GPa)	f_2 (GPa)	Type	l_1 (mm)	l_2 (mm)	Load	V_e (kN)	M_e (kNm)	P_e (kN)	V_p (kN)	P_p (kN)	V_{Oeh-1} (kN)	P_{Oeh} (kN)	V_{T-Y} (kN)	P_{T-Y} (kN)
Oehlers (1992)	62	1/2/S	130	5.00	210	0.27	S	100	550	4PB	29.6	3.0	29.6	44.6	43.1	24.3	20.9	48.0	44.8
	63	1/2/N	130	5.00	210	0.27	S	150	550	4PB	32.5	4.9	32.5	44.6	41.4	24.3	18.5	47.1	41.0
	64	1/3/S	130	5.00	210	0.27	S	250	550	4PB	25.8	6.5	25.8	44.6	37.2	24.3	14.9	45.0	33.4
	65	1/3/N	130	5.00	210	0.27	S	400	550	4PB	23.1	9.2	23.1	44.6	30.6	24.3	11.6	44.8	25.5
	66	2/1/N	130	5.00	210	0.27	S	300	550	4PB	26.1	7.8	26.1	45.4	35.1	25.0	16.8	46.6	31.5
	67	2/1/S	130	5.00	210	0.27	S	75	550	4PB	40.1	3.0	40.1	45.4	44.4	25.0	24.7	50.2	48.2
	68	2/2/N	130	5.00	210	0.27	S	300	550	4PB	24.9	7.5	24.9	47.0	35.9	25.0	16.8	46.8	31.6
	69	2/2/S	130	5.00	210	0.27	S	75	550	4PB	42.5	3.2	42.5	47.0	46.0	25.0	24.7	50.5	48.5
	70	2/3/N	130	5.00	210	0.27	S	300	550	4PB	27.9	8.4	27.9	49.0	36.7	25.0	16.8	47.2	31.7
	71	2/3/S	130	5.00	210	0.27	S	75	550	4PB	39.3	2.9	39.3	49.0	47.8	25.0	24.7	50.9	48.8
	72	2/4/N	130	5.00	210	0.27	S	300	550	4PB	32.2	9.7	32.2	51.3	37.7	25.0	16.8	47.7	31.9
	73	2/4/S	130	5.00	210	0.27	S	75	550	4PB	41.3	3.1	41.3	51.3	50.0	25.0	24.7	51.4	49.2
	74	5/1/N	130	5.00	210	0.27	S	400	550	4PB	24.0	9.6	24.0	51.7	32.6	25.3	15.5	49.2	27.1
	75	5/1/S	130	5.00	210	0.27	S	150	550	4PB	37.3	5.6	37.3	51.7	47.0	25.3	22.1	51.7	44.4
	76	6/1/-	130	5.00	210	0.27	S	625	925	4PB	19.3	12.1	19.3	46.2	23.6	25.9	11.8	40.1	18.6
	77	6/2/-	130	5.00	210	0.27	S	625	925	4PB	20.8	13.0	20.8	46.2	23.6	25.9	11.8	40.1	18.6
	78	6/3/-	130	5.00	210	0.27	S	825	1125	4PB	15.1	12.5	15.1	46.2	19.0	25.9	9.9	37.4	14.7
	79	6/4/-	130	5.00	210	0.27	S	825	1125	4PB	15.9	13.1	15.9	46.2	19.0	25.9	9.9	37.4	14.7
	80	7/1/N	130	5.00	210	0.27	S	1000	1400	4PB	10.3	10.3	10.3	45.5	15.5	25.3	9.2	33.6	12.1
	81	7/1/S	130	5.00	210	0.27	S	1000	1400	4PB	11.0	11.0	11.0	45.5	15.5	25.3	9.2	33.6	12.1
	82	8/1/N	130	5.00	210	0.27	S	1300	1700	4PB	9.7	12.5	9.7	43.3	11.6	23.4	6.2	28.5	8.9
	83	8/1/S	130	5.00	210	0.27	S	1300	1700	4PB	9.5	12.4	9.5	43.3	11.6	23.4	6.2	28.5	8.9
Oehlers &	84	S7/N1	120	5.00	210	0.21	S	468	825	4PB	35.9	16.8	35.9	45.0	29.1	22.2	13.0	32.2	22.2
Moran (1990)	85	S7/N2	120	5.00	210	0.21	S	375	825	4PB	46.9	17.6	46.9	45.0	32.6	22.2	14.4	33.0	25.0
	86	S7/N3	120	5.00	210	0.21	S	225	825	4PB	68.4	15.4	68.4	44.7	39.0	21.9	17.1	36.0	31.2
	87	S7/N4	120	5.00	210	0.21	S	125	825	4PB	82.4	10.3	82.4	44.7	42.7	21.9	20.1	37.1	35.2
	88	S8/N1	120	5.00	210	0.21	S	468	825	4PB	38.5	18.0	38.5	45.4	29.1	22.6	13.2	32.3	22.5
	89	S8/N2	120	5.00	210	0.21	S	375	825	4PB	55.2	20.7	55.2	45.4	32.7	22.6	14.7	33.0	25.2
	90	S8/N3	120	5.00	210	0.21	S	225	825	4PB	59.6	13.4	59.6	45.0	39.3	22.2	15.7	36.2	31.3
	91	S8/N4	120	5.00	210	0.21	S	125	825	4PB	90.4	11.3	90.4	45.0	42.9	22.2	19.0	37.2	35.3

Note: V_e & M_e = measured debonding strength; V_p; V_{Oeh-1}; & V_{T-Y} = prediction from Eqs 7.11; 7.6; & 7.10 respectively; P_p; P_{Oeh}; & P_{T-Y} = calculated load from Eqs 7.16; 7.13; & 7.15 respectively

7.4.4 Comparison of shear-bending interaction debonding strength models

The existing shear-bending interaction debonding strength models of Oehlers' (1992) and Teng and Yao's (2007) are compared with the proposed new interaction model, and all these models are assessed by the 91 test data shown in Figures 7.3a-c and Tables 7.6a-b. The interaction curve is plotted from the shear-bending interaction models discussed earlier. The ratio of test-to-predicted debonding shear force V_e/V_p is plotted against the corresponding bending moment ratio M_e/M_p for each interaction model as shown in Figures 7.3a-c. There are 68 test data on the vertical axis from the pure shear region and 67 test results on the horizontal axis from the pure bending region, which represent the two extreme boundary conditions to the interaction model. The remaining 91 data points in the shear-bending interaction region are shown scattered above and below the ideal interaction curve from respective interaction models. Note that these 91 data points have not been used in developing the interaction model. A large scatter for these data is evident. One possible explanation for this large scatter may be that not all the test beams failed in PED although they were reported so because it is not possible to identify whether the failure is due to PED or ICD after failure and both failure are and thus difficult to observe during the failure process.

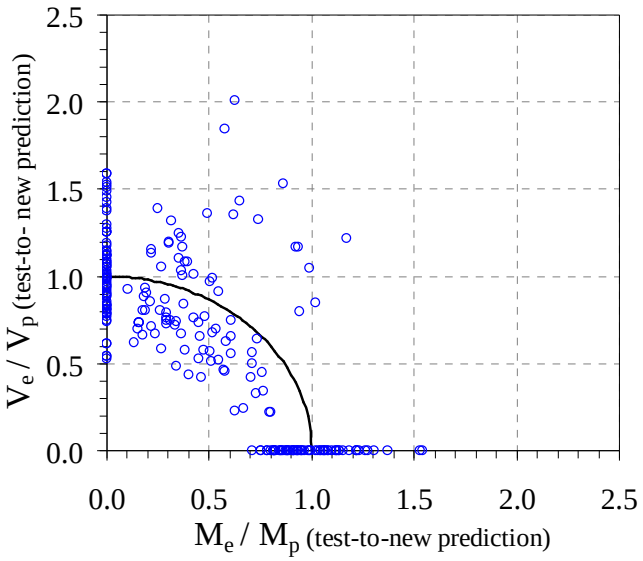

(a) Proposed interaction model

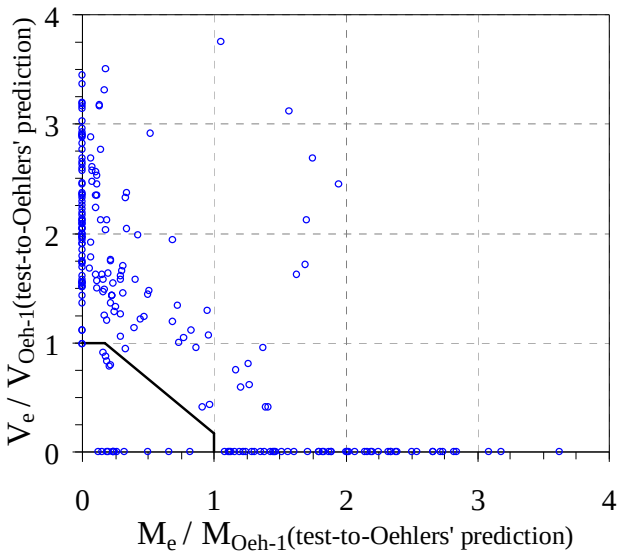

(b) Oehlers' (1992) interaction model

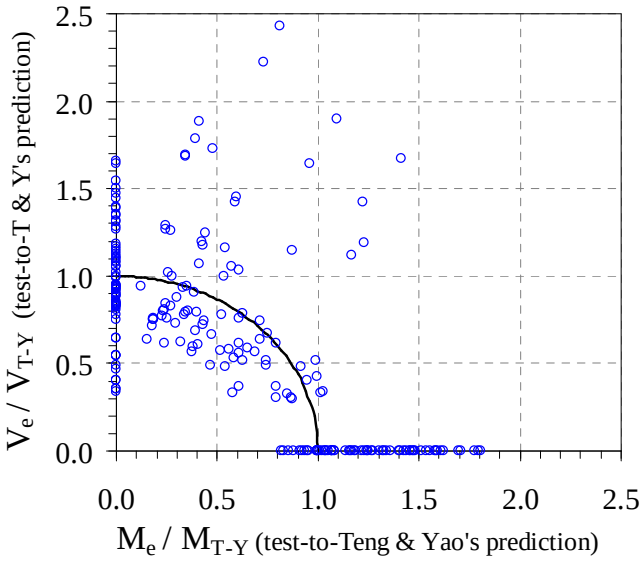

(c) Teng and Yao's (2007) interaction model

Figure 7.3. Shear-bending interaction debonding models: tests versus predictions

In order to further understand the performance of these interaction models quantitatively, the applied transverse load P_e corresponding to V_e and M_e is calculated knowing the type of applied load in the test database. The transverse load P (P_p from proposed new interaction model; P_{Oeh} from Oehlers's interaction model; and P_{T-Y} from Teng and Yao's interaction model) is predicted from the respective interaction models after expressing the shear force V and bending moment M in numerators of the respective interaction models in terms of P and substituting the predicted values of V and M appearing in denominators of respective interaction models from the respective shear and flexural debonding models. The transverse load corresponding to plate end

debonding failure obtained from test results P_e is compared with that calculated from the respective interaction models (P_p or P_{Oeh} or $P_{T\text{-}Y}$) in Figures 7.4a-c. It can be ascertained from the dispersion of the data points in Figures 7.3 and 7.4 that the predictions from the proposed new interaction model are much closer to the test results followed by Teng and Yao's (2007) and Oehlers' (1992). This is also evidenced from the statistical performances of these three models under assessment given in Tables 7.6a-b in terms of the test-to-predicted debonding load ratios.

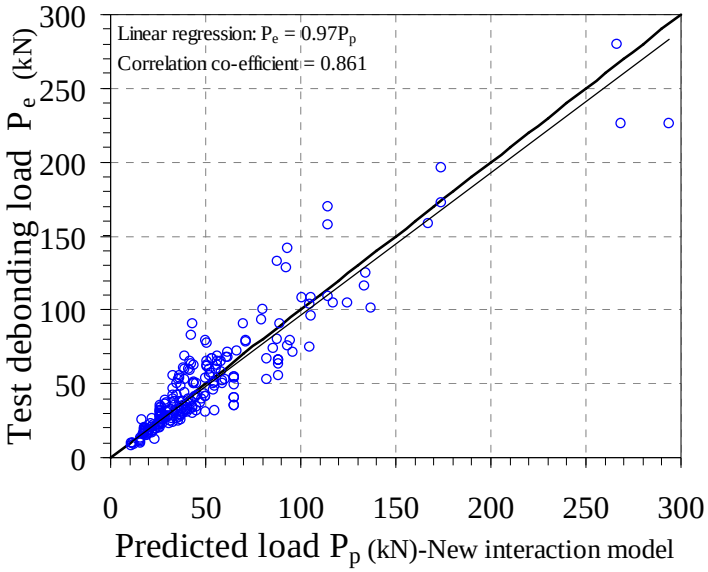

(a) Proposed interaction model

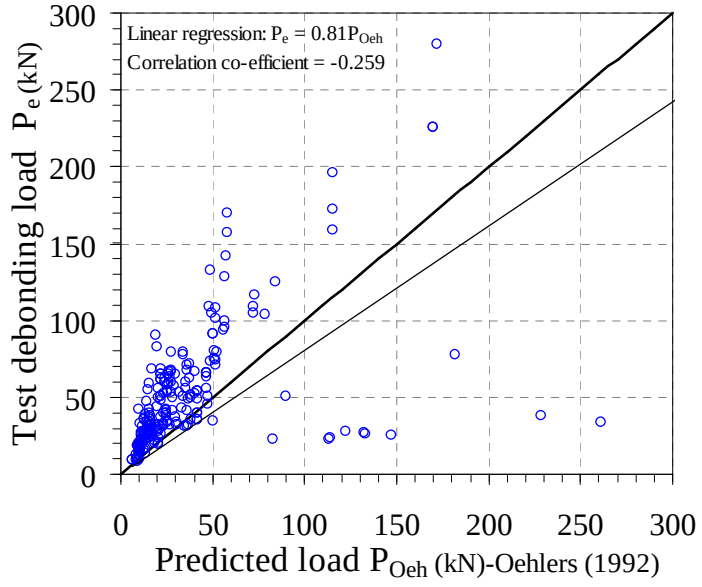

(b) Oehlers' (1992) interaction model

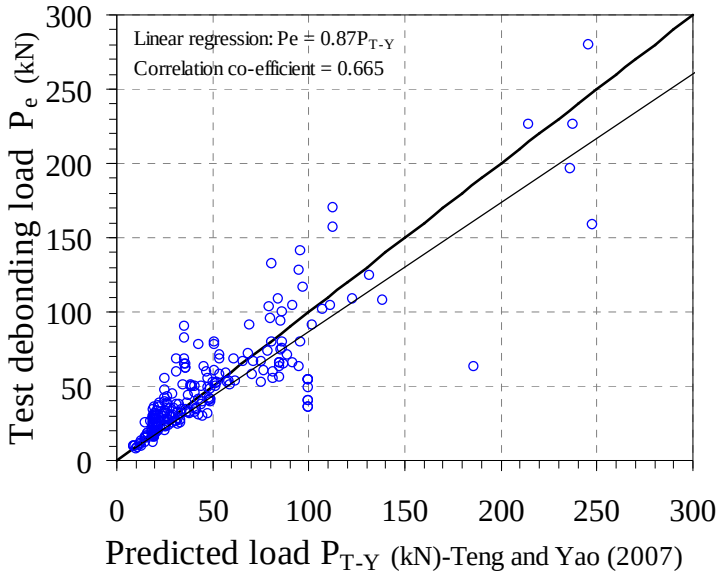

(c) Teng and Yao's (2007) interaction model

Figure 7.4. Shear-bending interaction debonding models: tests versus predictions.

Table 7.6a: Shear-bending interaction model- test-to-predicted debonding strength ratios

Model	Average	Coefficient of variation	Maximum	Minimum
Proposed model: (P_e/P_p)	1.005	0.261	2.105	0.530
Oehlers (1992): (P_e/P_{Oeh})	1.748	0.420	4.749	0.103
Teng & Yao (2007): (P_e/P_{T-Y})	1.099	0.330	2.560	0.338

Table 7.6b: Shear-bending interaction model-natural logarithm of test-to-predicted debonding strength ratios

Model	Average	Standard deviation	Maximum	Minimum
Proposed model: $\ln(P_e/P_p)$	-0.027	0.247	0.745	-0.636
Oehlers (1992): $\ln(P_e/P_{Oeh})$	0.437	0.584	1.558	-2.275
Teng & Yao (2007): $\ln(P_e/P_{T-Y})$	0.041	0.333	0.940	-1.085

The statistical performance of the natural logarithm of test-to-predicted debonding load ratios of the three interaction models are provided in Table 7.6b. Ideally, the average, maximum and minimum should be nearer to zero; and the standard deviation should be less for any good debonding model. The positive and negative sign in average, maximum and minimum can be considered as a representation of the extent of conservative and unconservative predictions respectively. Based on the above comparisons, it is found that the proposed interaction model offers good accuracy with

reasonable conservatism than the existing models and is easy to incorporate in any design codes.

7.5 Conclusions

FRP or steel plated RC beams are vulnerable to different types of premature plate end debonding failures. This chapter has presented a predictive debonding strength model for such failures which has advantages of accuracy and ease of application when compared with those of alternatives previously proposed by others. A large test database of plated RC beams reported to have failed by plate end debonding with 226 test results (including 67 flexural debonding tests; 68 shear debonding tests; and 91 tests for shear-bending interaction) collected from many existing experimental studies was used to assess the performance of existing and the proposed debonding strength models. The proposed shear debonding model for plates terminated in high shear-zero (or low) moment region is simple, accurate and provides an explicit prediction when compared against the existing models. This model considers the contribution from concrete, internal shear reinforcement and the bonded plate to the debonding strength. This model and an accurate flexural debonding model of Narayanamurthy et al. (2011) for plates terminated in pure bending region are shown to be the two extreme cases and any general case is an interaction of these two extremes whose coupling resulted in an accurate shear-bending interaction model applicable for plates terminated in any shear-bending interaction region. Comparisons between test results and the predictions of the debonding strength models demonstrated the simplicity and the accuracy of the proposed models that can easily be incorporated in any design codes and guidelines.

7.6 Notation

The following symbols are used in this chapter:

A = cross-sectional area;

b = width;

CoV = coefficient of variation;

d_e = effective depth of RC beam;

E = modulus of elasticity;

$(EI)_{c,p}$, $(EI)_{c,0}$ = flexural rigidity of the cracked and tensile reinforced plated and un-plated beam section respectively;

f_2 = tensile yield strength of steel or tensile strength of FRP plate;

f_c = cylinder compressive strength of concrete;

f_{cu} = cubic compressive strength of concrete;

f_t = tensile strength of concrete;

f_{yv} = yield strength of steel shear reinforcement;

4PB;3PB;UDL = 4 point bending; 3 point bending; and uniformly distributed load respectively;

G_f = mode-II interfacial fracture energy;

I = second moment of area;

l = effective span of the plated beam;

l_1 = distance from nearest support to the plate end;

l_2 = distance from nearest support to applied load P (shear span);

M (0) = bending moment at the plate end;

M = debonding moment;

p-1, p-2, p-3 = subscripts referring to the predictions from flexural debonding models 1, 2 and 3 respectively;

p; Oeh; Oeh-1; Oeh-2; Oeh-3;S-T; T-Y = subscripts referring to the predictions from proposed; Oehlers and Moran's (1990); Oehlers' (1992); Oehlers et al.'s (2004); Oehlers et al.'s (2005); Smith and Teng's (2002) and Teng and Yao's (2007) models respectively;

e = subscript referring to the experimental value from test database;

$M_{y,0}$ = theoretical first yield moment of the un-plated beam section;

$M_{u,0}$ = theoretical moment capacity of the un-plated beam section;

m_p = modular ratio of plate to beam;

P = transverse load on beam;

t = thickness;

V = debonding shear force;

V_{uc} = shear capacity of an unplated RC beam without stirrups from any design codes;

$V_{u,0}$ = shear capacity of a prestressed and unplated RC beam without stirrups from any design codes;

V_{st} = contribution of stirrups to the debonding shear strength;

y_1, y_2 = vertical distance from bottom of the beam and top of the plate to their respective centroids;

α = axial stiffness ratio between plate and original beam including steel tension reinforcement;

α_w, α_a, α_f = width ratio, and axial and flexural rigidity ratio respectively;

β_w = width ratio parameter ;

δ_f = maximum slip at initiation of debonding;

λ, m = parameters defined in Eqs 1b-c;

ρ = reinforcement ratio;

$\varepsilon_{v,e}$ = effective strain in vertical stirrups;

1; *a*; 2; s; sv = subscripts referring respectively to the beam; adhesive; plate; tension steel reinforcement; and steel shear reinforcement.

Chapter 8

Theoretical Formulation and Parametric Study of Intermediate Crack-Induced Debonding in Plated Beams

Abstract

Adhesively bonding FRP plate at the tension face of an RC beam can often significantly increase its strength. The behaviour of such a strengthened structure depends on the performance of the FRP-concrete interface in providing an effective stress transfer between the adherends. Debonding along this interface can lead to various premature failures. One of the common failure modes is the intermediate crack-induced debonding (ICD) which initiates at a major flexural or flexural-shear crack and propagates along the interface towards one of the plate ends. Correct modelling of the FRP-concrete interface bond behaviour is very important for understanding and mitigating these debonding failures. This bond behaviour has been extensively studied using a simple pull-off test specimen. However, the ICD behaviour of the interface between intermediate adjacent cracks in a plated beam is significantly different from that in a pull-off test.

This study is focussed on the ICD of the FRP-concrete interface between two adjacent cracks in a plated beam considering axial forces, transverse shear forces and bending moments in the adherends of the bonded joint using a softening bond-slip law. The interface deformation is related to the applied loading through two methods: the rotational spring method and the section analysis with partial interaction method and the merits and extent of their applicability are discussed. Theoretical formulation for interfacial shear stress, interfacial slip, plate stress and load-displacement response are

provided for different states of interfaces experienced by the FRP-concrete interface during different failure processes and the ductility and the ultimate ICD strength of the plated beam are predicted. A parametric study is further conducted to demonstrate the significant effect of bond length, moment ratio between two cracked ends, axial plate stiffness, beam depth and width, steel ratio and bending deformation on the load-displacement characteristics of the bonded joint.

8.1 Introduction

Adhesive bonding of FRP (or steel) plates on the tension face of an RC beam has gained wide acceptance and popularity in recent years as a viable strengthening and retrofitting technique. In this strengthening method, the stress transfer from the original beam to the external plate occurs through the adhesive interface and its performance is very important in maintaining the composite action between the bonded plate and the original beam. Experimental study (Teng et al., 2002; Yuan et al., 2004) has shown that the relative deformation (slip) between the FRP and concrete occurs within a very narrow transition zone consisting of a thin layer of adhesive and the adjacent concrete. Interfacial debonding along the FRP-concrete interface can lead to premature failure of the structure. Therefore, correct modelling of the FRP-concrete interface is very important for understanding and mitigating these debonding failures and to predict the ductility and ultimate behaviour of the plated beam.

Two types of debonding failures are commonly observed in experiments (Teng et al., 2002, 2003a, b). They are the plate end debonding (PED) and intermediate crack-induced interfacial debonding (ICD). PED is caused by the concentration of high interfacial stresses due to the presence of geometric discontinuity at the plate end and this interfacial stress and PED has been extensively studied in the literature (Narayanamurthy et al., 2010, 2011; Teng and Chen, 2009). ICD involves debonding of the plate which initiates at a major flexural or flexural-shear crack where the plate is under tension, and propagates along the FRP-concrete interface towards the stress-free end of the plate (type-1) or to an adjacent intermediate crack (type-2).

In type-1 (single crack), no crack exists between the free end of the plate and the crack where debonding initiates. This type is similar to the ICD arising from a shear crack in RC beams shear strengthened with bonded side plates and debonding in soffit plated beams having a single dominant flexural or flexural-shear crack. The stress state of the interface in type-1 ICD is similar to that in a simple pull-off test (single shear) specimen in which a plate is bonded to a concrete prism and pulled at one end and has been studied extensively by many researchers (e.g. Roberts, 1989; Taljsten, 1997; Brosens and Gamert, 1998; Chen and Teng, 2001; Teng et al., 2002, 2003a, b). Wu et al., (1997) conducted an experimental and numerical investigation. Yuan et al. (2001) developed a fracture mechanics based model and Sebastian (2001) recommended using a bond-slip

analysis based on experimental observations on type-1 ICD. Leung (2001), Neubauer and Rostasy (1999), Rabinovitch and Frostig (2001) and Lau et al. (2001) carried out a linear elastic bond slip analysis to study a cracked concrete beam flexurally strengthened with FRP. However, experimental studies have shown that the stress deformation relationship at the FRP-concrete interface is nonlinear (Chajes et al., 1995, 1996; Bizindavyi and Neale, 1999; Dai et al., 2005; Yao et al., 2005a, b) and suggested using a nonlinear bond-slip model to analyse this ICD. The bond-slip model relating the relative deformation at the FRP-concrete interface is essentially a cohesive zone model (CZM) where the locally damaged materials forming a narrow band of localised deformation in a large fracture processing zone (cohesive zone) is modelled by a nonlinear spring (Wang, 2006a). Using a bilinear bond-slip model, Yuan et al. (2004) developed formulations for the interfacial shear stress and plate stress and Lu et al. (2005a, b) carried out a numerical and experimental investigation on simple pull-off test specimens; and Wang (2006a, b) developed formulations for bond stress and plate stress considering bending moments and shear forces additionally and used a rotational spring method to model the local flexibility at the crack. Thereafter, Pan and Leung (2007), Wang (2007), Rabinovitch (2008a), Wang and Zhang (2008) further investigated this debonding mode by considering the interfacial normal stresses along with the interface separation on the FRP-concrete interface. Rabinovitch (2008b) compared the LEFM and CZM and highlighted their advantages, limitations and applicability for type-1 ICD process.

In type-2 ICD (multi crack), one or more significant cracks exists between the debonding initiation crack and the stress free plate end. The mechanics of debonding process in type-2 ICD is different from that of a simple pull-off test discussed above due to the interaction of the adjacent intermediate crack and only very few studies exist in the literature on this type of debonding (Teng and Chen, 2009). Teng et al. (2006) and Chen et al. (2007) conducted a theoretical investigation on different states of interface during different failure processes identified by them on the type-2 ICD through an FRP-to-concrete bonded joint model where the plate and concrete substrate are under axial forces at both ends. Chen et al. (2007) have demonstrated that neglecting the linear ascending branch representing the elastic deformation of the interface has an insignificant effect on the overall load-displacement response and the ultimate behaviour of the bonded joint, and provided a simplified solution. Recently, Chen and Qiao (2009) extended the type-1 ICD analysis of Wang (2006a, b) for type-2 ICD and

provided a solution applicable for one specific type of failure process identified in Chen et al. (2007). In ICD, the interface is dominated by shear stresses. It therefore differs from PED, where normal stresses perpendicular to the adhesive interface also play a significant role.

This study focuses on type-2 ICD in RC beams strengthened with an FRP plate using a thin adhesive layer. It extends Chen et al.'s (2007) study by utilising a more realistic bonded joint model considering bending moments, transverse shear forces and axial forces in the adherends. Closed-form solutions for the interfacial shear stress, interfacial slip and axial stress in the plate are obtained using a linearly softening bond-slip model for the different states experienced by the FRP-concrete interface during all the different failure processes. Crack initiation, propagation and complete debonding of FRP-concrete interface and load-displacement characteristics are analysed. This study employs two methods, namely the rotational spring method (RSM) and section analysis with partial interaction method (SA-PI), to relate the applied loading to the interface deformation during the debonding process. This requirement arises from the inclusion of bending moments and shear forces in the bonded joint model. Results of the present solution based on RSM and SA-PI are compared with Chen et al. (2007) after matching the end conditions. The load-displacement response and distribution of bond and plate stresses are provided through a typical illustration. A parametric study is conducted to analyse the effect of bond length, moment ratio at the two adjacent cracks, axial plate stiffness, beam depth and width, embedded steel ratio and bending deformation on the ICD behaviour of plated RC beams. This research represents a significant advance in understanding the behaviour of type-2 IC debonding failure, predicting the ductility and ultimate strength of plated beams and quantifying the influence of key parameters. It highlights for the first time the effect of bending deformation on IC debonding behaviour in plated beams.

8.2 Bonded Joint Model

Consider an FRP plated RC beam as shown in Figure 8.1. Note that a simply supported beam is shown as an example but the analysis presented in this paper is concerned with the behaviour between two intermediate cracks so it is generic and applicable to RC beams under any loading with any boundary conditions. Let L be the length of the

concerned segment between two intermediate cracks. The plated beam segment between these two cracks is idealised as a bonded joint which is subjected to axial forces $N_T(x)$, transverse shear forces $V_T(x)$ and bending moments $M_T(x)$ in the adherends on both sides. Consequently, both adherends are subjected to axial forces $N(x)$, transverse shear forces $V(x)$ and bending moments $M(x)$ as shown in Figure 8.2. The relationship between the total forces on the beam section and the forces on the adherends will be discussed later in the chapter. It is assumed that the sectional properties of the original beam between the two adjacent cracks remain constant. Let u and v be the horizontal and vertical displacements of the adherends respectively.

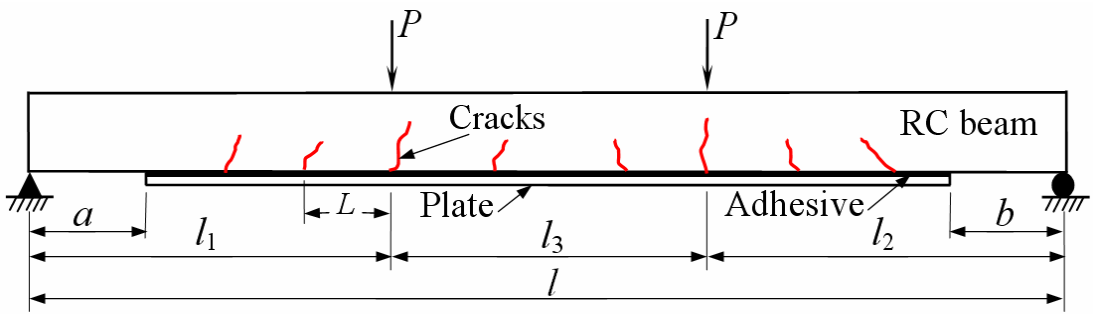

Figure 8.1. Plated beam

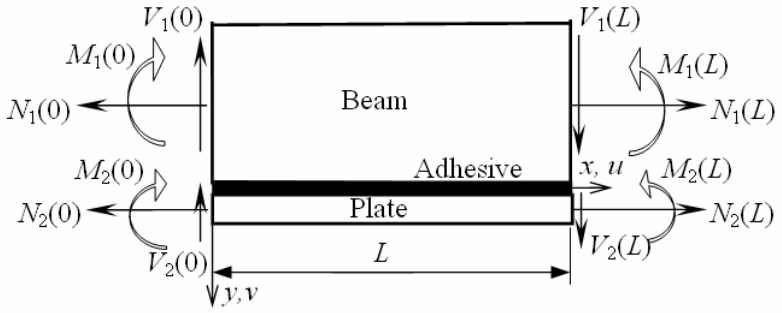

Figure 8.2. Bonded joint model between two adjacent cracks

Linear material behaviour is considered for the beam and plate only during initial derivation of formulation. A cracked RC beam section is considered when relating the applied loading to plate forces in SA-PI. It is assumed that interface deformations are dominated by Mode II. The thin adhesive layer is assumed to be uniform, have negligible bending and shear stiffnesses and the bond stress is constant through its thickness as in Teng et al. (2006) and Chen et al. (2007). The curvatures of the adherends are assumed to be the same in relating the bending moments of the

adherends. Fully composite action is assumed to exist at the FRP-concrete interface before local debonding is experienced.

The term "ultimate load" is used in this study to refer to the maximum loading capacity of the bonded joint instead of "bond strength" to avoid confusion with the local bond strength of the FRP-concrete interface (maximum shear stress in a bond-slip curve).

8.3 Governing Equations

The equilibrium, constitutive relations and the interface compatibility requirements for the differential segment of the plated beam between two adjacent cracks as shown in Figure 8.3 are necessary to derive the governing differential equations to analyse the initiation and propagation of debonding in the bonded joint. Let *t*, *b*, *E*, *A*, *I* represent the thickness, breadth, elastic modulus, cross-sectional area and second moment of area of the adherends respectively and subscripts 1 and 2 respectively refer to beam and plate. Longitudinal, vertical and moment equilibrium gives

$$\frac{dN_i(x)}{dx} = (-1)^i b_2 \tau(x) \qquad ; i = 1, 2 \tag{8.1}$$

$$\frac{dV_i(x)}{dx} = (-1)^i b_2 \sigma(x) \qquad ; i = 1, 2 \tag{8.2}$$

$$\frac{dM_i(x)}{dx} = V_i(x) - b_2 y_i \tau(x) \qquad ; i = 1, 2 \tag{8.3}$$

where $N_i(x)$, $V_i(x)$ and $M_i(x)$ are respectively axial force, transverse shear force and bending moment at any section of the adherend in the bonded joint; $\tau(x)$ and $\sigma(x)$ are respectively the interfacial shear and normal stresses in the bond; and y_1 and y_2 are distances from the bottom of beam and top of plate to their respective centroids.

The total axial force, shear force and moment at any section of the plated beam can be expressed as

$$N_T(x) = N_1(x) + N_2(x) \tag{8.4}$$

$$V_T(x) = V_1(x) + V_2(x) + b_2 t_a \tau(x) \tag{8.5}$$

$$M_T(x) = M_1(x) + M_2(x) + N_2(x)[t_1 + t_a + y_2 - y_c] - N_1(x)[y_c - (t_1 - y_1)] \tag{8.6}$$

where y_c is the distance of the centroid of the plated section from the top surface of the beam and t_a is the thickness of the adhesive layer.

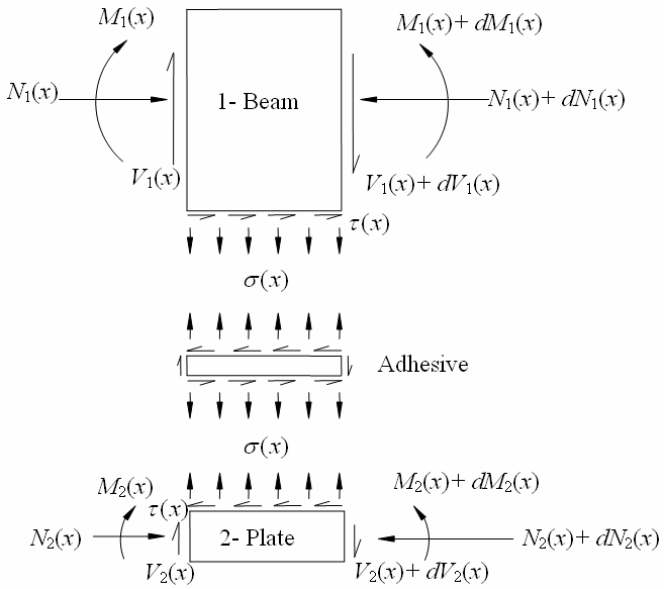

Figure 8.3. Differential segment in the bonded joint model

The constitutive relationship for the adherends provides the longitudinal strain at the bottom of adherend-1 $\varepsilon_1(x)$ and at the top of adherend-2 $\varepsilon_2(x)$ as:

$$\varepsilon_i(x) = \frac{du_i(x)}{dx} = (-1)^{i+1}\frac{y_i}{E_i I_i}M_i(x) + \frac{1}{E_i A_i}N_i(x); \qquad i = 1, 2 \tag{8.7}$$

The moment in the beam and the plate can be related assuming curvature compatibility as

$$R_b M_1(x) = M_2(x) \tag{8.8}$$

where R_b is the ratio between bending stiffness (EI) of the plate and the beam.

The interfacial slip $\delta(x)$ is the relative displacement between the beam and plate:

$$\delta(x) = u_2(x) - u_1(x) \tag{8.9}$$

Substituting Eqs 8.1 and 8.6-8.8 into Eq. 8.9 and introducing the parameters of interfacial fracture energy G_f and local bond strength τ_f give the following governing differential equation for the axial force in the plate:

$$N_2(x) = \frac{\tau_f^2 b_2}{2G_f\lambda^2}\left(\frac{d\delta(x)}{dx} + m\lambda^2 M_T(x)\right) \tag{8.10a}$$

where

$$\lambda^2 = \frac{\tau_f^2 b_2}{2G_f}\left[\frac{(y_1+y_2)(y_1+t_a+y_2)}{(E_1I_1+E_2I_2)} + \frac{1}{E_1A_1} + \frac{1}{E_2A_2}\right] \tag{8.10b}$$

$$m = \frac{1}{\lambda^2}\left[\frac{y_1 + y_2}{(E_1 I_1 + E_2 I_2)}\right] \tag{8.10c}$$

Differentiating Eq. 8.10a once with respect to x, substituting Eq. 8.1 into the resulting equation and replacing $\tau(x)$ by $f(\delta)$ yield the governing differential equation for the bonded joint (Figure 8.2) as

$$\frac{d^2\delta(x)}{dx^2} - \frac{2G_f\lambda^2}{\tau_f^2} f(\delta) + m\lambda^2 V_T(x) = 0 \tag{8.11}$$

The above equation can be solved if the local bond slip model $f(\delta)$ relating the local interfacial shear stress to the local interfacial slip is established.

8.4 Local Bond-Slip Model

Experimental studies (Sebastian, 2001; Chajes et al., 1995, 1996; Bizindavyi and Neale, 1999; Dai et al., 2005; Yao et al., 2005a, b) and analytical studies (Yuan et al., 2004; Lu et al., 2005a, b; Teng et al., 2006; Wang, 2006a, b) have shown that the stress deformation relationship at the interface between the adherends is nonlinear. This stress deformation relationship representing the large scale fracture processing zone is described as the bond-slip model or the cohesive zone model. This is a material property of the adhesive interface based on the nonlinear fracture mechanics approach of cohesive zone model developed by Dugdale (1960) and Barenblatt (1962).

A bilinear model with a linearly ascending branch (linear elastic stage) followed by a linearly descending branch (softening stage) represents a close approximation to the bond-slip behaviour of the bonded joint. In this model, the local interfacial shear stress $\tau(x)$ increases linearly with the increase in the interfacial slip $\delta(x)$ until it reaches the peak stress (bond strength) τ_f which is followed by the initiation of interfacial softening (micro-cracking). This is accompanied by a decrease in $\tau(x)$ and an increase in $\delta(x)$ until $\tau(x)$ reaches zero at an ultimate slip of δ_f which initiates macro cracking or debonding of the local bond element. Experimental studies have shown that the elastic deformation δ_1 at τ_f is much smaller than δ_f. For this reason, Chen et al. (2007) neglected the linearly ascending branch of the bond-slip law to derive a simplified and explicit formulation for the analysis of type-2 ICD failures in plated beams considering only the axial forces in

the bonded joint. Their comparison with the predictions of Teng et al. (2006) which is based on a bilinear bond-slip model revealed very close agreement and proven that such a simplification in the bond-slip model has an insignificant effect on the final predictions. This linearly softening bond-slip model as shown in Figure 8.4 is also adopted in the present study.

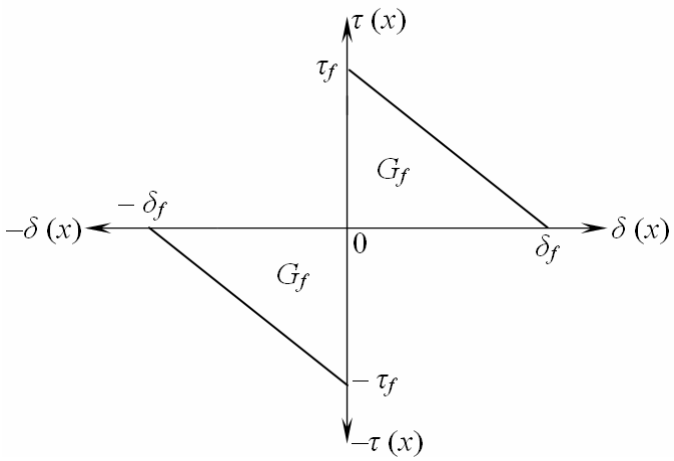

Figure 8.4. Local bond-slip model

Considering both positive and negative slips, the bond-slip model in Figure 8.4 can be described mathematically by the following equation:

$$\tau(x) = f(\delta) = \begin{cases} 0 & \text{when } \delta(x) = 0 \\ \dfrac{\tau_f}{\delta_f}[\delta_f - \delta(x)] & \text{when } 0 < \delta(x) \le \delta_f \\ \dfrac{\tau_f}{\delta_f}[-\delta_f - \delta(x)] & \text{when } -\delta_f \le \delta(x) < 0 \\ 0 & \text{when } |\delta(x)| > \delta_f \end{cases} \tag{8.12}$$

The friction and aggregate interlock in the debonded area is ignored leading to the absence of any residual shear strength after debonding. The bond-slip relationship is assumed to be fully reversible when local unloading is experienced before the slip reaches its ultimate value ± δ_f. This assumption can greatly simplify the analysis without significant loss of accuracy. The governing equation in Eq. 8.11 can be solved using Eq. 8.12 to find the shear stress (and interfacial slip) distribution along the interface and load-displacement response of the bonded joint.

8.5 States of the Bond Interface and Failure Processes

Let L_e be the effective bond length ($L_e = a_d + e_d$); a_u be the characteristic softening length of the bonded joint, a_d and e_d be the softening lengths on the left and right of the interface at the initiation of debonding; and β be the moment ratio between the left and right ends of the cracked bonded joint [$\beta = M(0)/M(L)$]. The moment ratio β here is equivalent to the load ratio in Chen et al. (2007), if the axial forces at two ends are equal in the present model. The left ($x = 0$) and right ($x = L$) of the bond interface are referred as left and right ends respectively in this chapter. It is assumed that $0 \leq \beta \leq 1$, i.e. the moment at the left end is always smaller than or equal to that at the right end and both have the same sign.

The entire interface is rigid initially because the adopted local bond–slip model neglects any elastic deformation. Under loading, a point of the interface can be in a rigid, softening, or debonded state. Letters R (rigid), S (softening) and D (debonding) are used below to describe the state of the interface from left to right. Depending on various parameters, the interface during the loading process experiences some of the following states:

1) rigid–softening (R–S) state. This state can occur only when $\beta = 0$ [i.e. $M(0) = 0$];
2) rigid–softening–debonding (R–S–D) state. This state can also occur only when $\beta = 0$;
3) softening–rigid–softening (S–R–S) state;
4) softening–rigid–softening–debonding (S–R–S–D) state;
5) softening–softening–debonding (S–S–D) state;
6) softening–debonding (S–D) state;
7) softening–softening (S–S) state;
8) softening (S) state, where the entire un-debonded part of the interface is in an unloading-softening state with the applied load reducing linearly until complete debonding;
9) debonding–softening–rigid–softening–debonding (D–S–R–S–D) state; and
10) debonding–softening–softening–debonding (D–S–S–D) state.

The interface between two (left and right) softening fronts remains rigid and has no interfacial stresses in the present analysis (Figure 8.5a), which makes the softening fronts abrupt whereas the stress distribution is smooth ahead of the softening fronts

during the whole loading process when a bilinear bond-slip model is used [as in Teng et al. (2006)].

When $\beta = 0$, the interface experiences progressively the R–S, R–S–D and S–D states, and then the linear unloading state to complete debonding. Only the general case with $\beta > 0$ is considered here and the interface during the entire loading process must experience one of the following five failure processes (FP), depending on the bond length L and the moment ratio β:

FP1: $\beta < 1$ and $L > L_e$: The interface experiences the S–R–S, S–R–S–D, S–S–D and S–D states.

FP2: $\beta < 1$ and $a_u < L < L_e$: The right end of the interface will be in a softening state even when the length of the rigid region in the middle of the interface reduces to zero. Debonding does not occur before the S–R–S interface becomes an S–S interface as the loading increases. The interface experiences the S–R–S, S–S, S–S–D and S–D states in this failure process. The solutions for the S–R–S, S–S–D and S–D states of interfaces are the same as in FP1.

FP3: $\beta < 1$ and $L < a_u$: Debonding does not occur progressively upon loading in this special case of small bond. Instead, the plate will be completely detached from the substrate in an instant. The interface experiences the S–R–S, S–S and S states in this failure process. The solutions for the S–R–S and the S–S states of interfaces are the same as in FP2.

FP4: $\beta = 1$ ($a_u = 0$, $a_d = e_d$) and $L > L_e = 2a_d$: The interface experiences the S–R–S, D–S–R–S–D and D–S–S–D states. The softening lengths in the S–R–S state and the softening and debonding lengths in the D–S–R–S–D and D–S–S–D states on both sides of the interface are the same in this failure process. The solutions for all the states in this FP4 are the same as in FP1. Due to symmetricity of the problem, solutions only for the region $(L/2) \leq x \leq L$) are sufficient.

FP5: $\beta = 1$ and $L < L_e$: The interface experiences the S–R–S and S–S states. Solutions for these two states are the same as in FP3.

The interfacial stress distribution and the sequence of debonding propagation for different failure processes involving different states of interfaces can be obtained from the respective solutions given in the following section. This is illustrated in Figure 8.5 for FP1 as an example.

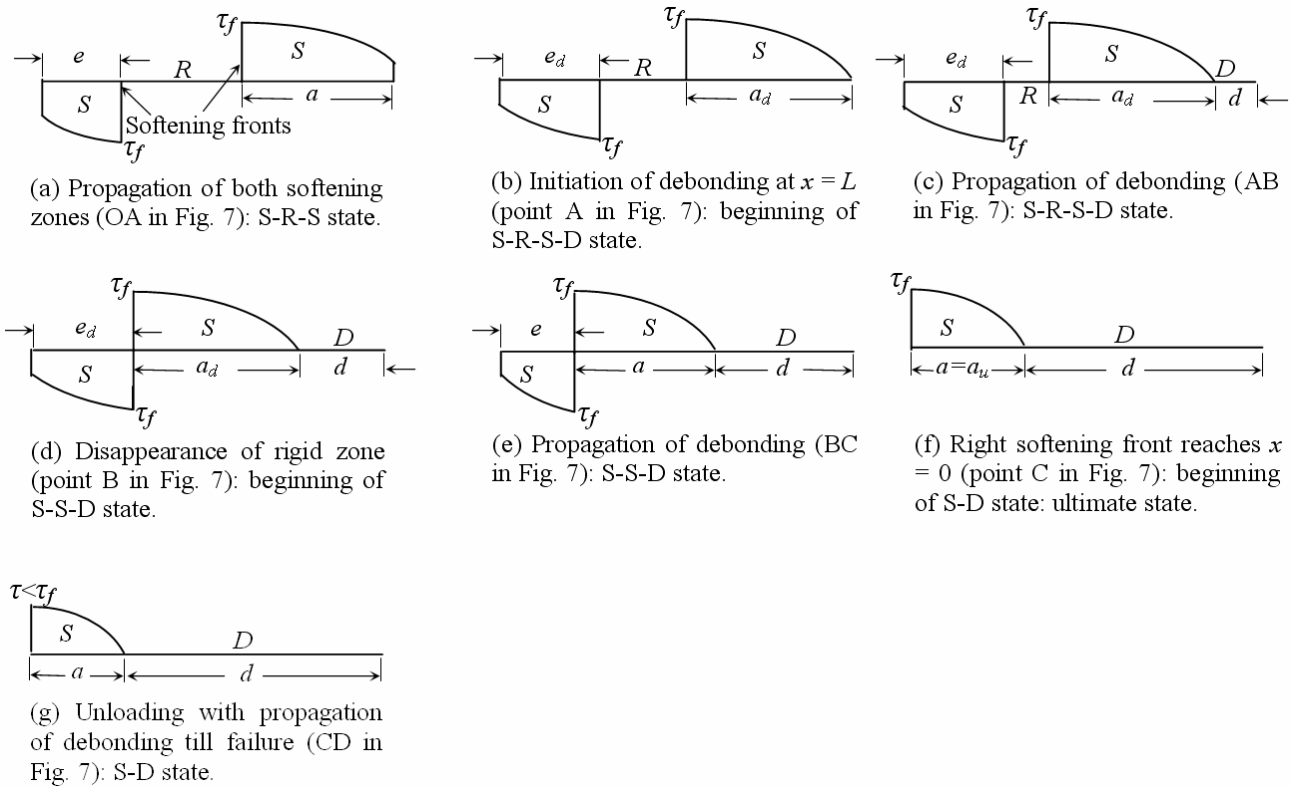

(a) Propagation of both softening zones (OA in Fig. 7): S-R-S state.

(b) Initiation of debonding at $x = L$ (point A in Fig. 7): beginning of S-R-S-D state.

(c) Propagation of debonding (AB in Fig. 7): S-R-S-D state.

(d) Disappearance of rigid zone (point B in Fig. 7): beginning of S-S-D state.

(e) Propagation of debonding (BC in Fig. 7): S-S-D state.

(f) Right softening front reaches $x = 0$ (point C in Fig. 7): beginning of S-D state: ultimate state.

(g) Unloading with propagation of debonding till failure (CD in Fig. 7): S-D state.

Figure 8.5. Distribution of interfacial shear stress in different states of the interface in the bonded joint: failure process FP1

8.6 Solutions for Different States of Interface

The solutions for the different states of interfaces that constitute five different failure processes described above are provided in this section. Substituting Eq. 8.12 for the case of $0 < |\delta(x)| \le \delta_f$ into Eq. 8.11 yield the governing equations respectively for the left and right softening interfaces as:

$$\frac{d^2\delta(x)}{dx^2} + \lambda^2\delta(x) = -\lambda^2\left(mV_T(x) + \delta_f\right) \qquad \text{for } -\delta_f \le \delta(x) < 0 \qquad (8.13a)$$

$$\frac{d^2\delta(x)}{dx^2} + \lambda^2\delta(x) = -\lambda^2\left(mV_T(x) - \delta_f\right) \qquad \text{for } 0 < \delta(x) \le \delta_f \qquad (8.13b)$$

The interfacial slip, the interfacial shear stress and the axial forces in the plate for the left and right softening regions can be found by solving Eqs 8.13a–b.

8.6.1 Softening–rigid–softening (S–R–S) interface

The interface remains in S–R–S state as shown in Figure 8.5a until the debonding moment M_{Td} is reached at the right end when the loads are increased gradually from zero. The general solution for the left softening region of the interface ($0 \le x \le e$) with $-\delta_f \le \delta(x) < 0$ is given by

$$\delta(x) = A_1 \sin[\lambda(x-e)] + B_1 \cos[\lambda(x-e)] - mV_T(x) - \delta_f \tag{8.14a}$$

$$\tau(x) = -\frac{\tau_f}{\delta_f}\left(A_1 \sin[\lambda(x-e)] + B_1 \cos[\lambda(x-e)] - mV_T(x)\right) \tag{8.14b}$$

$$N_2(x) = m_1\left(A_1\lambda \cos[\lambda(x-e)] - B_1\lambda \sin[\lambda(x-e)] + m\lambda^2 M_T(x)\right) \tag{8.14c}$$

and that for the right softening region ($L-a \le x \le L$) with $0 < \delta(x) \le \delta_f$ is given by

$$\delta(x) = C_1 \sin[\lambda(x-L+a)] + D_1 \cos[\lambda(x-L+a)] - mV_T(x) + \delta_f \tag{8.15a}$$

$$\tau(x) = -\frac{\tau_f}{\delta_f}\left(C_1 \sin[\lambda(x-L+a)] + D_1 \cos[\lambda(x-L+a)] - mV_T(x)\right) \tag{8.15b}$$

$$N_2(x) = m_1\left(C_1\lambda \cos[\lambda(x-L+a)] - D_1\lambda \sin[\lambda(x-L+a)] + m\lambda^2 M_T(x)\right) \tag{8.15c}$$

where

$$m_1 = \frac{\tau_f^2 b_2}{2G_f\lambda^2} \tag{8.15d}$$

The boundary and continuity conditions at the left and right ends and the softening fronts are:

$$N_2(x) = N_2(0) \text{ at } x = 0 \text{ and } N_2(x) = N_2(L) \text{ at } x = L \tag{8.16a}$$

$N_2(x)$ is continuous at $x = e$ and $x = L-a$ (8.16b)

$\delta(x) = 0$ at $x = e$ and $x = L-a$ (8.16c)

The constants of integration A_1 to D_1 are obtained by applying Eq. 8.16 to Eqs 8.14 and 8.15:

$$A_1 = C_1 = 0; \qquad B_1 = mV_T(e) + \delta_f; \qquad D_1 = mV_T(L-a) - \delta_f \tag{8.17a}$$

The first term in constants B_1 and D_1 is insignificant in magnitude [i.e mV_T (e) and mV_T (L-a) ≈ 0]. So, Eq. 8.17a becomes

$$A_1 = C_1 = 0; \qquad B_1 = \delta_f; \qquad D_1 = -\delta_f \tag{8.17b}$$

Substituting Eq. 8.17b into Eqs 8.14 and 8.15 yield the following equations from which the softening lengths *a* and *e* can be determined.

$$m_1 \lambda D_1 \sin(\lambda a) = m_1 m \lambda^2 M_T(L) - N_2(L) \tag{8.18}$$

$$m_1 \lambda B_1 \sin(\lambda e) = N_2(0) - m_1 m \lambda^2 M_T(0) \tag{8.19}$$

The softening lengths *a* and *e* increase gradually with the applied loading at the ends. The relative displacements (slips) between the adherends at the left and right ends, Δ_0 and Δ_l, can be obtained from Eqs 8.14a and 8.15a as:

$$\Delta_0 = B_1[\cos(\lambda e) - 1] \text{ and } \Delta_l = D_1[\cos(\lambda a) - 1] \tag{8.20a,b}$$

8.6.2 Softening–rigid–softening–debonding (S–R–S–D) interface

An S–R–S interface becomes an S–R–S–D interface (Figure 8.5b) when $\Delta_l = \delta_f$. Substituting this into Eq. 8.20b gives

$$a_d = \frac{\pi}{2\lambda} \tag{8.21}$$

The applied bending moment at the right end at the initiation of debonding M_{Td} and the corresponding left softening length e_d can be obtained from Eqs 8.18, 8.19 and 8.21. The shape and length of the softening regions and applied loading remains constant until the rigid region of the interface between the left and right softening fronts vanishes as debonding propagates. This is achieved by the movement of the right softening front steadily towards the left end by softening the rigid region in between while the left softening front remains stationary (Figure 8.5c).

Solutions given in Eqs 8.14 –8.19 are valid if *L* is replaced by (*L*–*d*) and *a* and *e* by a_d and e_d respectively where *d* is the debonded length at the right end of the interface. From Eq. 8.15c, the axial force at the right end of the plate can be obtained as given below in Eq. 8.22 and this is no longer sensitive to the softening lengths as in the S–R–S state of interface and remains constant as the variation in its second term is insignificant.

$$N_2(L) = m_1 \lambda [\delta_f + m \lambda M_T(L - d)] \tag{8.22}$$

Considering Eq. 8.10a, the displacement at $x = L$ during the debonding process can be obtained as

$$\Delta_l = \delta_f + \int_{L-d}^{L} \frac{d\delta(x)}{dx} dx = \delta_f + \frac{N_2}{m_1} d - m\lambda^2 \int_{L-d}^{L} M_T(x) dx . \tag{8.23}$$

where N_2 is the axial force in the debonded plate.

8.6.3 Softening–softening–debonding (S–S–D) interface

An S–R–S–D interface becomes an S–S–D interface when the length of the rigid region between the two softening fronts reduces to 0 and $d = L - (a_d + e_d)$ as shown in Figure 8.5d. Any further increase in the applied loading is accompanied by the decrease in the softening lengths a and e. Eqs 8.14 – 8.16 are valid if L is replaced by $(L–d)$ and the constants of integration $A_1 – D_1$ are replaced by $A_2 – D_2$. Consequently, $L = a + e + d$ and the two conditions in Eq. 8.16c are reduced to the same as $\delta = 0$ at $x = e = L – a – d$. To solve the problem, the following additional condition is required

$$\delta(x) = \delta_f \qquad \text{at } x = a + e = L - d \tag{8.24}$$

The constants of integration $A_2 – D_2$ and the softening lengths a and e are obtained by applying Eqs 8.16 and 8.24 to Eqs 8.14 and 8.15 after the above changes as

$$A_2 = C_2 = \frac{mV_T(e) - D_2 \cos(\lambda a)}{\sin(\lambda a)}; \qquad B_2 = mV_T + \delta_f; \qquad D_2 = mV_T - \delta_f \tag{8.25}$$

$$\sin(\lambda a) = \frac{m_1 \lambda \delta_f}{N_2(L-d) - m_1 m \lambda^2 M_T(L-d)} \tag{8.26}$$

$$\frac{\cos[\lambda(a-e)]}{\sin(\lambda a)} = \frac{N_2(0) - m_1 m \lambda^2 M_T(0)}{m_1 \lambda \delta_f} \tag{8.27}$$

The displacement at $x = L$ during the debonding process can be obtained from Eq. 8.23. The distribution of interfacial stress is shown in Figure 8.5e for this state which ends when $e = 0$, a = a_u and the corresponding applied moment at the right end becomes $M_T(L) = M_{Tu}$ (ultimate moment).

8.6.4 Softening–debonding (S–D) interface

An S–D interface (Figure 8.5f) begins from an S–S–D interface when $e = 0$. The general solution for the softening region of the interface ($0 \le x \le a_u$) with $0 < \delta(x) \le \delta_f$ obtained from Eq. 8.13b is given by

$$\delta(x) = A_3 \sin[\lambda(x-a)] + B_3 \cos[\lambda(x-a)] - mV_T(x) + \delta_f \tag{8.28a}$$

$$\tau(x) = -\frac{\tau_f}{\delta_f}\left(A_3 \sin[\lambda(x-a)] + B_3 \cos[\lambda(x-a)] - mV_T(x)\right) \tag{8.28b}$$

$$N_2(x) = m_1\left(A_3\lambda \cos[\lambda(x-a)] - B_3\lambda \sin[\lambda(x-a)] + m\lambda^2 M_T(x)\right). \tag{8.28c}$$

The boundary and continuity conditions at the left and right ends and the softening fronts are:

$$N_2(x) = N_2(0) \text{ at } x = 0 \tag{8.29a}$$

$$\delta(x) = \delta_f \text{ and } N_2(x) = N_2(a) = N_2(L) \text{ at } x = a = L–d \tag{8.29b}$$

The constants of integration A_3 and B_3 and the softening length a are obtained by application of Eq. 8.29 into Eq. 8.28:

$$A_3 = \frac{N_2(L) - m_1 m\lambda^2 M_T(L-d)}{m_1\lambda}; \qquad B_3 = mV_T(a) \tag{8.30}$$

$$\cos(\lambda a) = \frac{N_2(0) - m_1 m\lambda^2 M_T(0)}{N_2(L) - m_1 m\lambda^2 M_T(L-d)} \tag{8.31}$$

In the S-D state, the transfer of stress from beam to plate decreases considerably as debonding propagates. The Eq. 8.31 indicates that the softening length a reduces gradually to 0 (Figure 8.5g) with the reduction in the axial force in the plate N_2 to 0, i.e., complete debonding. This behaviour is different from that of a bonded joint subjected only to axial forces as in Teng et al. (2006) and Chen et al. (2007) where the softening length in the S-D state remains constant at a_u. The displacement at $x = L$ during the debonding process can be obtained from Eq. 8.23.

8.6.5 Softening–softening (S–S) interface

This state of interface is governed by Eqs 8.14 – 8.15 if the integration constants $A_1 - D_1$ are replaced by $A_4 - D_4$. In this case $L = a + e$, and the two conditions in Eq. 8.16c are reduced to one as $\delta = 0$ at $x = e = L - a$.

The constants of integration $A_4 - D_4$ and the softening lengths a and e are obtained as follows by applying Eq. 8.16 to Eqs 8.14 and 8.15 after the above changes:

$$B_4 = mV_T + \delta_f; \qquad D_4 = mV_T - \delta_f \tag{8.32a}$$

$$A_4 = \frac{N_2(0) - B_4 m_1 \lambda \sin[\lambda(L-a)] - m_1 m \lambda^2 M_T(0)}{m_1 \lambda \cos[\lambda(L-a)]} \tag{8.32b}$$

$$C_4 = \frac{N_2(L) + D_4 m_1 \lambda \sin(\lambda a) - m_1 m \lambda^2 M_T(L)}{m_1 \lambda \cos(\lambda a)} \tag{8.32c}$$

Also,

$$A_4 = C_4 \tag{8.32d}$$

The displacement at $x = L$ i.e. Δ_l during the debonding process can be obtained from Eq. 8.15a after changing $A_1 - D_1$ by $A_4 - D_4$. The S–S interface becomes an S–S–D interface when $\Delta_l = \delta_f$ and the corresponding softening lengths become a_d and e_d.

8.6.6 Softening (S) interface

In this state the whole interface is in a softening state ($L = a$) and it is governed by Eq. 8.28 with the integration constants $A_3 - B_3$ replaced by $A_5 - B_5$ and a replaced by L. The boundary conditions in Eq. 8.16*a* are still applicable here.

The constants of integration $A_5 - B_5$ and the softening length a are obtained as follows by applying Eq. 8.16*a* to Eq. 8.28 after the above changes:

$$A_5 = \frac{N_2(L) - m_1 m \lambda^2 M_T(L)}{m_1 \lambda} \tag{8.33a}$$

$$B_5 = \frac{N_2(0) - m_1 m \lambda^2 M_T(0) - \cos(\lambda L)[N_2(L) - m_1 m \lambda^2 M_T(L)]}{m_1 \lambda \sin(\lambda L)} \tag{8.33b}$$

The applied loading at the initiation of S state of interface can be obtained from Eq. 8.28a after replacing $A_3 - B_3$ by $A_5 - B_5$ and setting $\Delta_0 = 0$. The displacement at $x = L$ during the debonding process is given as

$$\Delta_l = B_5 - mV_T(L) + \delta_f \,. \tag{8.34}$$

8.7 Relationship between Applied Moment and Plate Axial Forces

The external loading in a plated beam is resisted by the plate in addition to the beam due to the transfer of forces between them through the adhesive bond interface. To obtain the final solutions for all the above states of interfaces (8.6.1 to 8.6.6), it is necessary to properly relate the applied bending moment $M_T(x)$ and the axial forces in the plate $N_2(x)$. Two methods are presented in this section to establish this relationship: (1) the rotational spring method (RSM) and (2) the section analysis with partial interaction (SA-PI) method.

8.7.1 Rotational spring method (RSM)

The flexural cracks occur in regions of low shear with high bending moment in an RC beam. This introduces a local flexibility at the cracked locations which may be modelled as a rotational spring at these locations (Figure 8.6). Wang (2006a, b) adopted this method to analyse type-1 ICD failure in a plated beam and has shown it to be realistic.

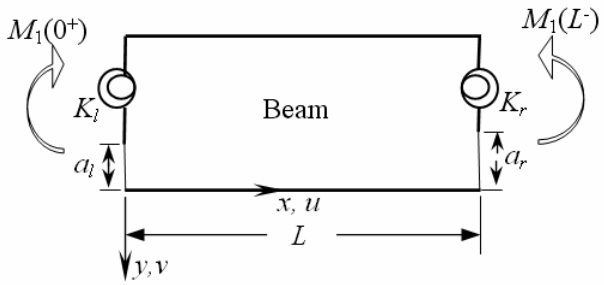

Figure 8.6. Rotational spring model for the RC beam

There exists a discontinuity in the rotation of the beam at the cracked section and a discontinuity in longitudinal displacement at the tensile face of the beam. These discontinuities are related to the rotational spring stiffness for a given applied moment and the crack depth at the crack location. The displacement and the rotation continuity conditions at the cracked locations yield

$$u_i\begin{pmatrix} x=0^- \\ x=L^- \end{pmatrix} = u_i\begin{pmatrix} x=0^+ \\ x=L^+ \end{pmatrix}; \quad v_i\begin{pmatrix} x=0^- \\ x=L^- \end{pmatrix} = v_i\begin{pmatrix} x=0^+ \\ x=L^+ \end{pmatrix} \tag{8.35a}$$

$$v_2'\begin{pmatrix} x=0^- \\ x=L^- \end{pmatrix} = v_2'\begin{pmatrix} x=0^+ \\ x=L^+ \end{pmatrix} \tag{8.35b}$$

where the subscript i = 1, 2 refer respectively to the beam and the plate.

Assuming that the slip at either side of the cracked section is the same in magnitude but opposite in sign, the slips at the two adjacent cracks can be related to the respective bending moment and rotational spring stiffness

$$\delta(0^+) = \delta(x)\Big|_{x=0^+} - \delta(x)\Big|_{x=0^-} = \frac{y_1}{2}\left[\frac{dv_1(x)}{dx}\Big|_{x=0^+} - \frac{dv_1(x)}{dx}\Big|_{x=0^-}\right] = \frac{y_1}{2K_l}M_1(0) \tag{8.36a}$$

$$\delta(L^-) = \delta(x)\Big|_{x=L^+} - \delta(x)\Big|_{x=L^-} = \frac{y_1}{2}\left[\frac{dv_1(x)}{dx}\Big|_{x=L^+} - \frac{dv_1(x)}{dx}\Big|_{x=L^-}\right] = -\frac{y_1}{2K_r}M_1(L) \tag{8.36b}$$

The rotational stiffness of the spring at the left and right cracks, K_l and K_r, may be estimated for a given crack geometry in the plain concrete beam (Paipetis and Dimarogonas, 1986) using the principle of fracture mechanics as

$$K_i = c_i(a_i, t_1)E_{1i}I_{1i} \tag{8.37}$$

where the subscript $i = l, r$ refer respectively to the left and right cracks; a_i is the crack depth; $E_{1i}I_{1i}$ is the flexural stiffness of the beam at the crack location; and c_i (a_i, t_1) is approximated for $(a_i/t_1) < 0.6$ as

$$c_i(a_i, t_1) = \frac{1}{5.346t_1}\left(\begin{array}{l} 1.8624\left(\frac{a_i}{t_1}\right)^2 - 3.95\left(\frac{a_i}{t_1}\right)^3 + 16.375\left(\frac{a_i}{t_1}\right)^4 - 37.226\left(\frac{a_i}{t_1}\right)^5 \\ + 76.81\left(\frac{a_i}{t_1}\right)^6 - 126.9\left(\frac{a_i}{t_1}\right)^7 + 172\left(\frac{a_i}{t_1}\right)^8 - 143.97\left(\frac{a_i}{t_1}\right)^9 + 66.56\left(\frac{a_i}{t_1}\right)^{10} \end{array}\right)^{-1} \tag{8.38}$$

An iterative method as proposed by Rabinovitch and Frostig (2001) may be used for an RC beam as it is difficult to get an explicit expression for K_i. The relationship between the axial forces in the plate $N_2(x)$ and the applied bending moment $M_T(x)$ using the above method are provided below for different states of the interface experienced during different failure processes.

Softening–rigid–softening (S–R–S) interface

Applying Eq. 8.36 to Eqs 8.14–8.15 provides the following expressions for the axial force in the plate:

$$N_2(L) = \frac{\rho_L M_T(L) - D_1[1-\cos(\lambda a)]}{\rho_L(y_1 + y_2 + t_a)} \tag{8.39}$$

$$N_2(0) = \frac{\rho_0 M_T(0) + B_1[1-\cos(\lambda e)]}{\rho_0(y_1 + y_2 + t_a)} \tag{8.40}$$

where

$$\rho_0 = \frac{y_1}{2K_l(1+R_b)}; \qquad \rho_L = \frac{y_1}{2K_r(1+R_b)} \tag{8.40a}$$

The softening lengths *a* and *e* for the given applied loading can be determined by substituting Eqs 8.39 and 8.40 respectively into Eqs 8.18 and 8.19.

Softening–rigid–softening-debonding (S–R–S–D) interface

The axial force from Eq. 8.22 is sufficient to solve this state of interface.

Softening–softening-debonding (S–S–D) interface

Modifying Eqs 8.14 and 8.15 as detailed in section 8.6.3 to extend its suitability to this state of interface and applying Eq. 8.36 gives

$$N_2(0) = \frac{[\rho_0 M_T(0) + \delta_f]\sin(\lambda a) - \delta_f \sin[\lambda(a-e)]}{\rho_0(y_1 + y_2 + t_a)\sin(\lambda a)}. \tag{8.41}$$

From Eqs 8.15, 8.36 and 8.41, it can be found that

$$N_2(L) = N_2(L-d) = \frac{\rho_L M_T(L) + \delta_f}{\rho_L(y_1 + y_2 + t_a)} \tag{8.42}$$

The softening lengths can be obtained by substituting Eqs 8.42 and 8.41 respectively in to Eqs 8.26 and 8.27.

Softening–debonding (S–D) interface

Application of RSM (Eq. 8.36) to Eq. 8.28 results in the following expressions for $N_2(0)$ and $N_2(L)$ which in combination with Eq. 8.31 provide the softening length for this state of the interface:

$$N_2(L) = \frac{m_1\lambda\left(\rho_L M_T(L) + \delta_f - m\lambda M_T(L-d)\sin[\lambda(L-a)]\right)}{m_1\lambda\rho_L(y_1 + y_2 + t_a) - \sin[\lambda(L-a)]}. \tag{8.43}$$

$$N_2(0) = \frac{m_1\lambda\rho_0 M_T(0) - m_1\lambda\delta_f + \sin(\lambda a)[N_2(L) - m_1 m\lambda^2 M_T(L-d)]}{m_1\lambda\rho_0(y_1 + y_2 + t_a)} \tag{8.44}$$

Softening–softening (S–S) interface

Modifying Eqs 8.14 and 8.15 as detailed in Section 8.6.5 to extend its suitability to this state of the interface and applying Eq. 8.36 gives

$$N_2(L) = \frac{\rho_L M_T(L) + C_4 \sin(\lambda a) + D_4 \cos(\lambda a) - mV_T(L) + \delta_f}{\rho_L (y_1 + y_2 + t_a)} \tag{8.45}$$

$$N_2(0) = \frac{\rho_0 M_T(0) + A_4 \sin[\lambda(L-a)] - B_4 \cos[\lambda(L-a)] + mV_T(0) + \delta_f}{\rho_0 (y_1 + y_2 + t_a)} \tag{8.46}$$

From Eqs 8.32, 8.45 and 8.46 the softening length *a* is obtained.

Softening (S) interface

Applying Eq. 8.36 to the general solution for this state of interface described in section 8.6.6 gives

$$N_2(L) = \frac{\rho_L M_T(L) + B_5 - mV_T(L) + \delta_f}{\rho_L (y_1 + y_2 + t_a)} \tag{8.47}$$

$$N_2(0) = \frac{\rho_0 M_T(0) + A_5 \sin(\lambda L) - B_5 \cos(\lambda L) + mV_T(0) - \delta_f}{\rho_0 (y_1 + y_2 + t_a)} \tag{8.48}$$

Eqs 8.33, 8.47 and 8.48 provide the solution for this state of the interface.

8.7.2 Section analysis with partial interaction method (SA-PI)

Force transfer from concrete to the reinforcements or strengthening plate in plated RC beams occurs through bond at the interfaces. Section analysis of a cracked RC beam as explained in Teng et al. (2002) may be employed to determine the axial forces in the plated beam due to the existence of full composite action between the RC beam and the bonded plate prior to the formation of flexural cracks at the tension face of the beam as reiterated in Liu et al. (2004). The strain distribution is linear through the depth of the cross section, i.e. the plane section assumption holds good and strain at the plate-beam interface remains same. After flexural cracking of the concrete, high bond stresses develop near the crack and as a result, interfacial slip is generated between the concrete beam and the plate. This means that the plate strain is no longer equal to the adjacent

concrete strain and the full composite action analysis discussed above is no longer valid. The partial interaction theory developed by Johnson (1994) for composite beams and advanced by Oehlers and Bradford (1995) for plated beams may be adopted in this case to achieve an accurate analysis. The region near a crack or between two adjacent cracks is termed a partial interaction region where the interfacial slip $\delta(x)$ and the slip strain $d\delta(x)/dx$ are non zero. Also, the concrete tensile strain at the plate-beam interface may approximately be taken as zero (it is zero if there is no tensile steel reinforcement) at sections very close to the crack. Therefore, in this region of partial interaction, the plate strain is the combination of the tensile strain at the tension face of the beam ε_{ct} obtained by section analysis and the slip strain due to partial interaction (Liu et al., 2004):

$$\varepsilon_2(x) = \varepsilon_{ct}(x) + \frac{d\delta(x)}{dx} \tag{8.49}$$

The section analysis detailed in Teng et al. (2002) in finding $\varepsilon_{ct}(x)$ involves two unknowns: the extreme compression fibre strain of concrete ε_{cf} and the neutral axis depth y from the compression fibre. These two parameters can be determined from axial force and moment equilibrium. The explicit expression for ε_{cf} in terms of y from the equilibrium analysis as in Teng et al. (2002) is as follows, which can be used to find the concrete tensile strain ε_{ct} based on plane section assumption.

Case-1: $\varepsilon_{cf} \le \varepsilon_{co}$; $|\varepsilon_s| < (f_y / E_s)$; $|\varepsilon_p| < (f_p / E_p)$

$$\varepsilon_{cf} = \alpha_1 + [\alpha_2 E_s (y - d_s) / f_y] \tag{8.50}$$

Case-2: $\varepsilon_{cf} \le \varepsilon_{co}$; $|\varepsilon_s| \ge (f_y / E_s)$; $|\varepsilon_p| < (f_p / E_p)$

$$\varepsilon_{cf} = 0.5[\alpha_1 \pm \sqrt{\alpha_1^2 - 4\alpha_2}] \tag{8.51}$$

Case-3: $\varepsilon_{co} < \varepsilon_{cf} \le 0.0035$; $|\varepsilon_s| < (f_y / E_s)$; $|\varepsilon_p| < (f_p / E_p)$

$$\varepsilon_{cf} = [-3 \pm \sqrt{9 + 4\alpha_3 \varepsilon_{co}}] / 2\alpha_3 \tag{8.52}$$

Case-4: $\varepsilon_{co} < \varepsilon_{cf} \le 0.0035$; $|\varepsilon_s| \ge (f_y / E_s)$; $|\varepsilon_p| < (f_p / E_p)$

$$\varepsilon_{cf} = [-\alpha_5 \pm \sqrt{\alpha_5^2 + 4\alpha_4 \varepsilon_{co}}] / 2\alpha_4 \tag{8.53}$$

where

$$\alpha_1 = 3\varepsilon_{co} + \left(\frac{3\varepsilon_{co}^2 E_p (y - d_p) A_p]}{0.67 f_{cu} b_c y^2} \right); \qquad \alpha_2 = \left(\frac{3\varepsilon_{co}^2 f_y A_s}{0.67 f_{cu} b_c y^2} \right) \tag{8.54a}$$

$$\alpha_3 = 3\left(\frac{E_s (y - d_s) A_s + E_p (y - d_p) A_p}{0.67 f_{cu} b_c y^2} \right) \tag{8.54b}$$

$$\alpha_4 = \left(\frac{3E_p (y - d_p) A_p]}{0.67 f_{cu} b_c y^2} \right); \qquad \alpha_5 = \left(3 - \frac{3 f_y A_s}{0.67 f_{cu} b_c y^2} \right) \tag{8.54c}$$

in which d_s and d_p are distances from the extreme concrete compression fibre to the centroid of steel rebars and plate respectively; b_c is the width of concrete beam; E and A are the elastic modulus and cross sectional area with subscripts s and p refer respectively to steel rebar and plate; f_y is the yield strength of steel rebar; f_p is the tensile strength of plate; f_{cu} is the cubic compressive strength of concrete and $\varepsilon_{co} = (f_{cu}^{0.5})/4100$. These nomenclatures are the same as those in Teng et al. (2002) for ease of reference.

Eqs 8.51-8.53 are quadratic and provide two values for ε_{cf} individually, out of which, one value that maintains the continuity of ε_{cf} with the previous case has to be considered.

The axial force in the plate $N_2(x)$ under the applied bending moment $M_T(x)$ can be determined from Eq. 8.49 and Eqs 8.55-8.65 provided below for the different states of the interface experienced during the different failure processes.

Softening–rigid–softening (S–R–S) interface

The axial force in the plate $N_2(x)$ at the two ends of the bonded joint during S–R–S state of interface can be obtained from Eqs 8.49 and 8.14-8.15 as:

$$N_2(L) = [\varepsilon_{ct}(L) - D_1 \lambda \sin(\lambda a)] E_2 A_2 \tag{8.55}$$

$$N_2(0) = [\varepsilon_{ct}(0) + B_1 \lambda \sin(\lambda e)] E_2 A_2 \tag{8.56}$$

The softening lengths a and e under the given applied loading can be determined by substituting Eqs 8.55 and 8.56 respectively into Eqs 8.18 and 8.19.

Softening–rigid–softening-debonding (S–R–S–D) interface

Replacing L with (L–d) in Eq. 8.15 and making use of Eq. 8.49 gives

$$N_2(L-d) = [\varepsilon_{ct}(L-d) + \delta_f \lambda)]E_2A_2 \tag{8.57}$$

The axial force obtained from Eq. 8.22 and 8.57 is the same so any one of them can be used to solve this state of interface.

Softening–softening-debonding (S–S–D) interface

Replacing L with (L–d) in Eqs 8.14-8.15, substituting Eq. 8.25 into the resulting expression and making use of Eq. 8.49 provide the axial force in the plate at x = 0 and x = L–d in the S–S–D state as:

$$N_2(L-d) = [\varepsilon_{ct}(L-d) + \frac{\delta_f \lambda}{\sin(\lambda a)}]E_2A_2 \tag{8.58}$$

$$N_2(0) = [\varepsilon_{ct}(0) + \frac{\delta_f \lambda \cos[\lambda(a-e)]}{\sin(\lambda a)}]E_2A_2 \tag{8.59}$$

Substituting Eqs 8.58 and 8.59 respectively into Eqs 8.26 and 8.27 provides the softening lengths. Eq. 8.58 gives the ultimate plate force at the right end (similar to the ultimate load in Chen et al. 2007) when e = 0 and $a = a_u$.

Softening–debonding (S–D) interface

Eqs 8.28 and 8.49 yield the axial force in the plate during S–D state as:

$$N_2(L) = [\varepsilon_{ct}(L-d) + A_3\lambda]E_2A_2 \tag{8.60}$$

$$N_2(0) = [\varepsilon_{ct}(0) + A_3\lambda\cos(\lambda a)]E_2A_2 \tag{8.61}$$

where

$$A_3 = \frac{\varepsilon_{ct}(L-d)E_2A_2 - m_1 m\lambda^2 M_T(L-d)}{\lambda(m_1 - E_2A_2)} \tag{8.61a}$$

Substituting Eqs 8.60 and 8.61 into Eq. 8.31 gives the softening length for this state of the interface.

Softening–softening (S–S) interface

Modifying Eqs 8.14 and 8.15 as detailed in section 8.6.5 to extend its suitability to this state of interface and using Eq. 8.49 gives

$$N_2(L) = [\varepsilon_{ct}(L) + C_4\lambda\cos(\lambda a) - D_4\lambda\sin(\lambda a)]E_2A_2 \tag{8.62}$$

$$N_2(0) = \{\varepsilon_{ct}(0) + A_4\lambda\cos[\lambda(L-a)] + B_4\lambda\sin[\lambda(L-a)]\}E_2A_2 \tag{8.63}$$

Eqs 8.32, 8.62 and 8.63 provide the softening lengths *a* and *e* for the S–S state of the interface.

Softening (S) interface

Applying Eq. 8.49 to the general solution Eq. 8.28 for this state of the interface as described in section 8.6.6 gives

$$N_2(L) = [\varepsilon_{ct}(L) + A_5\lambda]E_2A_2 \tag{8.64}$$

$$N_2(0) = [\varepsilon_{ct}(0) + A_5\lambda\cos(\lambda L) + B_5\lambda\sin(\lambda L)]E_2A_2 \tag{8.65}$$

The solution for this state of the interface can be obtained from Eqs 8.33, 8.64 and 8.65.

8.8 Comparison with Solution of Bonded Joint Model under Axial Forces Only

The present solution considering axial forces, shear forces and bending moments in the adherends is compared with Chen et al.'s (2007) solution that considered the same bonded joint model but only under axial forces in the plate and beam. Both solutions are based on a linearly softening bond-slip model. This comparison is carried out in this section through an illustrative example as detailed below.

8.8.1 An illustrative example

Consider an RC beam adhesively plated with CFRP and subjected to any loading. The geometrical and material properties of the adherends and adhesive are taken from Jones et al. (1988): b_1 = 155 mm; t_1 = 225 mm; E_1 = 28.6 GPa; f_{cu} = 27 MPa; 3 steel bars of ø20 mm centred at 190 mm from the extreme compressive fibre; E_s = 210 GPa; f_y = 410 MPa; b_2 = 125 mm; t_2 = 0.165 mm; E_2 = 256 GPa; f_p = 2500 MPa; and t_a = 1 mm. The same bond-slip parameters as those in Chen et al. (2007) are adopted: δ_1 = 0.034 mm; δ_f

= 0.16 mm; τ_f = 7.2 MPa; and G_f = 0.58 N/mm. The moment ratio β between the left and right ends of the bonded joint and the bond length L between adjacent cracks can vary and depend on the details of the geometry, material and loading of the beam, and the crack locations. L = 100 mm (which represents a typical crack spacing in an RC beam) and β = 0.8 are considered here as an example case. The coefficient of rotational springs are approximated as c_l = 0.0001167 and c_r = 0.0001060 which are close to the values used by Wang (2006a, b) in comparing the RSM with experimental results. These parameters remain the same in the rest of the chapter unless specified otherwise.

8.8.2 Load–displacement characteristics

Note that in the present solution the axial force ratio in beam to plate (η) varies during the loading process because the system is nonlinear and caused by the bending deformation. Chen et al. (2007) assumed a constant η value during the loading process. For comparison purpose, the average η value obtained from the present solution was used in Chen et al.'s (2007) solution.

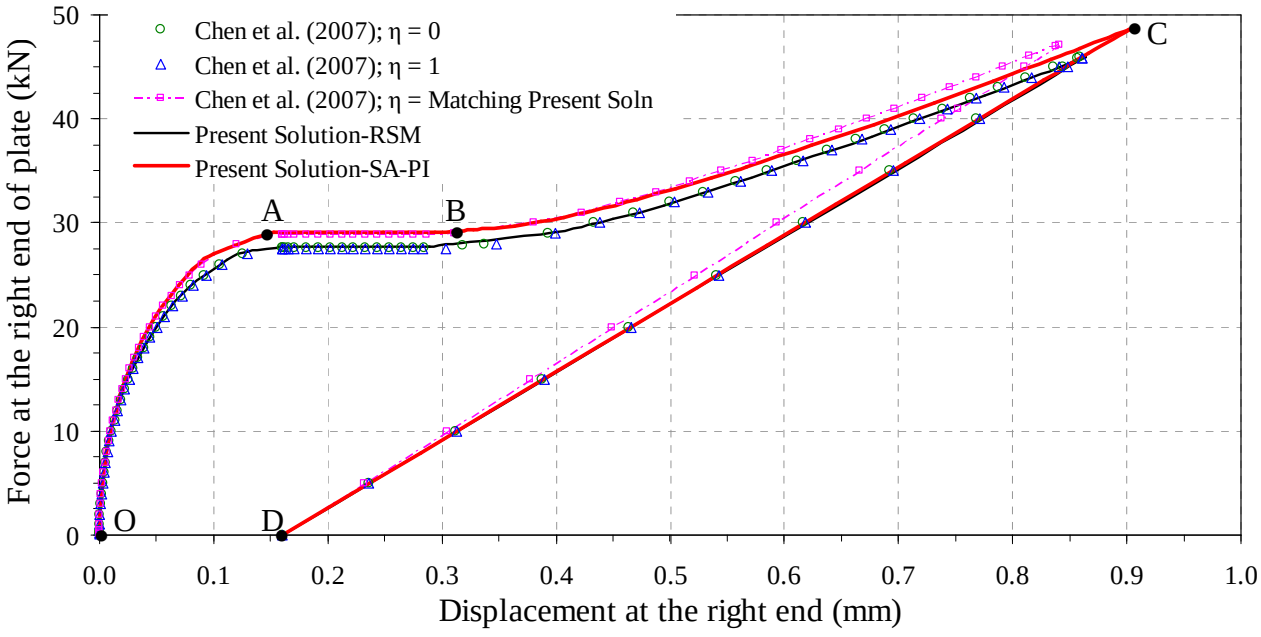

Figure 8.7. Load-displacement response of an example bonded joint

The load-displacement curves predicted from the present solution using both the RSM and SA-PI methods are compared with the predictions from reference solution (Chen et al., 2007) in Figure 8.7. Predictions from the RSM method matches closely with the reference solution when η = 0 or 1 but under-estimate when a matching η value is used.

This is due to the approximate nature of RSM method which can vary depending on the coefficient of rotational springs used in the analysis. These coefficients predicted from Eq. 8.38 do not give correct results even in Wang (2006 a, b) and are always approximated based on experimental or numerical results.

The salient points on the predictions using the SA–PI method are shown as O–A–C–D in Figure 8.7. The curve OA represents the S–R–S state of the interface, point A represents the initiation of debonding in the S–R–S state, the plateau AB refers to the S–R–S–D state, point B represents the meeting of left and right softening fronts (i.e., the end of the rigid zone between the left and right softening fronts), curve BC refers to the S–S–D state of the interface, and the ultimate point C represents the stage when the right softening front reaches the left end. The S–D state is shown by curve CD. The predictions from the SA–PI method and the reference solution with η taken as the average value obtained from the present solution are almost the same until the beginning of the S–S–D state. During the initial part of the S–S–D state the reference solution predicts a slightly higher capacity than SA–PI and this difference increases gradually as the displacement increases, with the reference solution under estimates by 3.1% of the ultimate capacity and 7.4% of the ultimate deformation. The under-estimation of the ultimate capacity from the reference solution may be attributed to the adopted η value which in reality varies, and the bending deformation considered in the present solution. Both solutions predict the same δ_f at the end of S–D state of the interface. Unlike the reference solution of Chen et al. (2007) which predicts a constant debonding zone during the S–D state until complete debonding, the present solution predicts a continuous debonding until complete interface failure. This difference is attributable to the inclusion of the bending moment and shear force in the adherends in the present solution.

Unless mentioned otherwise, the present solution using the SA–PI method is hereafter referred to as the present solution for simplicity.

8.8.3 Distribution of interfacial shear stress and axial plate stress

The interfacial shear stress and the axial stress in plate as predicted from the present solution are shown in Figures 8.8a–b along the length of the bonded joint for different slip at the right end Δ_l. Predictions for $\Delta_l < \delta_f$, $\Delta_l = \delta_f$, $\Delta_l > \delta_f$ and maximum Δ_l

represent the S–R–S, S–R–S–D, S–S–D and S–D states of the interface during the loading process. The axial forces in the plate at both end increases gradually as the load is increased. The axial force remains constant along the debonded interface in S–S–D and S–D states. However, this force increases with the load till the ultimate load is reached.

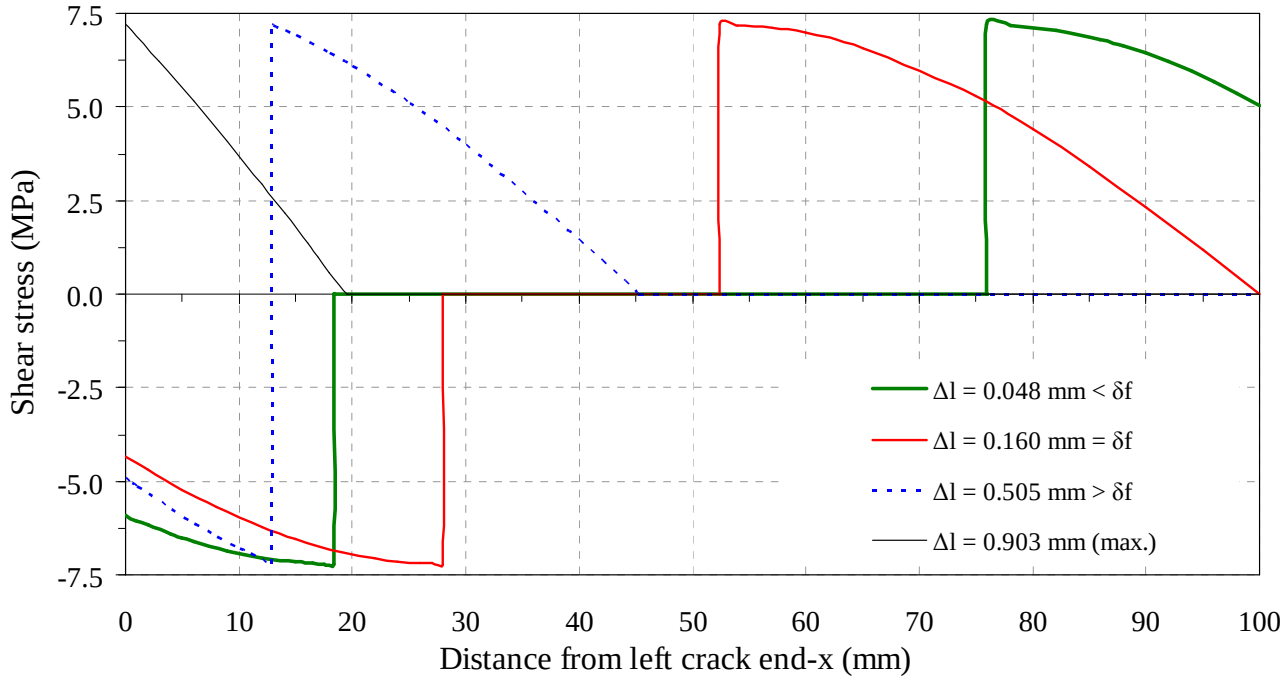

(a) Interfacial shear stress

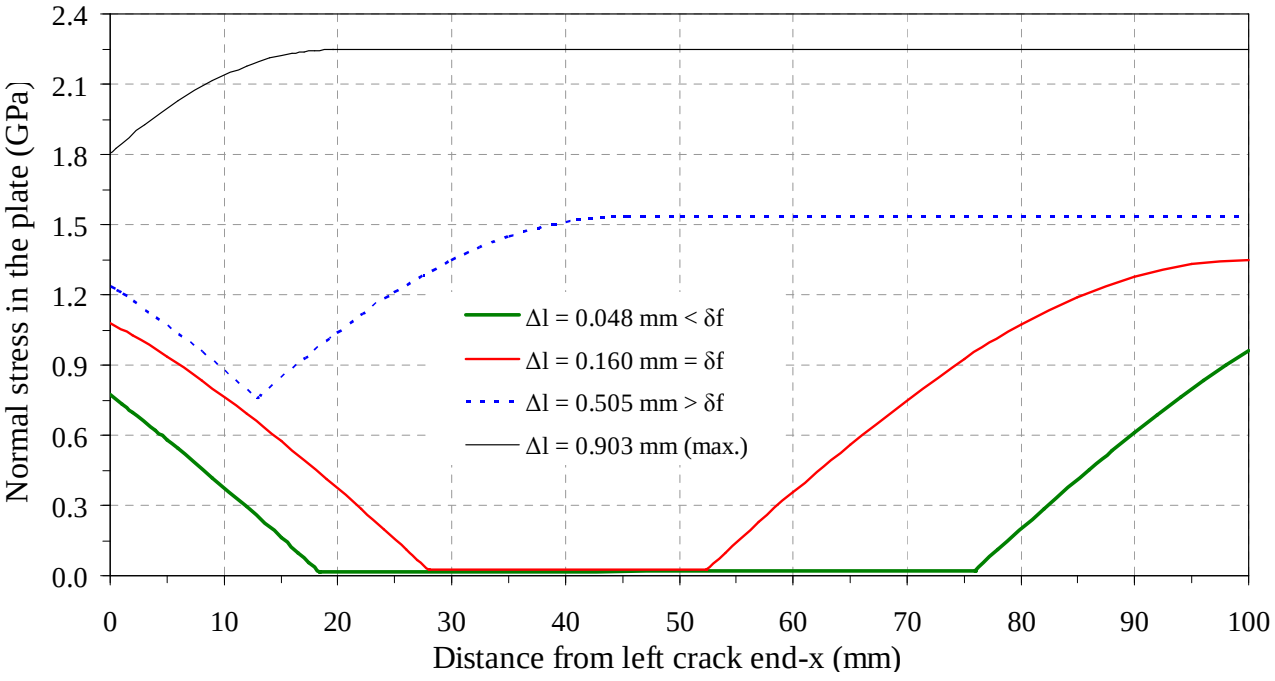

(b) Axial plate stress

Figure 8.8. Stress distribution along the bond length between two cracks

8.9 Parametric Study

The effect of bond length L (i.e. the distance between two adjacent cracks), the moment ratio β (similar to the load ratio in the reference solution), axial stiffness of plate E_2A_2, depth of the beam t_1, width of the beam b_1, the steel ratio ρ and bending deformation on the load-displacement characteristics are studied and analysed in this section using the present solution and the reference solution. This study highlights the differences between the predictions of the two solutions in addition to highlighting the effects of these parameters on the response of the bonded joint and thus the behaviour of ICD in plated RC beams. All geometrical and material properties of the adherends and adhesive, except the one being investigated, are the same as those in section 8.8.1 unless otherwise mentioned.

8.9.1 Effect of bond length L

The predictions from the present and reference solutions are obtained for five different bond lengths $L = L_e$ (effective bond length = $a_d + e_d$ = 76.3 mm), 80 mm, 100 mm, 125 mm and 150 mm. The load-displacement responses predicted from the two solutions for a given bond length are very close to each other as discussed in section 8.8.2. The plate force at the initiation of debonding and the ultimate load remains constant from both the solutions and unaffected by the bond length. However, while the prediction of the former is almost equal from both solutions, the latter predicted from present solution is constantly higher than the reference solution as shown in Figures 8.9a–b. The present solution predicts a slightly higher loading capacity (3.1%) and ductility (7.7%) than the reference solution irrespective of the bond length. Both the ultimate displacement at the right end and its difference between the present solution and the reference solution increases steadily with the bond length. The present solution predicts slightly higher displacement than the reference solution.

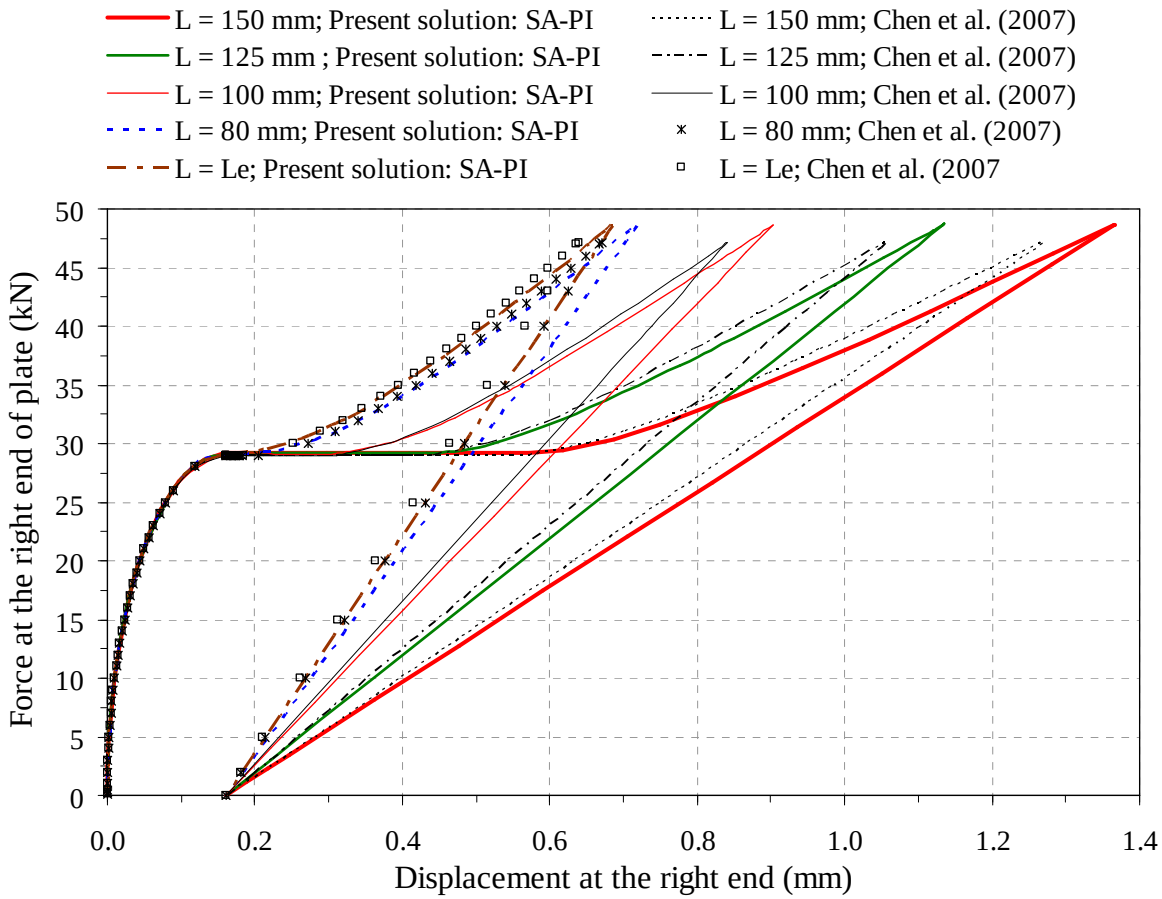

a) Load versus displacement at the right end

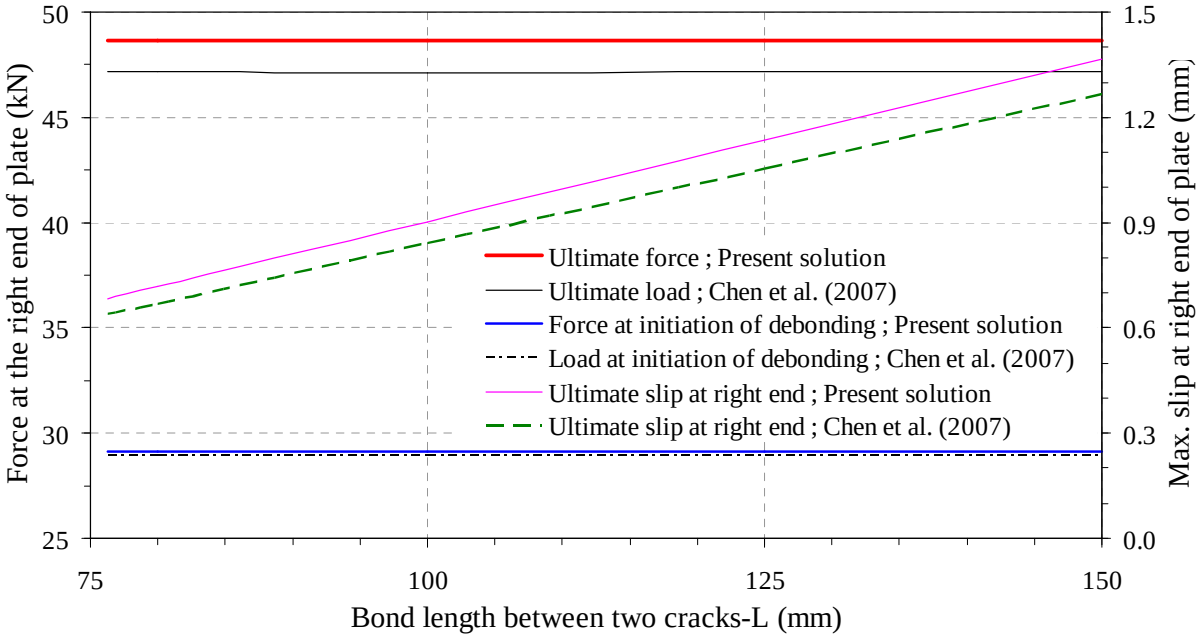

b) Force and displacement at right end of plate versus bond length.

Figure 8.9. Effect of bond length on plate end force and slip

8.9.2 Effect of moment (load) ratio β

Figures 10a-c show the predicted load-displacement responses with the moment ratio between the left and right ends β = 0, 0.7, 0.8, 0.85, 0.9, 0.95 and 0.98. The predicted force at the initiation of debonding (the height of the plateau) remains the same for both solutions and it is not affected by the moment ratio. The ultimate load and ultimate displacement at the right end increase almost linearly up to β = 0.7. They increase more quickly when β increases from 0.7 to 0.9, and steeply when it further increases from 0.9 to 1. The differences of the ultimate load and ultimate displacement from the present and the reference predictions increase from 0.2% to 3.6% and from 4.4% to 8.3% respectively with as β increase from 0 to 0.98.

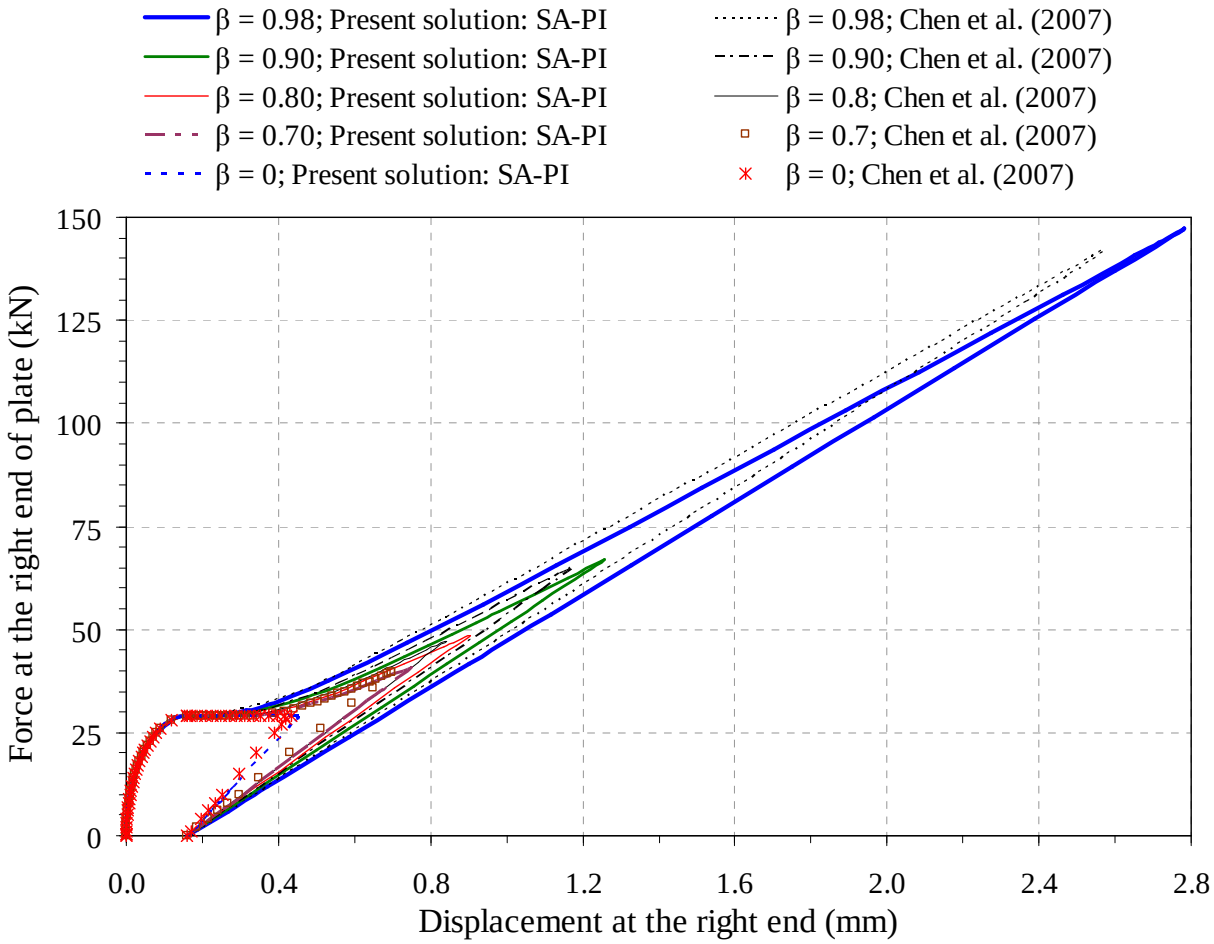

a) Load-displacement curve

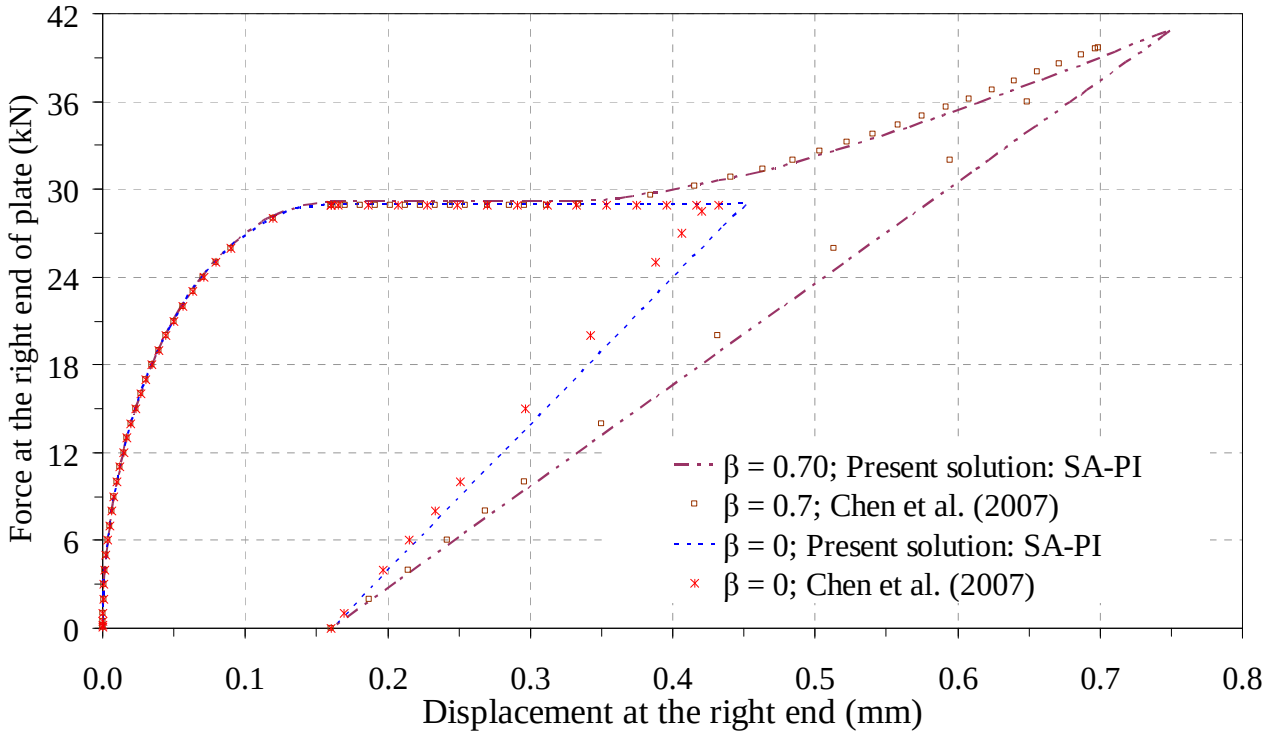

b) Load-displacement curve for β = 0 & 0.7

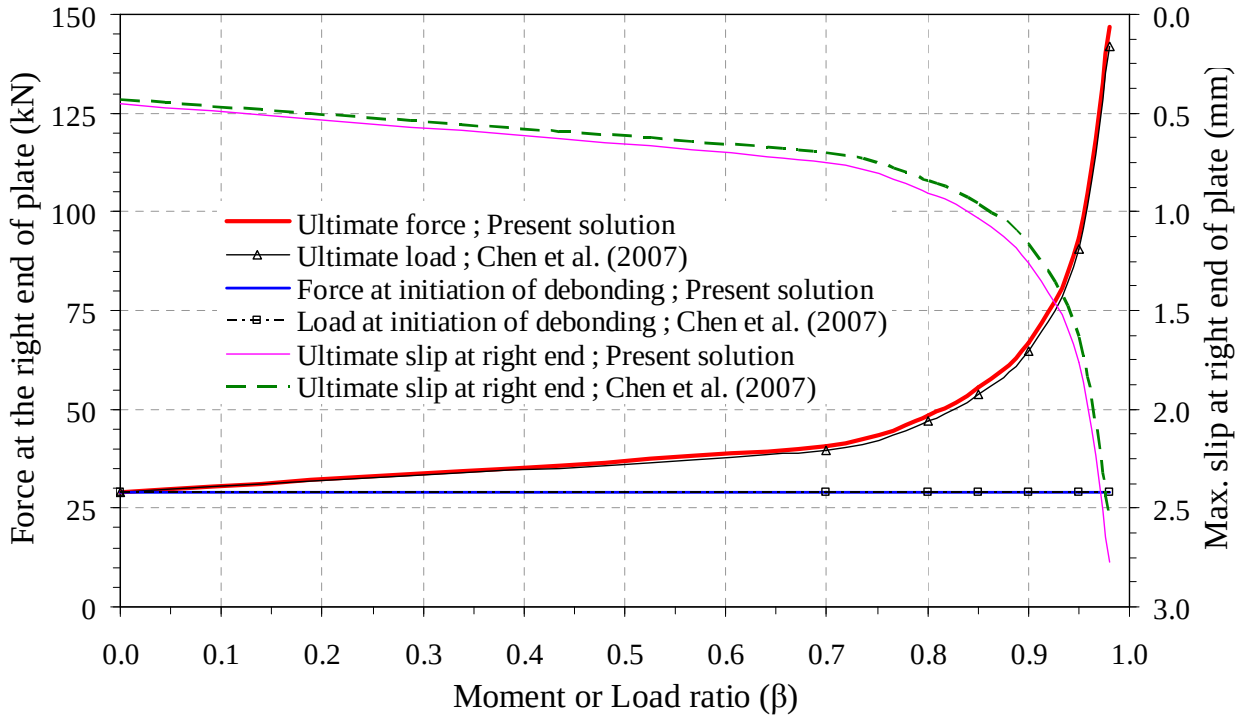

c) Effect of moment ratio β on force and displacement at right end of plate.

Figure 8.10. Effect of moment ratio β

8.9.3 Effect of axial stiffness of plate E_2A_2

The effect of the axial stiffness of the plate was studied with E_2A_2 = 0.001, 1, 3, 5.3, 10.6, 16 and 20 MN. The bond length is kept at 150 mm here as a small but the effective bond length exceeds 100mm in some of the cases. The force at the initiation of debonding remains almost the same in all the cases from both solutions and increases gradually with E_2A_2 (Figures 8.11a–b). The predicted ultimate load increases with the increase in E_2A_2. Its difference between the present solution and the reference solution also increases with E_2A_2 from 0.1% to 10.8% as shown in Figures 8.11a–b. The increase of the ultimate load occurs at the cost of ductility of the bonded joint. The ultimate displacement at the right end decreases steeply with the increase in E_2A_2 when it is small (E_2A_2 less than 3MN in Figure 8.11b) and reduces gradually with further increase in E_2A_2. The present solution predicts a 0.2% to 26% larger value than the reference solution within the considered range of E_2A_2 as in Figure 8.11b.

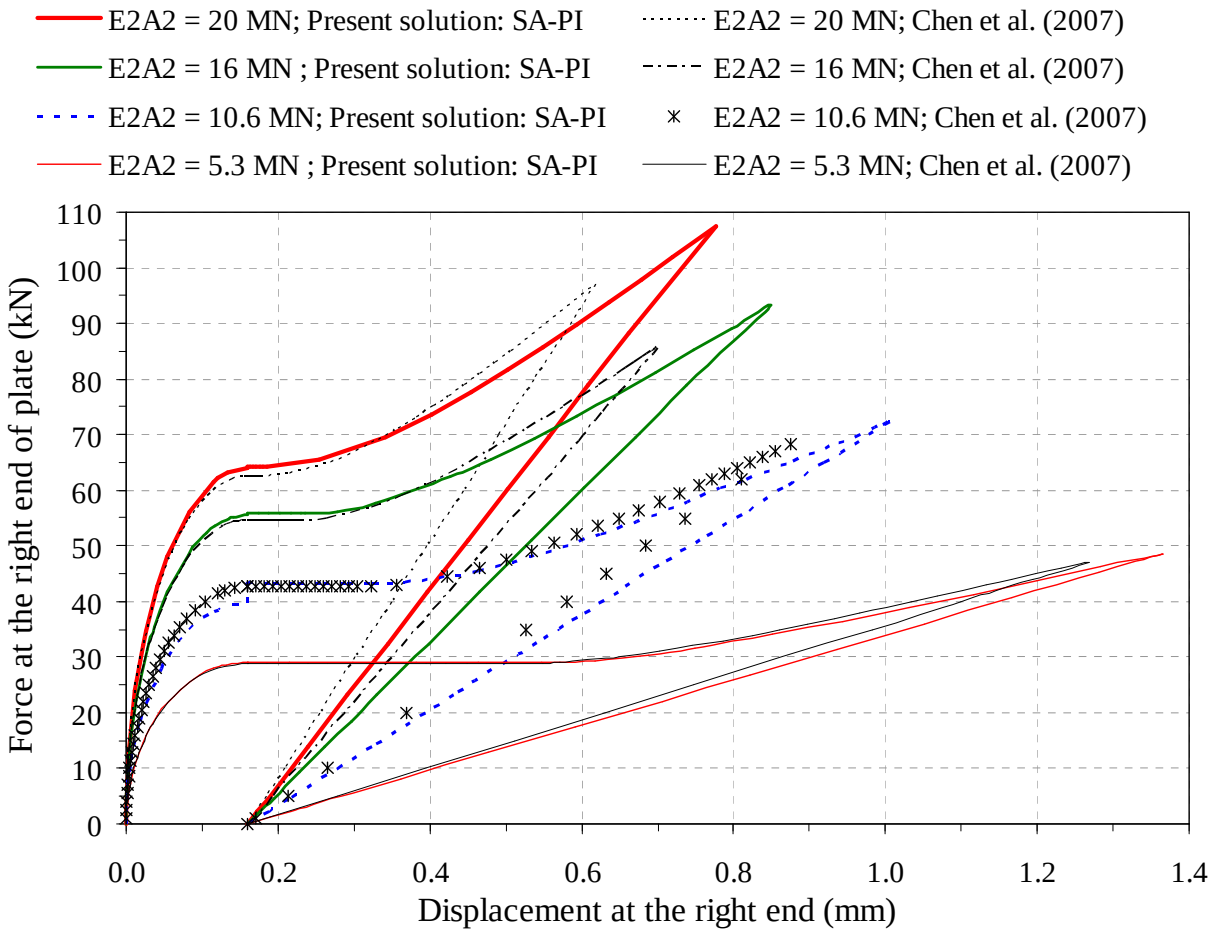

a) Load-displacement curves

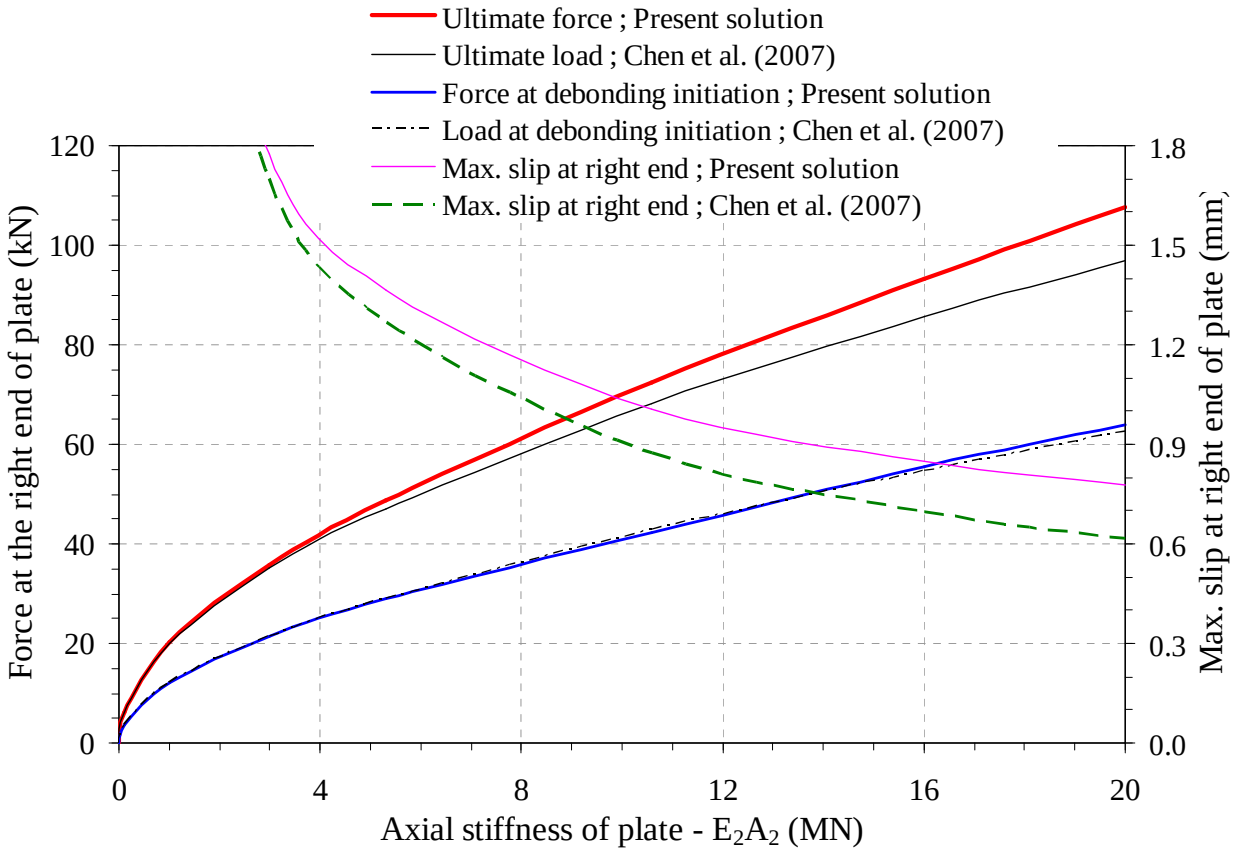

b) Effect of axial stiffness of plate on force and displacement at right end

Figure 8.11. Effect of axial stiffness of plate E_2A_2 on load-displacement characteristics and force and displacement at right end of plate

The distribution of interfacial shear stress and the axial normal stress in the plate at two different levels of the applied moment at the right end predicted from present solution are shown in Figures 8.12a–b. The bond stress at the two ends decreases when the plate axial stiffness E_2A_2 decreases at a given bending moment at the right end. The plate with lower E_2A_2 debonds before the one with higher E_2A_2. A higher axial stiffness effectively delays the debonding initiation and its propagation. The softening lengths near both ends and the axial normal stress in the plate increase with the decrease in E_2A_2 during S–R–S state under the same applied load.

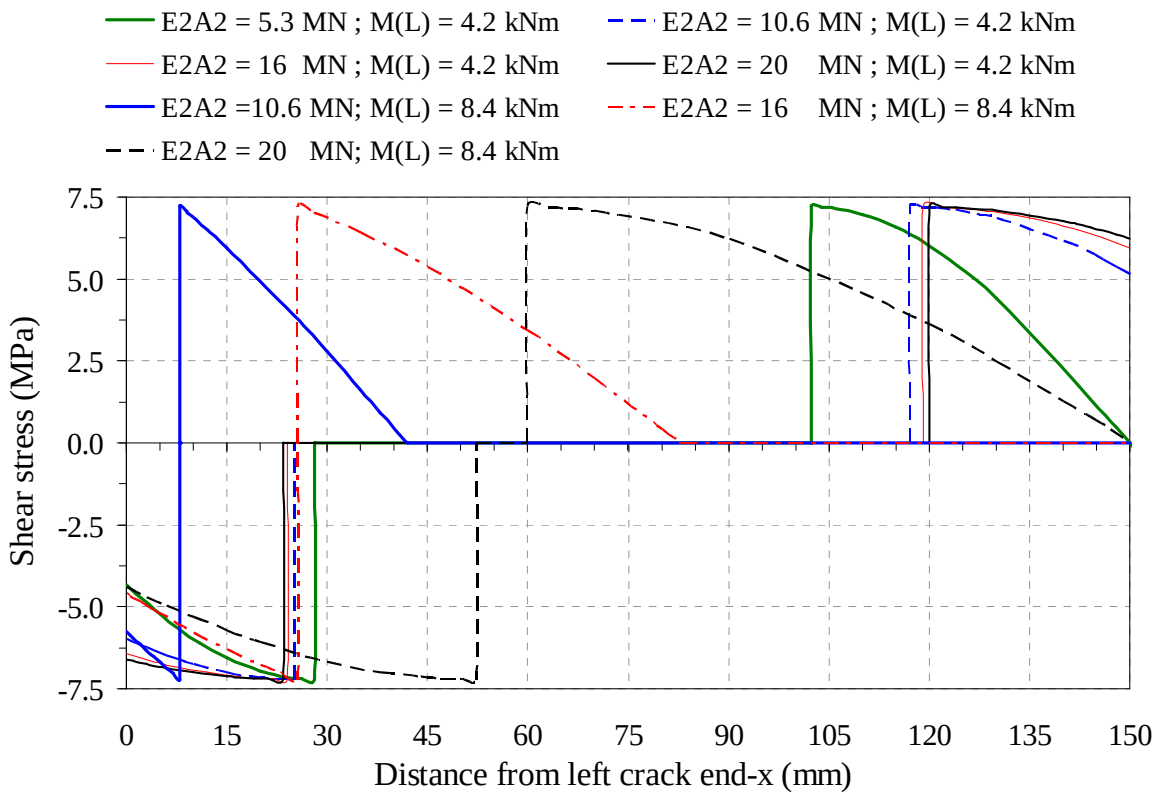

a) Interfacial shear stress

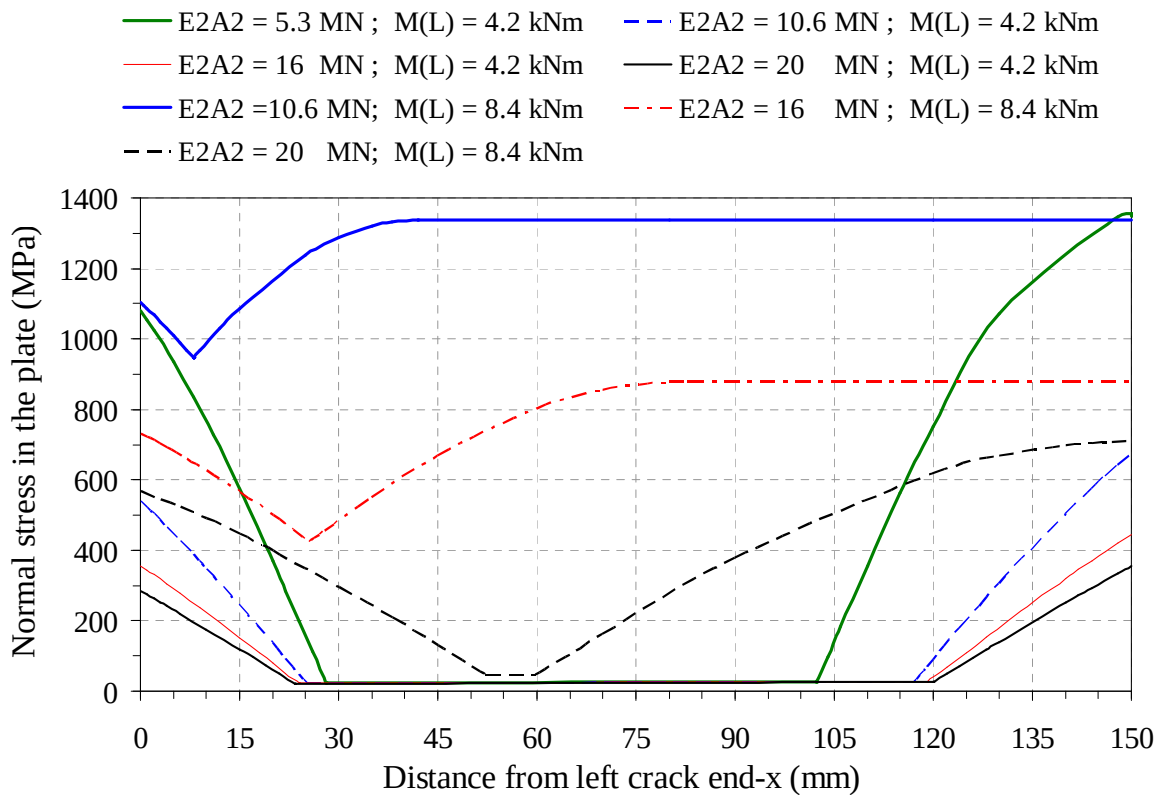

b) Axial normal stress in the plate

Figure 8.12. Effect of axial stiffness of plate E_2A_2 on distribution of interfacial shear stress and axial normal stress in the plate

8.9.4 Effect of beam depth t_1

The effect of beam depth is studied for L = 150 mm and E_2A_2 = 16.3 MN (with E_2 = 130 GPa and t_2 = 1 mm). The beam depth was varied with t_1 = 100, 125, 155, 190, 225, 300 and 400 mm. The force at the initiation of debonding decreases gradually with the increase in beam depth and its prediction from present solution is very marginally higher than that of the reference solution (Figures 8.13a-b). The ultimate load reduces with an increase of t_1. Its difference with the reference solution also decreases from 24.3% to 6.3% as t_1 increases. The ultimate displacement at the right end from present solution is 60.1% higher than the reference solution for t_1=100 mm but this difference decreases to 15.6% when t_1 = 400mm. The ultimate displacement decreases slowly with the increase in beam depth whilst the same prediction from reference solution increases.

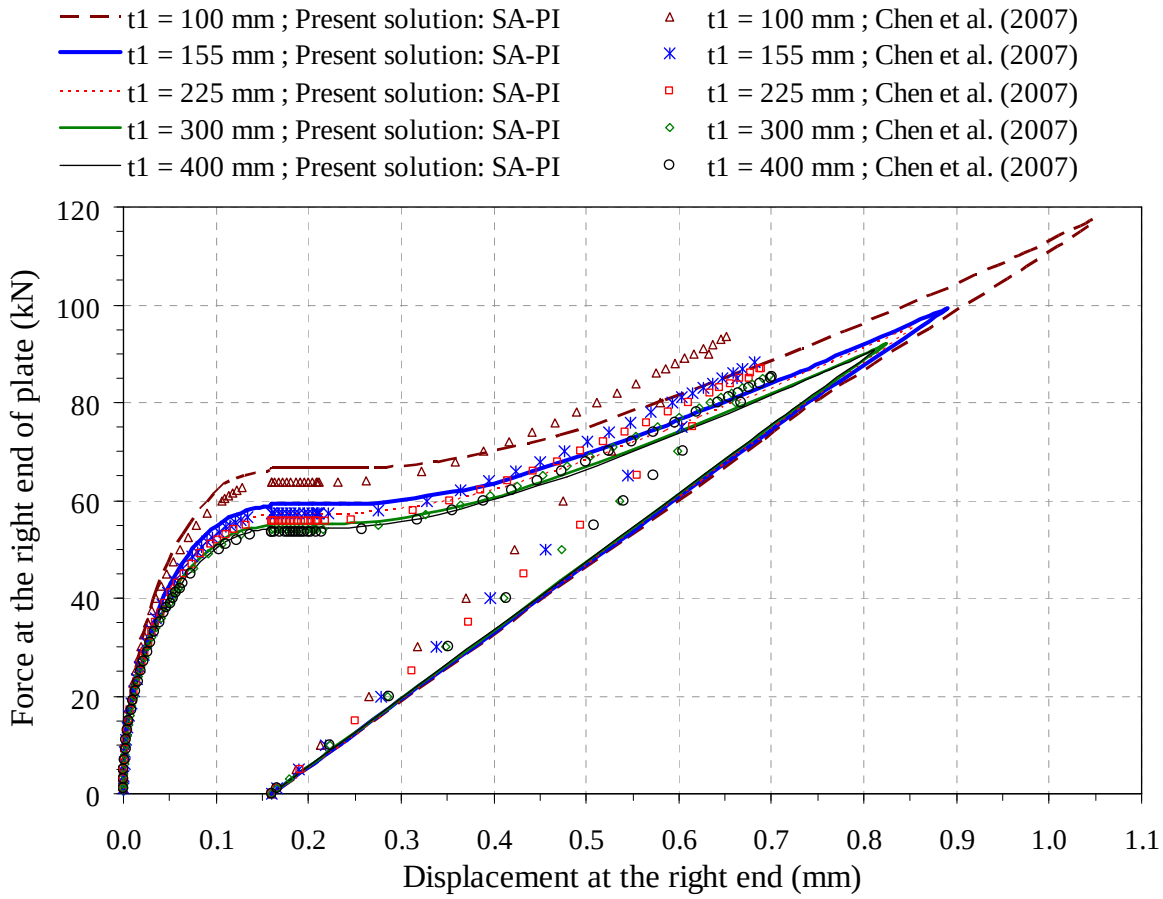

a) Load-displacement curve

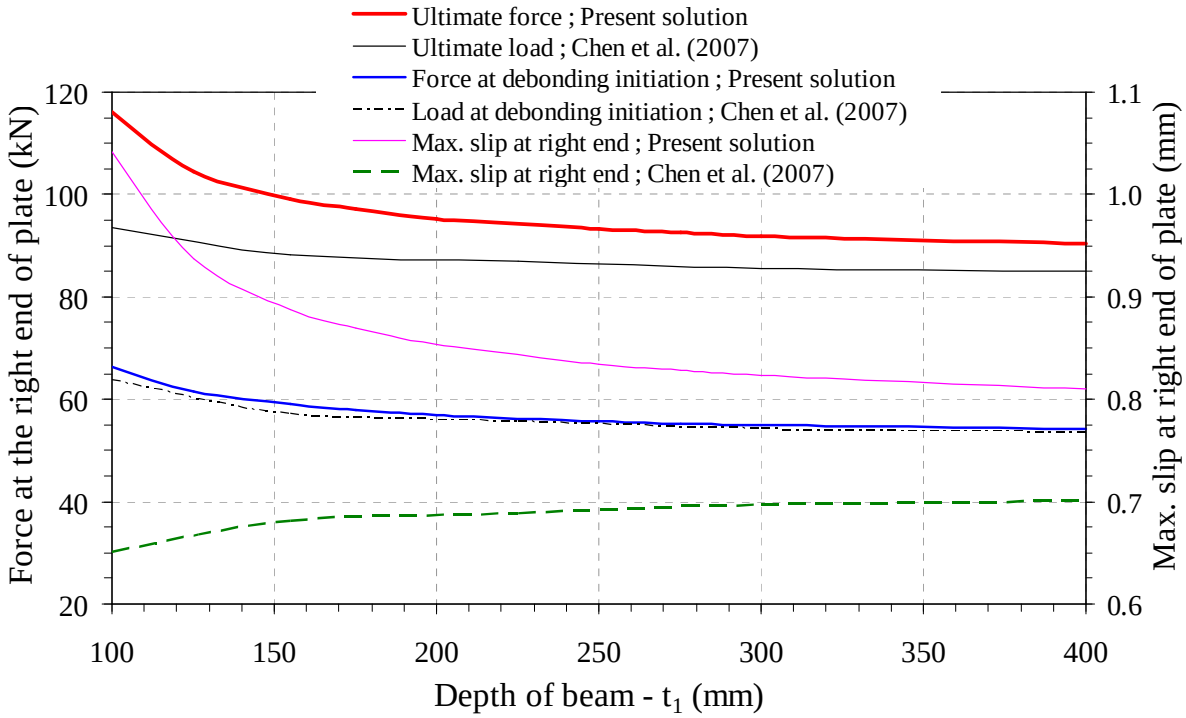

b) Effect of beam depth on force and displacement at right end of plate

Figure 8.13. Effect of beam depth t_1

8.9.5 Effect of beam width b_1

The effect of the width b_1 of the beam was studied with its value = 125, 155, 200 and 225 mm. The bond length and axial stiffness of plate were the same as in section 8.9.4. The beam width variation has less significant effect on the predictions as shown in Figures 8.14a–b, but the difference between the predictions of present and reference solutions remains similar to that discussed in section 8.8.2.

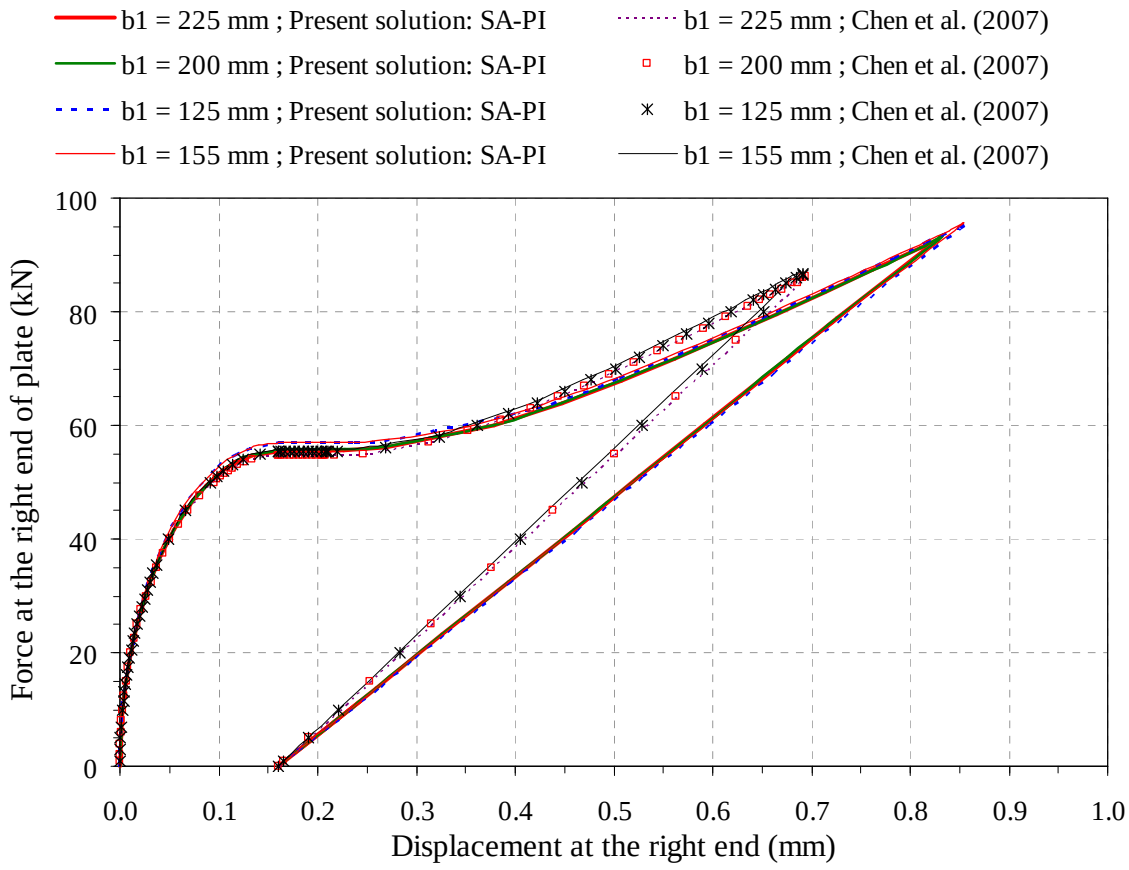

a) Load-displacement curve

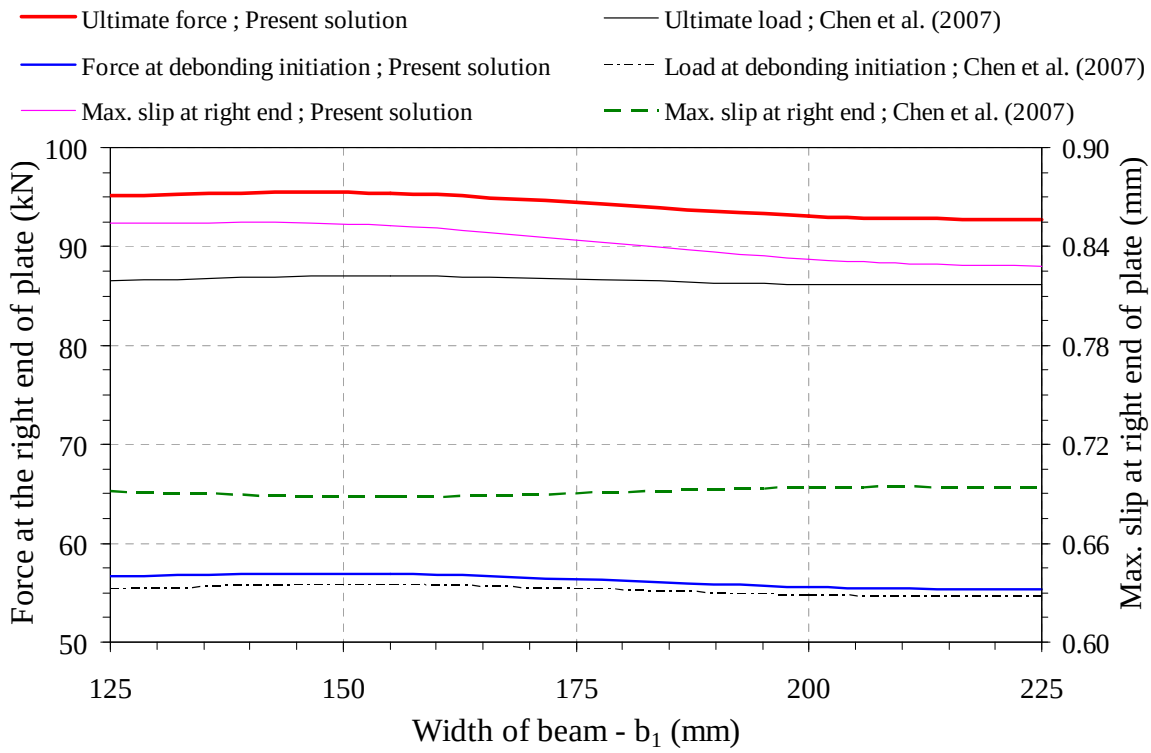

b) Effect of beam width b_1 on force and displacement at right end of plate

Figure 8.14. Effect of beam width b_1

8.9.6 Effect of steel ratio ρ

The bond length and axial stiffness of plate were the same as in section 8.9.4. The effect of tensile steel reinforcement ratio was investigated with ρ = 0.5, 1.0, 1.5 and 1.8%. Figures 8.15a–b show that the force at the initiation of debonding, ultimate load and ultimate slip at the right end decrease steadily with the increase in steel reinforcement ratio but their decrease becomes negligible after ρ = 1.5 %. This is because a small steel reinforcement ratio results in a higher curvature which in turn leads to higher axial forces in the strengthening plate. The prediction from reference solution is unaffected by changes in ρ.

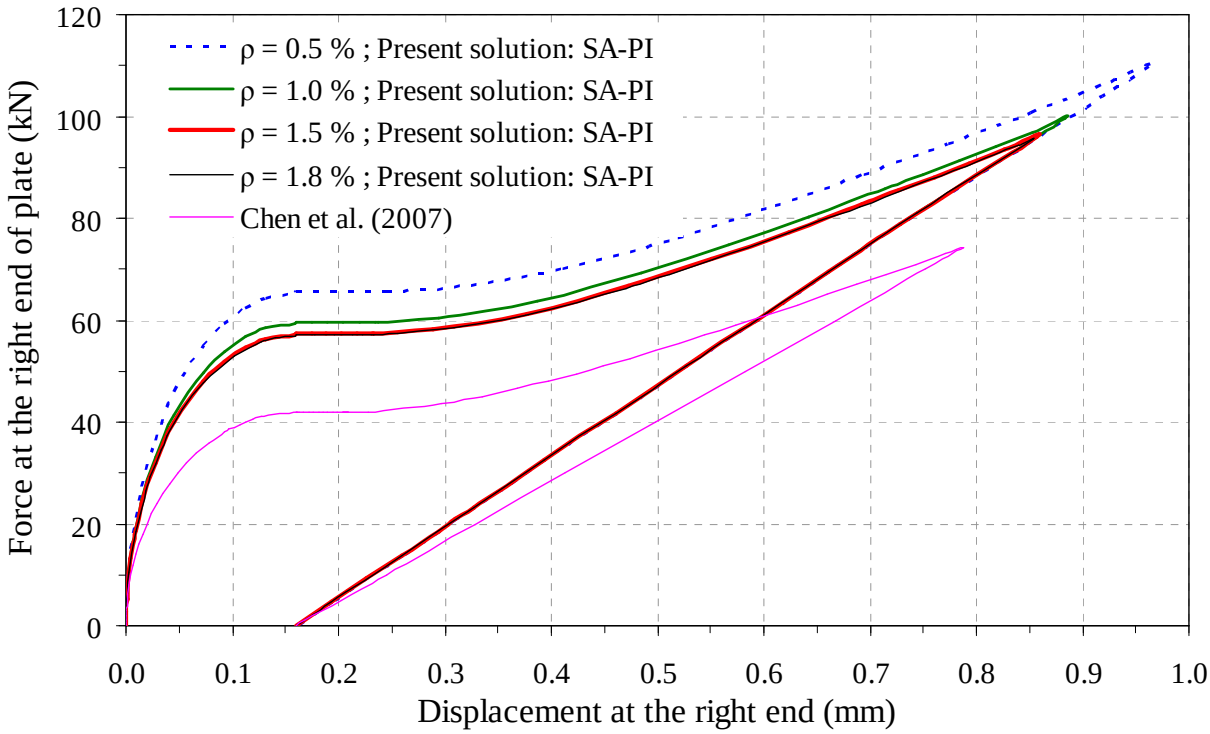

a) Load-displacement curves

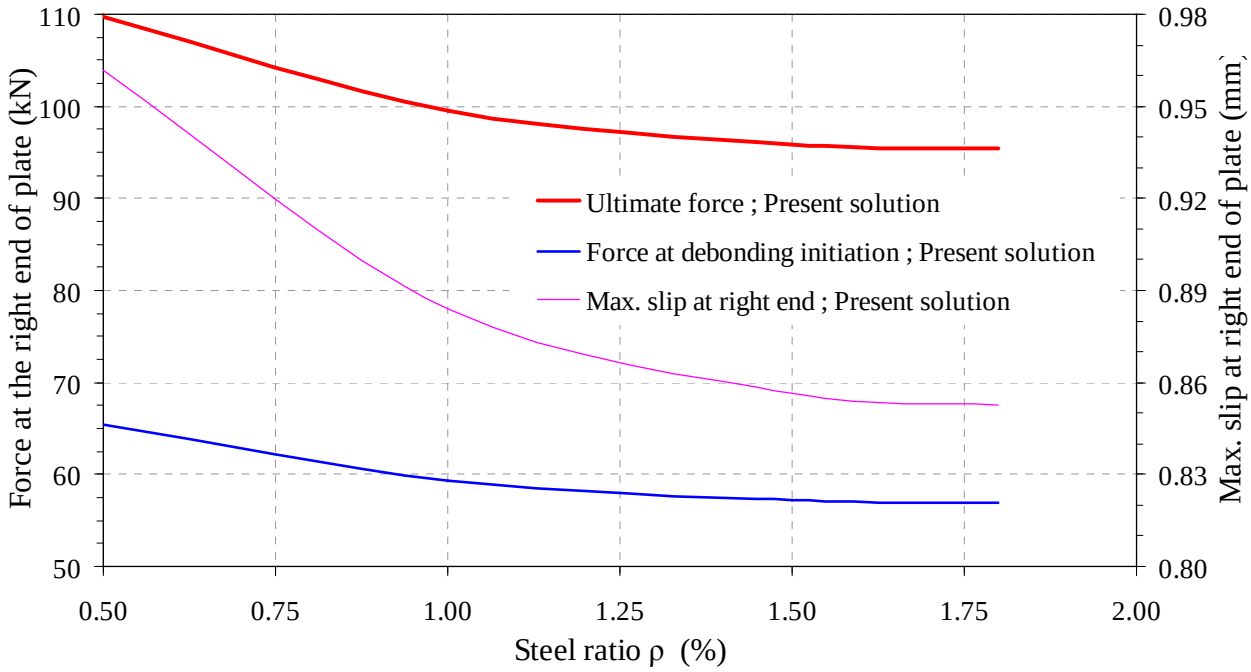

b) Effect steel ratio reinforcement ρ on force and displacement at right end of plate

Figure 8.15. Effect of steel ratio ρ

8.9.7 Effect of bending deformation

The effect of bending deformation was studied by fixing the flexural rigidity of beam and plate to a very large value. The predictions from present solution neglecting bending effects matches with the reference solution for $\eta = 0$ or 1 as shown in Figure 8.16. This is because when *EI* is very large, the present solution predicts $\eta = 0$ and curvature =0. Both the predicted ultimate capacity and ductility of the bonded joint are reduced when the bending deformation is ignored as in the reference solution. This shows that the effect of flexural deformation in adherends is beneficial in terms of ultimate capacity and slip.

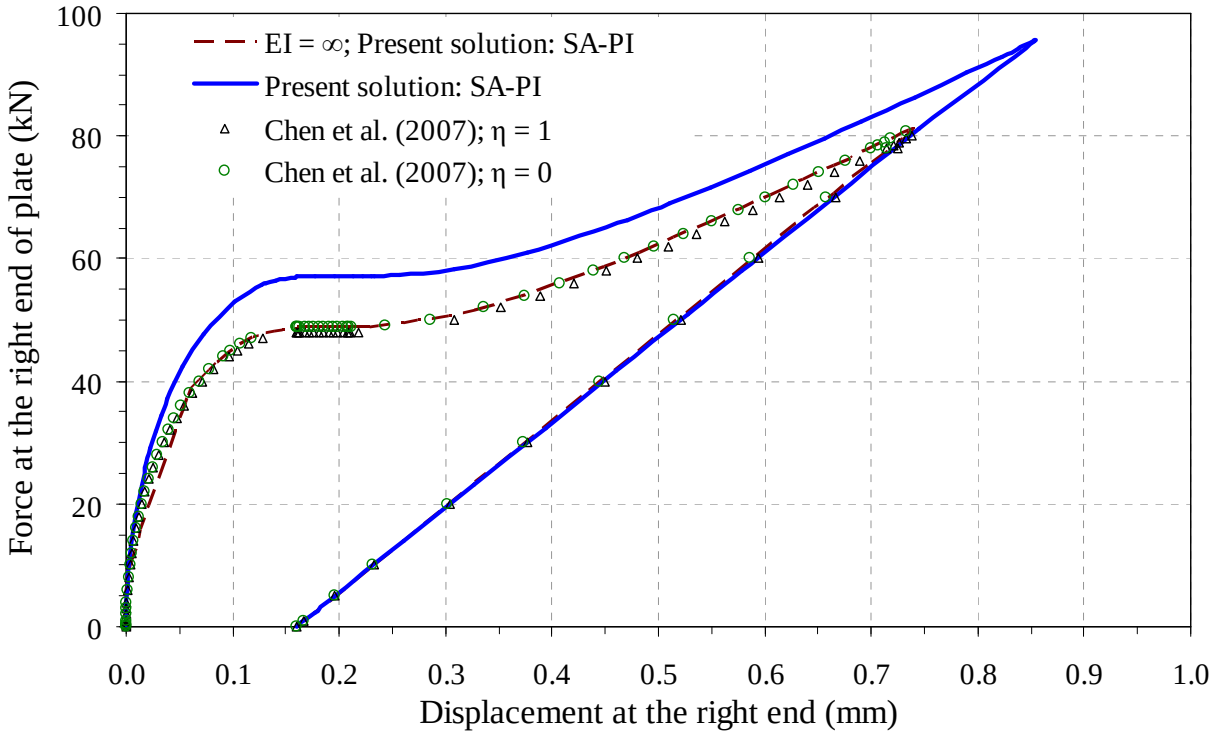

Figure 8.16. Effect of flexural deformation on load-displacement characteristics

8.10 Conclusions

This chapter has presented a study on the structural mechanics modelling of the full range of behaviour of intermediate crack induced debonding (ICD) failure of FRP or steel-concrete interface between two adjacent flexural cracks in plated reinforced concrete (RC) beams. The bonded joint is analysed considering axial forces, transverse shear forces and bending moments in the adherends employing a linearly softening bond-slip law. Full closed-form solutions for the entire loading process, including the stress and deformation distribution and load and deformation at various key stages such as debonding initiation and ultimate state have been developed.

In developing the solutions, the interface deformation has been related to the applied loading using two methods: the rotational spring method and the section analysis with partial interaction method. The accuracy of the RSM relies on the coefficients of the rotational springs which are used to simulate the local flexibility at the two cracks but these cannot be determined easily. On the other hand, the SA-PI method does not require any additional properties and more importantly, is accurate.

The solution provides a higher ultimate capacity and increased ductility compared to the bonded joint model based on double shear pull-off test specimen. Exploitation of the present solution in predicting the type-2 IC debonding failures in FRP strengthened RC members is being explored. Parametric studies demonstrated the significant effect of bond length, moment ratio between two cracked ends, axial plate stiffness, beam depth and width, steel ratio and flexural deformation on the load-displacement characteristics of the bonded joint.

8.11 Notation

The following symbols are used in this paper:

A = cross-sectional area;

b = width;

d_s , d_p = distances from the extreme concrete compression fibre to the centroid of steel rebar and plate respectively;

E = modulus of elasticity;

f_{cu} = cube compressive strength of concrete;

f_y = yield strength of steel reinforcements;

f_p = tensile strength of FRP;

G_f = fracture energy (area under the local bond-slip curve);

I = second moment of area;

L = bond length (distance between two adjacent cracks);

l = effective span of a plated beam;

$M(x)$ = bending moment;

$M_T(x)$ = total bending moment on a section in the plated beam;

M_{Td} = total bending moment at initiation of debonding;

M_{Tu} = total bending moment at ultimate state;

$N(x)$ = axial force;

$N_T(x)$ = total axial force at a section of the plated beam;

P = applied transverse load;

t = thickness;

u = longitudinal displacement;

v = vertical displacement;

$V(x)$ = shear force;

$V_T(x)$ = total shear force at a section of the plated beam;

y_1, y_2 = vertical distance from bottom of the beam and top of the plate to their respective centroids;

y = neutral axis depth of cracked plated section from the compression fibre;

β = ratio between moments at left and right adjacent cracks;

$\delta(x)$ = interfacial slip at x;

δ_1 = slip corresponding to the attainment of τ_f;

δ_f = maximum slip at initiation of debonding;

ε_{cf} = extreme compression fibre strain of concrete;

$\varepsilon_{ct}(x)$ = tensile strain at the soffit of beam;

η = ratio between axial forces in the beam and plate;

λ, m, m_1 = parameters defined respectively by Eqs 8.10b-c and 8.15d;

$\sigma(x)$ = interfacial normal stress;

$\tau(x)$ = interfacial shear stress;

τ_f = bond strength;

$1, a, 2, s$ = subscripts referring respectively to the beam, adhesive, plate and tensile steel reinforcement.

Chapter 9

Conclusions and Future Work

9.1 Introduction

Extensive research has proven that external adhesive bonding of a fibre reinforced polymer (FRP) composite, steel or any other metallic plate to the tension face of a reinforced concrete (RC), metal or timber beam can effectively enhance its strength and structural performance. This technique has found wide application in retrofitting and rehabilitating many existing structures around the world without disturbing the surrounding environment. Unfortunately, these plated beams are susceptible to premature debonding failure in service that occurs well before the full flexural capacity of the plated section is reached. Interfacial stress concentrations in the vicinity of the plate end and intermediate flexural/flexural-shear crack locations are attributed to be responsible for these premature failures. Further research is essential to more confidently relate these interfacial stresses directly to debonding failures. The research reported in this thesis presents a contribution towards this goal.

This research provides notable contributions to the theory of plated beams, particularly in analysis of the interfacial stresses; in understanding the real effect of shear deformation of beam and plate on interfacial stresses; developing the new technique of deducing interfacial stresses from experimental plate strain measurements; providing a first interfacial fracture mechanics flexural debonding model acquiescent for further improvement; proposing simple shear and shear-bending interaction debonding models; and advancing the current understanding of type-2 ICD behavior in plated beams.

This chapter highlights the key conclusions drawn from each core chapter and provides recommendations for extension of this research in the future.

9.2 Conclusions

9.2.1 Simple general theoretical solution for interfacial stresses

A simple, accurate and a robust interfacial stress solution applicable to any loading arrangements, any beam cross-section, any thickness of bonded plate and any material for plate and beam within linear elastic range has been provided in Chapter 2. This solution is based on the principle of superposition and compatibility of longitudinal and vertical deformations at adhesive interfaces between beam and plate. Accuracy is validated by comparison with the most famous solution of Smith and Teng (2001) and finite element (FE) analysis. The ability of the technique to treat arbitrary loading arrangements, beam cross-section, and material properties are demonstrated by suitable illustrations.

9.2.2 Effect of shear deformation on interfacial stresses

The first solution to consider the effect of adherends shear deformation on both interfacial shear and normal stresses is presented in Chapter 3. The shear deformation effect on interfacial shear stress is based on a reasonable approximation of displacement field and on interfacial normal stress is through Timoshenko's beam theory. This solution provides an assessment of shear deformation effects.

9.2.3 Rigorous closed-form solution for interfacial stresses

A rigorous closed-form theoretical solution for interfacial shear and normal stresses is provided in Chapter 4. This solution treats the plated beam as bi-Timoshenko beams and explains the real effect of shear deformation on interfacial shear and normal stresses. This provides a better understanding and accuracy in its predictions that agree well with FE predictions. This study has shown that the effect of the shear deformation of the adherends is insignificant for the interfacial shear stress, but significant for the interfacial normal stress.

9.2.4 A new technique for deduction of interfacial stresses from experiments

Chapter 5 discusses the development of a new technique to interpret interfacial stresses from experimentally measured plate strains. The advantage of this technique over the traditional deduction method is demonstrated. In addition to interfacial shear stresses it provides peeling stresses taken account of the effect of flexural deformations in beam and plate. The technique is applicable to all loading arrangements. This chapter also provides analysis of total, axial and bending strains in plate and its comparison with simple beam theory and experimental measurements.

9.2.5 Plate end flexural debonding models for plated beams

Chapter 6 reports the development of a first interfacial fracture mechanics based flexural plate end debonding (PED) model for the plates terminated in a pure bending region. This model provides a reasonable accuracy when assessed against a carefully constructed large flexural debonding test database of 67 FRP and steel plated RC beams reported to have failed by PED. A semi-empirical model with highest accuracy is developed based on theoretical model and test database. A phenomenological model entirely based on test results is also provided that is slightly less accurate but simpler than the semi-empirical model. The latter two models are shown to be the accurate among all existing and proposed models.

9.2.6 Strength model for plate end debonding in FRP and steel plated beams

A shear debonding model for plates terminated in high shear and zero (or low) moment regions is presented in Chapter 7. This model is simple, accurate and provides an explicit prediction comparing all existing models. This model and an accurate flexural debonding model in Chapter 6 are shown to be the two extreme cases and a better shear-bending interaction model applicable for plates terminated in any shear-bending interaction region is proposed by the coupling of these two extreme models. A large test database of plated RC beams reported to have failed by PED with 226 test results was used to assess the performance of existing and the proposed debonding strength models. Comparisons between test results and the predictions of the debonding strength models demonstrate the simplicity and the accuracy of the proposed model that can readily be incorporated in design codes and guidelines.

9.2.7 Theoretical formulation and parametric study of ICD in plated beams

A structural mechanics model that characterises type-2 intermediate crack induced interfacial debonding (ICD) behaviour using a local softening interface bond-slip law is provided in Chapter 8. Solutions for the full range of behaviour of ICD including debonding initiation, propagation and total failure of the FRP-concrete interface between two flexural cracks in an FRP strengthened RC member are presented that cover different states of interfaces in different possible failure processes. The interface deformation is related to the applied loading through the rotational spring method and the section analysis with partial interaction method and the merits and extent of applicability of both the methods are discussed. Parametric studies highlight the effect of flexural deformation on type-2 ICD behaviour. The present solution predicts higher ultimate capacity and deformation compared to Chen et al.'s (2007) solution that neglected the bending deformation of the adherends. While the emphasis of the study is on FRP-concrete bonded joints, the solution and methodology are applicable to similar joints between other materials such as FRP-to-steel or steel or aluminium-to concrete bonded joints.

9.2.8 Summary

This research in brief provides a simple-generic theoretical solution for assessment of interfacial stress concentrations at plate ends; clarifies the effect of adherend's shear deformation on interfacial stresses; offers a novel technique for interpreting interfacial shear and normal stresses from experiments; provides a first interfacial fracture mechanics based theoretical model of reasonable accuracy, a semi-empirical and an empirical model of improved accuracies for flexural PED; gives a simple and accurate pure shear and a shear-bending interaction PED models; and presents structural mechanics formulations for characterising type-2 ICD behaviour in plated RC beams that highlights the effect of flexural deformation and shows the application of a method to relate applied loading and interface deformations.

9.3 Future work

The study presented in this thesis has improved the understanding of the interfacial stresses and prediction of debonding failures in plated beams. Further studies that may be beneficial are recommended as follows.

9.3.1 Simplified generic solution for interfacial stresses

The simple generic solution presented in Chapter 1 can be further simplified; extended to curved plated beams; developed to analyse interfacial stresses in stepped plated beams; and extended to predict interfacial stresses in tension steel reinforcement-concrete interfaces.

9.3.2 Parametric study of the effect of shear deformation on interfacial stresses

A thorough parametric study using FE analysis of plated beams with Timoshenko beam elements and comparison with the present solution in Chapter 4 could provide a complete understanding of the effect of shear deformation of adherends on interfacial stresses.

9.3.3 Simplified technique to deduce interfacial stresses from experiments

There exists a possibility to simplify the technique presented in Chapter 5 so that it is well received and utilised by experimentalists in future.

9.3.4 Mixed mode interfacial fracture mechanics based plate end debonding model

Mode-I interfacial fracture effect can be included with the mode-II effect already considered in fracture mechanics based flexural debonding model to make it a more complete theoretical model whose accuracy may be better.

The above model can be applied to develop a pure shear debonding model and then a complete mechanics based shear-bending interaction model.

9.3.6 Interfacial stress based PED model

The simple interfacial stress solution in Chapter 1 and the large test database in Chapter 7 can be used together to evolve a better interfacial stress based plate end debonding model that will certainly be more accurate than the existing models of this kind.

This model can also be assessed with the phenomenological and interfacial fracture mechanics based plate end debonding models so that a very good plate end debonding model can be recommended for design use.

9.3.7 Interfacial fracture mechanics based ICD model

The solution presented in Chapter 8 could be utilised to develop a fracture mechanics based ICD model. A large test database similar to that in chapter 7 can be constructed to assess the accuracy of the proposed model that could be implemented in any design codes or guidelines.

9.3.7 Effect of adhesive on ICD behaviour

Effect of adhesive is not well understood in theory for both type-1 and type-2 IC debonding behaviour. Only experimental observations that lack any theoretical explanation currently exist and this requires further research.

References

Abdelouahed, T. (2006). "Improved theoretical solution for interfacial stresses in concrete beams strengthened with FRP plate". *International Journal of Solids and Structures*, 43, 4154–4174.

Abdelouahed, T., Hassaine, D.T., Benyoucef, S., and Adda bedia, E.A. (2009). "Interfacial stresses in FRP-plated RC beams: effect of adherend shear deformations". *International Journal of Adhesion and Adhesives*, 29 (4), 343–351.

ACI 318-02 (2002). *Building code requirements for structural concrete (318-02) and commentary (318R-02).* USA: American Concrete Institute (ACI).

ACI 440.2R-02 (2002). *Guide for the design and construction of externally bonded FRP systems for strengthening concrete structures*. USA: American Concrete Institute (ACI).

Ahmed, O. and van Gemert, D. (1999a). "Effect of longitudinal carbon fiber reinforced plastic laminates on shear capacity of reinforced concrete beams". *In: Dolan, C.W., Rizkalla, S.H. and Nanni, A., (eds.), Proceedings of the Fourth International Symposium on Fiber Reinforced Polymer Reinforcement for Reinforced Concrete Structures*, Maryland, USA, 933–943.

Ahmed, O. and van Gemert, D. (1999b). "Behaviour of RC beams strengthened in bending by CFRP laminates". *In: Forde, M.C., (ed.), Proceedings of the Eighth International Conference on Advanced Composites for Concrete Repair*, London, UK.

Ahmed, O., van Gemert, D. and Vanderwalle, L. (2001). "Improved model for plate end shear of CFRP strengthened RC beams". *Cement & Concrete Composites*, 23(1), 3–19.

Ali, M.S., Oehlers, D.J. and Park, S.M. (2001). "Comparison between FRP and steel plating of reinforced concrete beams". *Composites: Part A*, 32(9), 1319–1328.

ANSYS Release 10.0 (2005). *User's manual*. *ANSYS Inc*., USA.

Aprile, A. and Feo, L. (2007). "Concrete cover rip-off of R/C beams strengthened with FRP composites". *Composites: Part B* 38, 759–771.

Barenblatt, G.I. (1962). "The mathematical theory of equilibrium cracks in brittle fracture". *Advances in Applied Mechanics*, 7, 55–129.

Beber, A.J., Filho, A.C. and Campagnolo, J.L. (1999). "Flexural strengthening of RC beams with CFRP sheets". *In: Forde, M.C. (ed.), Proceedings of the Eighth International Conference on Advanced Composites for Concrete Repair*, London, UK.

Bizindavyi, B.L. and Neale, K.W. (1999). "Transfer lengths and bond strengths for composites bonded to concrete". *ASCE Journal of Composites for Construction,* 3, 153–160.

Breña, S.F. and Macri, B.M. (2004). "Effect of carbon-fiber-reinforced polymer laminate configuration on the behavior of strengthened reinforced concrete beams". *ASCE Journal of Composites for Construction*, 8(3), 229-40.

Brosens, K. and Van Gemert D. (1998). "Plate end shear design for external CFRP laminates". *In: Proceedings of FRAMCOS-3,* Freiburg (Germany): Aedificatio Publishers; 1793–1804.

BS 8110 (1997). *Structural use of concrete-part 1: Code of practice for design and construction.* London: British Standards Institute.

Casas, J.R. and Pascual, J. (2007). "Debonding of FRP in bending: Simplified model and experimental validation". *Construction and Building Materials*, 21,1940-1949.

Ceroni, F., Manfredi, G. and Pecce, M. (2001). "Crack width in RC beams strengthened with carbon fabrics". *In: Proceedings of the fifth international conference on FRP plastics for reinforced concrete structures,* 917–926.

Chajes, M.J., Finch Jr., W.W., Januszka, T.F. and Thomson Jr., T.A. (1996). "Bond and force transfer of composites materials plates bonded to concrete". *ACI Structural Journal*, 93, 209–217.

Chajes, M.J., Januszka, T.F., Mertz, D.R., Thomson Jr., T.A. and Finch Jr., W.W. (1995). "Shear strengthening of reinforced concrete beams using externally applied composite fabrics". *ACI Structural Journal*, 92, 295–303.

Chen, F. and Qiao, P. (2009). "Debonding analysis of FRP–concrete interface between two balanced adjacent flexural cracks in plated beams". *International Journal of Solids and Structures*, 46, 2618–2628.

Chen, J.F. and Teng, J.G. (2001). "Anchorage strength models for FRP and steel plates bonded to concrete". *ASCE Journal of Structural Engineering*, 127 (1), 784–791.

Chen, J.F., Teng, J.G. and Yao, J. (2006). "Strength model for intermediate crack debonding in FRP-strengthened concrete members considering adjacent crack interaction". *In: Proceedings of the Third International Conference on FRP Composites in Civil Engineering (CICE2006),* December 13-15, Miami, Florida, USA, 67-70.

Chen, J.F., Yang, Z.J. and Holt, G.D. (2001). "FRP or steel plate-to-concrete bonded joints: effect of test methods on experimental bond strength". *Steel and Composite Structures*, 1(2), 231-244.

Chen, J.F., Yuan, H. and Teng, J.G. (2007). "Debonding failure along a softening FRP-to-concrete interface between two adjacent cracks in concrete members". *Engineering Structures*, 29, 259–270.

Colotti, V., Spadea, G. and Swamy, R.N. (2004). "Structural model to predict the failure behaviour of plated reinforced concrete beams". *ASCE Journal of Composites for Construction*, 8(2), 104–122.

Dai, J., Ueda, T. and Sato, Y. (2005). "Development of the nonlinear bond stress-slip model of fiber reinforced plastics sheet–concrete interfaces with a simple method". *ASCE Journal of Composites for Construction*, 9, 52–62.

David, E., Djelal, C., Ragneau, E. and Bodin, F.B. (1999). "Use of FRP to strengthen and repair RC beams: experimental study and numerical simulations". *In: Forde, M.C., (ed.), Proceedings of the Eighth International Conference on Advanced Composites for Concrete Repair*, London, UK.

De Lorenzis, L., Teng, J.G. and Zhang, L. (2006). "Interfacial stresses in curved members bonded with a thin plate". *International Journal of Solids and Structures*, 43, 7501-7517.

De Lorenzis, L. and Zavarise, G. (2008). "Modeling of mixed-mode debonding in the peel test applied to superficial reinforcements". *International Journal of Solids and Structures*, 45, 5419–5436.

Deng, J., Lee, M.K. and Moy, S.J. (2004). "Stress analysis of steel beams reinforced with a bonded CFRP plate". *Composite Structures*, 65, 205–15.

Dugdale, D.S. (1960). "Yielding of steel sheets containing slits". *Journal of the Mechanics and Physics of Solids*, 8, 100–104.

Etman, E.E., and Beeby, A.W. (2000). "Experimental programme and analytical study of bond stress distributions on a composite plate bonded to a reinforced concrete beam". *Cement concrete composites*, 22(4), 281–291.

Gao, B., Leung, C.K.Y. and Kim, J.K. (2005). "Prediction of concrete cover separation failure for RC beams strengthened with CFRP strips". *Engineering Structures*, 27(2), 177–189.

Garden, H.N. and Hollaway, L.C. (1998). "An experimental study of the influence of plate end anchorage of carbon fibre composite plates used to strengthen reinforced concrete beams". *Composite Structures*, 42, 175–188.

Garden, H.N., Hollaway, L.C. and Thorne, A.M. (1997). "A preliminary evaluation of carbon fibre reinforced polymer plates for strengthening reinforced concrete members". *Proceedings of the Institution of Civil Engineers: Structures and buildings*, SB123, 127–142.

Hau, K.M. (1999). *Experiments on concrete beams strengthened by bonding fibre reinforced plastic sheets*. M.Sc. thesis. The Hong Kong Polytechnic University.

Hein, V.L. and Erdogan, F. (1971). "Stress singularities in a two-material wedge". *International Journal of Fracture Mechanics*, 7(3), 317-330.

Hollaway, L.C. and Teng, J.G. (eds.) (2008). *Strengthening and Rehabilitation of Civil Infrastructures using Fibre-Reinforced Polymer (FRP) Composites*. Cambridge, England: Woodhead Publishing limited.

Johnson, R.P. (1994). *Composite Structures of Steel and Concrete*. England: Blackwell Scientific Publications.

Jones, K.R., Swamy, R.N. and Charif, A. (1988). "Plate separation and anchorage of reinforced concrete beams strengthened by epoxy bonded steel plates". *The Structural Engineer*, 66 (5/1), 85–94.

Juvandes, L., Figueiras, J.A. and Marques, A.T. (1998). "Performance of concrete beams strengthened with CFRP laminates". *In: Proceedings of the Second International Conference on Composites in Infrastructure (ICCI)*, Arizona, USA.

Lau, K.T., Shi, S.Q. and Zhou, L.M. (2001). "Estimation of stress intensity factor (KI) for an FRP bonded concrete beam using the superposition method". *Magazine of Concrete Research*, 53, 31–41.

Leung, C.K.Y. (2001). "Delamination failure in concrete beams retrofitted with a bonded plate". *Journal of Materials in Civil Engineering*, 13, 106–113.

Liu, I., Oehlers, D.J. and Seracino, R. (2004). "Parametric study of intermediate crack debonding on adhesively plated beams". *In: Seracino, R., (ed.), Proceedings of FRP Composites in Civil Engineering*, Taylor & Francis Group, London, 515-521.

Lu, X.Z., Ye L.P., Teng, J.G. and Jiang, J.J. (2005a). "Meso-scale finite element model for FRP sheets/plates bonded to concrete". *Engineering Structures*, 27(4), 564–575.

Lu, X.Z., Teng, J.G., Ye, L.P. and Jiang, J.J. (2005b). "Bond–slip models for FRP sheets/plates bonded to concrete". *Engineering Structures*, 27(6), 920–937.

Luo, W. (1993). *Strengthening of post tensioned and reinforced concrete beams by bonding external steel plates*. MSc thesis, University of Adelaide.

Malek, A.M., Saadatmanesh, H., and Ehsani, M.R. (1998). "Prediction of failure load of RC beams strengthened with FRP plate due to stress concentration at the plate end". *ACI Structural Journal*, 95(1), 142–152.

Miller, T.C., Chajes, M.J., Mertz, D.R. and Hastings, J.N. (2001). "Strengthening of a steel bridge girder using CFRP plates". *ASCE Journal of Bridge Engineering*, 6(6), 514–522.

Mohammed Ali, M.S. (2000). *Peeling of plates adhesively bonded to RC beams*. PhD thesis, University of Adelaide.

Mukhopadhyaya, P. and Swamy, R.N. (2001). "Interface shear stress: a new design criterion for plate debonding". *ASCE Journal of Composites for Construction*, 5(1), 44-56.

Narayanamurthy, V., Chen, J. F. and Cairns, J. (2009). "A new approach for interfacial stress analysis of beams with a bonded soffit plate". *In: Oehlers, D.J. and Seracino, R. (eds.), Proceedings of the Ninth International Symposium on Fiber Reinforced Polymer Reinforcement for Reinforced Concrete Structures (FRPRCS-9)*, Sydney, Australia.

Narayanamurthy, V., Chen, J. F. and Cairns, J. (2009). "A solution for plated beam including shear deformation effect". *In: Proceedings of Advanced Composites in Construction, (ACIC-09)*, Edinburgh, UK.

Narayanamurthy, V., Chen, J. F. and Cairns, J. (2010). "A general analytical method for the analysis of interfacial stresses in plated beams under arbitrary loading". *Advances in Structural Engineering*, 13 (5), 975-988.

Narayanamurthy, V., Chen, J. F., Cairns, J. and Ananth, R. (2011). "Effect of shear deformation on interfacial stresses of plated beams subjected to arbitrary loading". *International Journal of Adhesion and Adhesives, (under review).*

Narayanamurthy, V., Chen, J. F., Cairns, J. and Oehlers, D.J. (2011). "Plate end flexural debonding model for plated beams". *ASCE Journal of Composites for Construction, (under review).*

Neubauer, U. and Rostasy, F.S. (1999). "Bond failure of concrete fiber reinforced polymer plates at inclined cracks-experimental and fracture mechanics model". *In: Dolan, D.W., Rizkalla, S.H. and Nanni, A. (eds.), Proceedings of the Fourth International Symposium of Nonmetallic (FRP) Reinforcement for Concrete Structures*, Baltimore, USA, 369–382.

Nguyen, D.M., Chan, T.K. and Cheong, H.K. (2001). "Brittle failure and bond development length of CFRPconcrete beams". *ASCE Journal of Composites for Construction*, 5(1), 12-17.

Oehlers, D.J. (1992). "Reinforced concrete beams with plates glued to their soffits". *ASCE Journal of Structural Engineering*, 118(8), 2023–2038.

Oehlers D.J. and Ali, M. (1998). Discussion on "Predictions of the maximum plate end stresses of FRP strengthened beams: Part II" by Quantrill, R.J, Hollaway, L.C. and Thorne, A.M. *Magazine of Concrete Research*, 50(1), 91–92.

Oehlers, D.J and Bradford, M.A. (1995). *Composite Steel and Concrete Structural Members: Fundamental Behaviour*. New York: Pergamon.

Oehlers, D.J., Liu, I.S.T. and Seracino, R. (2005). "Shear deformation debonding of adhesively bonded plates". *Proceedings of the Institution of Civil Engineers: Structures and Buildings*, 158(1), 77–84.

Oehlers, D.J., Liu, I.S.T., Seracino, R. and Mohamed Ali, M.S. (2004). "Prestress model for shear deformation debonding of FRP- and steel-plated RC beams". *Magazine of Concrete Research* 56(8), 475–486.

Oehlers, D.J. and Moran, J.P. (1990). "Premature failure of externally plated reinforced concrete beams". *ASCE Journal of Structural Engineering*, 116(4), 979–995.

Paipetis, S.A. and Dimarogonas, A.D. (1986). *Analytical Methods in Rotor Dynamics*. London: Elsevier Applied Science.

Pan, J. and Leung, C.K.Y. (2007). "Debonding along the FRP–concrete interface under combined pulling/peeling effects". *Engineering Fracture Mechanics*, 74 (1–2), 132–150.

Pham, H.B. and Al-Mahaidi, R. (2006). "Prediction models for debonding failure loads of carbon fiber reinforced polymer retrofitted reinforced concrete beams". *ASCE Journal of Composites for Construction*, 10(1), 48-59.

Pornpongsaroj, P. and Pimanmas, A. (2003). "Effect of end wrapping on peeling behaviour of FRP-strengthened RC beams". *In: Proceedings of the sixth international symposium on FRP reinforcement for concrete structures*, 277–286.

Quantrill, R.J., Hollaway, L.C. and Thorne, A.M. (1996a). "Experimental and analytical investigation of FRP strengthened beam response: Part I". *Magazine of Concrete Research*, 48(177), 331–342.

Quantrill, R.J., Hollaway, L.C. and Thorne, A.M. (1996b). "Predictions of the maximum plate end stresses of FRP strengthened beam: Part II". *Magazine of Concrete Research*, 48(177), 343–351.

Rabinovitch, O. (2008a). "Cohesive interface modeling of debonding failure in FRP strengthened beams". *Journal of Engineering Mechanics*, 134 (7), 578–588.

Rabinovitch, O. (2008b). "Debonding analysis of fiber-reinforced-polymer strengthened beams: cohesive zone modeling versus a linear elastic fracture mechanics approach". *Engineering Fracture Mechanics*, 75 (10), 2842–2859.

Rabinovich, O. and Frostig, Y. (2000). "Closed-form high-order analysis of RC beams strengthened with FRP strips". *ASCE Journal of Composites for Construction*, 4(2), 65–74.

Rabinovitch, O. and Frostig, Y. (2001). "Delamination failure of RC beams strengthened with FRP strip – a closed-form high-order and fracture mechanics approach". *Journal of Engineering Mechanics*, 127, 852–861.

Rahimi, H. and Hutchinson, Allan. (2001). "Concrete beams strengthened with externally bonded FRP plates". *ASCE Journal of Composites for Construction* 5(1), 44-56.

Raoof, M., El-Rimawi, J.A. and Hassanen, M.A. (2000). "Theoretical and experimental study on externally plated RC beams". *Engineering Structures*, 22, 85–101.

Ritchie, P.A., Thomas, D.A., Lu, L.W. and Conelly, G.M. (1991). "External reinforcement of concrete beams using fibre reinforced plastics". *ACI Structural Journal*, 88(4), 490–500.

Roberts, T.M. (1989). "Approximate analysis of shear and normal stress concentrations in the adhesive layer of plated RC beams". *The Structural Engineer*, 67(12), 229-233.

Roberts, T.M., and Haji-Kazemi, H. (1989). "Theoretical study of the behaviour of reinforced concrete beams strengthened by externally bonded steel plates". *Proceedings of the Institution of Civil Engineers*, 87(2), 39–55.

Ross, C.A., Jerome, D.M., Tedesco, J.W. and Hughes, M.L. (1999). "Strengthening of reinforced concrete beams with externally bonded composite laminates". *ACI Structural Journal*, 96(2), 212–220.

Saadatmanesh, H. and Ehsani, M.R. (1991). "RC beams strengthened with FRP plates I: An experimental study". *ASCE Journal of Structural Engineering*, 117(11), 3417–3433.

Sebastian, W.M. (2001). "Significance of midspan debonding failure in FRP-plated concrete beams". *ASCE Journal of Structural Engineering*, 127, 792–798.

Seracino, R., Saifulnaz, M.R. and Oehlers, D.J. (2007). "Generic debonding resistance of EB and NSM Plate-to-Concrete joints". *ASCE Journal of Composites for Construction*, 11 (1), 62–70.

Shen, H.S., Teng, J.G. and Yang, J. (2001). "Interfacial stresses in beams and slabs bonded with thin plate". *ASCE Journal of Engineering Mechanics*, 127(4), 399-406.

Smith, S.T. and Teng, J.G. (2001). "Interfacial stresses in plated beams". *Engineering Structures*, 23, 857–871.

Smith, S.T. and Teng, J.G. (2002a). "FRP-strengthened RC beams. I: Review of debonding strength models". *Engineering Structures*, 24 (4), 385–395.

Smith, S.T. and Teng, J.G. (2002b). "FRP-strengthened RC beams. II: Assessment of debonding strength models". *Engineering Structures*, 24 (4), 397–417.

Smith, S.T. and Teng, J.G. (2003). "Shear-bending interaction in debonding failures of FRP-plated RC beams". *Advances in Structural Engineering*, 6(3), 183–199.

Spadea, G., Bencardino, F. and Swamy, R.N. (1998). "Structural behaviour of composite RC beams with externally bonded CFRP". *ASCE Journal of Composites for Construction*, 2(3):132-137.

Stratford, T. and Cadei, J. (2006). "Elastic analysis of adhesion stresses for the design of a strengthening plate bonded to a beam". *Construction and Building Materials*, (20), 34–45.

Swamy, R.N, Jones, R. and Bloxham, J.W. (1987). "Structural behaviour of reinforced concrete beams strengthened by epoxy-bonded steel plates". *The Structural Engineer*, 65A(2), 59–68.

Taljsten, B. (1997). "Strengthening of beams by plate bonding". *ASCE International Journal of Materials in Civil Engineering*, 9(4), 206–212.

Taljsten, B. (1999). "Concrete beams strengthened for bending using CFRP-sheets. *In: Forde, M.C., (ed.), Proceedings of the Eighth International Conference on Advanced Composites for Concrete Repair*, London, UK.

Teng, J.G., Chen, J.F., Smith, S.T., Lam, L. (2002a). *FRP Strengthened RC Structures*. UK: John Wiley and Sons.

Teng, J.G., Zhang, J.W. and Smith, S.T. (2002b). "Interfacial stress in RC beams bonded with a soffit plate: a finite element study". *Construction and Building Materials*, 16(1), 1–14.

Teng, J.G. and Chen, J.F. (2009). "Mechanics of debonding in FRP-Plated RC beams". *Proceedings of ICE, Structures and Buildings*, 162(5), 335-345.

Teng, J.G., Chen, J.F., Smith, S.T. and Lam, L. (2003a). "Behaviour and strength of FRP-strengthened RC structures: a state-of-the-art review". *Proceedings of the Institution of Civil Engineers–Structures and Buildings*, 156 (1), 51–62.

Teng, J.G., Smith, S.T., Yao, J. and Chen, J.F. (2003b). "Intermediate crack-induced debonding in RC beams and slabs". *Construction and Building Materials*, 17 (6–7), 447–462.

Teng, J.G., Yuan, H. and Chen, J.F. (2006). "FRP-to-concrete interface between two adjacent cracks: Theoretical model for debonding failure". *International Journal of Solids and Structures*, 43, 5750-5778.

Teng, J.G. and Yao, J. (2007). "Plate end debonding in FRP-plated RC beams—II: Strength model". *Engineering Structures*, 29(10), 2472–2486.

Tsai, M.Y., Oplinger, D.W. and Mortaon, J. (1998). "Improved theoretical solutions for adhesive lap joints". *International Journal of Solids and Structures*, 35 (12), 1163-1185.

Tumialan, G., Serra, P., Nanni, A. and Belarbi, A. (1999). "Concrete cover delamination in reinforced concrete beams strengthened with carbon fiber reinforced polymer sheets". *In: Dolan, C.W., Rizkalla, S.H. and Nanni, A. (eds.), Proceedings of the Fourth International Symposium on Fiber Reinforced Polymer Reinforcement for Reinforced Concrete Structures*, Maryland, USA, 725–35.

Valcuende, M., Benlloch, J. and Parra, C.J. (2003). "Ductility of reinforced concrete beams strengthened with CFRP strips and fabric". *In: Proceedings of the Sixth International Symposium on FRP Reinforcement for Concrete Structures*, 337–346.

Vilnay, O. (1988). "The analysis of reinforced concrete beams strengthened by epoxy bonded steel plates". *International Journal of Cement Composites and Lightweight Concrete*, 10(2), 73–78.

Wang, J. (2006a). "Cohesive zone model of intermediate crack-induced debonding of FRP-plated concrete beam". *International Journal of Solids and Structures*, 43(21), 6630–6648.

Wang, J. (2006b). "Debonding of FRP-plated reinforced concrete beam, a bond-slip analysis. Part I: theoretical formulation". *International Journal of Solids and Structures*, 43 (21), 6649–6664.

Wang, J. (2007). "Cohesive zone model of FRP–concrete interface debonding under mixed-mode loading". *International Journal of Solids and Structures*, 44(20), 6551–6568.

Wang, J. and Zhang, C. (2008). "Nonlinear fracture mechanics of flexural-shear crack induced debonding of FRP strengthened concrete beams". *International Journal of Solids and Structures*, 45(10), 2916–2936.

Wu, Z., Matsuzaki, T. and Tanabe, K. (1997). "Interface crack propagation in FRP-strengthened concrete structures". *In: Proceedings of the Third International Symposium of Non-Metallic (FRP) Reinforcement for Concrete Structures*, Sapporo, Japan, 319–326.

Xu, R. and Wu., Y., F. (2009). "Analytical study of beams strengthened by adhesively bonded reinforcement with variable properties using state space method". *Composites Science and Technology*, 69, 1912–1918.

Yang, J., Chen, J.F. and Teng, J.G. (2002). "Interfacial stresses in plated RC beams under arbitrary symmetric loads: a higher-order closed form solution", *In: Proceedings of the First International Conference on the use of Advanced Composites in Construction*, Southampton University, UK, 153–163.

Yang, J., Chen, J.F. and J.G. Teng (2009). "Interfacial stress analysis of plated beams under symmetric mechanical and thermal loading". *Construction and Building Materials*, 23 (9), 2973–2987.

Yang, J., Teng, J.G. and Chen, J.F. (2004). "A high order closed-form solution for interfacial stresses in soffit plated RC beams under arbitrary loads". *Proceedings ICE: Structures and Buildings*, 157(1), 77-89.

Yang, J., and Wu, Y.F. (2007). "Interfacial stresses of FRP strengthened concrete beams: Effect of shear deformation". *Composite Structures*, 80, 343–351.

Yao, J., Teng, J.G. and Lam, L. (2005a). "Experimental study on intermediate crack debonding in FRP-strengthened RC flexural members". *Advances in Structural Engineering*, 8 (4), 365–396.

Yao, J., Teng, J.G. and Chen, J.F. (2005b). "Experimental study on FRP-to-concrete bonded joints". *Composites Part B: Engineering*, 36 (2), 99–113.

Yao, J. and Teng, J.G. (2007). "Plate end debonding in FRP-plated RC beams—I: Experiments". *Engineering Structures*, 29(10), 2457–2471.

Yuan, H., Teng, J.G., Seracino, R., Wu, Z.S. and Yao, J. (2004). "Full-range behaviour of FRP-to-concrete bonded joints". *Engineering Structures*, 26(5), 553–565.

Yuan, H., Wu, Z.S. and Yoshizawa, H. (2001). "Theoretical solutions on interfacial stress transfer of externally bonded steel/composite laminates". *JSCE Journal of Structural Mechanics and Earthquake Engineering*, 18(1), 27–39.

Zhang, J.P. (1997). "Diagonal cracking and shear strength of reinforced concrete beams". *Magazine of Concrete Research*, 49(178), 55–65.

Zhang, L. and Teng, J.G. (2010a). "Simple general solution for interfacial stresses in plated beams". *ASCE Journal of Composites for Construction*, 14 (4), 434-442.

Zhang, L. and Teng, J.G. (2010b). "Finite element prediction of interfacial stresses in structural members bonded with a thin plate". *Engineering Structures*, 32, 459-471.